Coastal surface circulation of the Gulf of Cadiz from satellite altimetry measurements

Ph.D Thesis

Roberto Mulero Martínez

Cádiz, 2024

Università degli Studi di Ferrara

DOCTORAL COURSE IN
EARTH AND MARINE SCIENCES (EMAS)

CYCLE XXXVI
Year 2020/2024

COORDINATOR Prof. Paolo Ciavola

Coastal surface circulation of the Gulf of Cadiz from satellite altimetry measurements

Scientific/Disciplinary Sector (SDS): GEO/12

Candidate
Roberto Mulero Martínez

Supervisor
Prof. Jesús Gómez Enri

UNIVERSIDAD DE CADIZ
FACULTAD DE CIENCIAS DEL MAR Y AMBIENTALES
DEPARTAMENTO DE FÍSICA APLICADA

Memoria presentada por Roberto Mulero Martínez para optar al grado de Doctor en Ciencias y Tecnologías Marinas – EMAS (Earth and Marine Sciences)
2020/2024

Coastal surface circulation of the Gulf of Cadiz from satellite altimetry measurements

Candidato
Roberto Mulero Martínez

Co-directores
Prof. Jesús Gómez Enri
Prof. Rafael Mañanes Salinas

D. JESÚS GÓMEZ ENRI, Profesor Titular del Departamento de Física Aplicada de la Universidad de Cádiz y D. RAFAEL MAÑANES SALINAS, Profesor Titular del Departamento de Física Aplicada de la Universidad de Cádiz, como sus directores HACEN CONSTAR:

Que esta memoria, titulada **"Coastal surface circulation of the Gulf of Cadiz from satellite altimetry measurements"**, presentada por D. ROBERTO MULERO MARTÍNEZ, resume su trabajo de Tesis y, considerando que reúne todos los requisitos legales, autorizan su presentación y defensa para optar al grado de Doctor por la Universidad de Cádiz.

Candidato

Roberto Mulero Martínez

Co-directores

Prof. Jesús Gómez Enri

Prof. Rafael Mañanes Salinas

Agradecimientos

En primer lugar, quiero expresar mi agradecimiento a mis directores de tesis, Jesús y Rafa, por compartir su experiencia y conocimiento conmigo, no solo durante el desarrollo de esta tesis, sino desde hace ya más de 8 años cuando comencé a interesarme por esto de la teledetección y la física del mar. Sus consejos y dedicación fueron fundamentales para la culminación de esta investigación.

De igual manera, tengo que agradecer a los investigadores de la Universidad del Algarve por su colaboración y valiosas ideas que enriquecieron significativamente este trabajo. Asimismo, agradezco a todo el personal del departamento de Física Aplicada por su apoyo y colaboración en los diferentes artículos que forman parte de esta tesis. Su disposición y compañerismo fueron claves para superar algún que otro proceso de revisión enrevesado y alcanzar los objetivos propuestos.

Por supuesto, a mi compañera, por su apoyo constante y comprensión en los momentos difíciles. Su paciencia y compañía fueron fundamentales durante todo este proceso. Finalmente, agradezco a mi familia y amigos por su apoyo y cariño.

La confianza que todas las personas involucradas han mostrado en mí ha sido una fuente de motivación clave para llegar hasta aquí.

Gracias.

Summary

The main objective of this thesis is to contribute to the understanding of coastal zone dynamics using high-resolution altimetry data. The study evaluates the possibility of studying mesoscale surface circulation in coastal areas, particularly in the Gulf of Cadiz, Spain, using high-resolution altimetry data with a posting rate of 20 Hz from CryoSat-2 (CS2). For this purpose, a specific filtering strategy for coastal areas was developed along with wind and bottom friction ageostrophic corrections to enhance the accuracy and realism of the outputs. The benefits of such methodology and corrections were assessed by comparison with measurements from high-frequency radar (HFR). The correction of these ageostrophic effects substantially enhanced the correlation between altimetry and HFR data, increasing from 0.61 (no correction) to 0.72 (corrected). Furthermore, the root mean square error (RMSE) decreases from 12.54 cm/s to 7.35 cm/s. Additionally, the research evaluates the quality and capabilities of altimetry-derived wind speed (WS) retrievals for validation/calibration of numerical weather prediction models (NWPM), specifically the Weather Research and Forecasting (WRF) model over the complex area of the Gulf of Cadiz. To assess the applicability of altimetry data for this purpose, the study compares Sentinel-3A/B (S3A/B) WS data with in-situ measurements and validates the WRF model with data from multiple stations in the area. The results show that S3A/B WS data align well with in-situ measurements and are trustworthy for model calibration/validation. The spatial variability of WS derived from the WRF model is compared with the along-track altimetry-derived WS under different wind conditions, demonstrating good agreement between the two datasets even under varying wind conditions. This illustrates that the spatial coverage of satellite altimetry can effectively validate high-resolution numerical weather prediction models in complex coastal areas. Based on the previously validated methodologies to obtain high-resolution satellite altimetry estimates of current velocities, along with high-resolution wind data from the WRF model, the research provides a comprehensive characterization of surface circulation over the northern shelf of the Gulf of Cadiz. The study compares high-resolution satellite altimetry-based surface zonal currents, corrected for bottom-drag and wind effects, with a publicly available altimetry dataset (generic CMEMS product) and validates them with in-situ measurements from Acoustic Doppler Current Profilers (ADCP). The findings indicate

that the corrected altimetry product outperforms the generic CMEMS product in terms of statistical metrics, accurately capturing surface circulation direction when compared with in-situ measurements. The research emphasizes the importance of considering both wind-driven and geostrophic components of the circulation in different sectors of the Gulf of Cadiz. It reveals that in the western basin, positive (eastward) surface currents are mainly driven by westerly winds, while occasional westward flows are mostly dominated by geostrophic forces. In contrast, in the eastern basin, both eastward and westward flows are primarily driven by favourable winds. Additionally, the analysis of Absolute Dynamic Topography (ADT) values along the entire basin highlights the presence of ADT gradients both cross and along-shore, with a greater significance attributed to the along-shore gradients. The research also conducts a seasonal analysis, showing that eastward circulation dominates during the spring and summer months, associated with upwelling and westerly winds. Conversely, westward flows prevail during the winter months, related to easterly winds and the effect of the along-shore sea level gradient during unfavourable upwelling conditions. While the research highlights the effectiveness of satellite altimetry data for studying coastal dynamics, it also acknowledges certain limitations, such as the inability to measure wind direction and the inability to capture variability at scales smaller than the across-track footprint length. Nonetheless, the results suggest that improved methodologies and higher-resolution altimetry measurements can significantly enhance our understanding of coastal zone dynamics, bringing it closer to that of the open ocean.

Resumen

El objetivo principal de esta tesis es contribuir a la comprensión de la dinámica de las zonas costeras utilizando datos altimétricos de alta resolución. En primer lugar, se evalúa la posibilidad de estudiar la circulación superficial de mesoescala en zonas costeras, particularmente en el Golfo de Cádiz, España, utilizando datos altimétricos de alta resolución (20 Hz) procedentes de CryoSat-2 (CS2). Para ello, se desarrolló una estrategia de filtrado específica para zonas costeras junto con correcciones ageostróficas de viento y fricción de fondo para mejorar la precisión y el realismo de los resultados. Las ventajas de esta metodología y de las correcciones se evaluaron comparándolas con las mediciones del radar de alta frecuencia (HFR). La corrección de estos efectos ageostróficos mejoró sustancialmente la correlación entre la altimetría y los datos del HFR, aumentando de 0,61 (sin corrección) a 0,72 (corregido). Además, el error cuadrático medio (RMSE) disminuye de 12,54 cm/s a 7,35 cm/s. Además, la investigación evalúa la calidad y las capacidades de las recuperaciones de la velocidad del viento (WS) derivadas de altimetría para la validación/calibración de modelos numéricos de predicción meteorológica (NWPM), en concreto el modelo Weather Research and Forecasting (WRF) sobre la compleja zona del Golfo de Cádiz. Para evaluar la aplicabilidad de los datos altimétricos para este propósito, el estudio compara los datos de WS de Sentinel-3A/B (S3A/B) con medidas in-situ y valida el modelo WRF con datos de múltiples estaciones de la zona. Los resultados muestran que los datos de WS de S3A/B se alinean bien con las mediciones in situ y son fiables para la calibración/validación del modelo. La variabilidad espacial de la WS derivada del modelo WRF se compara con la WS derivada de altimetría a lo largo de la traza bajo diferentes condiciones de viento, demostrando una buena concordancia entre los dos conjuntos de datos incluso bajo condiciones de viento variables. Esto demuestra que la cobertura espacial de la altimetría por satélite es de gran utilidad para validar eficazmente los modelos numéricos de predicción meteorológica de alta resolución en zonas costeras complejas. Basándose en las metodologías previamente validadas para obtener estimaciones de altimetría por satélite de alta resolución de las velocidades de las corrientes, junto con datos de viento de alta resolución del modelo WRF, la investigación proporciona una caracterización completa de la circulación superficial sobre la plataforma norte del Golfo de Cádiz. El estudio compara las corrientes zonales

superficiales de alta resolución basadas en altimetría por satélite, corregidas por los efectos del arrastre del fondo y del viento, con un conjunto de datos altimétricos disponibles públicamente (producto genérico CMEMS) y los valida con mediciones in situ de los Perfiladores Acústicos de Corrientes Doppler (ADCP). Los resultados indican que el producto altimétrico corregido supera al producto genérico CMEMS en términos de métricas estadísticas, capturando con precisión la dirección de la circulación superficial cuando se compara con las mediciones in situ. La investigación subraya la importancia de considerar tanto los componentes eólicos como geostróficos de la circulación en diferentes sectores del Golfo de Cádiz. Revela que en la cuenca occidental, las corrientes superficiales positivas (hacia el este) están impulsadas principalmente por los vientos del oeste, mientras que los flujos ocasionales hacia el oeste están dominados principalmente por fuerzas geostróficas. Por el contrario, en la cuenca oriental, tanto los flujos hacia el este como hacia el oeste son impulsados principalmente por vientos favorables. Además, el análisis de los valores de la Topografía Dinámica Absoluta (TDA) a lo largo de toda la cuenca pone de relieve la presencia de gradientes de TDA tanto transversales como a lo largo de la costa, atribuyéndose una mayor importancia a los gradientes a lo largo de la costa. La investigación también lleva a cabo un análisis estacional, mostrando que la circulación hacia el este domina durante los meses de primavera y verano, asociada al afloramiento y a los vientos del oeste. Por el contrario, los flujos hacia el oeste prevalecen durante los meses de invierno, relacionados con los vientos del este y el efecto del gradiente del nivel del mar a lo largo de la costa durante condiciones desfavorables de afloramiento. Aunque la investigación pone de relieve la eficacia de los datos de altimetría por satélite para estudiar la dinámica costera, también reconoce ciertas limitaciones, como la incapacidad para medir la dirección del viento y la incapacidad para captar la variabilidad a escalas menores que la longitud de la huella a través de la pista. No obstante, los resultados sugieren que la mejora de las metodologías y las mediciones altimétricas de mayor resolución pueden mejorar significativamente nuestra comprensión de la dinámica de las zonas costeras, acercándola a la del océano abierto.

Riassunto

L'obiettivo principale di questa tesi è di contribuire alla comprensione delle dinamiche della zona costiera utilizzando dati altimetrici ad alta risoluzione. Lo studio mira a investigare la circolazione superficiale a “mesoscala” nelle aree costiere, in particolare nel Golfo di Cadice, in Spagna, utilizzando dati altimetrici ad alta risoluzione con una frequenza di campionamento di 20 Hz dalla missione CryoSat-2 (CS2). A questo scopo, è stata sviluppata una specifica strategia di filtraggio per le aree costiere insieme all’utilizzo di correzioni ageostrofiche per il vento e dell’attrito sul fondale con l'obiettivo di migliorare l'accuratezza e il realismo dei risultati. I benefici di questa metodologia e delle correzioni sono stati valutati mediante un confronto con le misurazioni fornite dal radar ad alta frequenza (HFR). La correzione degli effetti ageostrofici ha notevolmente aumentato la correlazione tra l'altimetria e i dati HFR, passando da 0,61 (senza correzione) a 0,72 (con correzione). Inoltre, l'errore quadratico medio (RMSE) è diminuito da 12,54 cm/s a 7,35 cm/s. Lo studio si prefigge anche di valutare la qualità e il possibile utilizzo delle stime della velocità del vento derivate dall'altimetria (WS) per la validazione/calibrazione dei modelli numerici di previsione del tempo (NWPM), in particolare nel caso del modello Weather Research and Forecasting (WRF) nella complessa area del Golfo di Cadice. Per valutare l'applicabilità dei dati altimetrici a questo scopo, lo studio confronta i dati WS di Sentinel-3A/B (S3A/B) con misurazioni in situ e convalida il modello WRF con dati da varie stazioni nell'area. I risultati mostrano che i dati WS di S3A/B riproducono le misurazioni in situ e dimostrano l’utilizzo per la calibrazione/validazione del modello. La variabilità spaziale del WS derivato dal modello WRF viene confrontata con il WS derivato dall'altimetria lungo la traiettoria per condizioni di vento, mostrando un buon accordo tra i due set di dati anche in condizioni di vento variabili. Ciò conferma che la copertura spaziale dell'altimetria satellitare può convalidare efficacemente i modelli di previsione del tempo ad alta risoluzione in aree costiere complesse. Sulla base delle metodologie precedentemente validate per ottenere stime di altimetria satellitare ad alta risoluzione delle velocità delle correnti, insieme a dati di vento ad alta risoluzione dal modello WRF, lo studio fornisce una caratterizzazione completa della circolazione superficiale sulla piattaforma settentrionale del Golfo di Cadice. Vengono confrontate le correnti zonali superficiali basate sull'altimetria satellitare ad alta risoluzione, corrette per l'attrito sul fondo e gli effetti del vento, con un set di dati altimetrici disponibile

pubblicamente (prodotto CMEMS generico) e con misurazioni in situ da Profilatori Acustici Doppler delle Correnti (ADCP). I risultati indicano che il prodotto altimetrico corretto è più accurato del prodotto CMEMS generico utilizzando metriche statistiche, catturando in modo accurato la direzione della circolazione superficiale in confronto alle misurazioni in situ. I risultati sottolineano l'importanza di considerare sia i componenti guidati dal vento che quelli geostrofici della circolazione in settori diversi del Golfo di Cadice. Nel bacino occidentale, le correnti superficiali positive (verso Est) sono principalmente guidate dai venti di ponente, mentre i flussi occasionali verso Ovest sono dominati principalmente dalle forze geostrofiche. Al contrario, nel bacino orientale, sia i flussi verso Est che quelli verso Ovest sono principalmente guidati dai venti favorevoli. Inoltre, l'analisi dei valori della Topografia Dinamica Assoluta (ADT) lungo l'intero bacino evidenzia la presenza di gradienti ADT sia trasversali che lungo la costa, con una maggiore importanza attribuita ai gradienti lungo la costa. La ricerca conduce anche un'analisi stagionale, mostrando che la circolazione verso Est domina durante la primavera e l'estate, associata all' "upwelling" e ai venti di ponente. Al contrario, i flussi verso Ovest prevalgono durante i mesi invernali, legati ai venti di levante e all'effetto del gradiente del livello del mare lungo la costa durante condizioni di upwelling sfavorevoli. Mentre la ricerca sottolinea l'efficacia dei dati altimetrici satellitari nello studio delle dinamiche costiere, riconosce anche alcune limitazioni, come l'impossibilità di misurare la direzione del vento e di catturare la variabilità a scale più piccole della lunghezza dell'impronta lungo traccia. Tuttavia, i risultati suggeriscono che metodologie migliorate e misurazioni altimetriche ad alta risoluzione spaziale possono migliorare significativamente la nostra comprensione delle dinamiche delle zone costiere, avvicinandola a quella dell'oceano aperto.

Table of Contents

List of Figures

List of Tables

Acronyms

AEMET	Agencia Estatal de Meteorología
ADCP	Acoustic Doppler Current Profiler
ADT	Absolute Dynamic Topography
ASCAT	Advanced SCATterometer
CCMP	Cross-Calibrated Multiplatform
CCC	Coastal Countercurrent
CMEMS	Copernicus Marine Environment Monitoring Service
CODAR	Coastal Ocean Dynamics Applications Radar
CS2	CryoSat-2
CSM	Cape Santa Maria
CSV	Cape San Vicente
CT	Cape Trafalgar
DORIS	Doppler Orbitography and Radiopositioning Integrated by Satellite
DTU	Technical University of Denmark
ECV	Essential Climate Variables
ESA	European Space Agency
ETOPO	Earth TOPOgraphy
GCOS	Global Climate Observing System
GDOP	Geometric Dilution of Precision
GCC	Gulf of Cadiz Current
GPOD	Grid-Processing-On-Demand
GoC	Gulf of Cadiz

HFR	High-Frequency Radar
JCR	Journal Citation Reports
LOESS	Locally Estimated Scatterplot Smoothing
LRM	Low Resolution Mode
MDT	Mean Dynamic Topography
MODIS	Moderate Resolution Imaging Spectroradiometer
MO	Mediterranean Outflow
MSS	Mean Sea Surface
NRMSE	Nomalized Root Mean Square Error
NAO	North Atlantic Oscillation
P-PRO	Earth Console Parallel Processing Service
RMSE	Root Mean Square Error
RO	Relative Orbit
S3A/B	Sentinel-3A/B
SAGC	Surface Absolute Geostrophic Current
SAR	Synthetic Aperture Radar
SARin	Synthetic Aperture Radar Interferometry
SAMOSA	SAR Altimetry MOde Studies and Applications
SG	Strait of Gibraltar
SLA	Sea Level Anomaly
SST	Sea Surface Temperature
SSB	Sea State Bias
SSW	Sea Surface Wind

SSH	Sea Surface Height
STDE	Standard Deviation
SWH	Significant Wave Height
SWOT	Surface Water and Ocean Topography
U10	Wind Speed at 10 m
Vg	Geostrophic Current Velocity
WD	Wind Direction
WRF	Weather Research and Forecasting
WS	Wind Speed

Thesis Outline

The format of this thesis is manuscript-based, in which each of the three main chapters corresponds to a different research paper, all of them are already published in high-impact journals, located within the first quartile and decile of the Journal Citation Reports (JCR), respectively. Though the three studies are closely related, share some of the methods and data and are intended to fulfil the main objective of this thesis, the topics are sufficiently different to merit individual manuscripts and discussions. The manuscripts are presented identically to the publications with slight changes in formatting as well as the addition of final sections describing the connection of one chapter to the next, and each of them includes a specific discussion. All bibliographic references made throughout the thesis are summarized into a single bibliography section at the end. As a result, the final structure of the thesis is as follows:

- **Chapter 1. General Introduction**: Description of the scientific motivation behind the research presented in this dissertation, the hypothesis and the objectives, along with the fundamentals of satellite altimetry and its application for oceanographic purposes.
- **Chapter 2. Assessment of Near-Shore Currents from CryoSat-2 Satellite in the Gulf of Cadiz Using HF Radar-Derived Current Observations.** Mulero-Martínez, R.; Gómez-Enri, J.; Mañanes, R.; Bruno, M. *Remote Sens Environ 2021, 256, 112310, doi:10.1016/J.RSE.2021.112310.*
- **Chapter 3. The Use of Sentinel-3 Altimetry Data to Assess Wind Speed from the Weather Research and Forecasting (WRF) Model: Application over the Gulf of Cadiz**. Mulero-Martinez, R.; Román-Cascón, C.; Mañanes, R.;

Izquierdo, A.; Bruno, M.; Gómez-Enri, J. *Remote Sensing 2022, Vol. 14, Page 4036 2022, 14, 4036, doi:10.3390/RS14164036.*

- **Chapter 4. Spatiotemporal variability of the coastal circulation in the northern Gulf of Cadiz from Copernicus Sentinel-3A satellite radar altimetry measurements.** Mulero-Martinez, R.; Gómez-Enri, J.; De Oliveira Júnior, L.; Garel, E.; Relvas, P.; Mañanes, R. *Advances in Space Research 2024, doi: https://doi.org/10.1016/j.asr.2024.02.054.*
- **Chapter 5. General Conclusions:** Final discussion of the main results obtained, along with the connection between the different research works and the conclusions reached.
- **Chapter 6. Future Research Lines.** Further research and activities motivated by this work.
- **Chapter 7. References.** Cited references along the different chapters.
- **Annexes.** Original versions of the different manuscripts and Summary of Activities.

Chapter 1

General Introduction

This chapter includes an introductory section (Section 1.1) describing the scientific motivation behind the research presented in this dissertation, along with the fundamentals of satellite altimetry and its application for oceanographic purposes, particularly for the study of coastal areas (Section 1.2). This section aims to provide the reader with a general understanding of the main topics of this thesis to ease its reading. Finally, Section 1.3 presents the aims of this thesis through the description of the hypothesis and objectives.

1.1 Introduction

In recent decades, the scientific community has recognised oceans' significant role in regulating the planet's climate. It is well-established that the ocean exerts control over critical agents such as global temperature and carbon dioxide levels. In this context, it is imperative to observe, understand and model the diverse physical mechanisms that contribute to ocean circulation.

The surface layer of the ocean responds to the action of atmospheric factors (surface wind, temperature, pressure) through rapid changes in dynamics, reflected in events eddies, fronts, internal waves or upwellings (Barale et al., 2010), which, at the same time, are linked to high socio-economic and environmental impact activities (e.g. fisheries, offshore energy, navigation, oil spills) (Aguiar et al., 2020). Besides, surface circulation influences sea level variability (Han et al., 2019). Understanding coastal circulation and dynamics plays a key role in the management of coastal areas and hence in the life of more than 10% of the Earth's population exposed to the effects of sea level rise (Dinardo et al., 2018; Neumann et al., 2015). The Gulf of Cadiz is one of these exposed coastal areas and its surface circulation presents a complex dynamic, regarding its temporal and spatial variability, mainly due to its location, as it constitutes an inflow-outflow area between the Atlantic Waters with the Mediterranean Sea across the Strait of Gibraltar (Peliz et al., 2009). It is also linked to the North Atlantic Subtropical Gyre and to the Portuguese upwelling system (Laiz et al., 2019). In this context, satellite altimetry plays a key role in shedding light on understanding ocean dynamics.

During the last three decades, the use of satellite altimeters to measure sea level has made a significant contribution to the field of oceanography. Satellite altimetry is a very effective tool for understanding global sea level variability, large circulation patterns, and surface processes in the open ocean (Fu et al., 2010). However, in coastal areas and minor sub-

basins, the study of surface dynamics is more complex, since circulation in these areas is conditioned by local processes and ageostrophic components, such as the variability of the wind field or the drag forces related to abrupt and shallow bottom topographies, so they cannot be completely characterised applying the geostrophic approximation to the altimetry measurements. That is why the application of satellite altimetry measurements for the study of coastal areas requires a more in-depth assessment of the local conditions and specific editing methodologies for the altimetry data.

1.2 Theoretical background

The origins of satellite altimetry trace back to the 1970s, notably with the introduction of Seasat in 1978 and Geosat in 1985. Over time, advancements in radar techniques and orbit determination have progressively enhanced the precision, thereby increasing the practicality of satellite altimetry data. Notably, the deployment of ERS-1 in 1991 (accompanied by ERS-2 in 1995, Envisat in 2002, and Altika in 2013) and Topex/Poseidon in 1992 (alongside Jason-1 in 2001 and Jason-2 in 2008) marked the initiation of a continuous global altimetry observation era along repeated tracks. Even at the time this thesis is being written, there are ongoing development of new missions (i.e.: Sentinel-3C and Sentinel-3D) ensuring service continuity as evidenced by the recent introduction of the Surface Water and Ocean Topography (SWOT) mission, which aims to gather data across a 120 km wide swath (Abdalla et al., 2021; Srinivasan and Tsontos, 2023).

Radar altimeters measure the distance from the satellite to the surface below (range, Figure 1.2.1), through bounced-back echoes from transmitted radar pulses. The power of the signal as received by the satellite is registered in a time series called waveform. To extract geophysical information from these waveforms, it is necessary to conduct a processing step known as retracking (Chelton, 2001), which involves the fitting of a model response to the actual waveform. The upper limit of the range is estimated from the satellite position,

precisely known by the contribution of on-board navigation devices (Doppler Orbitography and Radio-positioning Integrated by Satellite instrument, DORIS; Global Positioning System, GPS, Satellite Laser Ranging, SLR) and referred to the ellipsoid. Below, the absolute elevation of surface or sea surface height (SSH), when measured over the ocean, is estimated by considering the difference between the orbit altitude and range, after applying corrections for atmospheric propagation and pulse reflection effects on the surface. Additionally, the characteristics of the echoes from the ocean's surface provide information on its roughness, directly related to wave heights and wind stress over the ocean (Vignudelli et al., 2011).

In coastal zones, satellite altimetry faces technical obstacles. First, the corrections required for the altimeter range, including geophysical such as tides and dynamic atmospheric correction, as well as environmental like ionospheric correction and corrections for dry and wet tropospheric conditions and sea state, become less reliable and more variable (Andersen and Scharroo, 2011). Secondly, the residual noise present in actual waveforms can significantly impact the accurate extraction of parameters of interest during the retracking process. This deviation occurs because the waveforms deviate from the expected theoretical open ocean shape. This phenomenon is particularly observed in the final 10 kilometers from the coastline, where both coastal waters and elevated terrain can produce returns within the altimeter's range window. Consequently, this alters the waveform shape from the anticipated pattern for a homogeneous surface. Additional agents that can affect the waveform in this regard includes potential abrupt alterations in the sea state (rapid changes in the bathymetry, wind-sheltered areas, wind gusts, etc) and the existence of land within the altimeter footprint (Deng et al., 2002).

In the last years, efforts have been made in the coastal altimetry community to improve the capabilities of current altimeters close to the coastal zone (Cipollini et al., 2010; Vignudelli

et al., 2019, 2011), including the application of improved range/geophysical corrections (Andersen and Scharroo, 2011; Handoko et al., 2017; Rieu et al., 2021), the development of

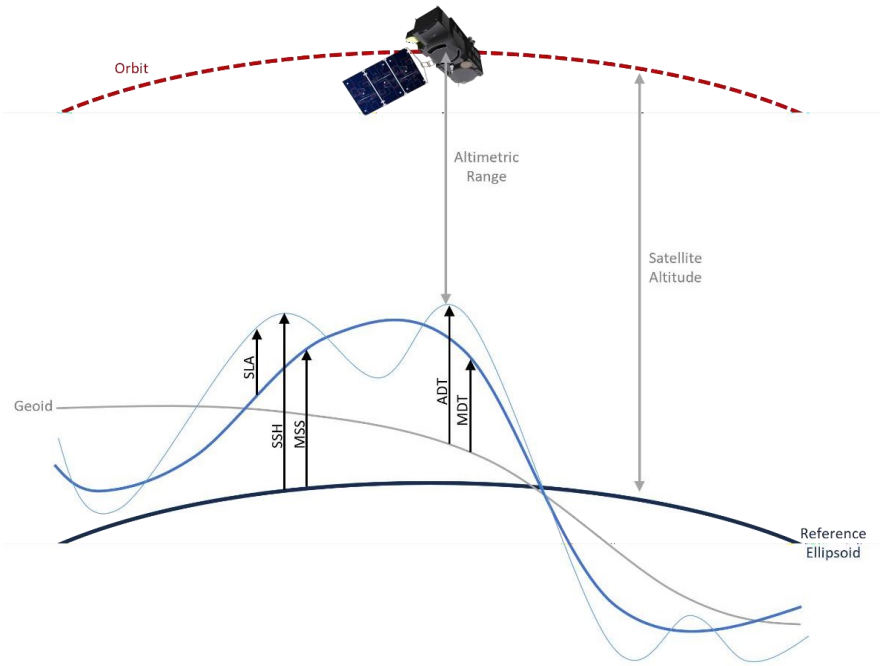

Figure 1.1 The principle of satellite altimetry, along with the different sea level variables (SSH, sea surface height; SLA, sea level anomaly; MSS, mean sea surface; MDT, mean dynamic topography; ADT, Absolute dynamic topography).

Having the capacity to gather sea surface height measurements across the entire ocean offers an opportunity not just to comprehend how sea level varies in space and time but also to analyze associated physical processes. Consequently, the deviation of sea level from the ocean surface's equipotential (the geoid) allows for the calculation of surface geostrophic currents (Fu et al., 1988).

The geostrophic approximation applied at the sea surface leads to a very simple relation between surface slope and surface current (Stewart, 1997). Considering a level surface (geoid) slightly below the sea surface (z). The level surface refers to the geoid, it is, the gravitational potential constant surface (Figure 1.2). The pressure gradient on the level surface is given by Equation 1.1:

$$p = \rho g\,(\Delta z) \tag{1.1}$$

assuming ρ and g are essentially constant in the upper few meters of the ocean.

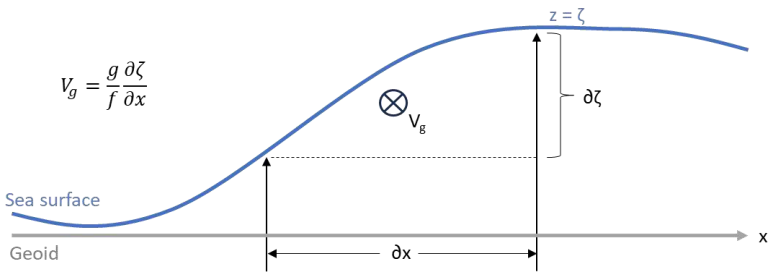

Figure 1.2. The slope of the sea surface relative to the geoid (∂ζ/∂x) is directly related to surface geostrophic currents, Vg.

Substituting Equation 1.1 into the geostrophic equations (Equation 1.2), the two components of the surface geostrophic currents are given by Equation 1.3.

$$\frac{1}{\rho}\frac{\partial p}{\partial x} = f \cdot v;\ \frac{1}{\rho}\frac{\partial p}{\partial y} = -f \cdot u \tag{1.2}$$

$$u_g = -\frac{g}{f}\frac{\partial\zeta}{\partial y};\ v_g = \frac{g}{f}\frac{\partial\zeta}{\partial x} \tag{1.3}$$

Where p is pressure, ρ is density, g is gravity, f is the Coriolis parameters, and ζ is the height of the sea surface above the level surface.

Considering that the ADT represents the dynamic signal indicating displacement relative to the geoid, influenced by interactions involving the atmosphere, topographical features of the ocean floor, and its boundaries, it is indeed possible to calculate an estimate of the absolute surface geostrophic circulation using altimeter measurements.

1.3 Aims & Objectives

Based on the above discussion about the limitations of using satellite altimetry data for studying ocean circulation over coastal areas, the main aim of this thesis is to contribute to one of the challenges of altimetry in the present decade: to reach a level of understanding of the coastal zones dynamic similar to that of the open ocean (Troupin et al., 2015). Therefore, the general objective is to make possible the assessment of surface circulation in coastal areas from altimetry data, starting from understanding the dynamics of the Gulf of Cadiz as a first stage. In order to achieve the general objective, the following specific objectives were proposed:

1) To characterize the contribution of different ageostrophic factors to the surface circulation of the Gulf of Cadiz, by comparing satellite altimetry-derived absolute surface geostrophic currents with high-frequency radar measurements.

2) To analyse the capabilities of satellite altimetry-derived wind speed retrievals for numerical wind model calibration/validation over the Gulf of Cadiz.

3) To use satellite altimetry-derived absolute surface geostrophic current estimates, along with ageostrophic corrections to improve the knowledge of the surface circulation patterns in the Gulf of Cadiz.

Chapter 2

Assessment of near-shore currents from CryoSat-2 satellite in the Gulf of Cadiz using high-frequency radar-derived current observations

This study evaluated the possibility of studying mesoscale surface circulation in coastal areas, such as the Gulf of Cadiz, Spain, using high-resolution altimetry data (20-Hz of posting rate) along with the use of wind and bottom friction ageostrophic corrections. Absolute cross-track surface zonal current velocities, derived from filtered along-track CryoSat-2 SIRAL-SARM Absolute Dynamic Topography (ADT) measurements, are compared with high-frequency radar (HFR) data in the coastal area of the Gulf of Cadiz. The filtering strategy followed in this study for the altimetry data is dependent on the HFR measurements for each track. Absolute surface geostrophic velocities obtained from 20-Hz altimetry data agree well with HFR further than 25 km from the coast. Close to land ([3–25] km) the ageostrophic component of the surface current (due to the wind drag and the bottom friction) needs to be considered in the altimeter data. On average, the correlation between altimetry and HFR improved from 0.61 (no correction) to 0.72 (correcting these effects). The root mean square error (RMSE) lowered from 12.54 cm/s to 7.35 cm/s. Furthermore, it has also been demonstrated that corrected altimeter measurements are useful for the study of dynamics and patterns of coastal areas.

Mulero-Martínez, R., Gómez-Enri, J., Mañanes, R., & Bruno, M. (2021). **Assessment of near-shore currents from CryoSat-2 satellite in the Gulf of Cadiz using HF radar-derived current observations**. Remote Sensing of Environment, 256(June 2020). https://doi.org/10.1016/j.rse.2021.112310

2.1 Introduction

Satellite altimetry has changed physical oceanography by enabling monitoring of global ocean topography from space (Fu et al., 1988). Consequently, large circulation patterns and processes in the open ocean are well characterised (Fu et al., 2010) using the geostrophic approximation. However, in coastal areas and minor sub-basins, the study of ocean dynamics is more complex since circulation in these areas is conditioned by local processes and ageostrophic components, such as tidal oscillations, changes in the field of winds, abrupt and shallow bottom topographies, river discharges and interactions between different water masses in small areas (Criado-Aldeanueva et al., 2006), and along-shore pressure gradients (Garel et al., 2016). The surface layer of the ocean responds to the action of these factors through rapid changes in dynamics, reflected in events such as coastal countercurrents, eddies, fronts, internal waves and upwellings (Barale et al., 2010), which, at the same time, are linked to activities of high socio-economic and environmental impact (fisheries, offshore energy, navigation, oil spills) (Aguiar et al., 2020). Moreover, surface circulation influences sea level variability (Han et al., 2019). Consequently, understanding coastal currents and ocean surface dynamics plays a key role in the management of coastal areas, where more than 10% of the Earth's population lives exposed to the effects of sea level rise (Neumann et al., 2015).

Technological advances in satellite altimeters, such as CryoSat-2 (CS2) and Sentinel-3A/B allow accurate measurements and improved spatial resolution measurements along the satellite's (pass) track, making them suitable tools for studying coastal zone dynamics (Morrow et al., 2017). Despite these improvements, coastal altimetry still faces two main challenges in retrieving accurate sea surface height: coastal zones are dominated by small and medium-scale structures and pro- cesses in the spatio-temporal domain; and the proximity to the coast implies the existence of anomalies in the altimeter measurements

related to the presence of land and/or calm water contamination within the altimeter's footprint (Gómez-Enri et al., 2010), as well as mis- characterised range/geophysical corrections (Gommenginger et al., 2011). In recent years, efforts have been made in the coastal altimetry community to improve the capabilities of current altimeters close to the coastal zone (Cipollini et al., 2010; Vignudelli et al., 2019, 2011), including the application of improved range/geophysical corrections (Andersen and Scharroo, 2011; Handoko et al., 2017) and validation with in-situ observations (Vignudelli et al., 2019 and references therein). Our work contributes toward overcoming one of the challenges of altimetry in the present decade: to reach a level of understanding of the ocean circulation in coastal zones similar to that of the open ocean (Troupin et al., 2015). To achieve this, quality-controlled data from high-frequency radar (HFR, henceforth) are used to validate the altimetry-derived ocean circulation in the coastal area. High-frequency radar is a useful tool to monitor coastal surface currents and it has been installed and used in a number of places around the world to study coastal mesoscale circulation (Mandal et al., 2019), monitor ocean dynamics and validate hydrodynamic and wave models (Wyatt, 2014).

Previous studies have compared HFR and altimetry concluding that the former represents a potential tool for the validation and improvement of altimetry products in coastal areas (Liu et al., 2014; Manso-Narvarte et al., 2018; Morrow et al., 2017; Powell and Leben, 2004; Roesler et al., 2013; Troupin et al., 2015). Related works obtained a high correlation between HFR and altimetry-derived circulation, up to 0.64 (e.g. Manso-Narvarte et al., 2018), using 1-Hz along-track altimeter measurements (~7 km between consecutive measurements). Very few studies, such as Troupin et al. (2015), which obtained consistent results up to 10 km from the coast, have compared surface currents derived from higher along-track spatial resolutions (20 Hz, 40 Hz) and HFR data close to the shore. Regarding the differences between the measurements derived from HFR (total surface circulation) and altimetry (surface geostrophic circulation), the application of ageostrophic corrections, such as wind-induced

surface currents, seems to increase the agreement between both datasets (Manso-Narvarte et al., 2018), but other ageostrophic components, such as those related to the bathymetry, remain to be analysed in detail (Morrow and Le Traon, 2012).

The main objective of this study was to validate improved estimates of altimeter-derived absolute cross-track surface zonal current velocities (Vg) at high along-track posting rate (20 Hz) from CryoSat-2 (CS2) satellite, using HFR data in the coastal zone (first 25 km from land) in the Gulf of Cadiz (GoC, henceforth) (Iberian Peninsula). Absolute cross-track (Vg) included the geostrophic signal plus two ageostrophic components based on the wind and the bottom friction effects. In addition, we assessed the capabilities of coastal altimetry data to detect meso/small-scale dynamics close to the coast in synergy with HFR data and supported by sea surface temperature (SST) data.

The study is organised as follows: Section 2.2 presents the GoC and its main surface circulation characteristics. Section 2.3 includes a description of the data sets, the edition strategies and the methods. The results and discussion are presented in Section 2.4, starting with the statistical outcomes from the comparison between hourly surface current velocity data from HFR and altimeter data for the 14 tracks analysed, including the impact of the ageostrophic corrections. We give some examples of the capabilities of the altimeter data with regard to the detection of coastal fine-scale circulation structures endorsed by HFR and SST data. Finally, Section 2.5 presents the conclusions and perspectives.

2.2 Study area

The present study is focused on the GoC, particularly on the easternmost part of the Gulf, the continental shelf area delimited by Cape Santa Maria (CSM) and Cape Trafalgar (CT). Figure 2.1a gives the bathymetry of the study area along with the main circulation patterns proposed by García-Lafuente et al. (2006) and Peliz et al. (2009), the CS2 tracks (red lines), and the area covered by the HFR system (blue dotted area) are shown in Figure 2.1b.

The surface circulation of the GoC presents complex dynamics, regarding its temporal and spatial variability, mainly due to its location, as it constitutes an inflow-outflow area between the Atlantic Ocean and the Mediterranean Sea across the Strait of Gibraltar (Peliz et al., 2009), and is also linked to the North Atlantic Subtropical Gyre (Laiz et al., 2019), a fact that significantly influences both local and Atlantic circulations.

Two linked systems can be differentiated when describing the circulation of the GoC: the upper slope current system; and the shelf circulation (Figure 2.1a). The first is generically composed of two flows. In deep layers, the upper Mediterranean outflow core (MO upper) circulates westward contouring the slope (Ambar and Howe, 1979; Peliz et al., 2009). The Gulf of Cadiz Current (GCC) flows toward the southeast into the Mediterranean Sea. The intensity and characteristics of this system are strongly linked to the Mediterranean inflow-outflow coupling (Peliz et al., 2009).

Regarding the circulation over the continental shelf, two modes can be characterised in the eastern section, located between CSM and CT, alternating westward/eastward circulation. Westward circulation, or cyclonic mode, is characterised by a coastal countercurrent (CCC) which comprises the northern boundary of a cyclonic cell located on the eastern shelf between CSM and the mouth of the Guadalquivir Estuary (García-Lafuente et al., 2006). This CCC seems to be controlled mainly by the imbalance of the along-shore pressure gradient, due to the relaxation of large-scale upwelling favourable wind (Garel et al., 2016). The eastward circulation, or anticyclonic mode, is defined by an eastward current (EC) that, unlike the CCC, is likely to originate from Ekman mechanisms that induce the upwelling of cold water along the coast (Garel et al., 2016).

In addition, abrupt changes in the orientation of the coastline and the presence of the Strait of Gibraltar connecting two basins with such different characteristics, favour the existence of a heterogeneous wind field, which strongly controls the zonal surface circulation by the

alternation of westerlies and easterlies (Peliz et al., 2007). Other agents, such as the runoff from the Guadiana and Guadalquivir rivers, affect the surface temperature, salinity, and other biogeochemical variables, mainly in the coastal fringe, near the river mouths (Laiz et al., 2013).

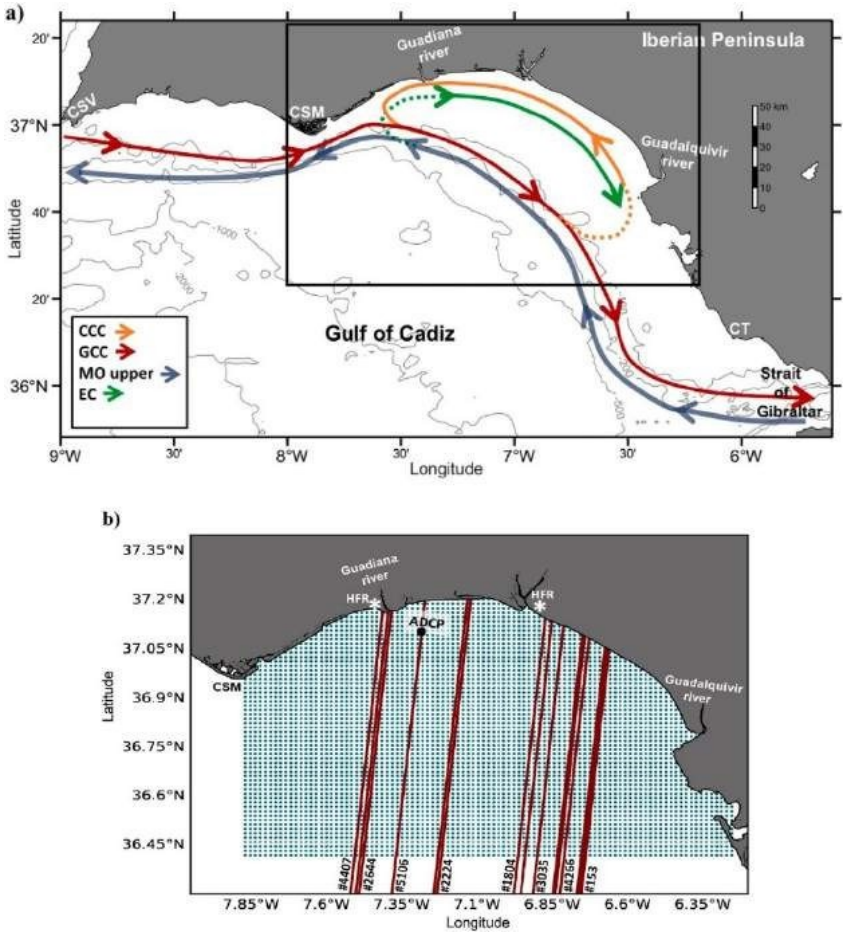

Figure 2.1 (a) The main feasible surface circulation characteristics of the GoC (following García-Lafuente et al. (2006) and Peliz et al. (2009)*, and some geographical features: CSV (Cape San Vicente), CSM (Cape Santa Maria), CT (Cape Trafalgar), CCC (Coastal Countercurrent), GCC (Gulf of Cadiz Current), MO (Mediterranean Outflow), EC (Eastward Current) (b) Location of the observational systems in the GoC: CS2 repetitive tracks and relative orbit number, red lines; HFR system potential covered area, blue dotted area; HFR, high-frequency radar system stations; ADCP, acoustic Doppler current profiler location.*

2.3 Data and Methods

Satellite altimetry

In this study, along-track Sea Level Anomaly (SLA) data from 14 CS2 tracks over the GoC were used to calculate cross-track zonal surface current. CS2 is a European Space Agency (ESA) satellite launched in April 2010 and its primary aim was to monitor changes in the thickness of the sea ice and continental ice sheets (Drinkwater et al., 2004; Wingham et al., 2006); however, CS2 altimetry data have been used for the exploitation of additional ocean products (Calafat et al., 2017) thanks to its main instrument, the synthetic interferometric altimeter (SIRAL), which operates in three modes depending on the purpose: Low Resolution Mode (LRM), mainly used over open ocean, Synthetic Aperture Radar (SAR) mode, for specific coastal areas, and SAR Interferometry (SARIn) mode, with the highest spatial resolution and used over continental water bodies and ice sheets (for more details see CryoSat-2 Product Handbook at https://earth.esa.int/documents). Over the study area, CS2 SIRAL has been working in SAR (Synthetic Aperture Radar) mode since the beginning of the mission in 2010. CryoSat-2 has a quasi-polar orbit of approximately 92◦, allowing nearly global coverage, reaching high latitudes of up to 88◦ N-S Latitude. The quasi-orthogonal product is posted at 20 Hz, which results in ~330 m along-track spatial resolution measurements. The altimetry product has been assessed by previous studies globally (Calafat et al., 2017), and focused on coastal areas, such as Gómez-Enri et al. (2018) over the GoC, obtaining a satisfactory performance further than 3–5 km to the shore. In addition, (Bouffard et al., 2018) demonstrated that the CryoSat-2 ocean products compare very well with in situ measurements and confirmed that the ocean products are perfectly suited for oceanographic applications.

The final SLA product from GPOD level 2, includes the range/ geophysical corrections listed in Table 2-1. In addition, a sea state bias (SSB) correction of 5% of the significant wave height (available in the GPOD product), was applied following previous studies (Fenoglio-Marc et al., 2015; Gómez-Enri et al., 2018). The Mean Sea Surface used was DTU18 MSS (Andersen et al., 2018).

The selection of tracks in the study area was made for the 2013 to 2018 period based on the availability of HFR data. In order to reduce the effect of land contamination in the footprint area of the radar measurements, only the tracks nearly orthogonal to the coastline were selected (Aldarias et al., 2020; Gómez-Enri et al., 2018). Therefore, relative orbits #153, #1804, #2224, #2644, #3035, #4266, #4407, and #5106 were used for a total of 14 tracks (Table 2-2).

Table 2-1 Range and geophysical corrections applied in CryoSat-2 SIRAL-SARM SLA data from SARvatore-GPOD used in this study.

Range corrections	**Geophysical corrections**	
Atmospheric	**Tidal**	**Ocean surface**
Dry Tropospheric	Ocean Tide (TPXO8-atlas model)	Dynamic Atmospheric Correction
Wet Tropospheric	Long-Period Equilibrium Tide	Sea State Bias (5% Significant Wave Height)
Ionospheric	Ocean Loading Tide	
	Solid Earth Tide	
	Geocentric Polar Tide	

SLA editing strategy

Raw 20-Hz along-track SLA data were edited, following the methods presented in Bouffard et al. (2010). The screening removes outliers and filters out high-frequency noise signals near the coast. Firstly, SLA values closer than 3 km to the coastline were rejected to maintain a distance of good quality (Aldarias et al., 2020). Previous studies with CS2 data demonstrated that land contamination might affect the sea level measurements close to the coast (Dinardo et al., 2018; Gómez-Enri et al., 2018). Secondly, SLA values larger than three

times the standard deviation were removed and replaced by linearly interpolated values; this processing was applied in a 10-times loop (Bouffard et al., 2010; Meloni et al., 2019). Finally, a Loess filter (Cleveland and Devlin, 1988) was applied along the track segments to filter out high-frequency noise (Manso-Narvarte et al., 2018); this is a common processing procedure for the study of oceanic mesoscale phenomena (Morrow et al., 2017). For each HFR-CS2 track comparison, a range of spatial cut-off values ([7–60] km) for the Loess filter was tested. This range was selected to resolve the scale of the baroclinic Rossby radius in the area (~6.5 km). The cut-off wavelength that gave the best results in terms of correlation and root mean square error at each track was selected (Morrow et al., 2017). The filter cut-off necessary for obtaining the best correlation among surface velocities obtained from altimetry and HFR is different for each track of the study, depending on the characteristics of the surface circulation at the moment of the satellite pass over the study area. The Loess filter cut-off values applied to each track are presented in Table 2-2.

Table 2-2Relative orbit number (RO), date of pass, filter cut-off window and angle coastline/track for each track.

Track # (RO)	Track date	Filter cut-off (km)	Angle coast/track
#4266	17-Oct-2013	25	64.43
#2644	30-Jun-2014	51	76.39
#1804	06-May-2015	54	68.62
#2224	04-Jun-2015	60	95.68
#4407	23-Oct-2015	60	63.73
#2644	09-Jul-2017	29	76.39
#3035	05-Aug-2017	60	76.80
#4266	29-Oct-2017	60	62.68
#153	21-Jan-2018	52	64.11
#1804	15-May-2018	35	68.55
#2224	13-Jun-2018	60	95.48
#2644	12-Jul-2018	60	78.74
#4266	01-Nov-2018	12	66.64
#153	25-Jan-2019	33	64.75

Figure 2.2 shows an example of the editing approach applied to the CS2 track #2644. High-frequency noise is clearly seen in the raw SLA profile (black line). No outlier is detected in

this track segment, but the Loess filter (60-km cut-off) removes most of the high-frequency noise (red line).

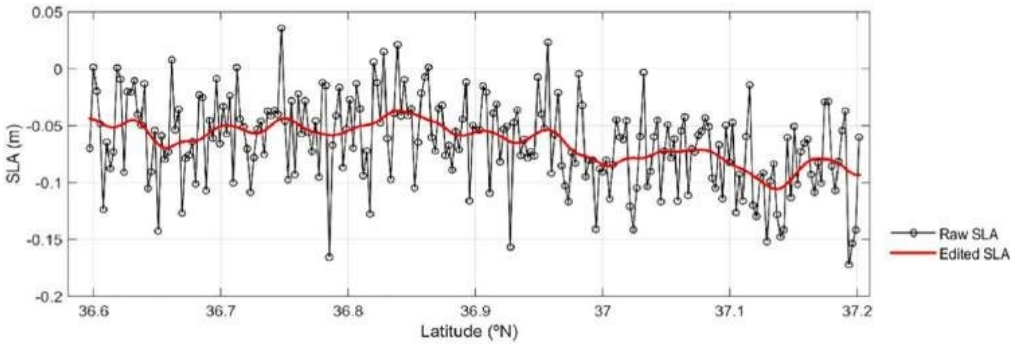

Figure 2.2. CryoSat-2 20 Hz original SLA (black) and edited SLA (red) for track #2644 (12-07-2018). (For interpretation of the references to colour in this figure legend, the reader is referred to the web version of this article.)

Absolute dynamic topography (ADT)

Along-track surface absolute geostrophic current (SAGC) is computed using the absolute dynamic topography (ADT). Absolute dynamic topography profiles were estimated by adding the mean dynamic topography (MDT) to the SLA. The DTU15MDT model (Knudsen et al., 2016), 1-min spatial resolution grid, was bilinearly interpolated to the CS2 along-track positions. DTU15MDT model was obtained by combining the latest version of the gravity field (EIGEN-6C4) with the Mean Sea Surface model (DTU15MSS) (Knudsen et al., 2016).

Surface absolute geostrophic current (SAGC)

Absolute dynamic topography is the dynamic signal that represents the displacement with respect to the equipotential surface (geoid) forced by the interactions with the atmosphere and the topographic contours of the bottom and sides of the ocean. Therefore, it is possible to obtain a good estimate of the surface geostrophic circulation from altimeter measurements from the spatial variations of ADT and consider the effect of the Earth's rotation movement, represented by the Coriolis force.

From an oceanographic point of view, on an axis of Cartesian coordinates in which the x-axis points to the east, y-axis to the north and the z-axis in the opposite direction to the gravity force, assuming that the water density is constant, the zonal (u) and meridional (v) components of the geostrophic current can be obtained using the geostrophic balance equations:

$$\begin{cases} f \cdot u = -\frac{1}{\rho} \cdot \frac{\partial p}{\partial y} \\ -f \cdot v = -\frac{1}{\rho} \cdot \frac{\partial p}{\partial x} \end{cases} \quad (2.1)$$

where ρ is seawater density; g is gravitational acceleration; f is the Coriolis parameter ($f=2\Omega sin\varphi$, where Ω is the angular rotation velocity of the Earth and φ the latitude); and p is pressure. Following the hydrostatic relation defined as:

$$-\frac{\partial p}{\partial z} = -\rho \cdot g, \quad (2.2)$$

and replacing the vertical variation (∂z) by the variation of the sea surface height over the geoid (∂h), Eq. (2.1) can be written as:

$$\begin{cases} f \cdot u = -g \cdot \frac{\partial h}{\partial y} \\ -f \cdot v = -g \cdot \frac{\partial h}{\partial x} \end{cases} \quad (2.3)$$

Considering that the zonal velocity is calculated along the satellite track, it is assumed that the variation of the sea surface height over the geoid along the x-axis does not exist, it is:

$$\frac{\partial h}{\partial x} = 0, \quad (2.4)$$

If h is replaced by absolute dynamic topography (ADT), it is possible to calculate the velocity values of the surface absolute geostrophic current (Vgabs) normal to the satellite tracks using the equation (Bouffard et al., 2010):

$$Vg_{abs} = -\frac{g}{f} \cdot \frac{\partial ADT}{\partial y} \quad (2.5)$$

The along-track altimetric gradient (slope) has been estimated by using the optimal filter developed by Powell & Leben (2004), following the methodology proposed by Bouffard et al. (2010), using a spatial frame of 1.5 km (equivalent to approximately five along-track altimeter measurements), which also addresses the spatial resolution of the high-frequency radar.

High-frequency radar data

Two CODAR SeaSondes stations installed in Mazagón (Spain) and Vila Real de Santo Antonio (Portugal) (Figure 2.1), that belong to the Red de Radares de Alta Frecuencia de Puertos del Estado (www.puertos.es), were used in this study. The stations work at 13.5 MHz frequency; this mode generates measurements with a spatial resolution of approximately 1.5 km and a range that reaches up to 60 km from the coast. The general reliability of HFR data has been demonstrated through extensive comparisons with independent measurements (drifters, ship-based sensor, acoustic Doppler current profilers) (Lorente et al., 2015) over different ocean conditions, providing typical root mean square errors (RMSE) of 7–20 cm/s (Cosoli and Bolzon, 2015; Lorente et al., 2015). Specifically, the HFR zonal velocity (HFRu) used in this study was previously validated with in-situ measurements from an acoustic Doppler current profiler (ADCP) moored in the GoC (37◦6′40” N, 7◦14′19” W, Fig. 1) for three months (from 16-Oct-2013 to 16-Jan-2014). The RMSE (5 cm·s-1) and correlation coefficient (0.86 for 95% of confidence level) resulting from the comparison of 2242 hourly measurements (Figure 2.3) were satisfactory, considering the magnitude of the standard deviations (ADCP:10.73 cm/s ; HFR: 13.09 cm/s) and results from previous studies using the same methodology and statistics (Cosoli et al., 2010; Cosoli and Bolzon, 2015).

A two-step editing methodology was applied to the HFR observations for the comparisons with altimetry data. Firstly, in order to remove high- frequency signals (mainly tidal oscillations), a 72-h average was computed (Roesler et al., 2013), using the 72 h prior to the dates of the satellite measurements. Finally, the HFRu velocity was bilinearly interpolated over the position of the altimeter track measurement positions. The performance of the SeaSonde software solves the geometric dilution of precision (GDOP) related problems, among the different possible sources of error (Lipa et al., 2006). We removed invalid data, for each period of 72-h of HFR data, retaining only the points with more than 60% of valid data (Figure 2.4). In most of the selected tracks the study area is fully covered by the HFR measurements. For this study, 60% of valid data ensures that a compromise is maintained between good spatial coverage of the data and adequate quality.

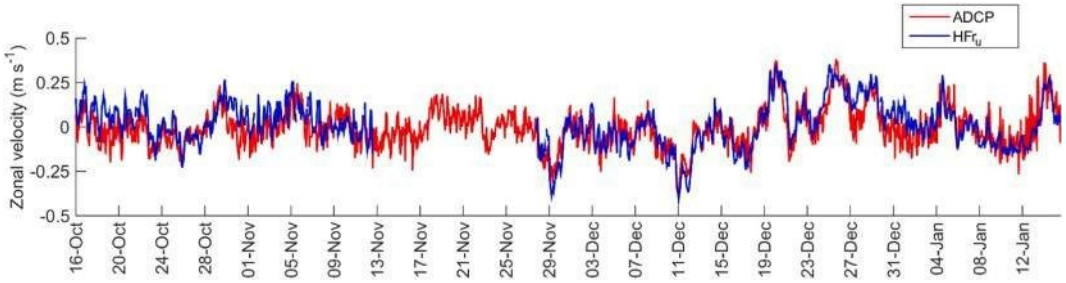

Figure 2.3. Hourly surface zonal velocity time-series recorded by the ADCP (red) and high-frequency radar (blue) from 16-Oct-2013 to 16-Jan-2014.

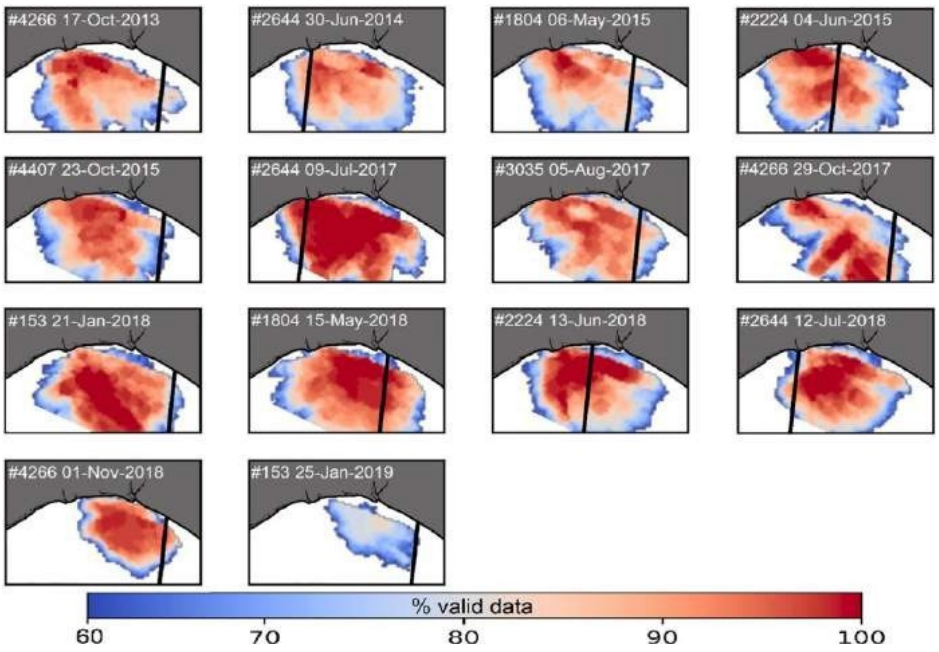

Figure 2.4. Fields of HFR valid data (>60%) for each track analysed.

Ageostrophic corrections of altimetry data

Wind

Zonal wind data from the Weather Research and Forecasting model (WRF; http://mandeo.meteogalicia.es/thredds/catalogos/WRF_2D/cat alog.html), provided by the meteorological agency of Galicia (https://www.meteogalicia.gal) with a spatial resolution of 12 km and temporal resolution of 1 h, were used in this study to calculate the ageostrophic wind-derived correction. WRF-simulated winds have proven to represent the wind regime in the GoC in good agreement with in-situ measurements from buoys (Carvalho et al., 2014; Teles-Machado et al., 2007). The correction does not assume the theoretical Ekman's solution since the study zone is far from the necessary assumption of infinitely deep ocean far from coastal boundaries that supports such a solution. In addition, Stanichny et al. (2016), using extensive drifting buoys and satellite data, demonstrated that surface wind-driven currents are directed almost in the direction of the wind, with a small rotation to the right (in the northern hemisphere) of ~10–15◦, with amplitudes equal to 2.8%. These parameters are not dependent on the Ekman layer depth and can be used in different ocean conditions, as it

has been demonstrated in a number of previous papers (Keulegan, 1951; Kim et al., 2010; Madsen, 1977; Weber, 1983; Wu, 1975). Finally, zonal surface wind-driven velocities (V_w) are computed as:

$$Vw = 0.03 \cdot W_{u10} \cdot \cos(10^{\circ}), \tag{2.6}$$

where W_{u10} is the zonal component of the wind speed at 10 m.

Following the procedure applied to the HFR measurements, the original hourly wind data from the WRF model was 72-h averaged and linearly interpolated over the position of the altimeter tracks. The wind-corrected velocity (Vg_w) was obtained following:

$$Vg_w = -\frac{g}{f} \cdot \frac{\partial ADT}{\partial y} + V_w \tag{2.7}$$

Bottom friction

In coastal areas, wind-induced surface currents are not the only ageostrophic agent since other factors, such as bottom friction and the along-shore pressure variations, also contribute to the overall dynamics. The effect of bottom friction is considerable even on the middle shelf area, able to counterbalance the surface wind stress in shallow waters (less than 25 m) (Kantha and Clayson, 2013). To evaluate and to correct the effect of the bottom friction over the surface circulation derived from altimetry in the coastal area, a bottom friction corrected surface velocity (Vg_d) was calculated. For this purpose, depth-averaged bottom friction terms were added to Eq. (2.3) as follows:

$$\begin{cases} f \cdot u = -g \cdot \dfrac{\partial h}{\partial y} - \dfrac{C_d |V| v}{d} \\ -f \cdot v = -g \cdot \dfrac{\partial h}{\partial x} - \dfrac{C_d |V| u}{d} \end{cases} \tag{2.8}$$

Where C_d is the bottom drag coefficient, $|V|$ is the current velocity modulus, h is the sea surface height over the geoid and d is the bottom depth. Admitting predominance of the zonal

component of the current over the meridional one (i.e. $|V| \sim |u|$) and considering the assumption given in Eq. (2.4), Eq. (2.8) can be written as:

$$\begin{cases} f \cdot u = -g \cdot \dfrac{\partial h}{\partial y} - \dfrac{C_d v}{d} \\ v = \dfrac{C_d |u| u}{f d} \end{cases} \tag{2.9}$$

We use the approximation $|u|u \sim 0.35u + 0.71u^3$, proposed by (Godin and Martinez, 1994). It is important to note that in this expression for typical maximum values of zonal current of 0.5 m/s, the linear term is roughly two times the non-linear one and, accordingly, we retain only the linear term in the approximation, which once substituted in Eq. (2.9), transforms the latter into the following:

$$\begin{cases} f \cdot u = -g \cdot \dfrac{\partial h}{\partial y} - \dfrac{C_d}{d} \cdot |u| v \\ v = \dfrac{0.35 C_d}{d} \cdot u = \dfrac{r}{f} \cdot u \end{cases} \tag{2.10}$$

Where $r = (0.35C_d)/d$ is a depth dependent parameter. Substitution of the second of the Eq. (2.10) into the first one, after admitting once again $|u|u \sim 0.35u$, produces:

$$u = \frac{-g}{\left(f + \dfrac{r^2}{f}\right)} \cdot \frac{\partial h}{\partial y} \tag{2.11}$$

Subsequently, replacing h with absolute dynamic topography (ADT), and using a typically accepted value of $C_d = 2.0\ 10^{-3}$ (Bowden, 1983), bottom drag corrected surface velocity (Vg_d) normal to the satellite track may be computed as:

$$Vg_d = \frac{-g}{\left(f + \dfrac{r^2}{f}\right)} \cdot \frac{\partial ADT}{\partial y} \tag{2.12}$$

Bathymetry data used were provided by ETOPO1 global relief model at 1-min resolution (Amante and Eakins, 2009).

Cross-track corrected velocity

Finally, in order to obtain the surface current including geostrophic and some of the main ageostrophic components, a bottom friction and wind-corrected surface velocity (Vg_{d+w}) was derived from the altimetry data, which includes both previously calculated ageostrophic corrections, and is expressed as:

$$Vg_{d+w} = \frac{-g}{\left(f + \frac{r^2}{f}\right)} \cdot \frac{\partial ADT}{\partial y} + Vw \qquad (2.13)$$

Sea surface temperature

An 8-day Level-3 binned SST from Moderate-resolution Imaging Spectroradiometer (MODIS) Aqua dataset with a spatial resolution of 4 km, from OceanColor (https://oceancolor.gsfc.nasa.gov/) was used in this study to complement the analysis of recorded surface circulation patterns. Sea surface temperature data were obtained for the closest date available prior to each CS2 track.

Data comparison

Altimetry derived velocities orthogonal to the satellite track were decomposed to obtain the zonal component of the velocity. The assessment of the altimeter Vg with the HFRu was performed by estimating two statistical parameters, the root mean square error (RMSE), also expressed as normalized root mean square error (NRMSE) regarding the range of the HFRu measurements (HFRu max - HFRu min), and the Pearson correlation coefficient (r).

2.4 Results and discussion

HFR-altimetry surface velocity statistical assessment

As reported in previous sections, HFR velocities were bilinearly interpolated over the position of the altimeter track measurement positions to perform an along-track comparison

using the altimeter cross-track derived zonal velocities (Vg_{abs}, Vg_{d}, Vg_{w}, Vg_{d+w}), and the zonal component from the high-frequency radar (HFRu). Table 3 provides the statistical results (r, RMSE and NRMSE) for the eight tracks analysed during the analysed time period (14 dates are available). The comparison between Vg_{abs} and HFRu shows r ranging between 0.28 and 0.93 (95% CL), RMSE between 5.08 cm/s and 29.76 cm/s, and NRMSE between 0.23 and 2.99. The average values of r and RMSE (0.61 and 12.54 cm·s-1, respectively) are in agreement with previous studies carried out in coastal areas of the Mediterranean Sea (Morrow et al., 2017; Troupin et al., 2015). A strong track-to-track variation in all the statistics stands out and may be related to different factors, such as the use of the 72-h HFR average window, which might not be suitable for all the comparisons since it could mask or over- smooth geostrophic structures captured by the altimeter. However, considering the method used to select valid HFR data points, the amount of valid data would be insufficient if the average window is reduced.

Impact of ageostrophic corrections

In this section, the effect of the ageostrophic component from the wind on the estimates of the surface current is analysed (Vg_{w}). Figure 2.5 shows the linear relation among the average along-track zonal wind velocity and zonal surface current from HFR for each track of the study, depicting the strong control that the wind exerts over the surface circulation in the area and, therefore, the importance of such a wind- related correction.

The track-to-track statistical values for Vg_{w} are given in Table 2-3. A significant improvement is observed in r/RMSE/NRMSE in most of the tracks (0.68/7.77 cm/s /0.78 in average), with respect to Vg_{abs}. In terms of RMSE this implies a reduction of almost 40%; also, the improvement in the NRMSE (from 1.19 to 0.78) shows the importance of the wind, which reduces this difference in intensity. The effectiveness of the wind-related correction is clearly shown in track #2644 (12-Jul- 2018), where r improves from 0.45 (Vg_{abs}) to 0.71

(Vg_w), proving the important control of the wind over the surface circulation as depicted in Figure 2.5.

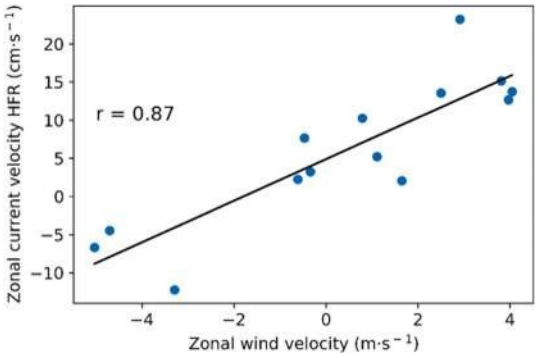

Figure 2.5. Scatter plot of the relation among average along-track zonal wind velocity and zonal surface current from HFR for each track. The linear Pearson's correlation coefficient is also shown (confidence level: 95%).

The ageostrophic correction due the bottom friction slightly improved the comparison with respect to Vg_{abs} in terms of r, RMSE and NRMSE in most of the tracks. The improvement in the correlation in track #4266 (17-Oct-2013) is particularly evident. The bottom friction component improved r = 0.88 (0.30) and RMSE = 14.86 cm/s (15.48 cm/s). This correction seems to be less effective than the one based on the wind effect, since it is restricted to shallower areas.

Table 2-3. Statistics of the comparison between the 14 CryoSat-2 tracks (relative orbit, RO) and high-frequency radar data. r is the correlation coefficient (95% Confidence Level), RMSE is the root mean square error and NRMSE is the normalized RMSE. Zonal wind column shows along-track averaged and standard deviation zonal wind velocity for each track.

Track #RO	Track date	Vg_{abs} - HFR			Vg_{w} - HFR			Vg_{d} - HFR			Vg_{d+w} - HFR			HFR		Zonal wind
		r	RMSE	NRMSE	r	RMSE	NRMSE	r	RMSE	NRMSE	r	RMSE	NRMSE	avg ± std.	Range	avg ± std
			(cm/s)			(cm/s)			(cm/s)			(cm/s)		(cm/s)	(cm/s)	(cm/s)
#4266	2013-10-17	0.3	15.48	2.39	0.49	16.56	2.56	0.88	14.86	2.3	0.92	15.95	2.47	7.65 ± 1.90	6.47	-0.47 ± 0.16
#2644	2014-06-30	0.9	23.34	1.22	0.65	13.85	0.72	0.88	23.18	1.21	0.7	13.7	0.72	15.16 ± 6.14	19.12	3.81 ± 0.47
#1804	2015-05-06	0.54	6.03	0.23	0.65	3.64	0.14	0.55	5.95	0.23	0.6	3.7	0.14	2.05 ± 4.18	25.67	1.65 ± 0.47
#2224	2015-06-04	0.59	12.72	0.49	0.81	2.24	0.09	0.49	12.65	0.49	0.8	2.14	0.08	-4.47 ± 1.94	26.00	-4.70 ± 1.96
#4407	2015-10-23	0.62	13.17	1.57	0.75	4.93	0.59	0.55	13	1.55	0.73	4.82	0.57	-12.22 ± 3.10	8.41	-3.29 ± 0.81
#2644	2017-07-09	0.93	5.21	1.29	0.93	4.02	1	0.89	5.3	1.32	0.89	3.46	0.86	13.57 ± 6.50	4.03	2.50 ± 0.26
#3035	2017-08-05	0.81	12.59	0.76	0.83	6.65	0.4	0.87	12.26	0.74	0.88	6.31	0.38	5.21 ± 5.28	16.46	1.11 ± 1.00
#4266	2017-10-29	0.28	13.49	1.84	0.51	3.43	0.47	0.23	13.07	1.79	0.52	2.91	0.4	-6.67 ± 1.57	7.31	-5.03 ± 1.91
#153	2018-01-21	0.73	5.08	0.52	0.78	5.42	0.56	0.77	4.92	0.5	0.81	5.25	0.54	3.25 ± 2.08	9.76	-0.34 ± 0.24
#1804	2018-05-15	0.64	5.97	0.28	0.62	4.15	0.2	0.69	5.62	0.27	0.68	3.76	0.18	2.25 ± 5.98	21.09	-0.61 ± 1.33
#2224	2018-06-13	0.73	20.04	1.13	0.88	11.25	0.63	0.69	20	1.13	0.88	11.24	0.63	12.68 ± 7.68	17.77	3.97 ± 0.79
#2644	2018-07-12	0.45	17.99	2.88	0.71	10.86	1.74	0.39	17.83	2.86	0.74	10.72	1.72	13.76 ± 7.64	6.24	4.05 ± 1.13
#4266	2018-11-01	0.84	29.76	2.99	0.84	22.7	2.28	0.83	28.19	2.83	0.83	20.99	2.11	23.22 ± 2.86	9.97	2.91 ± 0.46
#153	2019-01-25	0.78	7.19	0.29	0.78	6.92	0.28	0.78	5.56	0.22	0.78	5.29	0.21	0.78 ± 1.11	24.99	0.79 ± 0.21
Average value		0.61	12.54	1.19	0.68	7.77	0.78	0.63	12.16	1.16	0.72	7.35	0.73	5.71 ± 3.86	13.55	

The combined use of both ageostrophic corrections (Vg_{d+w}) improved the comparison (r, RMSE and NRMSE) against HFRu in most of the tracks. This is clearly observed in the averaged values in Table 2-3. As mentioned previously, the wind effect component has a major impact on increasing/reducing r/NRMSE considering the ageostrophic compo- nents. Tracks with good comparisons considering only the geostrophic component (Vg_{abs}), generally maintain good results when applying the different corrections, so the ageostrophic components seem to be circumstantially beneficial. Despite the variability of the wind field in the GoC, the wind correction might improve the results under different scenarios. Figure 2.6 gives the along-track averaged correlation (Figure 2.6a, b) and NRMSE (Figure 2.6c, d), split in two sectors: coastal (3–25 km) and offshore (> 25 km) considering the distance to the coastline. For the coastal sector, the use of the wind correction produces a strong improvement of the results, increasing/decreasing r/NRMSE. The effect of the bottom-friction correction is less important, but it still improves the results compared with the uncorrected measurements. The application of the ageostrophic component considering the bottom friction and wind (Vg_{d+w}) gives the best comparison against HFRu. Offshore, r shows a good performance even for the uncorrected measurements suggesting that the effect of the ageostrophic components further than 25 km is less significant. Again, the wind correction improves the results with respect to the bottom friction, and the best comparison is given when both corrections are added (more evident in NRMSE).

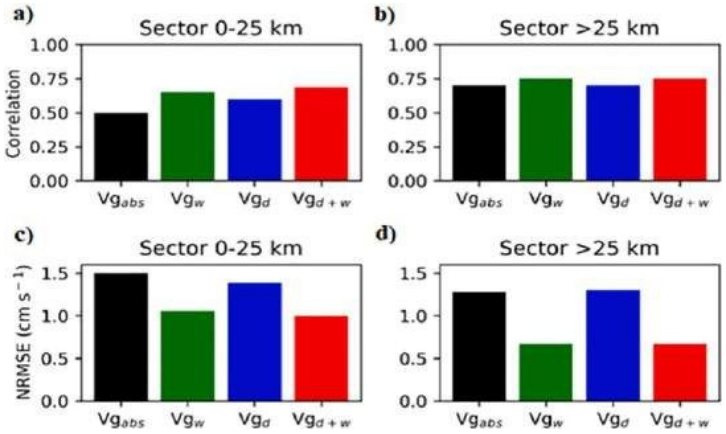

Figure 2.6. (a) Averaged correlation coefficient from the along-track comparison among Vg_{abs}, Vg_{w}, Vg_{d}, Vg_{d+w} from CS2 and surface zonal velocity from HFR for the 14 analysed tracks in the sector 3–25 km from the coastline; (b) Same as (a) for the offshore sector (>25 km from the coastline). (c) Same as (a) for the NRMSE; (d) Same as (b) for the NRMSE.

Figure 2.7 gives the along-track averaged values of HFRu, Vg_{abs}, Vg_{d}, Vg_{w}, Vg_{d+w} from the 14 analysed tracks depicted against the distance to the coastline (only the coastal sector is shown). The wind correction increased the altimeter-derived zonal velocity to the level observed in the radar close to the coast ([3–8] km). The effect of the bottom friction correction is clearly noticeable for distances closer than 5 km to the coast. The use of both corrections seems to underestimate Vg_{d+w} with respect to HFRu in the [9–25] km sector.

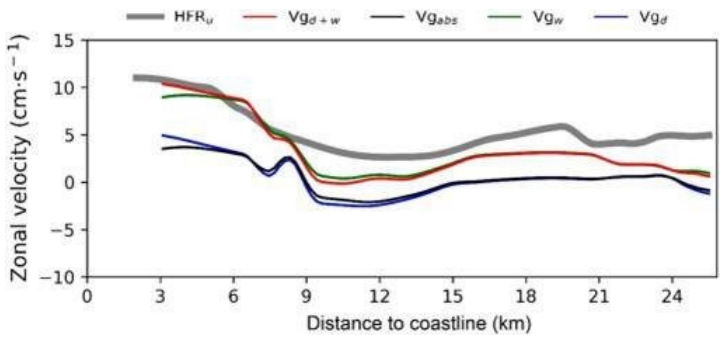

Figure 2.7. Along-track surface averaged velocities from Vg_{abs}, Vg_{w}, Vg_{d}, Vg_{d+w} and HFru.

Observability of fine-scale surface circulation

The surface circulation over the coastal area in the GoC is characterised by complex dynamics, regarding its spatio-temporal variability. The capability of CS2 measurements for detecting fine scale circulation variations over the study area is assessed in this section. Two examples are shown in which Vg_{d+w} and HFR measurements detect small variations in surface circulation related to the high variability of the coastal zone. Figure 2.8.a and Figure 2.8c show the total surface circulation in the GoC detected by the HFR and the 8-day SST. The along-track zonal CS2- Vg_{d+w} and HFRu current velocity are compared in Figure 2.8b

and 2.8d. The details of the CS2 tracks used are presented in Table 2-2. Figure 2.8a and b refer to CS2 track #1804 (06-May-2015). The surface circulation inferred from the HFR map is highly variable in the coastal area, while further south the circulation is mainly south-eastward. As depicted by SST data, a pool of warmer water close to the coastal area in the eastern sector of the GoC seems to exist, which could be generating an imbalance of the pressure gradient and, therefore, a possible west-bound current (Criado-Aldeanueva et al., 2006). Such a spatial variability is captured by the corrected altimetry data (Vg_{d+w}) in the same way as in HFR, but with a slight overestimation. Surface circulation from #2644 (09-Jul-2017) is presented in Figure 2.8c and d. An eastward current is observed along the whole transect from HFR, with decreasing velocities from coast to offshore. The same pattern is captured by the CS2 Vg_{d+w} measurements with a high level of agreement. This ocean surface variability could be related to a frontal structure generated by the vertical pumping of cold water (Barale et al., 2010) in the western sector of the area, as confirmed by the gradient in the water temperature close to the coast observed in the SST map.

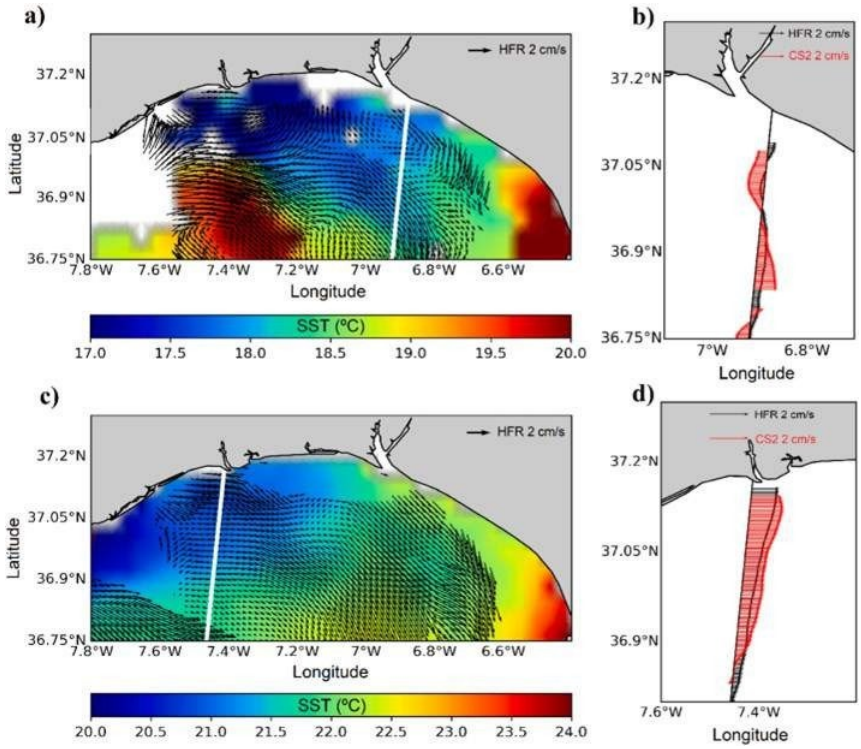

Figure 2.8. (a) Surface circulation observed from HFR overlaid with satellite SST for track #1804 (06-May-2015); (b) zonal surface circulation observed from CS2-Vg_{d+w} overlaid with zonal HFR surface velocity for track #1804; (c) same as (a) for track #2644 (09-Jul-2017); (d) same than (b) for track #2644.

2.5 Conclusions

This study assessed the performance of altimetry data from the CryoSat-2 SIRAL instrument in SAR-mode for estimating the surface circulation in coastal areas, along with the use of wind and bottom friction ageostrophic corrections to analyse the agreement with high-frequency radar measurements. In order to do this, we estimated cross-track surface velocities using along-track low-pass filtered Absolute Dynamic Topography measurements from 14 CS2 tracks over the area covered with valid HFR data in the GoC. The filtering strategy followed in this work is dependent on the HFR measurements for each track. This will be solved in future studies, in order to use HFR data only for validation purposes, avoiding their use in the processing of altimeter data to obtain along-track estimates of absolute dynamic topography. From the obtained results, the following conclusions are highlighted.

The absolute surface geostrophic velocity obtained from 20-Hz altimetry data (Vg_{abs}) agreed well ($r > 0.60$) with HFR data (HFRu) at along-track distances further than 25 km from land. In general, the geostrophic assumption needs to be considered with care in the GoC for distances between 3 and 25 km to the coast, since it is not realistic at these depths. The use of the wind ageostrophic component (Vg_w) improved the agreement in most of the tracks, despite the variability of the wind field along the time period analysed. Overall, we observed a reduction in NRMSE of ca. 35% once the wind correction was used in the estimates of the zonal velocity. The bottom friction ageostrophic component (Vg_d) just slightly improved the comparison (mainly for RMSE/NRMSE) in most of the tracks since the applied correction

is inherently a linear simplification. The use of both corrections (Vg_{d+w}) gave the best results in terms of r, RMSE, and NRMSE. This improvement was more significant in the 3–25 km sector. We concluded that ageostrophy plays a key role in the coastal fringe of the GoC (3–25 km). This study is a first attempt to consider the effect of the bottom friction on satellite altimetry data. Further studies are needed in order to obtain a better characterisation of the wind effect. A proper characterisation of ageostrophy could be of great benefit for the future of coastal altimetry and the understanding of the near-shore ocean dynamics, especially in coastal areas not covered by HFRs.

The qualitative comparison of the wind and bottom friction corrected altimetry surface measurements (Vg_{d+w}) with the HFR velocities along with SST data, exhibits the high potential of altimetry measurements for the study of dynamics and patterns of coastal areas. Surface velocities derived from CS2 detected surface structures and high- variability surface dynamics, with rapid changes in the current direction even for low velocities.

Satellite altimetry derived surface current velocities gave accurate measurements in coastal areas when the ageostrophic signals were corrected. Differences could be due to unsolved ageostrophic local factors which may also affect surface circulation such as the along-shore pressure variations, since our proposed ageostrophic corrections are just intended to address common issues for all coastal areas, which are the wind and bottom friction effect. The knowledge of ageostrophic and local processes in coastal areas is necessary for a better exploitation of altimetry data in coastal areas since they are highly tied to local metocean agents and their effects are not entirely understood. Our validation method has shown that the synergy between altimetry and HFR helped to unravel the effects of ageostrophic processes in coastal areas. This will help the validation of present (CryoSat-2, Sentinel-3A/B) and future (Jason-CS/Sentinel-6A/B and SWOT) missions. Thanks to this, it will be possible to: (i) make use of the whole dataset of satellite altimetry data since 1993 in order to obtain estimates of current velocities back in time when no HFR data were available in

our (and other) regions of the coastal zones around the world; and (ii) to extend this methodology to other areas where HFR are hardly available (e.g. Africa or South America) or countries which cannot cover all coastlines (e.g. Australia). Furthermore, the good agreement suggests that HFR systems may be a solid tool for the validation of altimetry derived surface currents in coastal areas. The methodology presented here will serve as a proof of concept for the validation of 2-D interferometric SAR altimeter missions (e.g. SWOT).

2.6 Connecting Text

This chapter shed light on the valuable insights that satellite altimetry, particularly utilizing data from the CryoSat-2 SIRAL instrument in SAR-mode, can offer in understanding the complex surface circulation of coastal areas such as the Gulf of Cadiz. The findings emphasized the significance of considering ageostrophic corrections, specifically wind and bottom friction, for accurate estimation of surface geostrophic velocity. Notably, the incorporation of both wind and bottom friction ageostrophic corrections demonstrated the most favorable results when using satellite altimetry data, especially in the 3–25 km coastal fringe sector.

One of the obvious questions that arises from the conclusions is: how can we address the ageostrophic components to fully characterize coastal circulation based on satellite altimetry data? This chapter stated the necessity of understanding the local variability of key agents controlling the ageostrophic circulation, mainly driven by the wind, without relying on just in-situ measurements, which are scarce in many coastal areas. In the following chapter, the capabilities of satellite altimetry, extending its utility beyond surface circulation to atmospheric variables like wind speed are assessed. In particular, it focuses on the spatial assessment of wind speed over the Gulf of Cadiz, comparing altimetry-derived wind speed with WRF model outputs under different wind synoptic conditions, emphasizing the potential of altimetry in assessing high-resolution numerical weather prediction models in complex areas, which provides valuable information for the understanding of ageostrophic circulation.

Chapter 3

The Use of Sentinel-3 Altimetry Data to Assess Wind Speed from the Weather Research and Forecasting (WRF) Model: Application over the Gulf of Cadiz

This work presents the quality performance and the capabilities of altimetry derived wind speed (WS) retrievals from the altimeters on-board Copernicus satellites Sentinel-3A/B (S3A/B) for the spatial assessment of WS outputs from the Weather Research and Forecasting (WRF) model over the complex area of the Gulf of Cadiz (GoC), Spain. In order to assess the applicability of the altimetry data for this purpose, comparisons between three different WS data sources over the area were evaluated: in-situ measurements, S3A/B 20 Hz altimetry data and WRF model outputs. Sen-tinel-3A/B WS data were compared against two different moored buoys to guarantee the quality of the data over the GoC, resulting in satisfying scores (Average results: RMSE = 1.21 m/s, r = 0.93 for S3A and RMSE = 1.36 m/s, r = 0.89 for S3B). Second, the WRF model was validated with in-situ data from 4 different stations to ensure the correct performance over the area. Finally, the spatial variability of the WS derived from the WRF model was compared with the along-track altimetry-derived WS. The analysis was carried out under different wind synoptic conditions. Qualitative and quantitative results (average RMSE < 1.0 m/s) showed agreement between

both data sets under low/high wind regimes, proving that the spatial coverage of satellite altimetry enables the spatial assessment of high-resolution numerical weather prediction models in complex water-covered zones.

Mulero-Martinez, R., Román-Cascón, C., Mañanes, R., Izquierdo, A., Bruno, M., & Gómez-Enri, J. (2022). **The Use of Sentinel-3 Altimetry Data to Assess Wind Speed from the Weather Research and Forecasting (WRF) Model: Application over the Gulf of Cadiz.** Remote Sensing 2022, Vol. 14, Page 4036, 14(16), 4036. https://doi.org/10.3390/RS14164036.

3.1 Introduction

Sea surface wind (SSW) plays an essential role in driving surface ocean currents, since it modulates the amount of energy available for the generation of ageostrophic Ekman currents (Kelly et al., 1999). Wind speed influences ocean surface circulation as well as climate variability, which is why surface wind speed and direction are included as Essential Climate Variables (ECV) in the Global Climate Observing System inventory (GCOS, 2016). Close to coastal areas, due to the occurrence of atmospheric thermal gradients, along with the existence of orographic constraints (Cerralbo et al., 2015), SSW is highly variable in the spatio-temporal domain. Accurate SSW maps are crucial in coastal areas for better monitoring and prediction of wind-related hazards such as storm surges or floodings (Lu et al., 2018). Moreover, SSW plays a key role in the estimation of realistic total ocean surface currents from altimetry, especially in coastal areas (Bôas et al., 2019; Mulero-Martínez et al., 2021a). The effect of the SSW on sea surface dynamics has been the focus of coastal altimetry and oceanography research in recent years. Significant progress has been made with products such as GlobCurrent (Rio et al., 2014) and the Near-Real-Time Version of the Cross-Calibrated Multiplatform (CCMP) Ocean Surface Wind Velocity Data Set (Mears et al., 2019). However, the spatial resolution of SSW products is still linked to scatterometer measurements, which generally contain a 25-50 km wide blind zone along the coast (Astudillo et al., 2017), except for specific products such as ASCAT 6.25-km, with a true spatial resolution of about 17 km. This is essential for studying dynamical mesoscale features, although they still present a significant coastal gap (Vogelzang et al., 2017), which limits the characterisation of mesoscale and fine scale circulation near the coast. The lack of information in the coastal fringe is also transferred to global atmospheric analysis and reanalysis products, which combine numerical weather prediction (NWP) with scatterometers and in-situ measurements, restricting the achievement of a realistic assessment of local conditions in coastal areas (Carvalho et al., 2017). In this context, WS

retrievals from synthetic aperture radar (SAR) imagery and altimeter-based techniques derived by the measurement of the backscattering coefficient (σ0) of the sea surface are of great value since they can provide high-resolution data near the coast.

Wind speed altimetry products provide WS at 10 m over the ocean surface (U10) (Abdalla, 2012), derived at along-track posting rates ranging from 1 Hz to 80 Hz (7 km / 85 m between consecutive measurements, respectively). Wind speed from altimetry is empirically estimated from the radar power returned from the sea surface. The returned power waveforms are affected by the sea surface roughness in the footprint area, which might be dominated by the wind-induced capillary waves. As wind increases, the sea surface roughness also increases and the backscattering coefficient (σ0) of the sea surface decreases, as measured by the altimeter (Witter and Chelton, 1991). Altimeter measurements of σ0 are therefore inversely related to sea surface WS. (Yang et al., 2020) proved consistency in the accuracy of WS data derived from Sentinel-3A/B (S3A/B) altimeters when validated against data from more than 80 moored buoys at different locations, with root mean square errors (RMSE) of 1.19 m/s and 1.13 m/s for S3A (from 1 March 2016 to 31 October 2019) and S3B (from 10 November 2018 to 31 October 2019), respectively. Wind speed data from Sentinel-3 mission are routinely evaluated by the Sentinel-3 Mission Performance Centre (S3MPC) tasked by the European Space Agency (ESA) to monitor and guarantee the provision of high-quality data to the users (Quartly et al., 2020). As officially reported in the S3 Wind and Waves Cyclic Performance Report (Abdalla, 2021) for the period from December 2020 to January 2021, the standard deviation of the difference (a proxy to the random error) is around 1.70 m/s and 1.80 m/s for S3A and S3B, when compared to in-situ (mainly buoys) measurements, using a maximum acceptable collocation distance and time interval between the collocated altimeter and buoy observation of 200 km and 2 hours, respectively.

Numerical weather prediction models such as the Weather Research and Forecasting (WRF) model (Powers et al., 2017; Skamarock et al., 2019), set with appropriate parametrizations, can provide wind speed data with high spatial and temporal resolution for any terrestrial, coastal, or open ocean area of the globe. WRF is a mesoscale numerical weather prediction system designed for both atmospheric research and operational forecasting applications (Powers et al., 2017). Commonly, NWP models such as WRF are calibrated/validated using in-situ observations from meteorological stations and buoys; however, due to spatial scarcity of these sources, the uncertainty in the WS of the coastal band persists (Astudillo et al., 2017). Therefore, there is a need for high-resolution measurements of the SSW over coastal areas for assessing NWP models, not only to enhance our knowledge in the mesoscale atmospheric circulation in these areas but also for a realistic characterisation of the surface current variability linked to it.

Although WS derived from altimetry is used for assimilation into forecasting models (Bhowmick et al., 2015), to our knowledge it is not yet used for spatial evaluation of NWP models in coastal areas, where scatterometer data are not available. Satellite altimeter WS measurements can be used to calibrate and validate wind models at any coastal area covered by the orbital configuration of the satellite, enabling the fine-tuning of NWP models over the complex land-sea transition zones.

The main objective of this study is to analyse the capability of S3A/B altimeters U10 retrievals to perform extensive spatial assessment of U10 from the WRF model over complex areas such as the Gulf of Cadiz (Figure 3.1), focusing on the possibilities of data comparison in the coastal area (up to 5 km from land due to altimeter limitations). Both datasets are also assessed through comparisons with moored buoy and weather station data. In addition, fine scale spatial variability of the wind at different dominant regimes in the study area is analysed using the outputs of the WRF model and the Sentinel-3 mission.

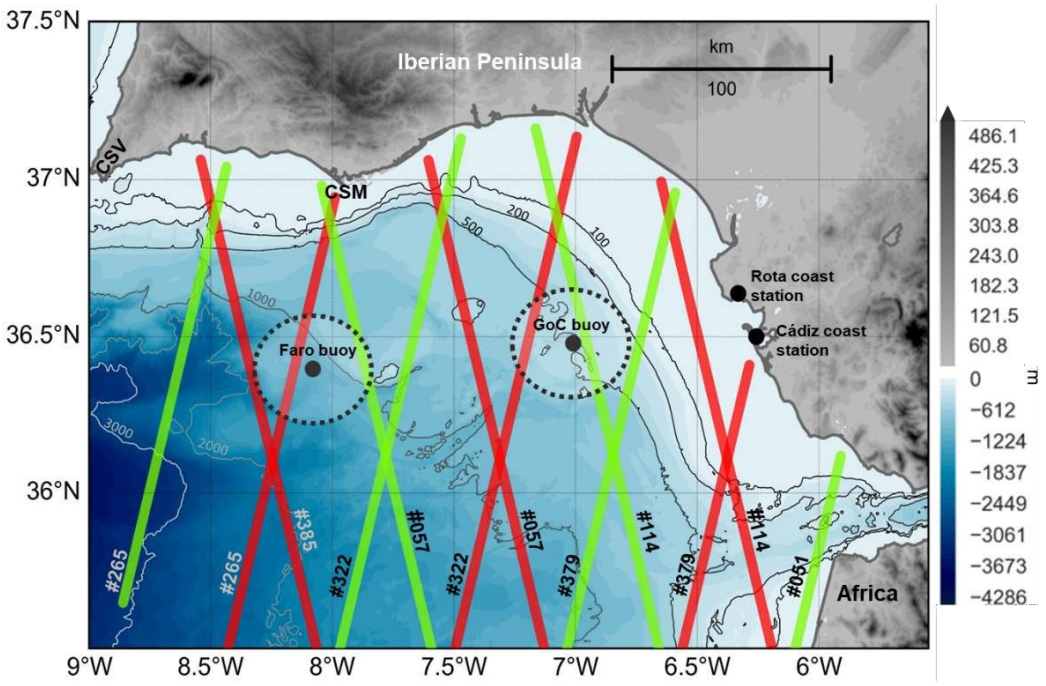

Figure 3.1. Study area (Gulf of Cadiz, southwestern coast of the Iberian Peninsula) along with the spatial distribution of the data sources used in this work and some geographical features: S3A tracks (red line), S3B tracks (green line), location of the moored (GoC buoy and Faro buoy) along with the 25 km radius area used to select S3A/B data for its validation (dotted contoured area), location of the land-based meteorological stations from the Spanish Meteorological Office (Cadiz coast station and Rota coast station), Cape Santa Maria (CSM), Cape San Vicente (CSV).

3.2 Materials and Methods

Study area

The study area extends from Cape San Vicente (CSV) to the entrance of the Strait of Gibraltar (SG) (Figure1), covering the Gulf of Cadiz (GoC), southern Spain. This area is characterised by abrupt changes in the orientation of the coastline, very complex coastal topography and links between two basins with different characteristics. Such features favour the existence of a heterogeneous wind field, with topography-induced atmospheric flows (Carvalho et al., 2014) that strongly control the zonal sea surface circulation (Mulero-

Martínez et al., 2021) and therefore, modulate variables of interest such as sea surface temperature (SST) and chlorophyll concentration (Navarro et al., 2013). Such sea surface circulation over the continental shelf alternates westward/eastward modes, the former characterised by a coastal countercurrent and the latter for inducing cold water upwellings along the coast (Garel et al., 2016; Mulero-Martínez et al., 2021). Moreover, due to differences in the surface temperatures of the land and the sea, the coastal area of the GoC, is characterised by a land-sea breeze circulation, which is generally perpendicular to the coastline and can be extended up to 200 km inland (Hernández-Ceballos et al., 2013). Apart from the local geographic characteristics, the wind field in the area is also controlled by the large scale. Different studies have demonstrated that the North Atlantic Oscillation (NAO) is significantly related with the wind field in the area through the modulation of the Azores anticyclone (Folkard et al., 1997; Hidalgo and Gallego, 2019). The zonal component of the SSW is the most important meteorological agent affecting the ocean circulation in the area. Its variability is directly related with the sea surface circulation over the GoC (Mulero-Martínez et al., 2021), but also with the across shore sea level variability of the strait, contributing to the modulation of the water exchange through it, as observed from modelling studies (Brandt et al., 2004), in-situ (Ross et al., 2000) and altimeter data (Gómez-Enri et al., 2019).

Altimetry data

The along-track WS data from altimetry are retrieved from the retracking of the altimeter waveforms. The satellites have a repeat cycle of 27 days. The radar instrument SRAL (Synthetic Aperture Radar Altimeter) has two measurement modes: Low Resolution (LRM) and SAR, the latter being the high-resolution along-track mode commonly used over the global ocean. Furthermore, the S3A/B SRAL generates level-2 data at 1 Hz and 20 Hz of the Ku and C bands (for more details see Sentinel-3 Altimetry Document Library at https://sentinel.esa.int/web/sentinel). The S3A/B level 2 data used were provided by the ESA Earth Console Parallel Processing Service (P-PRO) SAR versatile altimetric toolkit for

ocean research and exploitation (SARvatore) service (https://ui-ppro.earthconsole.eu/), applying the pre-defined processing set-up for coastal zones. The SAMOSA++ (SAR Altimetry MOde Studies and Applications) model (Dinardo et al., 2020) is used in the retracking process and the final product is posted at 20 Hz, which results in ~330 m along-track spatial resolution measurements. Along-track WS data come from 12 S3A/B tracks over the GoC, detailed in Table 3-2. For the validation of the altimetry WS data with in-situ measurements from the GoC buoy, only S3A/B data in a radius of 25 km around the position of the buoy have been used, so the altimetry data can be considered co-located with the in-situ data (Yang et al., 2020). Only data from relative orbits #265, #322, #385 from S3A and #057, #114 from S3B satisfy the 25 km radius criteria (see Figure 3.1). Raw 20-Hz along-track WS data were edited eliminating the first 5 km of data closer to the coast, since demonstrated by (Aldarias et al., 2020), S3-SRAL altimeters start to give accurate data 5 km from the coast, due to coastal and land reflections which might contaminate the radar waveforms, making the retrieval of estimates of the derived geophysical parameters less accurate (Gómez-Enri et al., 2018). Furthermore, the methods presented in (Bouffard et al., 2010) were applied, in order to remove outliers and filter out noise signals. The aforementioned editing methodology consists of removing values larger than three times the standard deviation and replacing them with linearly interpolated values; this processing was applied in a 10-times loop (Bouffard et al., 2010; Meloni et al., 2019).

In-situ data

The in-situ coastal wind data were extracted from four sources; (i) hourly time series of 10-m height WS and direction (WD), recorded by the weather station deployed by the Spanish Meteorology Agency (AEMET) in the city of Cadiz, (Cadiz coast station, Figure 3.1). (ii) same as (i) but located in Rota, (Rota coast station, Figure 3.1); (iii) in-situ offshore wind data collected by two moored multi-instrument buoys. These buoys (GoC buoy and Faro buoy, Figure 3.1) provide hourly time series of 3-m height WS and WD and are operated and

maintained by the Spanish Port Authorities and the Hydrographic Institute of Portugal, respectively. The hourly data, distributed for public use, are built from averaging 10 minutes of raw data each hour. It worth noting that these averages, related to spatially smoother wind fields (removing, for instance, small scale variability due to eddies), should match better with the S3A/B data which are averaged over the track segment inside the circular area with radius of 25 km. Considering that the buoy registers wind parameters at 3-m over the surface, it is necessary to extrapolate the buoy data to 10-m height wind speed, so it can be compared with altimetry derived WS data. For this purpose, the typically accepted logarithmic wind profile method (Carvalho et al., 2012; Paulson, 1970; Powell et al., 2003) was applied to extrapolate the measured winds by the buoy from 3 to 10 m over the sea surface (Carvalho et al., 2017). Although there are several methods and variations used for this purpose, e.g. stress equivalent winds (De Kloe et al., 2017) that considers the air mass density and stability. For practical reasons here we used the logarithmic wind profile method, which is suitable for our aim, requiring only WS and WD measurements and proven to be consistent over the first 30 m of sea surface (Emeis and Turk, 2007; Peña et al., 2008).

Weather Research and Forecasting model data

Model data were obtained using the mesoscale, non-hydrostatic WRF model version 4.2 (Skamarock et al., 2019). The model was used to produce dynamically downscaled hourly 10 m WS and WD over the complete study area during 2020, with a temporal resolution of 1 h and 3 km grid (d02). The d02 domain was one-way nested within a parent domain of 9 km grid (d01), as depicted in Figure 3.2, in order to allow communication from the parent (lower resolution) to the child domain (higher resolution), but not vice versa.

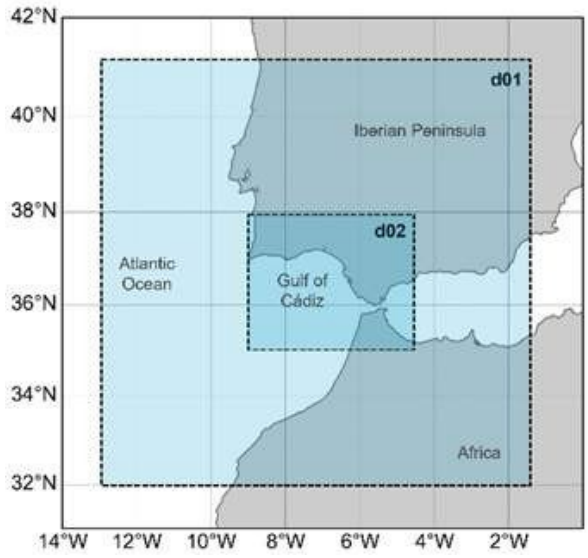

Figure 3.2. WRF model domains d01 (9 km grid) and d02 (3 km grid).

The initial and boundary conditions were supplied by the NCEP/NCAR operational Global Forecast System (GFS) with 0.25˚ of spatial resolution and 6 h of temporal sampling (National Centers for Environmental Prediction/National Weather Service/NOAA/US Department of Commerce, 2015). Boundary conditions are applied to the parent domain (d01). The dynamical set-up of the simulation was based on the optimized design presented by (Arasa et al., 2016) after having performed 4150 daily simulations over southern Spain (Table 3-1). Unlike previous studies in the area (Arasa et al., 2016; Carvalho et al., 2012; Salvação & Guedes Soares, 2018), which consider constant sea surface temperature (SST), in our study the SST was updated every 6 hours. Although the overall impact is expected to be small, it is a more realistic approach and might have an impact under specific conditions or in specific areas (Li et al., 2021).

Table 3-1. Configuration options selected for the WRF simulations.

Scheme or parameterization	Selected option
Initialization	NCEP/NARC GFS 0.25º
Microphysics	SBU-Lin
Longwave radiaion	RRTMG
Shortwave radiation	Dudhia
Cumulus	Kain-Fritsch
Surface layer	MM5 similarity
Planetary boundary layer	YSU
Vertical levels number	36
Diffusion 6th order option	Knievel
Damping	Rayleigh
Topography model	GTOPO30
Land uses	GLC
Nudging	Grid nudging (d01) / Observational nudging (d02) Sea surface temperature Updated every 6 h

Assessment of altimeter and model data

Prior to the comparisons, the WRF wind data were linearly interpolated to the position of in-situ instruments as well as to the S3A/B along-track measurement positions. Several statistical parameters were used to compare the wind speed and direction from altimeter and model, according to previous studies (Arasa et al., 2016; Carvalho et al., 2012; Marta-Almeida et al., 2016). Root mean square error (RMSE) (3.1), normalised root mean square error (NRMSE) (3.2), bias (3.3) and Pearson's correlation coefficient (r) (3.4) were used to evaluate wind speed, while bias and standard deviation error (STDE) (3.5) were applied to the wind direction comparisons results.

$$RMSE = \sqrt{\frac{\sum_{i=1}^{n} (P_i - O_i)^2}{n}} \quad (3.1)$$

$$NRMSE = \frac{RMSE}{max_i O - min_i O} \quad (3.2)$$

$$Bias = \frac{\sum_{i=1}^{n} (P_i - O_i)}{n} \quad (3.3)$$

$$r = \frac{\sum_{i=1}^{n} (O_i - \bar{O})(P_i - \bar{P})}{\left[\sum_{i=1}^{n} (O_i - \bar{O}) \sum_{i=1}^{n} (P_i - \bar{P})^2\right]^{1/2}} \quad (3.4)$$

$$STDE = [(RMSE^2 - bias^2)]^{\frac{1}{2}} \quad (3.5)$$

where P represents the co-located WS or WD from the data source that is being evaluated (model: WS, WD and altimetry: WS); O denotes the co-located WS or WD from the reference data source (in-situ stations). Note that WD is an angular variable, therefore, to avoid errors related to 0º and 360º overlapping, WD bias and WD STDE have been calculated for a new circular variable (d) (6), bounded between [-180,180], obtained from the observed (O) and predicted (P) wind directions as follows:

$$d_i = \begin{cases} d_i^p - d_i^o & if \ |d_i^p - d_i^o| < 180 \\ d_i^p - d_i^o - 360 & if \ d_i^p - d_i^o > 180 \\ d_i^p - d_i^o + 360 & if \ d_i^p - d_i^o < -180 \end{cases} \quad (3.6)$$

Table 3-2. Sentinel-3 A/B data availability (number of cycles, relative orbits and orientation) for the different comparisons among the datasets (the orientation of the different tracks is presented as ascending (A) or descending (D)).

Sentinel 3A				Sentinel 3B			
Relative orbit	Nº cycles S3A vs WRF	Nº cycles S3A vs buoy	Orientation	Relative orbit	Nº cycles S3B vs WRF	Nº cycles S3B vs buoy	Orientation
#057	13	-	A	#051	14	-	D
#114	13	-	A	#057	14	26	A
#265	14	33	D	#114	14	29	A
#322	14	53	D	#265	13	-	D
#379	14	-	D	#322	13	-	D
#385	14	34	A	#379	13	-	D
Analysed period	From Jan-2020 to Dec-2020	From Jan-2017 to Dec-2020			From Jan-2020 to Dec-2020	From Nov-2018 to Dec-2020	

3.3 Results and Discussion

Preliminary validation of the data sources

Altimetry wind speed validation using in-situ data

All available WS data derived from altimetry, and corresponding to relative orbits #265, #322 and #385 from S3A, and #057, #114 from S3B that matched the 25 km radius criteria, from January 6, 2017, to December 31, 2020, were compared against the moored GoC buoy and the Faro buoy, using some of the statistical parameters presented in previous sections, to ensure the correct performance of the altimetry sensors over the area of interest. The results from the comparison are shown in Figure 3.3. The scatterplots present the GoC buoy (Figure 3.3a) and Faro buoy (Figure 3.3b) WS measurements against the average of all the S3A and S3B measurements within the 25-km radius around the buoys; the corresponding standard deviation threshold of each track segment is also shown. Due to the different starting points of S3A (since 2016) and S3B (since 2018), the number of available data for the latter is lower than that of S3A.

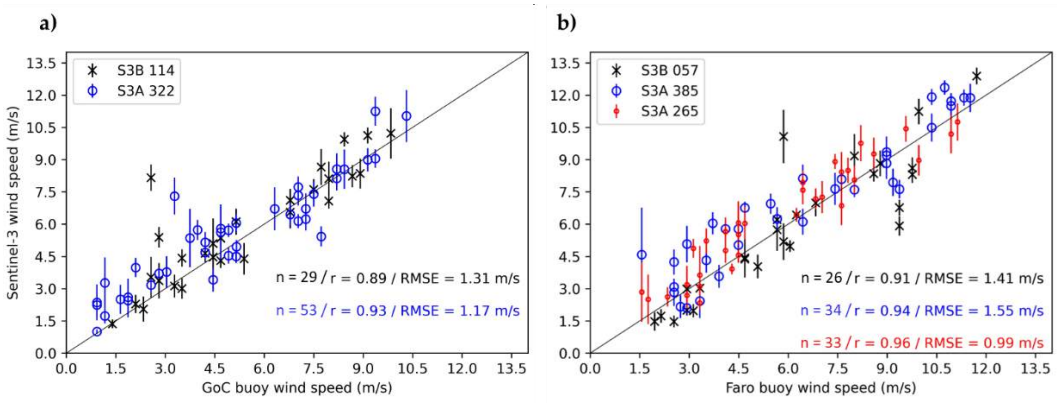

Figure 3.3. Scatterplot of the WS comparison among S3A (a)/S3B (b) and in-situ measurements from the GoC buoy. Vertical lines represent the standard deviation for each point based on the Sentinel-3 data inside the 25 km radius area (see Figure 3.1).

These results are in line with the reported accuracy in the S3 Wind and Waves Cyclic Performance Report for the period from December 2020 to January 2021 (Abdalla, 2021). They are also in agreement with those reported by (Yang et al., 2020), who compared WS from S3A/B with more than 80 moored buoys. There is a strong linear relationship between the altimeters and the GoC buoy dataset according to the average r coefficients (0.94 for S3A; 0.90 for S3B, 99% of Confidence Level). As it was expected, the best results correspond with the relative orbits closer to the location of the buoys, S3A #265.

The differences observed between the two data sources might be related with the representativeness of the spatio-temporal domains. Firstly, in the spatial domain, the in-situ data represent a local estimate and therefore include the wind variability over all scales (Stoffelen, 1998). However, the radar altimeter considers the entire footprint (Passaro et al., 2014). Secondly, the time difference between the satellite pass over the buoy and the operating period of the in-situ instrument. This difference has been calculated to be 30 minutes maximum. This temporal difference could also explain the presence of outliers since unlike the in-situ data, the altimeter WS is estimated from instantaneous measurements of the sea surface state. An example is the outlier observed in the S3B #114 vs. GoC buoy scatterplot (Figure 3.3a), which affects the statistical scores and could compromise the comparisons. This mismatch represents a S3B WS value of 8.00 m/s against an in-situ measurement of 2.50 m/s, approximately, and corresponds to 21:00 UTC in-situ data and 21:26 UTC altimetry data of 25-Nov-2020. As depicted in Figure 3.4e, where hourly WS from the GoC buoy for that day is presented, WS was highly variable during the entire day, especially between 14:00 UTC and 23:00 UTC, with WS ranging from 2.00 m/s to 11.50 m/s. Sentinel-3B passed over the GoC buoy position at 21:26 UTC and detected high variability in the spatial domain as shown in Figure 3.4a. The radargram of the power waveforms for S3B relative orbit #144 in the vicinity of the buoy is shown in Figure 4c, together with the along-track WS (Figure 3.4a) and the along-track backscattering coefficient

(σ0) (Figure 3.4b). Note that only the power from gates 320 to 365 are shown in the radargram; moreover, since the product used to generate this radargram has not yet been corrected by the retracking process, a leading edge deviation over latitude 36.30ºN is observed. Regarding the power represented in the radargram (Figure 3.4c), a fall is clearly observed in the segment between latitudes 35.80ºN and 36.25ºN. The strong decrease in power affects the retracking of the waveforms and, therefore, the retrieval of the geophysical parameters, as shown in (Aldarias et al., 2020). The retracking of these waveforms results in a strong decrease of the retrieved σ0 and therefore, a rise in the derived along-track WS. This may be related with the existence of a strong and sporadic wind gust, which would agree with the high spatio-temporal variability observed during the day by the in-situ sensor. Wind gusts can exceed 20 m/s over the area (Adame et al., 2018), also dramatically increasing the roughness of the sea surface. If the satellite crosses the area affected by the wind gust, a decrease in the returning signal received by the altimeter should be observed. However, this cannot be confirmed by the buoy data due to its sampling time (measurement recorded 26 minutes before the satellite pass).

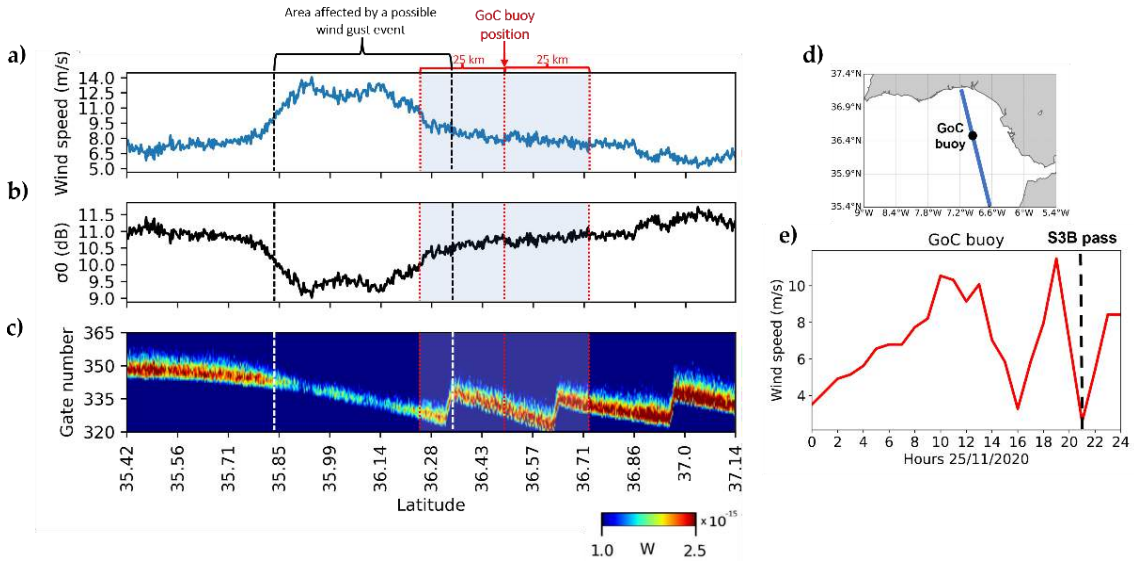

Figure 3.4. Along-track WS (a), σ0 parameter (b) and radargram of the waveforms (c) from the S3B relative orbit #144 (25-Nov-2020 at 21:26 UTC). Red dashed lines indicate the GoC buoy position and 25 km radius area; black dashed lines indicate the area

affected by a possible wind gust. (d) Satellite track (blue line) and GoC buoy position (black dot). (e) Hourly WS from the GoC buoy for the 25-Nov-2020.

WRF model wind velocity validation against in-situ data

In this section, hourly WS and WD data for 2020 obtained from the WRF model simulations are compared to in-situ data from the Cadiz and Rota coast meteorological stations and the GoC and Faro buoys, to ensure that the model performance over the study area is adequate. The wind rose diagrams representing the WD and WD data used to estimate the statistical parameters represented in Table 3-3, are shown in Figure 3.5, where it can be observed the predominant zonal component of the wind over the area. The four figures depict the high variability of the wind over the study area. The resulting scores, shown in Table 3-3, demonstrated the overall good performance of the dynamical set-up applied to the model, which are in line with similar studies (Arasa et al., 2016; Carvalho et al., 2012) usually performed only for open ocean comparisons. However, the model overestimates/underestimates the WS at the Faro and GoC buoy and Rota coast station/Cadiz coast station positions, respectively, as indicated for the bias scores in Table 3-3. Although there are differences among WS RMSE from the three stations, once the parameter is normalized (NRMSE) using the range of variation of the WS, these differences are reduced. The best results are obtained for the Faro buoy site, which is the farthest location from the coast.

Table 3-3. Statistical scores from the comparison among in-situ data from the different stations and buoys against simulations from the WRF model.

	Wind speed				Wind direction	
In-situ station	**Bias (m/s)**	**RMSE (m/s)**	**NRMSE (m/s)**	**r**	**Bias (º)**	**STDE (º)**
GoC buoy	0.74	1.93	0.12	0.80	6.74	47.10
Cádiz coast station	-0.13	1.74	0.12	0.74	5.78	54.49
Rota coast station	0.44	1.65	0.16	0.74	8.35	48.68
Faro buoy	0.33	1.59	0.10	0.85	5.54	33.84

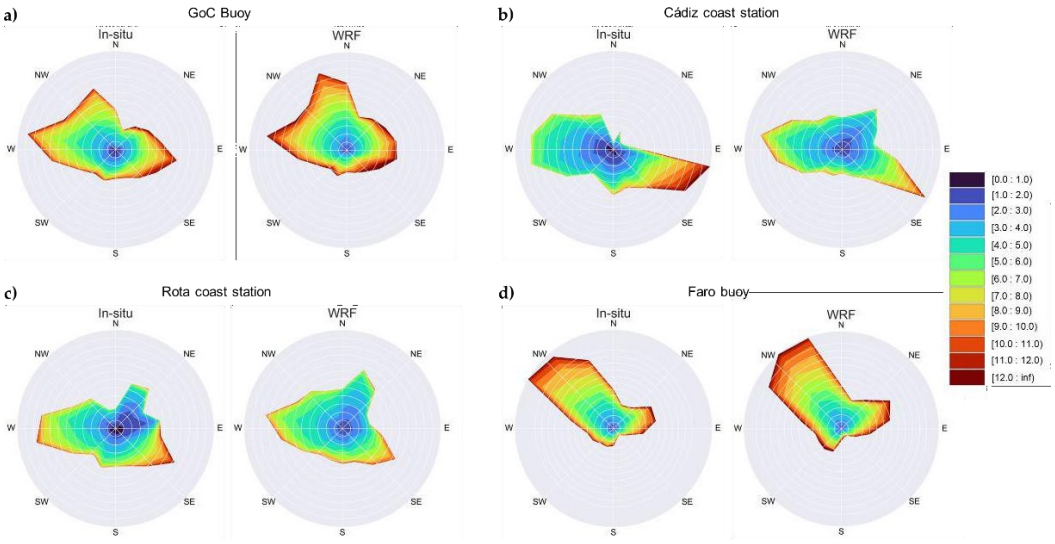

Figure 3.5. Wind rose diagrams (m/s) calculated at (a) GoC buoy, (b) Cadiz coast station, (c) Rota coast station and (d) Faro buoy, over the period January 2020 to December 2020 from both in-situ measurements and WRF simulations.

WRF model spatial assessment using altimetry data

In this section, the innovative use of altimetry WS for the spatial evaluation of WS from the WRF model over the study area is carried out through quantitative comparisons using WS retrievals from S3A and S3B altimeters. Special focus is on the coastal fringe, where other sensors such as the scatterometters cannot provide useful data for validating the model. The statistical results from the evaluation of WS data from the WRF model simulations with WS from the S3A/B tracks over the study area are presented here. In order to assess the accuracy of the WRF WS spatial variability, model outputs were linearly interpolated over the positions of the satellite track measurements for 2020. As depicted in Figure 3.6a and Figure 3.6b, the averaged WS spatial variability obtained from both altimetry (Figure 3.6a) and the WRF model (Figure 3.6b) matches for almost the whole study area. This agreement between the WRF model and the S3A/B WS data for the set of tracks used, is confirmed by the r Pearson's values, which are mostly over 0.80, being the average correlation value for all the tracks 0.85 (Confidence Level: 99%, Figure 3.6c). The RMSE (Figure 3.6d) is small for all

tracks, frequently below 1.0 m/s (Average RMSE: 0.65 m/s). Lower correlations and larger RMSEs are generally found near the coastal fringe. In the sector [5-20 km] from land the averages of the statistical parameters are r = 0.79 and RMSE 0.88 m/s, which is also evident in the WS average maps, since altimetry WS is slightly lower over the coastal area than the WS from WRF. Considering that the altimetry data over the 5 km closest to land were removed, the decrease in the statistical scores from the comparison adjacent to the coast is not due to the land contamination of the altimetry signal, but rather to the WRF simulations. The model WS overestimation in coastal areas is an issue previously described by (Ngan et al., 2013) and is most likely caused by the high spatial variability of the wind field over these areas due to the thermal atmospheric gradients (Cerralbo et al., 2015), which may not be properly reproduced by the WRF model at fine scales. Such misrepresentation could be related to the lack of information and crude representation of the land surface, that can considerably affect the simulation of the fluxes that will drive the associated boundary-layer processes (Román-Cascón et al., 2021). Although satellite tracks do not cover the entire WRF domain area, the results prove that using along-track WS from altimetry enables the estimation of the correlation coefficient and RMSE spatial maps for the area, which facilitate the assessment of the WRF model performance over the study area. Moreover, the presence of altimetry data up to 5 km from land, allows the detection of weaknesses in the model performance over the complex land-sea transition fringe.

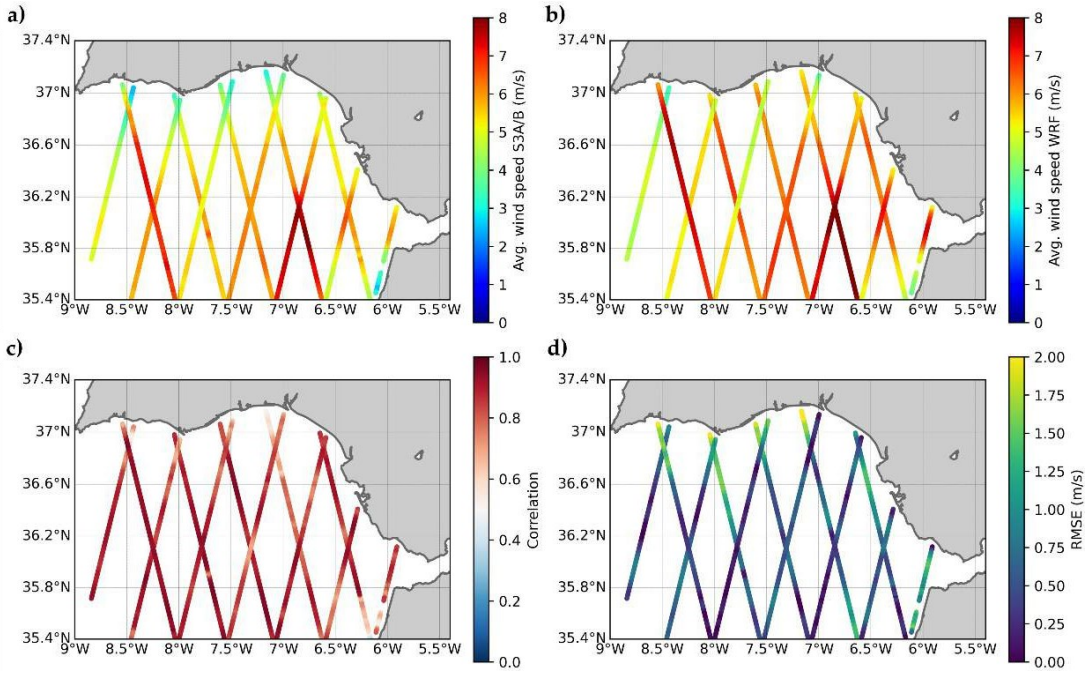

Figure 3.6. Average WS from S3A/B (a) and WRF (b); spatial distribution of the r Pearson's parameter (c) and RMSE (d) from the comparison among WS data from the WRF model and S3A/B tracks over the study area.

Observability of spatial variability

The wind field over the GoC is characterised by its high spatial variability and high-intensity events. In this section, a qualitative comparison of the spatial variability of the WS reproduced by the WRF model with the S3A/B data is presented to investigate the capabilities of using altimetry data for assessing the WRF model under complex conditions. For this purpose, WS from three S3A/B tracks under different atmospheric situations are compared with the wind field obtained from the corresponding WRF model simulations. The comparisons are shown in Figure 3.7. Figure 3.7a depicts the simulated wind field on 31-Dec-2020 at 11:00 UTC. The satellite crossed the area at 10:35 UTC. A weak northerly wind dominated over the whole GoC. The along-track spatial variability observed from the altimeter measurements agrees with the outputs of the WRF model, especially for the northernmost part of the track, stating the good performance of the WRF model even at the positions closer to the coast.

During the satellite pass on 25-Jun-2020 at 21:32 UTC the wind field reproduced by the model at 22:00 UTC (Figure 3.7b) over the GoC can be divided into two sectors: the westernmost area is dominated by mid intensity northwesterlies, while in the sector to the east, the wind is weaker and from west. Furthermore, as also shown by the along-track S3A WS, the intensity increases further from the coast from 6 to 10-12 m/s. Such spatial variability of the WS is well represented by both data sets; however, close to the coast the differences among the altimeter derived WS and the WRF model output increase. Such disagreement may be caused by two factors as previously mentioned in previous sections: The time difference between the satellite pass and the model simulation; and the precision of the WRF model at fine scales close to the complex land-sea boundary. Such discrepancies in the WRF model can be detected thanks to the presence of altimetry data in the coastal fringe.

Finally, Figure 3.7c shows an example of dominant easterlies over the GoC, as simulated by the WRF for the 21-Feb-2020 at 11:00 UTC. S3B crossed the area at 10:37 UTC. WRF output displays a heterogeneous wind field over the area, with a remarkable easterly jet coming from the Strait of Gibraltar and a generalised decrease towards the northern coast. This spatial pattern is also present in the along-track WS estimated by S3B (Figure 3.7b). However, over 36.8º latitude, a slight underestimation from the WRF model is observed, which coincides with the area covered by the Guadalquivir River mouth, an area characterised by high contrasts and variability.

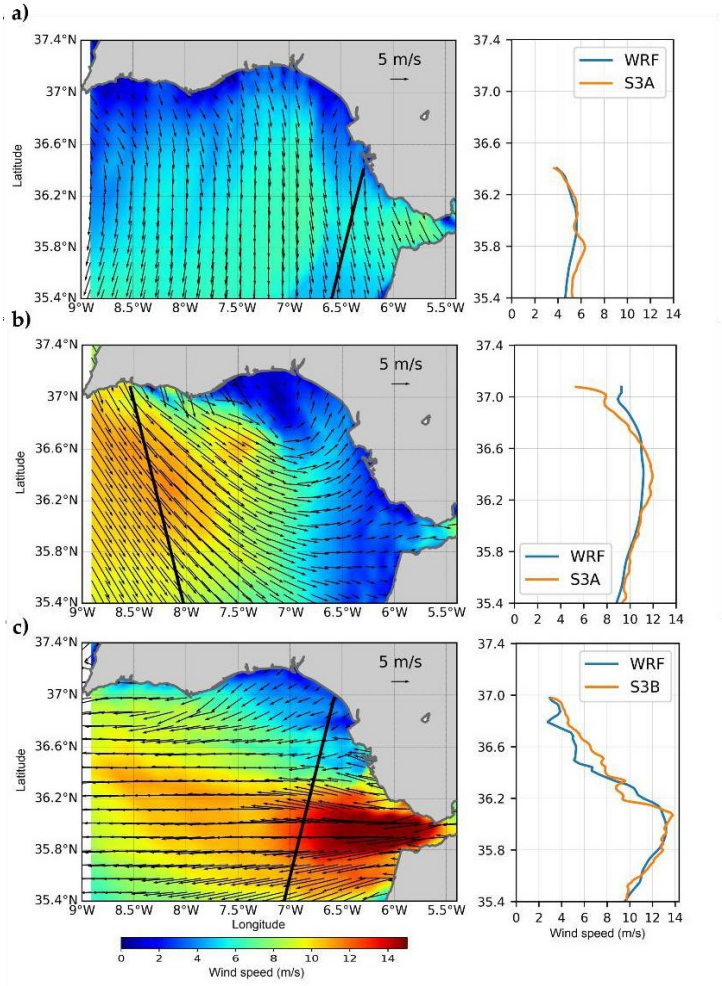

Figure 3.7. Wind field simulated by the WRF model overlaid with S3A/B track (left) and wind speed observed by S3A/B overlaid with interpolated WRF model data at the same positions for the closest available time. (a) 31-Dec-2020, WRF outputs for 11:00 UTC overlaid with S3A track at 10:35 UTC; (b) 25-Jun-2020, WRF outputs for 22:00 UTC overlaid with S3A track at 21:32 UTC; (c) 21-Feb-2020, WRF outputs for 11:00 UTC overlaid with S3B track at 10:37 UTC.

3.4 Conclusions

This study presents the quality and capabilities of WS from satellite altimetry for the spatial assessment of WS outputs from the WRF model over the complex area of the GoC. In order to achieve this, three WS data sources were compared: in-situ measurements, S3A/B satellite altimetry derived measurements at 20 Hz and the WRF model simulations from a nested

domain of 3 km grid and 1 h temporal resolution. From the results of the different comparisons, we conclude that the quality of the high-resolution (20 Hz) S3A/B WS data satisfies the general mission requirements over the study area, and even though the GoC buoy is located in a complex area affected by coastal-related processes, the results are in line with previous studies focused on the open ocean. Regarding the validation of the WRF model against in-situ data, the simulations of the surface WS over the area are of good quality; this confirms the goodness of the dynamical parameterizations proposed by (Arasa et al., 2016). Note that we introduced a modification in the configuration by updating the SST every 6 hours instead of maintaining a constant value, which makes the set-up more realistic. The spatial variability of the WS derived from the model has been compared with along-track altimetry derived WS data. This comparison, and considering the complex characteristics of the analysed region, exhibits the potential of the altimetry data for the spatial evaluation of numerical models. In this case, the altimetry data enable the detection of a certain level of degradation of the WRF outcomes near the coastal fringe, which is in line with previously detected WS overestimation of the WRF model in coastal areas, which supports the need to conduct further analyses into the dynamical phenomena and the effect of using a more accurate surface representation. It is important to note that these model deficiencies in the coastal band are detected thanks to the presence of altimetry data up to 5 km from the land, enabling the fine-tuning and evaluation of NWP models over the complex coastal fringe. Qualitatively, we proved the agreement between altimetry and WRF model data sets under low/high wind speed conditions. However, it is important to note the limitations related to altimetry as the fact that it is not possible to obtain the wind direction. Besides, altimetry data are instantaneous and events of time scales shorter than the time resolution of the model may lead to mismatches. Moreover, perpendicular to the track, the altimeters do not measure the variability in scales smaller than the across track footprint length. In this sense, it is important to highlight the need for continuous improvement of satellite altimetry and model

outputs in the coastal fringe in order to obtain realistic geophysical parameters in these areas. Present and future satellite altimetry missions will allow the exploitation of fully-focused SAR data for a better characterization of ocean processes in the 0 – 5 km coastal band. This study proves the high quality of Sentinel-3A/B WS retrievals over complex areas and aims to foster the use of this data for the improvement of knowledge of WS and sea surface circulation over areas where the availability of in-situ measurements is limited or inexistent. We have shown how the spatial coverage of satellite altimetry enables the spatial assessment of high-resolution NWP models in water-covered surfaces, including coastal areas up to 5 km from land, a feature that sets altimetry as a complementary data source to improve the study and prediction of the wind in coastal areas together with some of the current systems, such as scatterometers, high frequency radars and SAR wind fields.

3.5 Connecting Text

This chapter proved the quality and capabilities of WS retrievals from satellite altimetry for spatially assessing WS outputs from the WRF model over the complex Gulf of Cadiz. The findings emphasized the high quality of the 20 Hz S3A/B WS data and its application for a successful validation of the WRF model over the area, along with an additional comparison against in-situ data. Those results, added to the insights related to the capabilities for studying surface circulation from satellite altimetry data presented in Chapter 2, build up a solid baseline and database, founded on satellite altimetry data, for the comprehensive study of total surface circulation over coastal areas, including both geostrophic and main ageostrophic components.

The next chapter focuses on a generalized characterization of surface circulation over the northern shelf of the GoC, utilizing four years of high-resolution satellite altimetry data and the wind model dataset, developed in the present chapter, to provide oceanographic insights on the influence of the different components of the circulation, related local processes and its seasonality.

Chapter 4

Spatiotemporal variability of the coastal circulation in the northern Gulf of Cadiz from Copernicus Sentinel-3A satellite radar altimetry measurements

This study presents a generalised characterisation of the surface circulation over the northern shelf of the Gulf of Cadiz, based on 4 years of high-resolution satellite altimetry data from Sentinel-3A and wind model data. The altimetry-based surface zonal currents, adjusted for bottom-drag and wind effects, are compared with a generic CMEMS product and validated against in-situ ADCP measurements. The proposed altimetry product demonstrates superior performance than the CMEMS product, accurately reflecting surface circulation direction compared to in-situ measurements (r = 0.77, RMSE = 0.10 m/s, bias = 0.01 m/s). The use of the bottom-drag and wind-corrected/uncorrected altimetry product for spatiotemporal analysis of the shelf circulation revealed the distinct contributions of wind-driven and geostrophic components in different basin sectors. The results show that over the western basin, positive (eastward) surface currents were predominantly driven by westerly winds, while only occasionally, westward flows coincided with easterly winds, suggesting a higher control of the geostrophic component over the westward flows. In contrast, over the eastern basin, both eastward and westward flows were found to be primarily driven by favourable winds. Additionally, the analysis of Absolute Dynamic Topography (ADT) values along the whole basin showed the presence of ADT gradients both along-shore and cross-shore over

the shelf, contributing to geostrophic flows. Finally, the seasonal analysis showed that eastward circulation tends to dominate during the spring and summer months, related to the upwelling season in the Gulf of Cadiz and associated westerly winds. Westward flows prevail during the winter months, related to easterly winds and the rebalancing of the along-shore sea level gradient during relaxed upwelling conditions. The findings demonstrate a significant improvement in the use of satellite altimetry data to study complex oceanographic dynamics in coastal areas, where both spatial and temporal variability are high. Moreover, the similarity of our results to those obtained from in-situ systems supports the use of altimetry data and publicly available wind models to support oceanographic studies in remote or resource-limited areas.

Mulero-Martinez, R.; Gómez-Enri, J.; De Oliveira Júnior, L.; Garel, E.; Relvas, P.; Mañanes, R. **Spatiotemporal variability of the coastal circulation in the northern Gulf of Cadiz from Copernicus Sentinel-3A satellite radar altimetry measurements**. Advances in Space Research (2024), doi: https://doi.org/10.1016/j.asr.2024.02.054

4.1 Introduction

The use of satellite altimetry had a transformative impact on the discipline of physical oceanography by providing a comprehensive global perspective on ocean topography from space (Fu et al. 2010). This advancement has made significant contributions to our understanding of large-scale circulation patterns and processes in the open ocean through the application of geostrophic approximation methods. Studying ocean dynamics becomes notably complex in coastal areas and smaller sub-basins where the geostrophic approximation by itself might not be enough to explain the circulation due to local phenomena and non-geostrophic factors like complex variations in wind fields, shallow bottom topographies, river discharges, and interactions between different water masses (Criado-Aldeanueva et al. 2006; Mulero-Martínez et al. 2021). Nonetheless, more in-depth knowledge of the ocean dynamics over coastal areas (including the potential effects of sea level rise) has significant socio-economic and environmental implications, potentially improving the management of activities such as fisheries, offshore energy or navigation-related risks.

Recent advancements in radar altimetry have greatly enhanced the accuracy and resolution of sea surface height (SSH) measurements along the satellite's tracks, allowing the study of coastal ocean circulation by providing observations at short spatial scales critical for coastal regions (Morrow et al. 2017; Raney 2012). In particular, Synthetic Aperture Radar (SAR) Delay-Doppler altimetry achieves a resolution which is an order of magnitude finer compared to conventional radar altimetry. The Sentinel-3A (S3A) satellite altimeter currently provides SAR-mode data in the whole ocean enabling the application of this innovative data processing approach to coastal ocean studies (Feng et al. 2023). Besides, satellite altimetry continues evolving and represents a fast-developing technology,

exemplified by the recent launch of the Surface Water and Ocean Topography (SWOT) mission that will collect data across a 120 km wide swath (Srinivasan and Tsontos 2023).

This study aims to present the capacities of S3A SAR mode datasets for assessing coastal sea surface circulation over the Gulf of Cadiz. In addition, the study shows how the value of such a dataset, characterised by its enhanced and consistent time and spatial coverage, can be improved when accounting for the effect of ageostrophic factors such as the bottom-drag effects and the wind-driven surface circulation. On a final basis, this work aims to contribute to achieving a level of understanding of ocean circulation in coastal zones from altimetry similar to that of the open ocean (Troupin et al. 2015), even in areas with a lack of either in-situ measurements or local hydrodynamical models. The overarching goal of this study is to complement regional coastal oceanographic studies by providing the highest quality altimeter measurements of Absolute Dynamic Topography (ADT) and ADT-derived geostrophic current (Vt), over the northern GoC coastal zone. This objective entails an investigation into the quality of different altimetry-based products but also about the different mechanisms affecting the sea surface circulation over the continental shelf of the GoC along its sub-basins. The approach relies upon previous coastal oceanographic studies (Manso-Narvarte et al. 2018; Mulero-Martínez et al. 2021) based on altimetry and local oceanographic studies (Garel et al. 2016; De Oliveira Junior et al. 2021; De Oliveira Junior et al. 2022) based on various measurement devices such as high-frequency radar (HFR) and Acoustic Doppler current profiler (ADCP).

The chapter is organized as follows. Section 4.2 provides a concise overview of the study region and presents recent research findings about the ocean circulation in the area. Section 4.3 describes the datasets and methods applied, including the detailed filtering strategy applied to the raw altimetry data and the approach to obtain estimates of the geostrophic velocity. Results and discussions are presented in Section 4.4, starting with the comparison of altimetry-derived surface current velocity from different products with in-situ ADCP

measurements. Next, the GoC shelf circulation is characterised based on current velocity estimated with the most accurate product from the previous comparison with ADCP, including the assessment of the alongshore ADT gradients, the different contributions of both the bottom-drag corrected geostrophic and the wind-driven circulation to the total circulation and the spatiotemporal variability of the circulation over the shelf. Finally, the summary and conclusions are presented in Section 4.5.

4.2 Study area

The GoC is located between the northwestern coast of Africa and the southwestern tip of the Iberian Peninsula. The northern shelf spans from the eastern Strait of Gibraltar to Cape San Vicente (CSV) in the west. It is divided by Cape Santa Maria (CSM) into a narrower western shelf and a broader eastern shelf (Figure 4.1). The complex dynamics of the surface circulation in this region are influenced by factors such as bathymetry, wind patterns, river discharges and water mass exchanges through the Strait of Gibraltar (Criado-Aldeanueva et al. 2006; García-Lafuente et al. 2006).

The wind field along the GoC is influenced by various factors, including topography, atmospheric flows, and temperature variations between land and sea (Carvalho et al. 2014; Mulero-Martinez et al. 2022). The wind patterns in the GoC exhibit alternating flows known as Ponientes (westerly) and Levantes (easterly). These winds can occur consistently throughout the year with a periodicity of approximately 2-3 days (De Oliveira Júnior et al. 2021) but generally respond to a seasonal cycle forced by the seasonal displacement of the Azores high (Criado-Aldeanueva et al. 2009; Ortega et al. 2023). During the winter and autumn months (December to February and September to November, respectively), there is a high degree of variability in wind direction accompanied by frequent intense weather events, including strong Levantes. In spring, northwest winds become less dominant, occasionally giving way to stronger eastward winds. Summer experiences predominantly

calm winds with a prevailing northwest component (De Oliveira Júnior et al. 2021). Northerly winds along western Portugal rotate anti-clockwise from CSV, providing the conditions for local upwelling along the southern coast. East of Cape Santa Maria, the intensity of the wind-related upwelling events decreases due to the widening continental shelf being non-significant by the middle of the eastern basin (De Oliveira Júnior et al. 2022).

The large-scale (> 100 km) sea surface circulation in the GoC generally displays a south-eastward background circulation superimposed on the anticyclonic pattern delineated by the presence of the Gulf of Cadiz Current (GCC) that is strongest in summer (Criado-Aldeanueva et al. 2006; García-Lafuente et al. 2006; Garel et al. 2016; Sánchez and Relvas 2003). Shifts to north-westward flow can be observed throughout the year, but predominantly in late autumn and early winter, particularly in December and January (Folkard et al. 1997; Sánchez and Relvas 2003). Over the continental shelf, the flow is alongshore, alternating between eastward and westward at a time scale of 2-3 days, following a similar pattern to the wind field. The alongshore velocities, mostly zonal due to the coastline orientation, can reach up to approximately 0.4 m/s, while cross-shore (meridional) velocities, mainly dominated by tidal forces, are one order of magnitude weaker (Garel et al. 2016; De Oliveira Júnior et al. 2021). The shelf circulation along the GoC is highly linked to the southward flows along Portugal's western coast and its upwelling system. Eastward cold-water flows along the GoC shelf originated either under northerly winds, due to the rotation of the poleward Portugal's current around CSV or locally under westerly wind conditions (Folkard et al. 1997; De Oliveira Júnior et al. 2022). In contrast, westward coastal flows, commonly expressed as Coastal Counter Currents (CCC) (Garel et al. 2016; Laiz et al. 2019; De Oliveira Júnior et al. 2021, 2022; Teles-Machado et al. 2007) due to their opposite direction to the characteristic south-eastward slope of the GCC, develop along a relatively narrow strip spanning up to 15-20 km off the coast (De Oliveira Júnior et al. 2021). Recent studies of surface currents derived from High-Frequency Radar (HFR) and numerical

model simulations found the coastal margin of the westernmost side of the Strait of Gibraltar as the initiation point of the CCCs events (Sirviente et al. 2023). Opposite to the eastward flows, CCCs tend to increase coastal temperatures during summer through the transport of warm water from areas surrounding the mouth of the Guadalquivir River and Cadiz Bay marshes (Relvas and Barton 2002). Such transport does not only affect water temperature but also nutrient availability and the transport of pollutants throughout the basin, playing a key role in the biogeochemistry of the area (Laiz et al. 2019). The occurrence of CCCs has been associated with an unbalanced along-shore pressure gradient during periods of weakened upwelling-favourable winds (Garel et al. 2016; De Oliveira Júnior et al. 2021, 2022). In addition to local wind stress, it is crucial to take into account the impact of remote factors such as wind forcing over the Alboran Sea and the eastern side of the Strait of Gibraltar. A recent study also suggested a potential relation with the sea level atmospheric pressure forcing over the Ligurian Sea (Sirviente et al. 2023). However, understanding the primary driving mechanisms for CCCs in this region is challenging since those events result from various intricated factors that vary spatially and temporally.

Considering the different features that characterise the GoC circulation, a generic glimpse of the ocean surface circulation can be defined as a predominant anticyclonic system, regarding the open ocean circulation, with episodic inversions to north-westward circulation under strong and persistent easterly winds. The shelf circulation is characterised by the presence of two transient cyclonic cells over the eastern and western basins, driven by CCC events in the north and delimited by the GCC in the south (Criado-Aldeanueva et al. 2009).

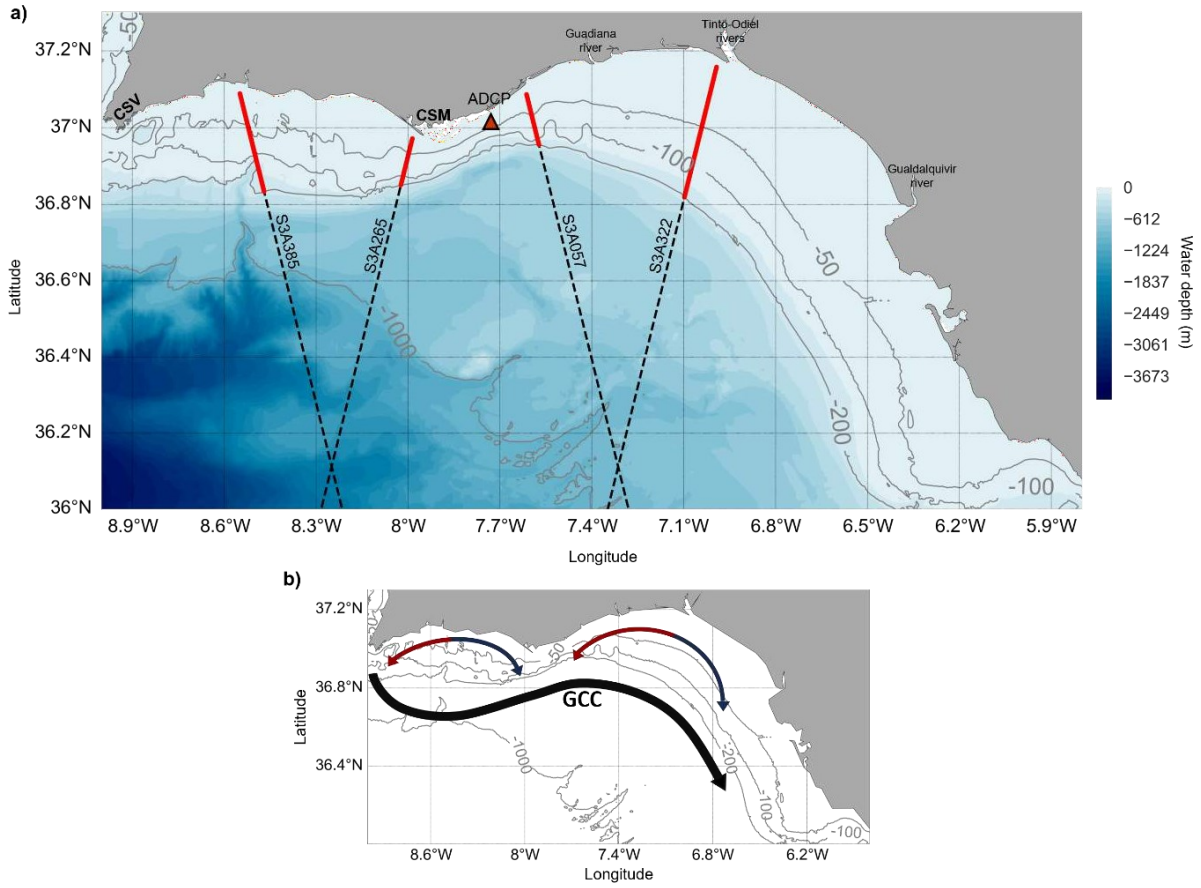

Figure 4.1. (a) Study area along with the Sentinel-3A tracks (red lines indicate the sectors considered over the continental shelf, with depth ≤ 200 m) selected for the study and the location of the Armona ADCP (ADCP). The main geographical characters are also presented: Cape San Vicente (CSV); Cape Santa Maria (CSM). (b) Representative scheme of the surface circulation in the northern margin of the GoC based on (De Oliveira Júnior et al., 2022)*, where the GCC remains stable almost all year round, while over the shelf, the blue lines represent the circulation under favourable upwelling conditions and the red lines represent the circulation under weakened upwelling conditions and/or strong Levantes.*

4.3 Data and methods

Satellite altimetry data from Sentinel-3A

This study is based on high-resolution along-track ADT obtained from Sea Level Anomaly (SLA) measurements from 4 different Sentinel-3A tracks crossing the continental shelf of the GoC (Figure 2.1), during the period: 2017-2021. Each track has a repeat cycle of 27 days and is identified by its specific relative orbit number: S3A-385, S3A-265, S3A-057 and S3A-322.

The synthetic aperture radar altimeter (SRAL) instrument onboard Sentinel-3A can measure in two different modes, namely, low resolution (LRM) and synthetic aperture radar (SAR). The latter mode, SAR, is renowned for its high-resolution along-track capabilities and is widely utilised across the global ocean. Additionally, the data from the SRAL instrument on Sentinel-3A can be post-processed to generate level-2 data at frequencies of 1 Hz, 20 Hz and 80 Hz for the Ku and C bands. Detailed information regarding these data can be found in the Sentinel-3 Altimetry Document Library, accessible at https://sentinel.esa.int/web/sentinel. Sentinel-3A level 2 data for this study were accessed through the ESA Earth Console Parallel Processing Service (P-PRO) SAR versatile altimetric toolkit for ocean research and exploitation, known as P-PRO SARvatore (https://ui-ppro.earthconsole.eu). These data were processed using the predefined setup designed for coastal zones. In addition, the retracking process was based on the SAR Altimetry MOde Studies and Applications (SAMOSA++) model (Dinardo et al., 2021). The product extracted consists of SLA measurements at a frequency of 20 Hz, yielding an along-track spatial resolution of approximately 330 meters. Finally, a set of range and geophysical corrections, presented in Table 4-1, are applied following the recommendations in (Feng et al., 2023; Fenoglio-Marc et al., 2015; Gómez-Enri et al., 2018; Mulero-Martínez et al., 2021), including a sea state bias (SSB) correction based on 5% of the significant wave height (SWH), as suggested by (Fenoglio-Marc et al., 2015; Gómez-Enri et al., 2018).

Table 4-1. Range and geophysical corrections applied to the original Sea Level Anomaly (SLA) measurements.

Range corrections	Geophysical corrections	
Atmospheric	**Tidal**	**Ocean surface**
Dry Tropospheric	Ocean Tide (TPXO8-atlas model)	Dynamic Atmospheric Correction
Wet Tropospheric	Long-Period Equilibrium Tide	Sea State Bias (5% Significant Wave Height)
Ionospheric	Ocean Loading Tide	
	Solid Earth Tide	
	Geocentric Polar Tide	

Sea level anomaly (SLA) filtering strategy

To obtain valid SLA data up to 3 km from the coast over the GoC, 20-Hz along-track SLA data from 4 different Sentinel-3A relative orbits over the area for the period 2017-2021 were edited as follows: Firstly, raw SLA values closer than 3 km to the coastline were rejected to maintain a distance of good quality. This criterion is based on (Aldarias et al. 2020), which suggested that good quality data can be obtained within S3-A tracks up to 3 km from the coast in our study area. Secondly, values larger than three times the standard deviation of the SLA were removed and replaced by linearly interpolated values; this processing was applied in a 10-times loop (i.e.: the process is applied 10 times) (Bouffard et al. 2010; Meloni et al. 2019; Mulero-Martínez et al. 2021) along each pass (along-track) and along all passes from the same relative orbit (along-time) to ensure the removal of outliers spatially and temporally. Finally, a LOESS (locally weighted smoothing) filter (Cleveland and Devlin, 1988) was applied along each track segment individually to filter out high-frequency noise (Manso-Narvarte et al., 2018); this is a common and proven valid processing procedure for the study of oceanic mesoscale phenomena (Morrow et al., 2017; Mulero-Martínez et al., 2021). After applying this procedure, the resulting SLA is suitable for being used for oceanographic purposes. Figure 4.2 shows an example of track S3A-057 before (Fig. 2.a) and after (Fig. 2.b) the filtering process.

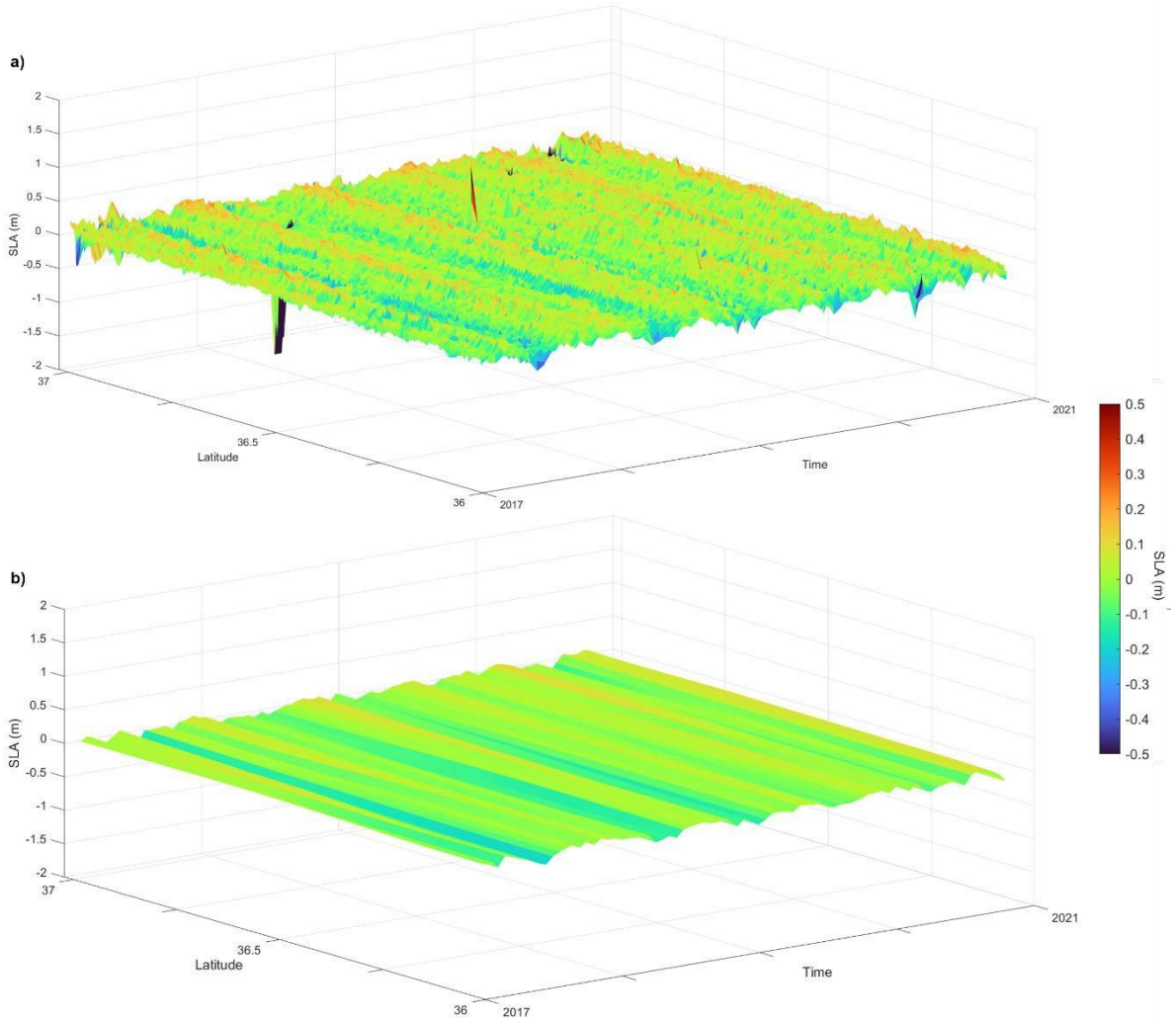

Figure 4.2. Latitude-time variability of the SLA from S3A-057 before (a) and after (b) applying the filtering strategy.

Absolute Dynamic Topography (ADT) and surface circulation

Absolute dynamic topography (ADT) profiles were estimated by adding the mean dynamic topography (MDT) to the SLA. Though the ADT can also be computed by extracting a geoid model from the sea surface height (SSH), the MDT-based approach has been found to provide the best estimates when used to calculate derived geostrophic velocities. The DTU15MDT model (Knudsen et al., 2016) was used to calculate the final ADT. This MDT model has been previously used by (Mulero-Martínez et al., 2021) over the eastern basin of

the GoC for estimating geostrophic currents from CryoSat-2 satellite altimetry data with good results. While the MDT data were interpolated from the original model grid to the satellite' tracks positions, the EGM2008 (Pavlis et al., 2008) and EIGEN6C4 (Förste et al., 2014) geoid models data were extracted along with the raw altimetry data from the P-PRO SARvatore service, at the same 20 Hz posting rate.

Given that the ADT characterises the dynamic signal denoting displacement relative to the equipotential surface (geoid) influenced by interactions involving the atmosphere and the topographical features of the ocean floor and its boundaries, it is feasible to derive an estimate of the absolute surface geostrophic circulation using altimeter measurements. This estimation relies on analysing the spatial fluctuations in ADT while accounting for the impact of the Earth's rotational motion, represented by the Coriolis force. Briefly, it is possible to obtain estimates of the absolute geostrophic component of the surface circulation (V_{gAbs}) normal to the satellite tracks using the following Equation 4.1:

$$V_{gAbs} = \frac{-g}{f} \cdot \frac{\partial ADT}{\partial y}, \tag{4.1}$$

where g (m·s-2) is the gravitational acceleration; y (m) is the along-track distance; f (s-1) is the Coriolis parameter ($f = 2\Omega sin\varphi$, where Ω is the angular rotation velocity of the Earth and φ the latitude). The along-track ADT (m) gradient (slope) is estimated by using the optimal filter developed by (Powell and Leben 2004). In addition, (Mulero-Martínez et al. 2021) suggested that, in coastal areas, the effect of both the wind-induced velocity component and the bottom friction must be considered to improve estimates of the surface circulation. Following (Mulero-Martínez et al. 2021), Equation 4.2 and Equation 4.3 provide an estimation of the bottom-drag corrected surface geostrophic velocity (V_{gd}, m·s-1) and the zonal surface wind-driven velocities (V_w, m·s-1), respectively:

$$V_{gd} = \frac{-g}{\left(f + \frac{r^2}{f}\right)} \cdot \frac{\partial ADT}{\partial y}, \quad (4.2)$$

$$V_w = 0.03 \cdot W_{u10} \cdot \cos(10^\circ), \quad (4.3)$$

where r = (0.35C_d)/d (m-1) is a depth-dependent parameter, using a typically accepted value of C_d = 2.0 10-3 (Bowden 1983), and U_{10} (m·s-1) is the zonal component of the wind speed at 10 m above the mean sea level.

Finally, Equation 4.4 allows the estimation of a more complete along-track total surface velocity (V_t), accounting for the main geostrophic component derived from altimetry and corrected for the bottom friction and wind drag effects on the surface circulation, as proposed by (Mulero-Martínez et al., 2021).

$$V_t = \frac{-g}{\left(f + \frac{r^2}{f}\right)} \cdot \frac{\partial ADT}{\partial y} + 0.03 \cdot U_{10} \cdot \cos(10°), \quad (4.4)$$

where r is a depth-dependent parameter and U_{10} is the zonal component of the wind speed. An in-depth development of Equation 4.2 can be found in (Mulero-Martínez et al., 2021). In addition, the resulting cross-track velocities are rotated to obtain the zonal component of the current.

Figure 4.3 summarizes the complete methodology from the original raw SLA measurements to the final V_t product.

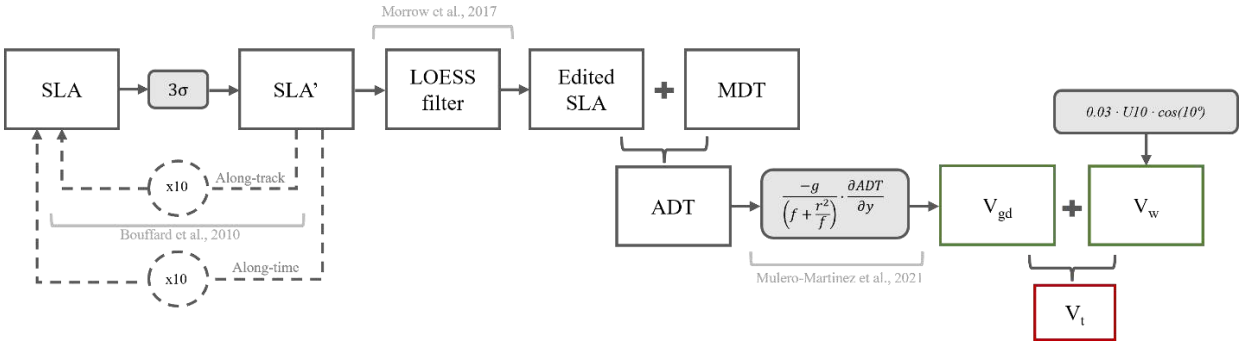

Figure 4.3. Schematic representation of the complete methodology for editing satellite sea level anomaly and calculating the along-track total surface velocity.

Model wind data

Wind data used to compute the wind component of the circulation for the period 2017-2021 was extracted from the National Center for Environmental Prediction (NCEP) operational Global Forecast System (GFS) with 0.25˚ (approximately 25 km) of grid resolution and 6 h of temporal sampling (https://rda.ucar.edu/datasets/ds084.1/). A previous study on the GoC found the NCEP-GFS model as a reliable source of wind data, obtaining the best results in terms of error and correlation, for both wind speed and direction, when assessed against in-situ measurements and compared with other equivalent publicly available models (Carvalho et al. 2014). NCEP GFS wind data was used for the estimation of the wind-driven surface current in Section 4.2. However, for the detailed evaluation of surface current velocities from different altimetry-based products against ADCP measurements during the period 2020-2021, presented in Section 4.1, an alternative source with higher spatial and temporal resolutions, and locally calibrated, was used to accurately reproduce the wind conditions, though with a higher computation cost. Specifically, the wind data for the study was obtained using the Weather Research and Forecasting (WRF) model v.4.2 (Skamarock et al. 2019), which is a mesoscale non-hydrostatic model. The WRF model was used to produce dynamically downscaled hourly 10 m wind speed and direction over the complete GoC area. The 3 km resolution domain was one-way nested within a larger parent domain with a resolution of 9 km. The initial and boundary conditions were provided by the NCEP-GFS model described earlier and applied to the parent domain. The dynamical set-up of the simulations follows the scheme presented in (Mulero-Martinez et al. 2022), as it was proved to successfully reproduce the wind conditions in the area.

In-situ ADCP measurements

Acoustic Doppler current profiler (ADCP) measurements were obtained from Armona coastal station (37.0108ºN, 7.7413ºW) (Figure 4.1), where the water depth is 22 m. For the

data collection a Sentinel V 500 kHz ADCP, manufactured by TRDI, was bottom-mounted 4 times for periods ranging from January 2020 to December 2021. The instrument recorded hourly velocities in cells of 0.5 m thick along the water column. The resulting data was de-tided by applying a low-pass filter of a 40-h cut-off period. This study was based only on the spatial average of the two uppermost valid cells (Garel et al., 2016), typically within the initial 2 to 3 meters from the water surface. For the comparisons against satellite altimetry data, presented in Section 4.1, 72 h averages of ADCP measurements previous to the satellite pass were used. Using 72 h averages is suggested in (Mulero-Martínez et al., 2021; Roesler et al., 2013) for comparisons with altimetry data since it is representative of a synoptic circulation, similar to the estimates using altimetry data, mainly based on geostrophic processes.

CMEMS gridded product

Gridded absolute geostrophic current velocities were gathered from the Copernicus Marine Environment Monitoring Service (CMEMS). The gridded product is based on multi-mission satellite altimetry (including Sentinel-3A) SLA measurements. The final gridded data is estimated by optimal interpolation, merging the level-3 along-track measurement from the different altimeter missions available and providing daily estimates with a 1/8°x1/8° spatial resolution. A more detailed description of the development and quality of the products can be found in https://doi.org/10.48670/moi-00142.

4.4 Results and discussion

Comparison and validation with in-situ current measurements

The S3A-057 satellite track passes over the GoC southbound (descending track), covering a narrow part of the continental shelf east of the CSM (Figure 4.1). The Armona ADCP was

moored 15 km from this track. Different surface current estimates from S3A-057 altimetry measurements and gridded CMEMS products were compared with in situ measurements from the ADCP moored at Armona station.

Evaluation of ADT constructions

Results of the comparison between ADCP surface zonal velocities and the three different S3-V_t products, computed with ADTs from the different approaches (S3-V_tMDT, S3-V_tEGM and S3-V_tEIGEN), are presented in Figure 4.4. The comparison of different methods yielded the best result in terms of Pearson's correlation and root mean square error when using S3-V_tMDT (correlation coefficient=0.77; RMSE=0.10 m/s). The S3-V_tEGM and S3-V_tEIGEN estimates also performed well but had slightly lower correlation coefficients and larger RMSE compared to S3-V_tMDT. This finding aligns with a previous study (Feng et al., 2023) conducted in the Northwest Atlantic Shelf, particularly in the Gulf of Maine, which also concluded that constructing ADT based on MDT provides more accurate results when used for geostrophic current estimations, mainly due to increasing geoid errors near the coast.

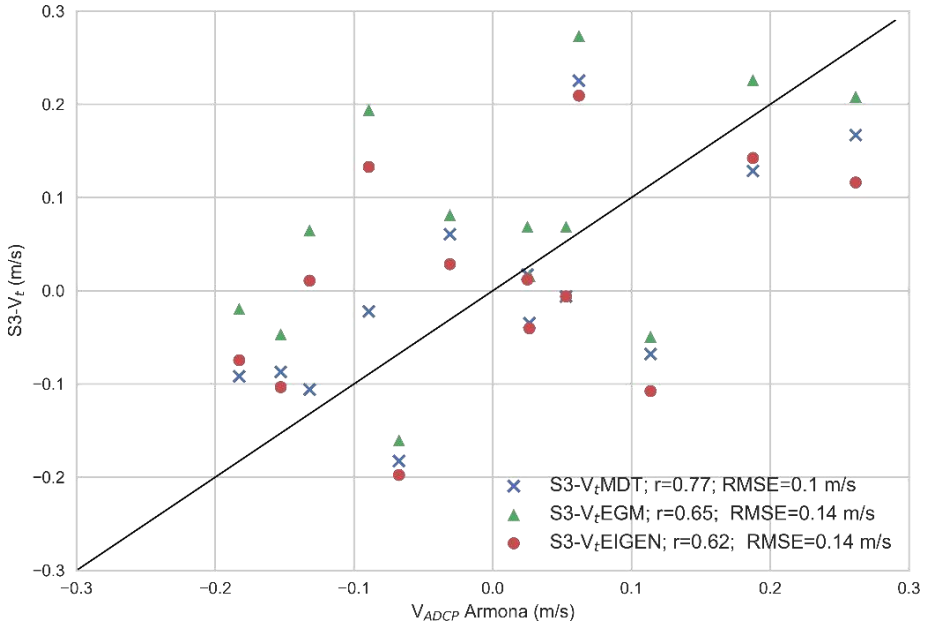

Figure 4.4. Scatter plot of the different satellite altimetry-derived surface geostrophic velocity approaches against in-situ ADCP measurements. S3-V_tMDT refers to geostrophic

velocities estimated using the ADT based on MDT, while S3-V_tEGM and S3-V_tEIGEN refer to the geostrophic velocities estimated using geoid models EGM2008 and EIGEN6C4, respectively.

Inter-products comparison

The comparison presented in Figure 4.5 shows the current velocity estimated from several altimetry-based products against in-situ ADCP surface current measurements. Specifically, the altimetry-based products are the bottom-friction corrected geostrophic current (V_{gd}), the total current velocity accounting for the bottom-friction corrected geostrophic and wind components (V_t), generated from both high-resolution altimetry data along S3A-057 (S3-V_{gd} and S3-V_t) and the CMEMS product (C-V_{gd} and C-V_t). The wind information used for the estimation of the V_t was extracted from the high-resolution locally downscaled WRF model. The statistical parameters resulting from the comparison (r-correlation, RMSE, and bias) used to quantify the performance of the different products are presented in Table 4-2.

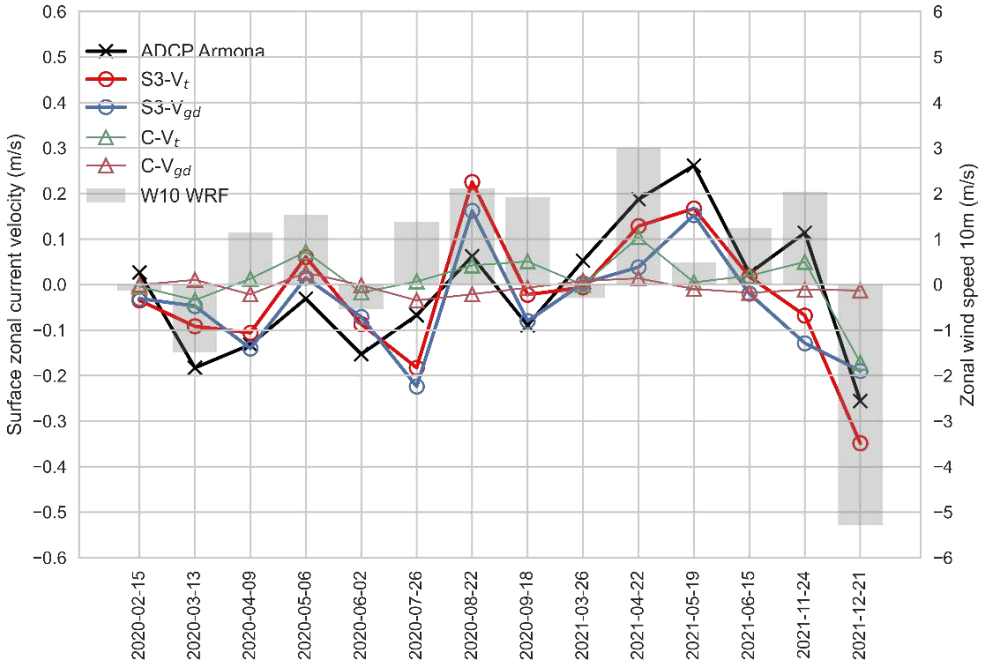

Figure 4.5. Match-up time series of altimetry-based current velocities (S3-V_{gd}, S3-V_t, C-V_{gd}, C-V_t) and in-situ ADCP Armona surface current velocities, along with the simultaneous zonal wind speed from WRF. Note that the time interval is not constant.

The comparison with in-situ measurements shows that the C-V_{gd} product produced the worst results (r = 0.10, RMSE = 0.14 m/s, Bias = -0.01 m/s), which is expected considering that it mainly represents the geostrophic current, corrected only for the bottom friction, in addition to the low resolution and high smoothing of both the final product and altimetric data (1 Hz) used for its development. The CMEMS product improved when applying an estimate of surface wind current (C-V_t), (r = 0.62, RMSE = 0.12 m/s, Bias = 0.01 m/s), especially in terms of correlation. This improvement is due to the greater similarity between the compared variables, resulting from the important role of the wind on the surface circulation of the GoC (De Oliveira Júnior et al., 2022; Mulero-Martínez et al., 2021).

The best results of the comparison derive from the use of the products generated with high-resolution altimetric measurements (20 Hz), S3-V_{gd} and S3-V_t. S3-V_{gd} showed a higher correlation than C-V_t, even without the application of wind current estimation (r = 0.67,

RMSE = 0.11 m/s, Bias = 0.03 m/s). The higher spatial resolution of the altimetric data used to generate this product allows for a better representation of nearshore circulation along the continental shelf. However, the lack of a wind component penalizes the results of this comparison in terms of bias. Finally, the S3-V_t product provided the best representation of the surface circulation, with the best results for all calculated statistics (r = 0.77, RMSE = 0.10 m/s, Bias = 0.01 m/s). The S3-V_t product not only has the advantage of being generated with high spatial resolution altimetric data but also includes the variability provided by the estimation of the wind-induced current component. The high variability of the zonal circulation in the continental shelf sector during the analysis period can be observed. This variability, which is highly dependent on the wind field in the area, is well represented by the S3-V_t product, which correctly reproduced the ADCP current direction more than 70% of the time, even considering weak flows that might be produced by surface gradients of low magnitude, difficult to be resolved by altimetry (Marechal & Ardhuin, 2022).

Despite the good results, it should be noted that the comparison shows current values obtained independently and in various ways. The ADCP measures at a single point and directly measures the total circulation that is taking place at each moment, while the altimetric products estimate the geostrophic component of the circulation based on the elevation gradient of the ocean surface along the satellite track (Feng et al., 2023). In addition, the distance between the satellite track and the ADCP could also affect the comparison. Such differences stand a limitation when performing this kind of comparison and should be considered when interpreting the statistical results. These results demonstrate the benefits of including the wind effect in the estimation of the surface circulation from altimetry.

Table 4-2. Statistical results (correlation coefficient, r; root mean square error, RMSE; and bias, Bias) from the comparison between altimetry-based current velocities (S3-Vgd, S3-Vt, C-Vgd, C-Vt) and in-situ ADCP Armona surface current velocities.

Product	r	p-value	RMSE (m/s)	Bias (m/s)
C-V_{gd}	0.10	0.742	0.14	-0.01
C-V_t	0.62	0.018	0.12	0.01
S3-V_{gd}	0.67	0.009	0.11	0.03
S3-V_t	0.77	0.001	0.10	0.01

Characterisation of the GoC shelf circulation

Since S3-V_t showed the best validation results, the same methodology has been extended to tracks S3A-385, 265, and 322, in addition to the already mentioned 057, for a longer period: 2017-2021. The use of different satellite tracks along the area allows for analysing the spatiotemporal variability of the surface circulation along the continental shelf in the GoC. It is worth mentioning that unlike in the previous section, the S3-V_t products analysed in this section, have been generated with an estimation of the wind-induced surface current (V_w) based on lower resolution data from NCEP-GFS instead of the locally calibrated WRF downscaling, due to computation limitations. Since the NCEP-GFS was used as boundary conditions for the WRF model, they were found to equivalently represent the synoptic conditions.

Contribution of the geostrophic and wind components

The different time-series presented in Figure 4.6 show the along-track average zonal circulation along the continental shelf of the GoC, from tracks S3A-385 (a), 265 (b), 057 (c) and 322 (d), respectively. Specifically, estimates of the total current (V_t), the bottom-friction corrected geostrophic components (V_{gd}) and the wind component (V_w) of the surface

circulation are presented to provide a comprehensive understanding of how the different components contribute to the alongshore circulation in the GoC northern shelf.

Tracks S3A-285, 265 and 057 (Figure 4.6a-c) present similar characteristics regarding the contribution of V_{gd} and V_w to V_t. Positive flows are mainly driven by westerly winds, as indicated by the correspondence of positive V_t and V_w, agreeing with the wind field over the area, since west of CSM westerly and north-westerly winds dominate (De Oliveira Júnior et al., 2022; Folkard et al., 1997b), while easterlies are less recurrent and weaker than over the southern part of the eastern basin (Mulero-martinez et al., 2022). In contrast, westward V_t flows are likely to occur along with both westward V_{gd} and V_w, but also just linked to V_{gd}, suggesting that westward flows, such as CCCs, are not necessarily linked to strong easterly winds, but also to geostrophic adjustments. Marked events (E1, 2, 3, 4 and 5) in Figure 4.6a represent the different scenarios detected with track S3A-385 along the western basin regarding the contribution of both Vgd and Vw to the westward flows. Events E1 (21-Apr-2017), E4 (25-Feb-2019) and E5 (23-Feb-2021) show Vt negative flow events driven by both westward Vgd and Vw, while during events E2 (30-Sep-2017) and E3 (6-Dec-2018) the Vt flows directed to the west are purely controlled by a negative Vgd flow. Several authors have suggested the existence of an alongshore pressure (sea level) gradient over the shelf that is likely to promote westward flows without favourable winds and would explain most of the flow variability during CCCs events in the western basin (De Oliveira Júnior et al., 2022, 2021; Garel et al., 2016). The new findings show that the cross-shore gradients may contribute as well to these events. The actual presence of both sea level gradients (i.e., cross-shore and alongshore) over the shelf is further analysed in Section 0. Regarding track S3A-322 (Figure 4.6d), crossing the eastern basin of the GoC, both V_{gd} and V_w components agree on most of the occasions on the direction of the circulation, aligning with V_t. This observation suggests that in contrast to the western basin, both eastward and westward flows along the shelf in this region are predominantly driven by favourable winds as suggested by

previous studies using ADCP measurements (Criado-Aldeanueva et al., 2009). These winds also contribute to the development of cross-shelf sea level gradients through the piling up or down of water at the coast by Ekman transport, as previously reported in nearby areas (Gómez-Enri et al., 2019), which enhances the total flow through the additional contribution of a geostrophic component. The different V_{gd}-V_w interplays along the different basins are reassured when comparing with ADCP measurements with the correlation coefficients for V_{gd}-V_w, being 0.12 for S3A-385 (western basin) and 0.46 for S3A-322 (eastern basin). It can be also observed that, on average, the wind-driven flow is eastward for all the tracks, due to the dominance of westerly winds over the area, while the geostrophic flow tends to be westward along the whole basin.

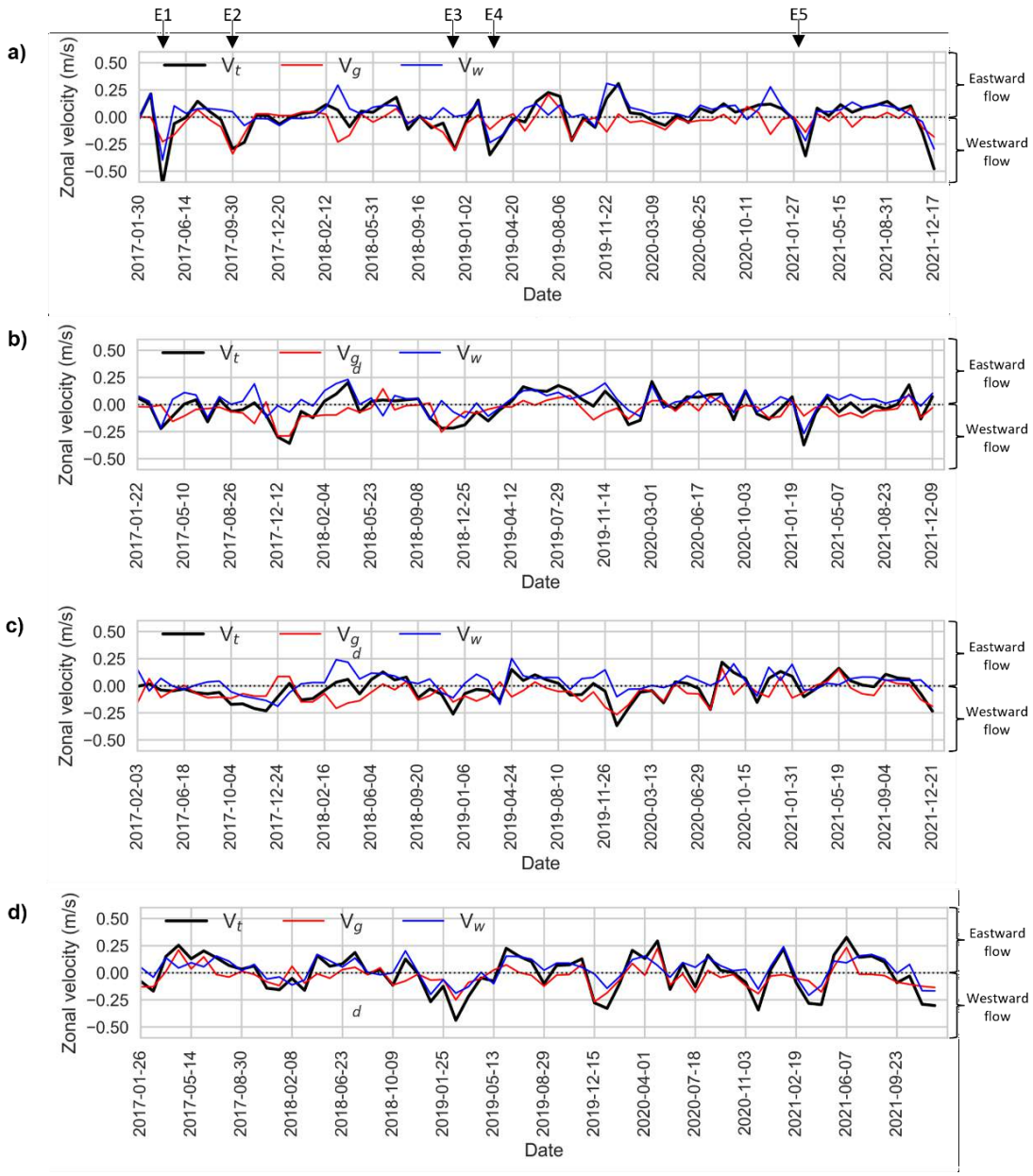

Figure 4.6. Time series of shelf average V_{gd} (red lines), V_w (blue lines) and V_t (black lines) from tracks S3A-385 (a), S3A-265 (b), S3A-057 (c) and 322 (d).

Alongshore and cross-shore sea level gradients

The 5 years average (2017-2021) of ADT for the continental shelf sector traversed by the different tracks is presented in Figure 4.7. The results show the existence of ADT gradients both alongshore and cross-shore, the former of much larger amplitude. Alongshore ADT average differences reach up to 4 cm between the easternmost and the westernmost tracks. This result is in line with previous studies, such as (Relvas and Barton, 2002; Sánchez et al.,

2006), that estimated an average slope of 5 cm/100 km for the same area based on tide gauges. This difference in ADT along the basin implies the existence of an unbalance in the along-shore pressure gradient. To be rebalanced, such alongshore gradient would lead to a westward flow (De Oliveira Júnior et al., 2021; García-Lafuente et al., 2006) during periods of weakened westerly winds and would be enhanced under easterly wind conditions. Additionally, the cross-shore sea level gradients would also support the westward circulation over the shelf, as for the physical basis of this research, a north-south ADT gradient (higher ADT values close to the coast and lower off the coast) would develop a westward geostrophic flow. Such interpretation of the potential effects of the alongshore and cross-shore sea level gradients (ADT gradients) matches with the previously analysed contribution of the different components to the total shelf circulation at the different locations. The results also agree with several studies that suggested the existence of an alongshore pressure gradient as the main factor driving the commonly known coastal countercurrent (CCC) over the GoC shelf during weak wind conditions (Garel et al. 2016; De Oliveira Júnior et al. 2021, 2022) and with the observations from (Sirviente et al. 2023) of sea surface height across-shore gradients directed seawards for days when the CCC in the GoC is present. The average net geostrophic flow resulting from the existence of the ADT gradients presented in Figure 4.7 can be summed up as a westward flow in the absence of any other components. Such a flow would support the circulation represented by red lines in Figure 4.1.

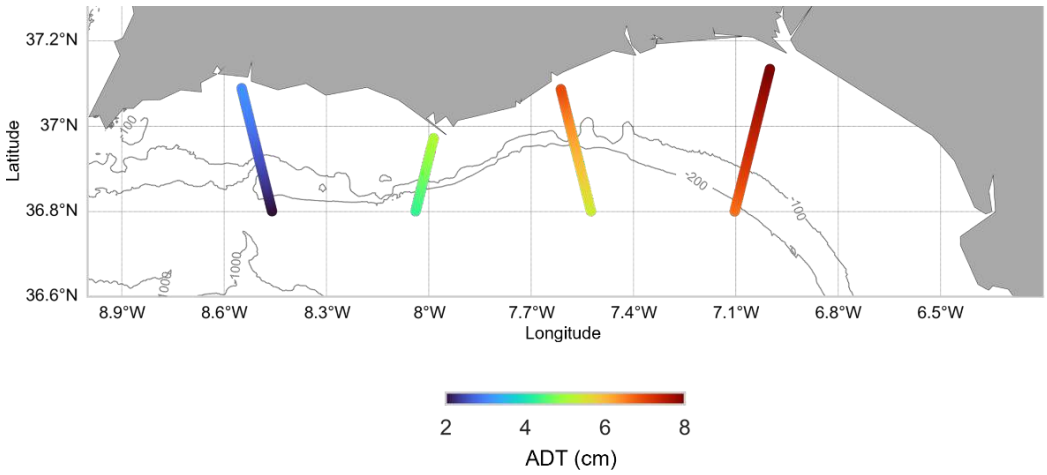

Figure 4.7. Along-track ADT average for the period 2017-2021 over the continental shelf of the GoC.

Spatio-temporal variability

The spatial and temporal variability of the zonal component of surface circulation along the GoC is evaluated by a Hovmöller (HM) diagram (Figure 4.8). The figure shows an HM diagram of the satellite total zonal velocity (V_t) variability against latitude and time for the tracks S3A-385 (a) and S3A-322 (b), representing the western and eastern basins, respectively. Tracks S3A-265 and S3A-057 are not presented due to the narrowness of the shelf at these locations. The use of time-latitude HM diagrams enables qualitatively identifying the alternance among periods dominated by either eastward or westward circulation, in addition, to providing the latitudinal variability of the main flows. Even though the different tracks are not contemporary, it is possible to appreciate a generic and common winter-summer seasonality.

For track S3A-385 (Figure 4.8a), the HM diagram shows some intense westward events extending along the entire transect (E1, E4 and E5). Those events can also be identified in Figure 6 and seem to be the result of the joint action of both V_w and V_{gd} west-bounded components. These events are not limited to the shelf section but extend further offshore, potentially due to the action of Levantes along the whole basin. Additional westward events

can be found more limited to the northern section and the shelf (i.e., E2 and E3), agreeing with the expected configuration of intense CCC events. As can be observed in Figure 4.6, E2 and E3 are mainly explained by the V_{gd} flow, suggesting that westward flows due to geostrophic forces might result in narrower coastal flows than those where also the V_w contribute. Considering that the wind-driven flows would be due to a homogeneous wind field blowing toward the west all over the GoC, they can be expected to cover an extension as wide as the mentioned wind field. On the other hand, the extension of westward flows caused only or mainly by geostrophic forces could result in narrower extensions due to constraints such as bathymetry. The southern half of the HM diagram in Figure 4.8a presents the highest positive flow velocities mostly limited up to 36.6ºN, agreeing with the spatial characteristics of the GoC Current (GCC). Results from track S3A-322 (Figure 4.8b) show remarkably high-intensity negative flows over the southern section of the analysed transect, which most of the time extend up to the northern limits. As previously mentioned, (De Oliveira Júnior et al., 2022) performed a similar analysis based on HFR data over the GoC, and, for the eastern basin found that negative flows tend to occur mostly over the outer shelf, in line with these results that show how the most intense negative flows tend to occur more detached from the coast. Such setup of the circulation might be explained by the proximity to the Strait of Gibraltar where easterly winds are canalised into the GoC and would drive the surface circulation since, as previously stated, is mainly controlled by the wind component over the eastern basin.

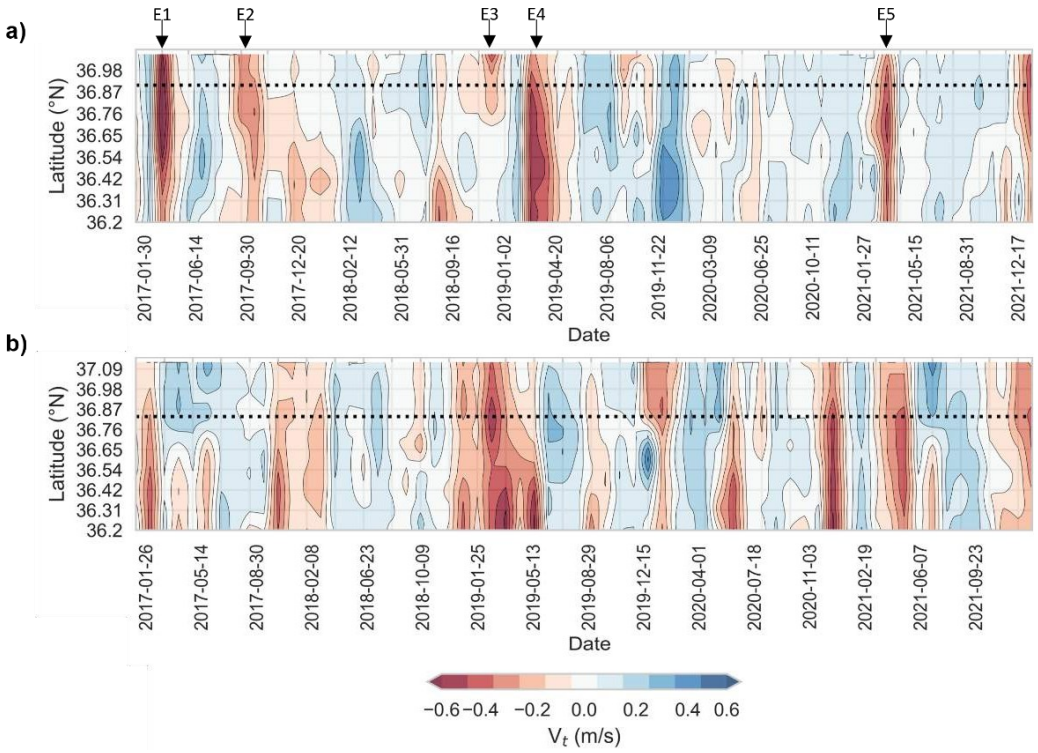

Figure 4.8. *Latitude-time Hovmöller diagrams of the total surface zonal velocity for the period 2017-2021 from tracks S3A-385 (a) and S3A-322 (b) Horizontal dotted lines indicate the latitude corresponding to the 200 m depth isobath.*

The percentage of occurrence of positive and negative flows over the different months, as estimated from the different tracks for the shelf section are presented in Table 4-3. This table provides a global perspective of the temporal and seasonal variability of the dominant flow direction along the year. For all four tracks, eastward circulation prevails during May, June, July and August. The prevalence of eastward flows during the spring-summer months agrees with the upwelling season, though such seasonality over the GoC is not clearly defined, during these months westerly winds are most likely to drive the surface circulation over the area (De Oliveira Júnior et al., 2022; Garel et al., 2016; Sánchez and Relvas, 2003). The opposite situation is observed for winter months, from December to February, when the circulation is predominantly westward. More prevailing westward flows during winter months are associated with strong easterly winds and the effect of the along-shore sea level gradient during relaxed upwelling conditions. The resulting all-year percentages for all tracks are

mainly balanced, agreeing with the results presented in (Teles-Machado et al. 2007), and with the latest study over the area (Sirviente et al. 2023) which, based on HFR measurements and numerical model simulations, found that for summer months westward flows are of smaller amplitude, and greater amplitudes are observed in eastward flows. It is worth noting that the values presented in Table 4-3 are based on satellite passes with 27-day cycles, resulting in approximately 5 passes per track and month for the whole period analysed.

Table 4-3. Monthly percentage of occurrence of westward and eastward circulation and zonal wind over the continental shelf of the GoC from Sentinel-3A tracks #385, #365, #057, #322 and NCEP-GFS wind model. Periods coloured in blue represent the dominance of eastward circulation, while those coloured in red stand for the dominance of westward circulation.

S3A Tracks	V_t Direction	Jan	Feb	Mar	Apr	May	Jun	Jul	Aug	Sep	Oct	Nov	Dec
#385	Westward	42.86	50.00	40.00	80.00	42.86	20.00	0.00	16.67	57.14	60.00	33.33	42.86
	Eastward	57.14	50.00	60.00	20.00	57.14	80.00	100.00	83.33	42.86	40.00	66.67	57.14
#365	Westward	66.67	60.00	42.86	60.00	20.00	16.67	28.57	40.00	40.00	50.00	83.33	66.67
	Eastward	33.33	40.00	57.14	40.00	80.00	83.33	71.43	60.00	60.00	50.00	16.67	33.33
#057	Westward	66.67	100.00	66.67	40.00	40.00	33.33	33.33	40.00	60.00	50.00	100.00	66.67
	Eastward	33.33	0.00	33.33	60.00	60.00	66.67	66.67	60.00	40.00	50.00	0.00	33.33
#322	Westward	75.00	100.00	60.00	33.33	40.00	0.00	16.67	28.57	20.00	60.00	60.00	83.33
	Eastward	25.00	0.00	40.00	66.67	60.00	100.00	83.33	71.43	80.00	40.00	40.00	16.67
Zonal Wind	**Direction**	**Jan**	**Feb**	**Mar**	**Apr**	**May**	**Jun**	**Jul**	**Aug**	**Sep**	**Oct**	**Nov**	**Dec**
	Westward	47.52	52.66	45.97	40.67	37.16	18.33	15.16	24.68	41.00	50.81	43.67	50.97
	Eastward	52.48	47.34	54.03	59.33	62.84	81.67	84.84	75.32	59.00	49.19	56.33	49.03

4.5 Summary and conclusions

This study presents a generic methodology for assessing the surface circulation over the northern shelf of the Gulf of Cádiz, based on satellite altimetry measurements and considering the effects of ageostrophic factors such as the bottom-drag and wind-driven circulation. The results from the applied methodology were validated against in-situ measurements over the GoC's shelf. After ensuring the good performance of the methods, the outputs were applied for a characterisation of the surface circulation over the GoC northern shelf, specifically, based on 4 years of high-resolution satellite altimetry data from Sentinel-3A and wind model data. The resulting spatiotemporal characteristics agree with

the general description of the literature, furthermore, the results bring additional details about the sea level variability along the GoC.

The following summary and conclusions are derived from the different sections and analyses.

The use of the ADT construction employing MDT, for computing surface geostrophic velocities, yielded the best correlation (0.77) and the lowest root mean square error (0.10 m/s) when compared to ADCP measurements from near-shore moorings. While geoid-based methods also provided reasonable results, they exhibited slightly lower correlation coefficients and larger RMSE values. This analysis is consistent with results from prior studies in other coastal regions, such as coastal areas over the Northwest Atlantic Shelf (Feng et al., 2023), emphasizing the importance of constructing ADT based on MDT for improved accuracy, particularly in areas near the coast. Thus, the present work provides valuable insights into the choice of ADT construction methods for enhancing the reliability of satellite-derived ocean current velocity data in coastal regions.

The comparison of surface bottom-drag corrected geostrophic (V_{gd}) and total (V_t) zonal current velocity estimates derived from different altimetry-based sources, including high-resolution along-track Sentinel-3A data (S3-V_{gd} and S3-V_t) and Copernicus Marine Environment Monitoring Service (CMEMS) products (C-V_{gd} and C-V_t), with in-situ ADCP measurements, revealed that the CMEMS's geostrophic current product (C-V_{gd}) had the poorest performance due to its limited resolution. However, when incorporating wind-driven current estimates (C-V_t), the product improved significantly, emphasizing the importance of wind on the surface circulation (Mulero-Martínez et al., 2021). The best results were achieved with high-resolution altimetry data (S3A-V_{gd} and S3A-V_t). S3A-V_{gd} showed a high correlation even without wind data, with a slight bias. S3-V_t, which included wind-driven current variability, outperformed all other products in terms of statistical metrics, accurately

capturing surface circulation direction most of the time. These findings encourage the use of high-resolution altimetry data as inputs for global products/models, even over coastal areas. In addition, they highlight the necessity of properly characterising local effects as wind-driven currents to reach a good understanding of the circulation over complex coastal areas.

The analysis of the surface circulation along the continental shelf aimed to assess the contributions of the bottom-friction corrected geostrophic (V_{gd}) and wind-driven (V_w) flow components to the total surface current (V_t). The results showed distinct characteristics over the different parts of the GoC. Tracks S3A-385 and 265, located in the western basin, suggested that positive (eastward) surface currents were predominantly driven by westerly winds, while only occasionally, westward flows coincided with easterly winds. These patterns suggest a higher control of the geostrophic component over westward flows, which are mainly driven by cross-shore and alongshore sea level gradients. In contrast, track S3A-322, located in the eastern basin, displayed a stronger correspondence between both V_{gd} and V_w with V_t. This fact suggests that both eastward and westward flows along the shelf in this region were primarily driven by favourable winds. These winds also induced cross-shelf sea level gradients through Ekman transport, enhancing the westward geostrophic component of the flow. Related to that, the analysis of ADT values along the whole basin showed the presence of ADT gradients, both along-shore and cross-shore, along the GoC's shelf, with a greater amplitude attributed to alongshore gradients. Notably, average alongshore ADT differences reached up to 4 cm between the easternmost and westernmost tracks. This discrepancy in ADT along the basin supports the fact that an imbalance in the along-shore pressure gradient would induce a westward flow during periods of weakened westerly winds and intensify under easterly wind conditions. These findings are consistent with the observed contributions of different components to the total shelf circulation over the different basins. They also corroborate previous studies suggesting that an alongshore pressure gradient is a primary driver of the coastal CCC under weak wind conditions. These findings are consistent

with the observed contributions of different components to the total shelf circulation over the different basins. They also corroborate previous studies suggesting that an alongshore pressure gradient is a primary driver of the coastal CCC under weak wind conditions (De Oliveira Júnior et al. 2021, 2022) and with the observations from (Sirviente et al. 2023) of sea surface height across-shore gradients directed seawards for days when the CCC in the GoC is present. in the GoC.

Regarding the spatiotemporal characterisation of the surface circulation, the results for the continental shelf of the western basin showed the occurrence of westward flows primarily in the northern half of the transect, aligning with the expected configuration of CCC events in this area. The southern half of the transect exhibited a higher occurrence of positive (eastward) flows, typically limited to latitudes up to 36.6ºN, consistent with the Gulf of Cadiz Current (GCC). These findings supported previous research that found negative flows extending toward the shelf break 60-70% of the time, with positive flows dominating further offshore. In contrast, results for the eastern basin displayed notably high-intensity negative flows, primarily in the southern section of the transect. These observations were in line with previous studies indicating that negative flows tend to occur mostly over the outer shelf and detached from the coast at the eastern basin (De Oliveira Júnior et al., 2022), as easterly winds channelled into the Gulf of Cadiz played a significant role in driving surface circulation. Across all four tracks, the eastward circulation dominated during the spring and summer months (May, June, July, and August). This eastward flow pattern correlated with the upwelling season in the Gulf of Cadiz, driven by westerly winds. In contrast, westward flows prevailed during the winter months (December to February). This westward flow predominance in winter might be associated with a higher occurrence of easterly winds and the rebalancing of the along-shore sea level gradient during relaxed upwelling conditions.

These results represent an advance in the use of satellite altimetry data for oceanographic applications in coastal areas where both the spatial and temporal variability of the circulation

are highly complex. Furthermore, considering the similarity of the results with previous studies based on in-situ systems that entail more costs for the user, such as HFR and ADCP, the use of altimetry data and publicly accessible wind models is an advantage for the evaluation of oceanographic characteristics in areas with difficult access or few resources, which can contribute to a better understanding and management of coastal areas.

4.6 Connecting Text

This chapter, relying upon the knowledge gathered from Chapters 2 and 3, fulfil the third objective of the thesis, *"to use satellite altimetry-derived absolute surface geostrophic current estimates, along with ageostrophic corrections to improve the knowledge of the surface circulation patterns in the Gulf of Cadiz"*. In addition, this chapter tries to increase the reliability of satellite altimetry measurements for understanding the circulation over coastal areas and provide solid insights about its potential for assessing fine-scale processes. The findings proved that the altimetry-based dataset provided valuable knowledge for the oceanographic community and agreed with previous results from site-based measurements. More generally, those results back up and reinforce the use of satellite altimetry measurements for filling the gap in those regions with the scarcity of site-measurements. Finally, Chapters 2, 3 and 4 are intended to fulfil the main aim of this thesis, which is to contribute to one of the challenges of altimetry in the present decade: to reach a level of understanding of the coastal zones dynamic similar to that of the open ocean.

Chapter 5

General Conclusions

- The methodology proposed for filtering high-resolution satellite altimetry measurements for the estimation of absolute surface geostrophic velocities is suitable for coastal areas such the Gulf of Cadiz, as proved with the comparison with HFR measurements.

- Satellite altimetry derived surface current velocities became more accurate when the ageostrophic signals were added. The main unsolved ageostrophic local factors affecting the surface circulation were successfully corrected by applying bottom-friction and wind-driven component estimates.

- Ageostrophic-corrected surface velocities from altimetry measurements can be used to detect surface structures and high-variability surface dynamics, including events with rapid changes in the current direction even for low velocities.

- HFR systems were found to be a solid tool for the validation of altimetry derived surface currents and the synergy between altimetry and HFR helps to unravel the effects of ageostrophic processes in coastal areas.

- The quality of the high-resolution S3A/B wind speed data satisfies the general mission requirements over the complex area affected by coastal-related processes which is the Gulf of Cadiz, as demonstrated from the comparison with in-situ measurements.

- The good quality and spatial coverage of satellite altimetry wind speed data allows the spatio-temporal validation/calibration of numerical weather prediction models such as the WRF model over complex coastal areas.

- The main limitations related to altimetry as a source of validation for NWP models are related to the fact that it is not possible to obtain the wind direction and that the

altimeters do not measure the variability in scales smaller than the across track footprint length.

- The resulting surface current velocities estimates from high-resolution along-track altimetry data, obtained by applying the proposed methodology for coastal areas, outperformed the equivalent generic CMEMS product when compared with in-situ ADCP measurements, reinforcing the idea of using an improved methodology for coastal areas along with higher resolution altimetry measurements.

- The analysis of surface circulation along the continental shelf of the Gulf of Cadiz showed distinct insights over the different basins regarding the contribution of the different surface current components.

- Over the western basin, positive (eastward) surface currents were predominantly driven by westerly winds, while only occasionally, westward flows coincided with easterly winds, suggesting a higher control of the geostrophic component over the westward flows, mainly driven by cross-shore and along-shore sea level gradients.

- Over the eastern basin, both eastward and westward flows along the shelf primarily driven by favourable winds. These winds also induced cross-shelf sea level gradients through Ekman transport, enhancing the westward geostrophic component of the flow.

- Along the Gulf of Cadiz both along-shore and cross-shore ADT gradients exist, with a greater significance attributed to the along-shore gradients. The observed unbalance in the along-shore pressure gradient would induce a westward flow during periods of weakened westerly winds and would intensify under easterly wind conditions.

- The shelf circulation over the northern shelf of the Gulf of Cadiz is dominated by eastward circulation during the spring and summer months (May to August),

correlated with the upwelling season in the Gulf of Cadiz. Westward flows prevailed during the winter months (December to February), associated with easterly winds and the rebalancing of the along-shore sea level gradient during relaxed upwelling conditions.

Chapter 6

Future Research Lines

The results obtained along this dissertation are consistent with the proposed hypothesis and the defined objectives. However, they provide a baseline for a new set of questions, along with the current state of the art, that motivate further research and activities to expand on the findings. The following details the primary areas for future exploration:

- To extend the different methodologies presented in this document to the whole satellite altimetry dataset, including past and present missions, for different coastal areas, in order to have a better perspective of the effects of climate change over the coastal circulation. In addition to explore the capabilities of new systems and missions (i.e.: SWOT) for assessing fine scale circulation over coastal areas.

- To encourage the use of high-resolution satellite altimetry data (from 20 Hz upwards) for assimilation on global and regional analysis/reanalysis systems applying retracking processes and corrections specific for coastal areas. In this regard, those systems could benefit from all the derived parameters from altimetry measurements, including wind speed, wave height, sea level and geostrophic circulation.

- To further analyse the Gulf of Cadiz circulation attending different factors, including local and remote, found to be critical for understanding the surface dynamic at different scales. For this, a complete dataset based on past and present satellite altimetry missions would play a key part to shed light not only into the surface circulation itself but into the role of sea level variability and related pressure gradients along the different basins connected with the GoC.

Chapter 7

References

Abdalla, S. (2012). Ku-Band Radar Altimeter Surface Wind Speed Algorithm. Marine Geodesy, 35(SUPPL. 1), 276–298. https://doi.org/10.1080/01490419.2012.718676

Abdalla, S., Abdeh Kolahchi, A., Ablain, M., Adusumilli, S., Aich Bhowmick, S., Alou-Font, E., Amarouche, L., Andersen, O. B., Antich, H., Aouf, L., Arbic, B., Armitage, T., Arnault, S., Artana, C., Aulicino, G., Ayoub, N., Badulin, S., Baker, S., Banks, C., … Zlotnicki, V. (2021). Altimetry for the future: Building on 25 years of progress. Advances in Space Research, 68(2), 319–363. https://doi.org/10.1016/j.asr.2021.01.022

Abdalla, S., Dinardo, S., Benveniste, J., & Janssen, P. A. E. M. (2018). Assessment of CryoSat-2 SAR mode wind and wave data. Advances in Space Research, 62(6), 1421–1433. https://doi.org/10.1016/j.asr.2018.01.044

Adame, J. A., Lope, L., Hidalgo, P. J., Sorribas, M., Gutiérrez-Álvarez, I., del Águila, A., Saiz-Lopez, A., & Yela, M. (2018). Study of the exceptional meteorological conditions, trace gases and particulate matter measured during the 2017 forest fire in Doñana Natural Park, Spain. Science of the Total Environment, 645(2), 710–720. https://doi.org/10.1016/j.scitotenv.2018.07.181

Aguiar, E., Mourre, B., Juza, M., Reyes, E., Hernández-Lasheras, J., Cutolo, E., Mason, E., & Tintoré, J. (2020). Multi-platform model assessment in the Western Mediterranean Sea: impact of downscaling on the surface circulation and mesoscale activity. Ocean Dynamics, 70(2), 273–288. https://doi.org/10.1007/s10236-019-01317-8

Aldarias, A., Gomez-Enri, J., Laiz, I., Tejedor, B., Vignudelli, S., & Cipollini, P. (2020a). Validation of Sentinel-3A SRAL Coastal Sea Level Data at High Posting Rate: 80 Hz. IEEE Transactions on Geoscience and Remote Sensing, 58(6), 3809–3821. https://doi.org/10.1109/TGRS.2019.2957649

Amante, C., & Eakins, B. W. (2009). {ETOPO}1 Global Relief Model converted to {PanMap} layer format. NOAA-National Geophysical Data Center.

Ambar, I., & Howe, M. R. (1979). Observations of the mediterranean outflow-II the deep circulation in the vicinity of the gulf of cadiz. Deep Sea Research Part A, Oceanographic Research Papers. https://doi.org/10.1016/0198-0149(79)90096-7

Andersen, O. B., & Scharroo, R. (2011). Range and geophysical corrections in coastal regions: And implications for mean sea surface determination. In Coastal Altimetry. https://doi.org/10.1007/978-3-642-12796-0_5

Andersen, O., Knudsen, P., & Stenseng, L. (2018). A New DTU18 MSS Mean Sea Surface – Improvement from SAR Altimetry. 25 Years of Progress in Radar Altimetry Symposium, Portugal.

Arasa, R., Porras, I., Domingo-Dalmau, A., Picanyol, M., Codina, B., González, M. Á., & Piñón, J. (2016). Defining a Standard Methodology to Obtain Optimum WRF Configuration for Operational Forecast: Application over the Port of Huelva (Southern Spain). Atmospheric and Climate Sciences, 06(02), 329–350. https://doi.org/10.4236/acs.2016.62028

Astudillo, O., Dewitte, B., Mallet, M., Frappart, F., Rutllant, J. A., Ramos, M., Bravo, L., Goubanova, K., & Illig, S. (2017). Surface winds off Peru-Chile: Observing closer to the coast from radar altimetry. Remote Sensing of Environment, 191, 179–196. https://doi.org/10.1016/j.rse.2017.01.010

Barale, V., Gower, J. F. R., & Alberotanza, L. (2010). Oceanography from space: Revisited. Oceanography from Space: Revisited, 1–375. https://doi.org/10.1007/978-90-481-8681-5

Bhowmick, S. A., Modi, R., Sandhya, K. G., Seemanth, M., Balakrishnan Nair, T. M., Kumar, R., & Sharma, R. (2015). Analysis of SARAL/AltiKa Wind and Wave over Indian Ocean and its Real-time Application in Wave Forecasting System at ISRO. Marine Geodesy, 38(July 2014), 396–408. https://doi.org/10.1080/01490419.2015.1006380

Bouffard, J., Naeije, M., Banks, C. J., Calafat, F. M., Cipollini, P., Snaith, H. M., Webb, E., Hall, A., Mannan, R., Féménias, P., & Parrinello, T. (2018). CryoSat ocean product quality status and future evolution. Advances in Space Research. https://doi.org/10.1016/j.asr.2017.11.043

Bouffard, J., Pascual, A., Ruiz, S., Faugère, Y., & Tintoré, J. (2010a). Coastal and mesoscale dynamics characterization using altimetry and gliders: A case study in the Balearic Sea. Journal of Geophysical Research: Oceans, 115(10). https://doi.org/10.1029/2009JC006087

Bowden, K. F. (1983). Physical oceanography of coastal waters. E. Horwood. https://books.google.com/books/about/Physical_Oceanography_of_Coastal_Waters.html?hl=es&id=UppNAQAAIAAJ

Brandt, P., Rubino, A., Sein, D. V., Baschek, B., Izquierdo, A., & Backhaus, J. O. (2004). Sea level variations in the western Mediterranean studied by a numerical tidal model of the Strait of Gibraltar. Journal of Physical Oceanography, 34(2), 433–443. https://doi.org/10.1175/1520-0485(2004)034<0433:SLVITW>2.0.CO;2

Calafat, F. M., Cipollini, P., Bouffard, J., Snaith, H., & Féménias, P. (2017). Evaluation of new CryoSat-2 products over the ocean. Remote Sensing of Environment, 191, 131–144. https://doi.org/10.1016/J.RSE.2017.01.009

Carvalho, D., Rocha, A., Gómez-Gesteira, M., & Santos, C. (2012). A sensitivity study of the WRF model in wind simulation for an area of high wind energy. Environmental Modelling and Software, 33, 23–34. https://doi.org/10.1016/j.envsoft.2012.01.019

Carvalho, D., Rocha, A., Gómez-Gesteira, M., & Silva Santos, C. (2014). Offshore wind energy resource simulation forced by different reanalyses: Comparison with observed data in the Iberian Peninsula. Applied Energy, 134, 57–64. https://doi.org/10.1016/j.apenergy.2014.08.018

Carvalho, D., Rocha, A., Gómez-Gesteira, M., & Silva Santos, C. (2017). Offshore winds and wind energy production estimates derived from ASCAT, OSCAT, numerical weather prediction models and buoys – A comparative study for the Iberian Peninsula Atlantic coast. Renewable Energy. https://doi.org/10.1016/j.renene.2016.10.063

Cerralbo, P., Grifoll, M., Moré, J., Bravo, M., Sairouní Afif, A., & Espino, M. (2015). Wind variability in a coastal area (Alfacs Bay, Ebro River delta). Advances in Science and Research, 12(1), 11–21. https://doi.org/10.5194/asr-12-11-2015

Chelton, D. B. (2001). Satellite Altimetry. In Academic Press (Ed.), Satellite Altimetry And Earth Sciences: A Handbook Of Techniques And Applications (Vol. 69, pp. 1–131).

Cipollini, P. (2010). The role of altimetry in coastal observing systems. Oceanography, 23(4), 150–159.

Cipollini, P., Beneviste, J., Bouffard, J., Emery, W., Fenoglio-Marc, L., Gommenginger, C., … Zavala-Garay, J. (2010). The role of altimetry in coastal observing systems.

Cleveland, W. S., & Devlin, S. J. (1988). Locally weighted regression: An approach to regression analysis by local fitting. Journal of the American Statistical Association, 83(403), 596–610. https://doi.org/10.1080/01621459.1988.10478639

Cosoli, S., & Bolzon, G. (2015). Accuracy of surface current mapping from High-Frequency (HF) ocean radars. Bollettino Di Geofisica Teorica Ed Applicata, 56(1), 55–70. https://doi.org/10.4430/bgta0132

Cosoli, S., Mazzoldi, A., & Gačić, M. (2010). Validation of surface current measurements in the northern Adriatic Sea from high-frequency radars. Journal of Atmospheric and Oceanic Technology. https://doi.org/10.1175/2009JTECHO680.1

Criado-Aldeanueva, F., Garcia-Lafuente, J., Navarro, G., & Ruiz, J. (2009). Seasonal and interannual variability of the surface circulation in the eastern Gulf of Cadiz (SW Iberia). Journal of Geophysical Research: Oceans, 114(1), 0–11. https://doi.org/10.1029/2008JC005069

Criado-Aldeanueva, F., García-Lafuente, J., Vargas, J. M., Del Río, J., Vázquez, A., Reul, A., & Sánchez, A. (2006). Distribution and circulation of water masses in the Gulf of Cadiz from in situ observations. Deep-Sea Research Part II: Topical Studies in Oceanography, 53(11–13), 1144–1160. https://doi.org/10.1016/j.dsr2.2006.04.012

De Kloe, J., Stoffelen, A., & Verhoef, A. (2017). Improved Use of Scatterometer Measurements by Using Stress-Equivalent Reference Winds. IEEE Journal of Selected Topics in Applied Earth Observations and Remote Sensing, 10(5), 2340–2347. https://doi.org/10.1109/JSTARS.2017.2685242

De Oliveira Júnior, L., Garel, E., & Relvas, P. (2021). The structure of incipient coastal counter currents in South Portugal as indicator of their forcing agents. Journal of Marine Systems, 214(October 2020), 103486. https://doi.org/10.1016/j.jmarsys.2020.103486

De Oliveira Júnior, L., Relvas, P., & Garel, E. (2022). Kinematics of surface currents at the northern margin of the Gulf of Cádiz. Ocean Science, 18(4), 1183–1202. https://doi.org/10.5194/os-18-1183-2022

Deng, X., Featherstone, W. E., Hwang, C., & Berry, P. A. M. (2002). Estimation of contamination of ERS-2 and POSEIDON satellite radar altimetry close to the coasts of Australia. Marine Geodesy, 25(4), 249–271. https://doi.org/10.1080/01490410214990

Dinardo, S., Fenoglio-Marc, L., Becker, M., Scharroo, R., Fernandes, M. J., Staneva, J., Grayek, S., & Benveniste, J. (2021). A RIP-based SAR retracker and its application in North East Atlantic with Sentinel-3. Advances in Space Research, 68(2), 892–929. https://doi.org/10.1016/j.asr.2020.06.004

Dinardo, S., Fenoglio-Marc, L., Buchhaupt, C., Becker, M., Scharroo, R., Joana Fernandes, M., & Benveniste, J. (2018). Coastal SAR and PLRM altimetry in German Bight and West Baltic Sea. Advances in Space Research, 62(6), 1371–1404. https://doi.org/10.1016/j.asr.2017.12.018

Drinkwater, M. R., Francis, R., Ratier, G., & Wingham, D. J. (2004). The European Space Agency's Earth Explorer Mission CryoSat: Measuring variability in the cryosphere. Annals of Glaciology. https://doi.org/10.3189/172756404781814663

Emeis, S., & Turk, M. (2007). Comparison of Logarithmic Wind Profiles and Power Law Wind Profiles and their Applicability for Offshore Wind Profiles. Wind Energy, December, 61–64. https://doi.org/10.1007/978-3-540-33866-6_11

Feng, H., Egido, A., Vandemark, D., & Wilkin, J. (2022). Exploring the potential of Sentinel-3 delay Doppler altimetry for enhanced detection of coastal currents along the Northwest Atlantic shelf. Advances in Space Research, 71(1), 997–1016. https://doi.org/10.1016/j.asr.2022.09.011

Fenoglio-Marc, L., Dinardo, S., Scharroo, R., Roland, A., Dutour Sikiric, M., Lucas, B., Becker, M., Benveniste, J., & Weiss, R. (2015). The German Bight: A validation of CryoSat-2 altimeter data in SAR mode. Advances in Space Research, 55(11), 2641–2656. https://doi.org/10.1016/J.ASR.2015.02.014

Folkard, A. M., Davies, P. A., Fiúza, A. F. G., & Ambar, I. (1997). Remotely sensed sea surface thermal patterns in the gulf of-cadiz and the strait of Gibraltar: Variability, correlations, and relationships with the surface wind field. Journal of Geophysical Research C: Oceans, 102(C3), 5669–5683. https://doi.org/10.1029/96JC02505

Fu, L. L., Chelton, D. B., Le Traon, P. Y., & Morrow, R. (2010). Eddy dynamics from satellite altimetry. Oceanography, 23(4), 15–25. https://doi.org/10.5670/OCEANOG.2010.02

Fu, L.-L., Chelton, D., & Zlotnicki, V. (1988). Satellite Altimetry: Observing Ocean Variability From Space. Oceanography. https://doi.org/10.5670/oceanog.1988.01

García-Lafuente, J., Delgado, J., Criado-Aldeanueva, F., Bruno, M., del Río, J., & Miguel Vargas, J. (2006). Water mass circulation on the continental shelf of the Gulf of Cádiz. Deep-Sea Research Part II: Topical Studies in Oceanography, 53(11–13), 1182–1197. https://doi.org/10.1016/j.dsr2.2006.04.011

Garel, E., Laiz, I., Drago, T., & Relvas, P. (2016a). Characterisation of coastal counter-currents on the inner shelf of the Gulf of Cadiz. Journal of Marine Systems, 155, 19–34. https://doi.org/10.1016/j.jmarsys.2015.11.001

Godin, G., & Martinez, A. (1994). Friction on the Propagation O F Tides in a Channel. Continental Shelf Research, 14(7), 723–748.

Gómez-Enri, J., González, C. J., Passaro, M., Vignudelli, S., Álvarez, O., Cipollini, P., Mañanes, R., Bruno, M., López-Carmona, M. P., & Izquierdo, A. (2019). Wind-induced cross-strait sea level variability in the Strait of Gibraltar from coastal altimetry and in-situ measurements. Remote Sensing of Environment, 221(October 2018), 596–608. https://doi.org/10.1016/j.rse.2018.11.042

Gómez-Enri, J., Vignudelli, S., Cipollini, P., Coca, J., & González, C. J. (2018). Validation of CryoSat-2 SIRAL sea level data in the eastern continental shelf of the Gulf of Cadiz (Spain). Advances in Space Research, 62(6), 1405–1420. https://doi.org/10.1016/j.asr.2017.10.042

Gómez-Enri, J., Vignudelli, S., Quartly, G. D., Gommenginger, C. P., Cipollini, P., Challenor, P. G., & Benveniste, J. (2010). Modeling Envisat RA-2 waveforms in the coastal zone: Case study of calm water contamination. IEEE Geoscience and Remote Sensing Letters, 7(3), 474–478. https://doi.org/10.1109/LGRS.2009.2039193

Gommenginger, C., Thibaut, P., Fenoglio-Marc, L., Quartly, G., Deng, X., Gómez-Enri, J., Challenor, P., & Gao, Y. (2011). Retracking Altimeter Waveforms Near the Coasts. Coastal Altimetry, 61–101. https://doi.org/10.1007/978-3-642-12796-0_4

Han, W., Stammer, D., Thompson, P., Ezer, T., Palanisamy, H., Zhang, X., Domingues, C. M., Zhang, L., & Yuan, D. (2019). Impacts of Basin-Scale Climate Modes on Coastal Sea Level: a Review. In Surveys in Geophysics. https://doi.org/10.1007/s10712-019-09562-8

Handoko, E. Y., Fernandes, M. J., & Lázaro, C. (2017). Assessment of altimetric range and geophysical corrections and mean sea surface models-Impacts on sea level variability around the Indonesian seas. Remote Sensing. https://doi.org/10.3390/rs9020102

Hernández-Ceballos, M. A., Adame, J. A., Bolívar, J. P., & De la Morena, B. A. (2013). A mesoscale simulation of coastal circulation in the Guadalquivir valley (southwestern

Iberian Peninsula) using the WRF-ARW model. Atmospheric Research, 124, 1–20. https://doi.org/10.1016/j.atmosres.2012.12.002

Hidalgo, P., & Gallego, D. (2019). A historical climatology of the easterly winds in the strait of Gibraltar. Atmosfera, 32(3), 181–195. https://doi.org/10.20937/ATM.2019.32.03.02

Kantha, L. H., & Clayson, C. A. (2013). Numerical Models of Oceans and Oceanic Processes. In International Geophysics Series. https://doi.org/10.1016/S0074-6142(00)80027-3

Kelly, K. A., Dickinson, S., & Yu, Z. (1999). NSCAT tropical wind stress maps: Implications for improving ocean modeling. Journal of Geophysical Research: Oceans, 104(C5), 11291–11310. https://doi.org/10.1029/1998JC900036

Keulegan, G. H. (1951). Wind tides in small closed channels. Journal of Research of the National Bureau of Standards. https://doi.org/10.6028/jres.046.041

Kim, S. Y., Cornuelle, B. D., & Terrill, E. J. (2010). Decomposing observations of high-frequency radar-derived surface currents by their forcing mechanisms: Locally wind-driven surface currents. Journal of Geophysical Research: Oceans. https://doi.org/10.1029/2010JC006223

Knudsen, P., Andersen, O., & Maximenko, N. (2016). The updated geodetic mean dynamic topography model - DTU15MDT. EGUGA, 18, EPSC2016-5052. https://ui.adsabs.harvard.edu/abs/2016EGUGA..18.5052K/abstract

Laiz, I., Gómez-Enri, J., Tejedor, B., Aboitiz, A., & Villares, P. (2013). Seasonal sea level variations in the gulf of Cadiz continental shelf from in-situ measurements and satellite altimetry. Continental Shelf Research, 53, 77–88. https://doi.org/10.1016/j.csr.2012.12.008

Laiz, I., Plecha, S., Teles-Machado, A., González-Ortegón, E., Sánchez-Quiles, D., Cobelo-García, A., Roque, D., Peliz, A., Sánchez-Leal, R. F., & Tovar-Sánchez, A. (2019). The role of the Gulf of Cadiz circulation in the redistribution of trace metals between the Atlantic Ocean and the Mediterranean Sea. Science of the Total Environment. https://doi.org/10.1016/j.scitotenv.2019.134964

Li, H., Claremar, B., Wu, L., Hallgren, C., Körnich, H., Ivanell, S., & Sahlée, E. (2021). A sensitivity study of the WRF model in offshore wind modeling over the Baltic Sea. Geoscience Frontiers, 12(6), 101229. https://doi.org/10.1016/j.gsf.2021.101229

Lipa, B., Nyden, B., Ullman, D. S., & Terrill, E. (2006). SeaSonde radial velocities: Derivation and internal consistency. IEEE Journal of Oceanic Engineering. https://doi.org/10.1109/JOE.2006.886104

Liu, Y., Weisberg, R. H., Vignudelli, S., & Mitchum, G. T. (2014). Evaluation of altimetry-derived surface current products using Lagrangian drifter trajectories in the eastern Gulf of Mexico. Journal of Geophysical Research: Oceans, 119(5), 2827–2842. https://doi.org/10.1002/2013JC009710

Lorente, P., Piedracoba, S., & Fanjul, E. A. (2015). Validation of high-frequency radar ocean surface current observations in the NW of the Iberian Peninsula. Continental Shelf Research. https://doi.org/10.1016/j.csr.2014.11.001

Lu, Y., Zhang, B., Perrie, W., Mouche, A., Li, X., & Wang, H. (2018). A C-band Geophysical Model Function for Determining Coastal Wind Speed Using Synthetic Aperture Radar. Progress in Electromagnetics Research Symposium, 2018-Augus(7), 1440–1446. https://doi.org/10.23919/PIERS.2018.8598163

Madsen, O. L. (1977). A realistic model of the wind-induced Ekman boundary layer. In Journal of Physical Oceanography. https://doi.org/10.1175/1520-0485(1977)007<0248:ARMOTW>2.0.CO;2

Mandal, S., Sil, S., Pramanik, S., Arunraj, K. S., & Jena, B. K. (2019). Characteristics and evolution of a coastal mesoscale eddy in the Western Bay of Bengal monitored by high-frequency radars. Dynamics of Atmospheres and Oceans. https://doi.org/10.1016/j.dynatmoce.2019.101107

Manso-Narvarte, I., Caballero, A., Rubio, A., Dufau, C., & Birol, F. (2018). Joint analysis of coastal altimetry and high-frequency (HF) radar data: Observability of seasonal and mesoscale ocean dynamics in the Bay of Biscay. Ocean Science, 14(5), 1265–1281. https://doi.org/10.5194/os-14-1265-2018

Marechal, G., & Ardhuin, F. (2022). Surface Currents and Significant Wave Height Gradients: Matching Numerical Models and High-Resolution Altimeter Wave Heights

in the Agulhas Current Region. Journal of Geophysical Research: Oceans. https://doi.org/10.1002/ESSOAR.10505343.1

Marta-Almeida, M., Teixeira, J. C., Carvalho, M. J., Melo-Gonçalves, P., & Rocha, A. M. (2016). High resolution WRF climatic simulations for the Iberian Peninsula: Model validation. Physics and Chemistry of the Earth, 94, 94–105. https://doi.org/10.1016/j.pce.2016.03.010

Mears, C. A., Scott, J., Wentz, F. J., Ricciardulli, L., Leidner, S. M., Hoffman, R., & Atlas, R. (2019). A Near-Real-Time Version of the Cross-Calibrated Multiplatform (CCMP) Ocean Surface Wind Velocity Data Set. Journal of Geophysical Research: Oceans, 124(10), 6997–7010. https://doi.org/10.1029/2019JC015367

Meloni, M., Bouffard, J., Doglioli, A. M., Petrenko, A. A., & Valladeau, G. (2019). Toward science-oriented validations of coastal altimetry: Application to the Ligurian Sea. Remote Sensing of Environment, 224(February), 275–288. https://doi.org/10.1016/j.rse.2019.01.028

Morrow, R., Carret, A., Birol, F., Nino, F., Valladeau, G., Boy, F., Bachelier, C., & Zakardjian, B. (2017). Observability of fine-scale ocean dynamics in the northwestern Mediterranean Sea. Ocean Science, 13(1), 13–29. https://doi.org/10.5194/OS-13-13-2017

Morrow, R., & Le Traon, P. Y. (2012). Recent advances in observing mesoscale ocean dynamics with satellite altimetry. Advances in Space Research. https://doi.org/10.1016/j.asr.2011.09.033

Mulero-Martínez, R., Gómez-Enri, J., Mañanes, R., & Bruno, M. (2021). Assessment of near-shore currents from CryoSat-2 satellite in the Gulf of Cádiz using HF radar-derived current observations. Remote Sensing of Environment, 256(June 2020). https://doi.org/10.1016/j.rse.2021.112310

Mulero-Martinez, R., Román-Cascón, C., Mañanes, R., Izquierdo, A., Bruno, M., & Gómez-Enri, J. (2022). The Use of Sentinel-3 Altimetry Data to Assess Wind Speed from the Weather Research and Forecasting (WRF) Model: Application over the Gulf of Cadiz. Remote Sensing 2022, Vol. 14, Page 4036, 14(16), 4036. https://doi.org/10.3390/RS14164036

Navarro, G., Escudier, R., Pascual, A., Caballero, I., & Vázquez, A. (2013). Singular Value Decomposition of Ocean Surface Chlorophyll and Sea Level Anomalies in the Gulf of Cadiz (South-Western Iberian Peninsula). November 2014.

Neumann, B., Vafeidis, A. T., Zimmermann, J., & Nicholls, R. J. (2015). Future coastal population growth and exposure to sea-level rise and coastal flooding - A global assessment. PLoS ONE. https://doi.org/10.1371/journal.pone.0118571

Ngan, F., Kim, H., Lee, P., Al-Wali, K., & Dornblaser, B. (2013). A study of nocturnal surface wind speed overprediction by the WRF-ARW model in Southeastern Texas. Journal of Applied Meteorology and Climatology, 52(12), 2638–2653. https://doi.org/10.1175/JAMC-D-13-060.1

Ortega, M., Sánchez, E., Gutiérrez, C., Molina, M. O., & López-Franca, N. (2023). Regional winds over the Iberian Peninsula (Cierzo, Levante and Poniente) from high-resolution COSMO-REA6 reanalysis. International Journal of Climatology, 43(2), 1016–1033. https://doi.org/10.1002/joc.7860

Passaro, M., Cipollini, P., Vignudelli, S., Quartly, G. D., & Snaith, H. M. (2014). ALES: A multi-mission adaptive subwaveform retracker for coastal and open ocean altimetry. Remote Sensing of Environment, 145, 173–189. https://doi.org/10.1016/j.rse.2014.02.008

Passaro, M., Müller, F. L., Abulaitijiang, A., Andersen, O. B., Dettmering, D., Høyer, J. L., Johansson, M., Oelsmann, J., Rautiainen, L., Ringgaard, I. M., Rinne, E., Särkkä, J., Scarrott, R., Schwatke, C., Seitz, F., Madsen, K. S., Tuomi, L., Ambrozio, A., Restano, M., & Benveniste, J. (2020). Using the Baltic Sea to advance algorithms to extract altimetry-derived sea-level data from complex coastal areas, featuring seasonal sea-ice. EGU2020. https://doi.org/10.5194/EGUSPHERE-EGU2020-6773

Paulson (1970). The Mathematical Representation of Wind Speed and Temperature Profiles in the Unstable Atmospheric Surface Layer. Journal of Applied Meteorology, 9, 857–861.

Pavlis, N. K., Holmes, S. A., Kenyon, S. C., & Factor, J. K. (2008). An Earth Gravitational Model to Degree 2160: EGM2008. Geophysical Research Abstracts, 10, 2008–01891.

Peliz, A., Dubert, J., Marchesiello, P., & Teles-Machado, A. (2007). Surface circulation in the Gulf of Cadiz: Model and mean flow structure. Journal of Geophysical Research: Oceans. https://doi.org/10.1029/2007JC004159

Peliz, A., Marchesiello, P., Santos, A. M. P., Dubert, J., Teles-Machado, A., Marta-Almeida, M., & Le Cann, B. (2009). Surface circulation in the Gulf of Cadiz: 2. Inflow-outflow coupling and the Gulf of Cadiz slope current. Journal of Geophysical Research: Oceans. https://doi.org/10.1029/2008JC004771

Peña, A., Gryning, S. E., & Hasager, C. B. (2008). Measurements and modelling of the wind speed profile in the marine atmospheric boundary layer. Boundary-Layer Meteorology, 129(3), 479–495. https://doi.org/10.1007/s10546-008-9323-9

Powell, B. S., & Leben, R. R. (2004). An optimal filter for geostrophic mesoscale currents from along-track satellite altimetry. Journal of Atmospheric and Oceanic Technology, 21(10), 1633–1642. https://doi.org/10.1175/1520-0426(2004)021<1633:AOFFGM>2.0.CO;2

Powell, M. D., Vickery, P. J., & Reinhold, T. A. (2003). Reduced drag coefficient for high wind speeds in tropical cyclones. Nature, 422(6929), 279–283. https://doi.org/10.1038/nature01481

Powers, J. G., Klemp, J. B., Skamarock, W. C., Davis, C. A., Dudhia, J., Gill, D. O., … Duda, M. G. (2017). The Weather Research and Forecasting Model: Overview, System Efforts, and Future Directions. Bulletin of the American Meteorological Society, 98(8), 1717–1737. https://doi.org/10.1175/BAMS-D-15-00308.1

Quartly, G. D., Nencioli, F., Raynal, M., Bonnefond, P., Garcia, P. N., Garcia-Mondéjar, A., de la Cruz, A. F., Cretaux, J. F., Taburet, N., Frery, M. L., Cancet, M., Muir, A., Brockley, D., Mcmillan, M., Abdalla, S., Fleury, S., Cadier, E., Gao, Q., Escorihuela, M. J., … Lucas, B. (2020). The roles of the S3MPC: Monitoring, validation and evolution of sentinel-3 altimetry observations. Remote Sensing, 12(11). https://doi.org/10.3390/rs12111763

Raney, R. K. (2012). CryoSat SAR-mode looks revisited. IEEE Geoscience and Remote Sensing Letters, 9(3), 393–397. https://doi.org/10.1109/LGRS.2011.2170052

Relvas, P., & Barton, E. D. (2002). Mesoscale patterns in the Cape São Vicente (Iberian Peninsula) upwelling region. Journal of Geophysical Research: Oceans, 107(C10), 28–1. https://doi.org/10.1029/2000JC000456

Rieu, P., Moreau, T., Cadier, E., Raynal, M., Clerc, S., Donlon, C., Borde, F., Boy, F., & Maraldi, C. (2021). Exploiting the Sentinel-3 tandem phase dataset and azimuth oversampling to better characterize the sensitivity of SAR altimeter sea surface height to long ocean waves. Advances in Space Research, 67(1), 253–265. https://doi.org/10.1016/J.ASR.2020.09.037

Rio, M. H., Mulet, S., & Picot, N. (2014). Beyond GOCE for the ocean circulation estimate: Synergetic use of altimetry, gravimetry, and in situ data provides new insight into geostrophic and Ekman currents. Geophysical Research Letters, 41(24), 8918–8925. https://doi.org/10.1002/2014GL061773

Roesler, C. J., Emery, W. J., & Kim, S. Y. (2013). Evaluating the use of high-frequency radar coastal currents to correct satellite altimetry. Journal of Geophysical Research: Oceans, 118(7), 3240–3259. https://doi.org/10.1002/JGRC.20220

Román-Cascón, C., Lothon, M., Lohou, F., Hartogensis, O., Vila-Guerau De Arellano, J., Pino, D., Yagüe, C., & Pardyjak, E. R. (2021). Surface representation impacts on turbulent heat fluxes in the Weather Research and Forecasting (WRF) model (v.4.1.3). Geoscientific Model Development, 14(6), 3939–3967. https://doi.org/10.5194/gmd-14-3939-2021

Ross, T., Garrett, C., & Traon, P. Y. Le. (2000). Western Mediterranean sea-level rise: Changing exchange flow through the strait of Gibraltar. Geophysical Research Letters, 27(18), 2949–2952. https://doi.org/10.1029/2000GL011653

Sánchez, R. F., Mason, E., Relvas, P., da Silva, A. J., & Peliz, Á. (2006). On the inner-shelf circulation in the northern Gulf of Cádiz, southern Portuguese shelf. Deep Sea Research Part II: Topical Studies in Oceanography, 53(11–13), 1198–1218. https://doi.org/10.1016/J.DSR2.2006.04.002

Sánchez, R. F., & Relvas, P. (2003). Spring-summer climatological circulation in the upper layer in the region of Cape St. Vincent, Southwest Portugal. ICES Journal of Marine Science. https://doi.org/10.1016/S1054-3139(03)00137-1

Sirviente, S., Bolado-Penagos, M., Gomiz-Pascual, J. J., Romero-Cózar, J., Vázquez, A., & Bruno, M. (2023). Dynamics of Atmospheric-Driven Surface Currents on The Gulf of Cadiz Continental Shelf and its link with The Strait of Gibraltar and The Western Alboran Sea. Progress in Oceanography, 219. https://doi.org/10.1016/j.pocean.2023.103175

Skamarock, W. C., Klemp, J. B., Dudhia, J., Gill, D. O., Zhiquan, L., Berner, J., Wang, W., Powers, J. G., Duda, M. G., Barker, D. M., & Huang, X.-Y. (2019). A Description of the Advanced Research WRF Model Version 4. NCAR Technical Note NCAR/TN-475+STR, 145. http://library.ucar.edu/research/publish-technote

Srinivasan, M., & Tsontos, V. (2023). Satellite Altimetry for Ocean and Coastal Applications: A Review. Remote Sensing 2023, Vol. 15, Page 3939, 15(16), 3939. https://doi.org/10.3390/RS15163939

Stanichny, S. V., Kubryakov, A. A., & Soloviev, D. M. (2016). Parameterization of surface wind-driven currents in the Black Sea using drifters, wind, and altimetry data. Ocean Dynamics, 66(1), 1–10. https://doi.org/10.1007/S10236-015 0901-3/FIGURES/7

Stewart, R. H. (1997). Introduction To Physical Oceanography.

Stoffelen, A. (1998). Toward the true near-surface wind speed: Error modeling and calibration using triple collocation. Journal of Geophysical Research: Oceans, 103(3334), 7755–7766. https://doi.org/10.1029/97jc03180

Teles-Machado, A., Peliz, Á., Dubert, J., & Sánchez, R. F. (2007). On the onset of the Gulf of Cadiz Coastal Countercurrent. Geophysical Research Letters, 34(12), 1–5. https://doi.org/10.1029/2007GL030091

Troupin, C., Pascual, A., Valladeau, G., Pujol, I., Lana, A., Heslop, E., Ruiz, S., Torner, M., Picot, N., & Tintoré, J. (2015). Illustration of the emerging capabilities of SARAL/AltiKa in the coastal zone using a multi-platform approach. Advances in Space Research, 55(1), 51–59. https://doi.org/10.1016/J.ASR.2014.09.011

Vignudelli, S., Kostianoy, A. G., Cipollini, P., & Benveniste, J. (2011). Coastal altimetry. In Coastal Altimetry. https://doi.org/10.1007/978-3-642-12796-0

Vignudelli, S., Scozzari, A., Abileah, R., Gómez-Enri, J., Benveniste, J., & Cipollini, P. (2019). Water surface elevation in coastal and inland waters using satellite radar

altimetry. In Extreme Hydroclimatic Events and Multivariate Hazards in a Changing Environment. https://doi.org/10.1016/b978-0-12-814899-0.00004-3

Vogelzang, J., Stoffelen, A., Lindsley, R. D., Verhoef, A., & Verspeek, J. (2017). The ASCAT 6.25-km Wind Product. IEEE Journal of Selected Topics in Applied Earth Observations and Remote Sensing, 10(5), 2321–2331. https://doi.org/10.1109/JSTARS.2016.2623862

Weber, J. E. (1983). Steady Wind- and Wave-Induced Currents in the Open Ocean. Journal of Physical Oceanography. https://doi.org/10.1175/1520-0485(1983)013<0524:swawic>2.0.co;2

Wingham, D. J., Francis, C. R., Baker, S., Bouzinac, C., Brockley, D., Cullen, R., de Chateau-Thierry, P., Laxon, S. W., Mallow, U., Mavrocordatos, C., Phalippou, L., Ratier, G., Rey, L., Rostan, F., Viau, P., & Wallis, D. W. (2006). CryoSat: A mission to determine the fluctuations in Earth's land and marine ice fields. Advances in Space Research. https://doi.org/10.1016/j.asr.2005.07.027

Witter, D. L., & Chelton, D. B. (1991). A Geosat altimeter wind speed algorithm and a method for altimeter wind speed algorithm development. Journal of Geophysical Research, 96(C5), 8853–8860. https://doi.org/10.1029/91JC00414

Wu, J. (1975). Wind-induced drift currents. Journal of Fluid Mechanics, 68(1), 49–70. https://doi.org/10.1017/S0022112075000687

Wyatt, L. R. (2014). High frequency radar applications in coastal monitoring, planning and engineering. Australian Journal of Civil Engineering. https://doi.org/10.7158/C13-023.2014.12.1

Yang, J., Zhang, J., Jia, Y., Fan, C., & Cui, W. (2020). Validation of Sentinel-3A/3B and Jason-3 altimeter wind speeds and significant wave heights using buoy and ASCAT data. Remote Sensing, 12(13). https://doi.org/10.3390/rs12132079

Annex

Original versions of the different manuscripts already published.

Universidad de Cádiz
Escuela de Doctorado UCA
Edificio Hospital Real
Plaza Falla nº 8
11003 Cádiz
http://escueladoctoral.uca.es/
escuela.doctoral@uca.es

Modelo de consentimiento de coautores para inclusión de trabajos en la modalidad de tesis por compendio de publicaciones

Los investigadores/as:

Gómez-Enri, J., Mañanes, R., y Bruno, M., como coautores/as del artículo/libro/capítulo de libro:

Assessment of near-shore currents from CryoSat-2 satellite in the Gulf of Cadiz using HF radar-derived current observations, publicado en *Remote Sensing of Environment*, por la presente dan su consentimiento para que esta publicación sea incorporada a la tesis doctoral titulada *Coastal surface circulation of the Gulf of Cadiz from satellite altimetry measurements* cuyo autor/a es Roberto Mulero Martínez, renunciando a presentar estos resultados como parte de otra tesis doctoral en cualquier Universidad.

En Cádiz, a 06 de marzo de 2024

Fdo. Jesús Gómez Enri

GOMEZ ENRI JESUS - 34048944C

Firmado digitalmente por GOMEZ ENRI JESUS - 34048944C
Nombre de reconocimiento (DN): cn=GOMEZ ENRI JESUS - 34048944C, sn=GOMEZ ENRI, givenName=JESUS, c=ES, serialNumber=IDCES-34048944C
Fecha: 2024.03.07 15:06:40 +01'00'

Fdo. Rafael Mañanes Salinas

Firmado por MAÑANES SALINAS RAFAEL - ***0751** el día 07/03/2024 con un certificado emitido por AC FNMT Usuarios

Fdo. Miguel Bruno Mejías

BRUNO MEJIAS MIGUEL - 42824979Z

Firmado digitalmente por BRUNO MEJIAS MIGUEL - 42824979Z
Nombre de reconocimiento (DN): c=ES, serialNumber=IDCES-42824979Z, givenName=MIGUEL, sn=BRUNO MEJIAS, cn=BRUNO MEJIAS MIGUEL - 42824979Z
Fecha: 2024.03.06 13:59:47 +01'00'

Remote Sensing of Environment 256 (2021) 112310

Contents lists available at ScienceDirect

Remote Sensing of Environment

journal homepage: www.elsevier.com/locate/rse

Assessment of near-shore currents from CryoSat-2 satellite in the Gulf of Cádiz using HF radar-derived current observations

R. Mulero-Martínez *, J. Gómez-Enri, R. Mañanes, M. Bruno

Applied Physics Department, University of Cádiz, Puerto Real, Cádiz, Spain

ARTICLE INFO

Keywords:
Altimetry
Surface circulation
Coastal areas
CryoSat-2
HF radar

ABSTRACT

This study evaluated the possibility of studying mesoscale surface circulation in coastal areas, as is the Gulf of Cádiz, Spain, using high-resolution altimetry data (20-Hz of posting rate) along with the use of wind and bottom friction ageostrophic corrections. Absolute cross-track surface zonal current velocities, derived from filtered along-track CryoSat-2 SIRAL-SARM Absolute Dynamic Topography (ADT) measurements, are compared with high-frequency radar (HFR) data in the coastal area of the Gulf of Cádiz. The filter strategy followed in this study for the altimetry data is dependent on the HFR measurements for each track. Absolute surface geostrophic velocities obtained from 20-Hz altimetry data agree well HFR further than 25 km from the coast. Close to land ([3–25] km) the ageostrophic component of the surface current (due to the wind drag and the bottom friction) needs to be considered in the altimeter data. On average, the correlation between altimetry and HFR improved from 0.61 (no correction) to 0.72 (correcting these effects). The root mean square error (RMSE) lowered from 12.54 cm·s^{-1} to 7.35 cm·s^{-1}. Furthermore, it has also been demonstrated that corrected altimeter measurements are useful for the study of dynamics and patterns of coastal areas.

1. Introduction

Satellite altimetry has changed physical oceanography by enabling monitoring of global ocean topography from space (Fu et al., 1988). Consequently, large circulation patterns and processes in open ocean are well characterised (Fu et al., 2010) using the geostrophic approximation. However, in coastal areas and minor sub-basins the study of ocean dynamics is more complex since circulation in these areas is conditioned by local processes and ageostrophic components, such as tidal oscillations, changes in the field of winds, abrupt and shallow bottom topographies, river discharges and interactions between different water masses in small areas (Criado-Aldeanueva et al., 2006), and along-shore pressure gradients (Garel et al., 2016). The surface layer of the ocean responds to the action of these factors through rapid changes in dynamics, reflected in events such as coastal countercurrents, eddies, fronts, internal waves and upwellings (Barale et al., 2010), which, at the same time, are linked to activities of high socio-economic and environmental impact (fisheries, offshore energy, navigation, oil spills) (Aguiar et al., 2020). Moreover, surface circulation influences sea level variability (Han et al., 2019). Consequently, understanding coastal currents and ocean surface dynamics plays a key role in the management of coastal areas, where more than 10% of the Earth's population lives exposed to the effects of sea level rise (Neumann et al., 2015).

Technological advances in satellite altimeters, such as CryoSat-2 (CS2) and Sentinel-3A/B allow accurate measurements and improved spatial resolution measurements along the satellite's (pass) track, making them suitable tools for studying coastal zone dynamics (Morrow et al., 2017). Despite these improvements, coastal altimetry still faces two main challenges in retrieving accurate sea surface height: coastal zones are dominated by small and medium-scale structures and processes in the spatio-temporal domain; and the proximity to the coast implies the existence of anomalies in the altimeter measurements related to the presence of land and/or calm water contamination within the altimeter's footprint (Gómez-Enri et al., 2010), as well as mischaracterised range/geophysical corrections (Gommenginger et al., 2011). In recent years, efforts have been made in the coastal altimetry community to improve the capabilities of current altimeters close to the coastal zone (Cipollini et al., 2010; Vignudelli et al., 2019, 2011), including the application of improved range/geophysical corrections (Andersen and Scharroo, 2011; Handoko et al., 2017; among others) and validation with in-situ observations (Vignudelli et al., 2019, and references therein). Our work contributes toward overcoming one of the

* Corresponding author.
E-mail address: roberto.mulero@uca.es (R. Mulero-Martínez).

https://doi.org/10.1016/j.rse.2021.112310
Received 8 June 2020; Received in revised form 13 January 2021; Accepted 15 January 2021
Available online 25 January 2021

challenges of altimetry in the present decade: to reach a level of understanding of the ocean circulation in coastal zones similar to that of the open ocean (Troupin et al., 2015). To achieve this, quality-controlled data from high-frequency radar (HFR, henceforth) are used to validate the altimetry derived ocean circulation in the coastal area. High-frequency radar is a useful tool to monitor coastal surface currents and it has been installed and used in a number of places around the world to study coastal mesoscale circulation (Mandal et al., 2019), monitor ocean dynamics and validate hydrodynamic and wave models (Wyatt, 2014).

Previous studies have compared HFR and altimetry concluding that the former represents a potential tool for the validation and improvement of altimetry products in coastal areas (Liu et al., 2014; Manso-Narvarte et al., 2018; Morrow et al., 2017; Powell and Leben, 2004; Roesler et al., 2013; Troupin et al., 2015). Related works obtained high correlation between HFR and altimetry derived circulation, up to 0.64 (e.g. Manso-Narvarte et al., 2018), using 1-Hz along-track altimeter measurements (~7 km between consecutive measurements). Very few studies, such as Troupin et al. (2015), which obtained consistent results up to 10 km from the coast, have compared surface currents derived from higher along-track spatial resolutions (20 Hz, 40 Hz) and HFR data close to the shore. Regarding the differences between the measurements derived from HFR (total surface circulation) and altimetry (surface geostrophic circulation), the application of ageostrophic corrections, such as wind-induced surface currents, seems to increase the agreement between both datasets (Manso-Narvarte et al., 2018), but other ageostrophic components, such as those related to the bathymetry, remain to be analysed in detail (Morrow and Le Traon, 2012).

The main objective of this study was to validate improved estimates of altimeter-derived absolute cross-track surface zonal current velocities (Vg) at high along-track posting rate (20 Hz) from CryoSat-2 (CS2) satellite, using HFR data in the coastal zone (first 25 km from land) in the Gulf of C´adiz (GoC, henceforth) (Iberian Peninsula). Absolute cross-track (Vg) included the geostrophic signal plus two ageostrophic components based on the wind and the bottom friction effects. In addition, we assessed the capabilities of coastal altimetry data to detect *meso*/small-scale dynamics close to the coast in synergy with HFR data and supported by sea surface temperature (SST) data.

The paper is organised as follows: Section 2 presents the GoC and its main surface circulation characteristics. Section 3 includes the description of the data sets, the edition strategies and the methods. The results and discussion are presented in Section 4, starting with the statistical outcomes from the comparison between hourly surface current velocity data from HFR and altimeter data for the 14 tracks analysed, including the impact of the ageostrophic corrections. We give some examples of the capabilities of the altimeter data with regard to the detection of coastal fine-scale circulation structures endorsed by HFR and SST data. Finally, Section 6 presents the conclusions and perspectives.

2. Study area

The present study is focused on the Gulf of C´adiz (GoC), particularly on the easternmost part of the Gulf, the continental shelf area delimited by Cape Santa Maria (CSM) and Cape Trafalgar (CT). Fig. 1a gives the bathymetry of the study area along with the main circulation patterns proposed by García-Lafuente et al. (2006) and Peliz et al. (2009); the CS2 tracks (red lines), and the area covered by the HFR system (blue dotted area) are shown in Fig. 1b.

The surface circulation of the GoC presents complex dynamics, regarding its temporal and spatial variability, mainly due to its location,

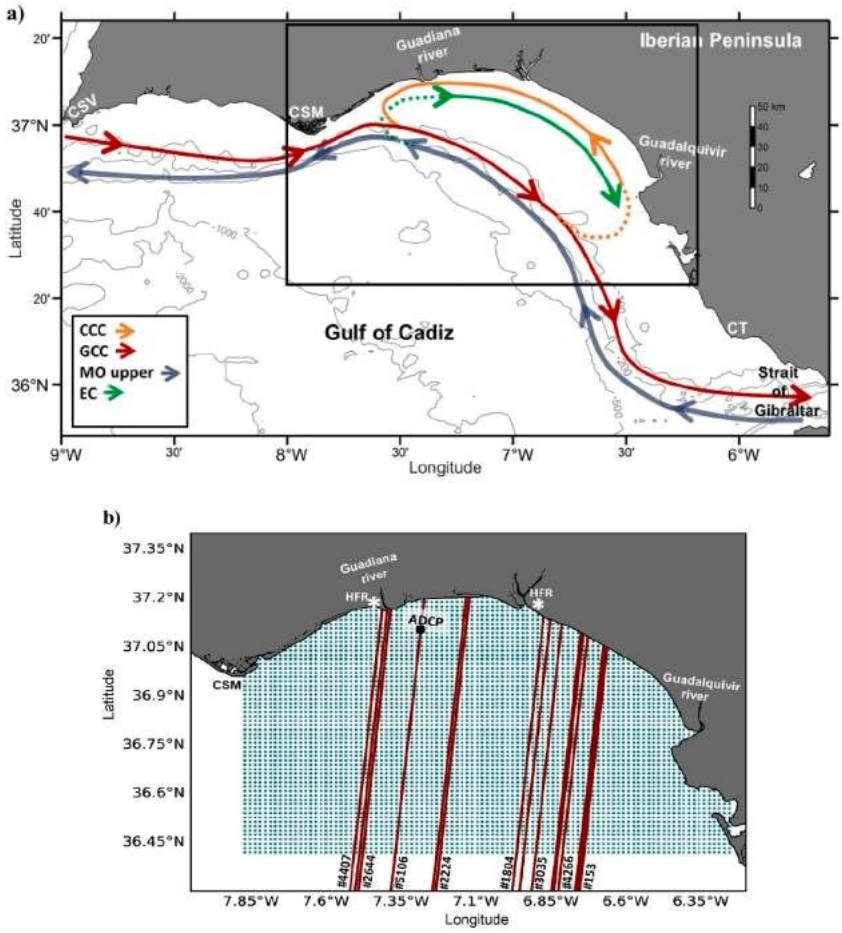

Fig. 1. (a) Main feasible surface circulation characteristics of the GoC (following García-Lafuente et al., 2006 and Peliz et al., 2009), and some geographical features: CSV (Cape San Vicente), CSM (Cape Santa Maria), CT (Cape Trafalgar), CCC (Coastal Countercurrent), GCC (Gulf of Ca´diz Current), MO (Mediterranean Outflow), EC (Eastward Current) **(b)** Location of the observational systems in the GoC: CS2 repetitive tracks and relative orbit number, red lines; HFR system potential covered area, blue dotted area; HFR, high-frequency radar system stations; ADCP, acoustic Doppler current profiler location. (For interpretation of the references to colour in this figure legend, the reader is referred to the web version of this article.)

as it constitutes an inflow-outflow area between the Atlantic Ocean and the Mediterranean Sea across the Strait of Gibraltar (Peliz et al., 2009), and is also linked to the North Atlantic Subtropical Gyre (Laiz et al., 2019), a fact that significantly influences both local and Atlantic circulations.

Two linked systems can be differentiated when describing the circulation of the GoC: the upper slope current system; and the shelf circulation (Fig. 1a). The first is generically composed of two flows. In deep layers, the upper Mediterranean outflow core (MO upper) circulates westward contouring the slope (Ambar and Howe, 1979; Peliz et al., 2009). The Gulf of C´adiz Current (GCC) flows toward the southeast into the Mediterranean Sea. The intensity and characteristics of this system are strongly linked to the Mediterranean inflow-outflow coupling (Peliz et al., 2009).

Regarding the circulation over the continental shelf, two modes can be characterised in the eastern section, located between CSM and CT, alternating westward/eastward circulation. Westward circulation, or cyclonic mode, is characterised by a coastal countercurrent (CCC) which comprises the northern boundary of a cyclonic cell located on the eastern shelf between CSM and the mouth of the Guadalquivir Estuary (García-Lafuente et al., 2006). This CCC seems to be controlled mainly by the imbalance of the along-shore pressure gradient, due to the relaxation of large-scale upwelling favourable wind (Garel et al., 2016). The eastward circulation, or anticyclonic mode, is defined by an eastward current (EC) that, unlike the CCC, is likely to originate from Ekman mechanisms that induce the upwelling of cold water along the coast (Garel et al., 2016).

In addition, abrupt changes in the orientation of the coastline and the presence of the Strait of Gibraltar connecting two basins with such different characteristics, favour the existence of a heterogeneous wind field, which strongly controls the zonal surface circulation by the alternation of westerlies and easterlies (Peliz et al., 2007). Other agents, such as the runoff from the Guadiana and Guadalquivir rivers, affect the surface temperature, salinity, and other biogeochemical variables, mainly in the coastal fringe, near the river mouths (Laiz et al., 2013).

3. Data and methods

3.1. Satellite altimetry

In this study, along-track Sea Level Anomaly (SLA) data from 14 CS2 tracks over the GoC were used to calculate cross-track zonal surface current. CS2 is a European Space Agency (ESA) satellite launched in April 2010 and its primary aim was to monitor changes in the thickness of the sea ice and continental ice sheets (Drinkwater et al., 2004; Wingham et al., 2006); however, CS2 altimetry data have been used for the exploitation of additional ocean products (Calafat et al., 2017) thanks to its main instrument, the synthetic interferometric altimeter (SIRAL), which operates in three modes depending on the purpose: Low Resolution Mode (LRM), mainly used over open ocean, Synthetic Aperture Radar (SAR) mode, for specific coastal areas, and SAR Interferometry (SARIn) mode, with the highest spatial resolution and used over continental water bodies and ice sheets (for more details see CryoSat-2 Product Handbook at https://earth.esa.int/documents). Over the study area, CS2 SIRAL has been working in SAR (Synthetic Aperture Radar) mode since the beginning of the mission in 2010. CryoSat-2 has a quasi-polar orbit of approximately 92°, allowing nearly global coverage, reaching high latitudes of up to 88° N-S Latitude. The quasi-orthogonal orbit inclination with respect to the equator allows a nearly zonal component of the geostrophic current when computed across track.

CryoSat-2 level 2 data used in this work were provided by the ESA Grid Processing On Demand (GPOD) SAR versatile altimetric toolkit for ocean research and exploitation (SARvatore) service (https://gpod.eo.esa.int/), using the pre-defined processing configuration for coastal zones. The SAMOSA+ (SAR Altimetry MOde Studies and Applications) model (Dinardo et al., 2018) is used in the retracking process and the final product is posted at 20 Hz, which results in ~330 m along-track spatial resolution measurements. The altimetry product has been assessed by previous studies globally (Calafat et al., 2017), and focused on coastal areas, such as Go´mez-Enri et al. (2018) over the GoC, obtaining a satisfactory performance further than 3–5 km to the shore. In addition, Bouffard et al. (2018) demonstrated that the CryoSat-2 ocean products compare very well with in situ measurements and confirmed that the ocean products are perfectly suited for oceanographic applications.

The final SLA product from GPOD level 2, includes the range/geophysical corrections listed in Table 1 (Webb and Hall, 2016). In addition, a sea state bias (SSB) correction of 5% of the significant wave height (available in the GPOD product), was applied following previous studies (Fenoglio-Marc et al., 2015; Go´mez-Enri et al., 2018). The Mean Sea Surface used was DTU18 MSS (Andersen et al., 2018).

The selection of tracks in the study area was made for the 2013 to 2018 period based on the availability of HFR data. In order to reduce the effect of land contamination in the footprint area of the radar measurements, only the tracks nearly orthogonal to the coastline were selected (Aldarias et al., 2020; Go´mez-Enri et al., 2018). Therefore, relative orbits #153, #1804, #2224, #2644, #3035, #4266, #4407, and #5106 were used for a total of 14 tracks (Table 2).

3.1.1. SLA editing strategy

Raw 20-Hz along-track SLA data were edited, following the methods presented in Bouffard et al. (2010). The screening removes outliers and filters out high-frequency noise signals near the coast. Firstly, SLA values closer than 3 km to the coastline were rejected to maintain a distance of good quality (Aldarias et al., 2020). Previous studies with CS2 data demonstrated that land contamination might affect the sea level measurements close to the coast (Dinardo et al., 2018; Go´mez-Enri et al., 2018). Secondly, SLA values larger than three times the standard deviation were removed and replaced by linearly interpolated values; this processing was applied in a 10 times loop (Bouffard et al., 2010; Meloni et al., 2019). Finally, a Loess filter (Cleveland and Devlin, 1988) was applied along the track segments to filter out high-frequency noise (Manso-Narvarte et al., 2018); this is a common processing procedure for the study of oceanic mesoscale phenomena (Morrow et al., 2017). For each HFR-CS2 track comparison, a range of spatial cut-off values ([7–60] km) for the Loess filter was tested. This range was selected to resolve the scale of the baroclinic Rossby radius in the area (~6.5 km). The cut-off wavelength that gave the best results in terms of correlation and root mean square error at each track was selected (Morrow et al., 2017). The filter cut-off necessary for obtaining the best correlation among surface velocities obtained from altimetry and HFR is different for each track of the study, depending on the characteristics of the surface circulation at the moment of the satellite pass over the study area. The Loess filter cut-off values applied to each track are presented in Table 2.

Fig. 2 shows an example of the editing approach applied to the CS2 track #2644. High-frequency noise is clearly seen in the raw SLA profile (black line). No outlier is detected in this track segment, but the Loess filter (60-km cut-off) removes most of the high frequency noise (red

Table 1
Range and geophysical corrections applied in CryoSat-2 SIRAL-SARM SLA data from SARvatore-GPOD used in this study.

Range corrections	Geophysical corrections	
Atmospheric Corrections	Tidal Corrections	Ocean Surface Corrections
Dry Tropospheric	Ocean Tide (TPXO8-atlas model)	Dynamic Atmospheric Correction
Wet Tropospheric	Long-Period Equilibrium Tide	Sea State Bias (5% Significant Wave Height)
Ionospheric	Ocean Loading Tide	
	Solid Earth Tide	
	Geocentric Polar Tide	

Table 2
Relative orbit number (RO), date of pass, filter cut-off window and angle coastline/track for each track.

Track # (RO)	Track date	Filter cut-off (km)	Angle coast/track
#4266	17-Oct-2013	25	64.43
#2644	30-Jun-2014	51	76.39
#1804	06-May-2015	54	68.62
#2224	04-Jun-2015	60	95.68
#4407	23-Oct-2015	60	63.73
#2644	09-Jul-2017	29	76.39
#3035	05-Aug-2017	60	76.80
#4266	29-Oct-2017	60	62.68
#153	21-Jan-2018	52	64.11
#1804	15-May-2018	35	68.55
#2224	13-Jun-2018	60	95.48
#2644	12-Jul-2018	60	78.74
#4266	01-Nov-2018	12	66.64
#153	25-Jan-2019	33	64.75

line).

3.1.2. Absolute dynamic topography (ADT)

Along-track surface absolute geostrophic current (SAGC) is computed using the absolute dynamic topography (ADT). Absolute dynamic topography profiles were estimated by adding the mean dynamic topography (MDT) to the SLA. The DTU15MDT model (Knudsen et al., 2016), 1-min spatial resolution grid, was bilinearly interpolated to the CS2 along-track positions. DTU15MDT model was obtained by combining the latest version of the gravity field (EIGEN-6C4) with the Mean Sea Surface model (DTU15MSS) (Knudsen et al., 2016).

3.1.3. Surface absolute geostrophic current (SAGC)

Absolute dynamic topography is the dynamic signal that represents the displacement with respect to the equipotential surface (geoid) forced by the interactions with the atmosphere and the topographic contours of the bottom and sides of the ocean (Pinardi et al., 2017). Therefore, it is possible to obtain a good estimate of the surface geostrophic circulation from altimeter measurements from the spatial variations of ADT and considering the effect of the Earth's rotation movement, represented by the Coriolis force.

From an oceanographic point of view, on an axis of Cartesian coordinates in which the *x-axis* points to the east, *y-axis* to the north and the *z-axis* in the opposite direction to the gravity force, assuming that the water density is constant, the zonal *(u)* and meridional (v) components of the geostrophic current can be obtained using the geostrophic balance equations:

$$\begin{cases} f \cdot u = -\frac{1}{\rho}\frac{\partial p}{\partial y} \\ -f \cdot v = -\frac{1}{\rho}\frac{\partial p}{\partial x} \end{cases} \quad (1)$$

where ρ is seawater density; g is gravitational acceleration; f is the Coriolis parameter ($f = 2\Omega sin\varphi$, where Ω is the angular rotation velocity of the Earth and φ the latitude); and p is pressure. Following the hydrostatic relation defined as:

$$\frac{\partial p}{\partial z} = -\rho \cdot g, \quad (2)$$

and replacing the vertical variation (∂z) by the variation of the sea surface height over the geoid (∂h), Eq. (1) can be written as:

$$\begin{cases} f \cdot u = -g \cdot \frac{\partial h}{\partial y} \\ -f \cdot v = -g \cdot \frac{\partial h}{\partial x} \end{cases} \quad (3)$$

Considering that the zonal velocity is calculated along the satellite track, it is assumed that the variation of the sea surface height over the geoid along the *x-axis* does not exist, it is:

$$\frac{\partial h}{\partial x} = 0, \quad (4)$$

If h is replaced by absolute dynamic topography (ADT), it is possible to calculate the velocity values of the surface absolute geostrophic current (Vg_{abs}) normal to the satellite tracks using the equation (Bouffard et al., 2010):

$$Vg_{abs} = \frac{-g}{f} \cdot \frac{\partial ADT}{\partial y}, \quad (5)$$

The along-track altimetric gradient (slope) has been estimated by using the optimal filter developed by Powell and Leben (2004), following the methodology proposed by Bouffard et al. (2010), using a spatial frame of 1.5 km (equivalent to approximately five along-track altimeter measurements), which also addresses the spatial resolution of the high-frequency radar.

3.2. High-frequency radar data

Two CODAR SeaSondes stations installed in Mazagón (Spain) and Vila Real de Santo Antonio (Portugal) (Fig. 1), that belong to the *Red de Radares de Alta Frecuencia de Puertos del Estado* (www.puertos.es), were used in this study. The stations work at 13.5 MHz frequency; this mode generates measurements with a spatial resolution of approximately 1.5 km and a range that reaches up to 60 km from the coast. The general reliability of HFR data has been demonstrated through extensive comparisons with independent measurements (drifters, ship-based sensor, acoustic Doppler current profilers) (Lorente et al., 2015) over different ocean conditions, providing typical root mean square errors (RMSE) of 7–20 cm s^{-1} (Cosoli and Bolzon, 2015; Lorente et al., 2015). Specifically, the HFR zonal velocity (HFR_u) used in this study was previously validated with in-situ measurements from an acoustic Doppler current profiler (ADCP) moored in the GoC (37°6′40″ N, 7°14′19″ W, Fig. 1) for three months (from 16-Oct-2013 to 16-Jan-2014). The RMSE (5 cm·s^{-1}) and correlation coefficient (0.86 for 95% of confidence level) resulting

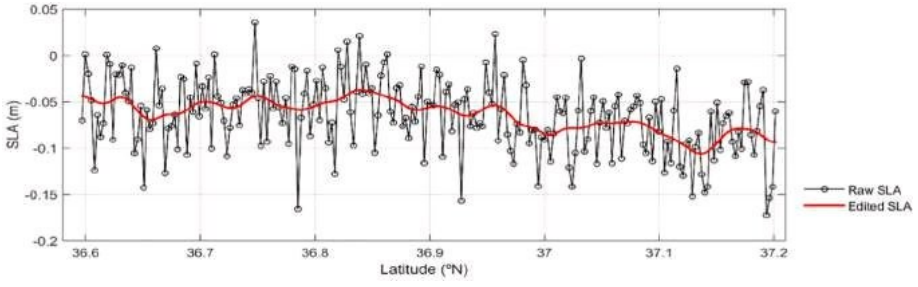

Fig. 2. CryoSat-2 20 Hz original SLA (black) and edited SLA (red) for track #2644 (12-07-2018). (For interpretation of the references to colour in this figure legend, the reader is referred to the web version of this article.)

from the comparison of 2242 hourly measurements (Fig. 3) were satisfactory, considering the magnitude of the standard deviations (ADCP: 10.73 cm·s^{-1}; HFR: 13.09 cm·s^{-1}) and results from previous studies using the same methodology and statistics (Capodici et al., 2019; Cosoli et al., 2010, 2005).

A two-step editing methodology was applied to the HFR observations for the comparisons with altimetry data. Firstly, in order to remove high-frequency signals (mainly tidal oscillations), a 72-h average was computed (Roesler et al., 2013), using the 72 h prior to the dates of the satellite measurements. Finally, the HFR_u velocity was bilinearly interpolated over the position of the altimeter track measurement positions. The performance of the SeaSonde software solves the geometric dilution of precision (GDOP) related problems, among the different possible sources of error (Lipa et al., 2006). We removed invalid data, for each period of 72-h of HFR data, retaining only the points with more than 60% of valid data (Fig. 4). In most of the selected tracks the study area is fully covered by the HFR measurements. For this study, 60% of valid data ensures that a compromise is maintained between good spatial coverage of the data and adequate quality.

3.3. Ageostrophic corrections of altimetry data

3.3.1. Wind

Zonal wind data from the Weather Research and Forecasting model (WRF; http://mandeo.meteogalicia.es/thredds/catalogos/WRF_2D/catalog.html), provided by the meteorological agency of Galicia (https://www.meteogalicia.gal) with a spatial resolution of 12 km and temporal resolution of 1 h, were used in this study to calculate the ageostrophic wind-derived correction. WRF simulated winds have proven to represent the wind regime in the GoC in good agreement with in-situ measurements from buoys (Carvalho et al., 2014; Teles-Machado et al., 2007). The correction does not assume the theoretical Ekman's solution since the study zone is far from the necessary assumption of infinitely deep ocean far from coastal boundaries that supports such a solution. In addition, Stanichny et al. (2016), using extensive drifting buoys and satellite data, demonstrated that surface wind-driven currents are directed almost in the direction of the wind, with a small rotation to the right (in the northern hemisphere) of ~10–15°, with amplitudes equal to 2.8%. These parameters are not dependent on the Ekman layer depth and can be used in different ocean conditions, as it has been demonstrated in a number of previous papers (Keulegan, 1951; Kim et al., 2010; Madsen, 1977; Weber, 1983; Wu, 1975). Finally, zonal surface wind-driven velocities (V_w) are computed as:

$$V_w = 0.03 \cdot w_{u10} \cdot \cos(10^{\circ}) \tag{6}$$

where w_{u10} is the zonal component of the wind speed at 10 m.

Following the procedure applied to the HFR measurements, the original hourly wind data from the WRF model was 72-h averaged and linearly interpolated over the position of the altimeter tracks. The wind-corrected velocity (Vg_w) was obtained following:

$$Vg_w = \frac{-g}{f}\frac{\partial ADT}{\partial y} + V_w \tag{7}$$

3.3.2. Bottom friction

In coastal areas, wind-induced surface currents are not the only ageostrophic agent since other factors, such as bottom friction and the along-shore pressure variations, also contribute to the overall dynamics. The effect of bottom friction is considerable even on the middle shelf area, able to counterbalance the surface wind stress in shallow waters (less than 25 m) (Kantha and Clayson, 2013). To evaluate and to correct the effect of the bottom friction over the surface circulation derived from altimetry in the coastal area, a bottom friction corrected surface velocity (Vg_d) was calculated. For this purpose, depth-averaged bottom friction terms were added to Eq. (3) as follows:

$$\begin{cases} f \cdot u = -g \cdot \dfrac{\partial h}{\partial y} - \dfrac{C_d |V| v}{d} \\ -f \cdot v = -g \cdot \dfrac{\partial h}{\partial x} - \dfrac{C_d |V| u}{d} \end{cases} \tag{8}$$

Where C_d is the bottom drag coefficient, $|V|$is the current velocity modulus, h is the sea surface height over the geoid and d is the bottom depth. Admitting predominance of the zonal component of the current over the meridional one (i.e. $|V| \sim |u|$) and considering the assumption given in Eq. (4), Eq. (8) can be written as:

$$\begin{cases} f \cdot u = -g \cdot \dfrac{\partial h}{\partial y} - \dfrac{C_d v}{d} \\ v = \dfrac{C_d |u| u}{fd} \end{cases} \tag{9}$$

We use the approximation $|u|u \sim 0.35u + 0.71u^3$, proposed by Godin and Martinez (1994). It is important to note that in this expression for typical maximum values of zonal current of 0.5 m s^{-1}, the linear term is roughly two times the non-linear one and, accordingly, we retain only the linear term in the approximation, which once substituted in Eq. (9), transforms the latter into the following:

$$\begin{cases} f \cdot u = -g \cdot \dfrac{\partial h}{\partial y} - \dfrac{C_d}{d} \dfrac{|u|}{v} \\ v = \dfrac{0.35 C_d}{df} u = \dfrac{r}{f} u \end{cases} \tag{10}$$

Where $r = (0.35 C_d)/d$ is a depth dependent parameter. Substitution of the second of the Eq. (10) into the first one, after admitting once again $|u|u \sim 0.35u$, produces:

$$u = \frac{-g}{\left(f + \frac{r^2}{f}\right)} \frac{\partial h}{\partial y} \tag{11}$$

Subsequently, replacing h with absolute dynamic topography (ADT), and using a typically accepted value of $C_d = 2.0\ 10^{-3}$ (Bowden, 1984), the bottom drag corrected surface velocity (Vg_d) normal to the satellite

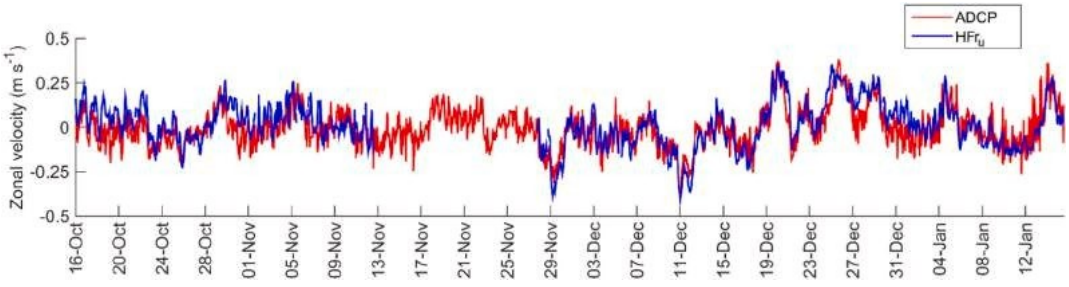

Fig. 3. Hourly surface zonal velocity time-series recorded by the ADCP (red) and high-frequency radar (blue) from 16-Oct-2013 to 16-Jan-2014. (For interpretation of the references to colour in this figure legend, the reader is referred to the web version of this article.)

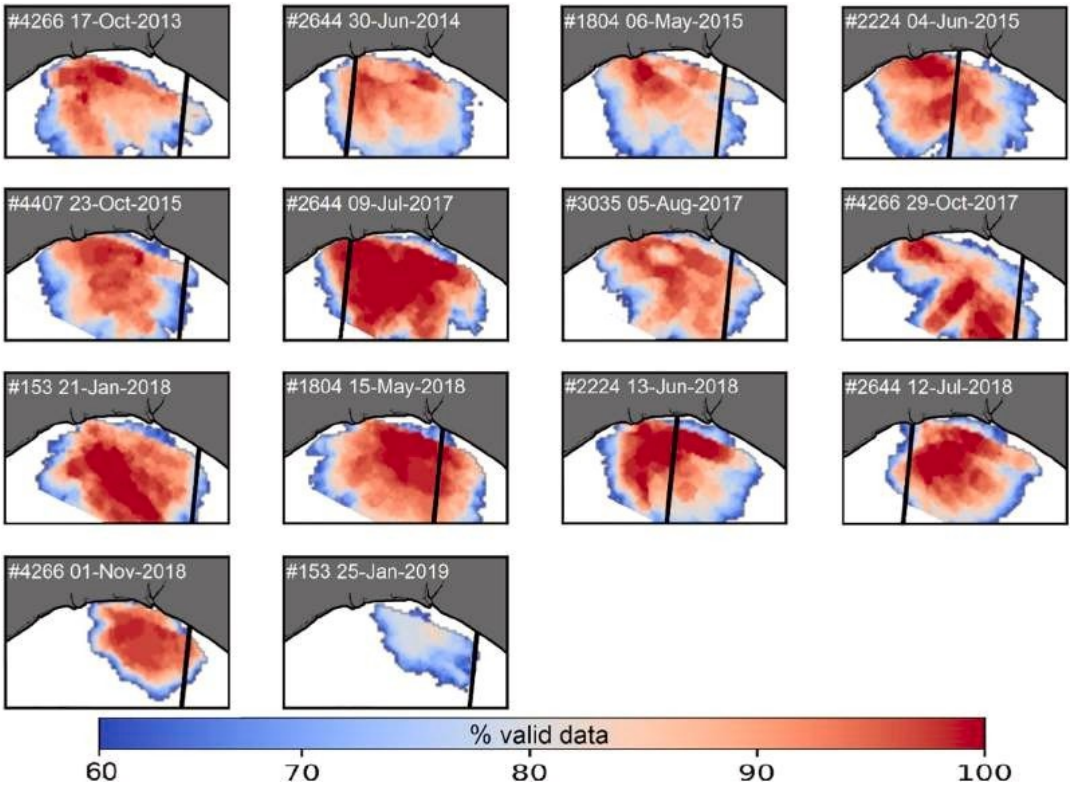

Fig. 4. Fields of HFR valid data (>60%) for each track analysed.

track may be computed as:

$$Vg_d = \left(\frac{-g}{f + r^2 f}\right) \cdot \frac{\partial ADT}{\partial y} \quad (12)$$

Bathymetry data used were provided by ETOPO1 global relief model at 1-min resolution (Amante and Eakins, 2009).

3.3.3. Cross-track corrected velocity

Finally, in order to obtain the surface current including geostrophic and some of the main ageostrophic components, a bottom friction and wind-corrected surface velocity (Vg_{d+w}) was derived from the altimetry data, which includes both previously calculated ageostrophic corrections, and is expressed as:

$$Vg_{d+w} = \left(\frac{-g}{f + r^2 f}\right) \cdot \frac{\partial ADT}{\partial y} + Vw \quad (13)$$

3.4. Sea surface temperature

An 8-day Level-3 binned SST from Moderate-resolution Imaging Spectroradiometer (MODIS) Aqua dataset with a spatial resolution of 4 km, from OceanColor (https://oceancolor.gsfc.nasa.gov/) was used in this study to complement the analysis of recorded surface circulation patterns. Sea surface temperature data were obtained for the closest date available prior to each CS2 track.

3.5. Data comparison

Altimetry derived velocities orthogonal to the satellite track were decomposed to obtain the zonal component of the velocity. The assessment of the altimeter Vg with the HFR_u was performed by estimating two statistical parameters, the root mean square error (RMSE), also expressed as normalized root mean square error (NRMSE) regarding the range of the HFR_u measurements ($HFR_{u\ max}$ - $HFR_{u\ min}$), and the Pearson correlation coefficient (r).

4. Results and discussion

4.1. HFR-altimetry surface velocity statistical assessment

As reported in Section 3.2, HFR velocities were bilinearly interpolated over the position of the altimeter track measurement positions to perform an along-track comparison using the altimeter cross-track derived zonal velocities (Vg_{abs}, Vg_d, Vg_w, Vg_{d+w}), and the zonal component from the high-frequency radar (HFR_u).

Table 3 provides the statistical results (r, RMSE and NRMSE) for the eight tracks analysed during the analysed time period (14 dates are available). The comparison between Vg_{abs} and HFR_u shows r ranging between 0.28 and 0.93 (95% CL), RMSE between 5.08 $cm \cdot s^{-1}$ and 29.76 $cm \cdot s^{-1}$, and NRMSE between 0.23 and 2.99. The average values of r and RMSE (0.61 and 12.54 $cm \cdot s^{-1}$, respectively) are in agreement with previous studies carried out in coastal areas of the Mediterranean Sea (Morrow et al., 2017; Troupin et al., 2015). A strong track-to-track variation in all the statistics stands out and may be related to different factors, such as the use of the 72-h HFR average window, which might not be suitable for all the comparisons since it could mask or over-smooth geostrophic structures captured by the altimeter. However, considering the method used to select valid HFR data points, the amount of valid data would be insufficient if the average window is reduced.

4.1.1. Impact of ageostrophic corrections

In this section, the effect of the ageostrophic component from the wind on the estimates of the surface current is analysed (Vg_w). Fig. 5 shows the linear relation among the average along-track zonal wind velocity and zonal surface current from HFR for each track of the study, depicting the strong control that the wind exerts over the surface circulation in the area and, therefore, the importance of such a wind-related correction.

Table 3
Statistics of the comparison between the 14 CryoSat-2 tracks (relative orbit, RO) and high-frequency radar data. r is the correlation coefficient (95% Confidence Level), RMSE is the root mean square error and NRMSE is the normalized RMSE. Zonal wind column shows along-track averaged and standard deviation zonal wind velocity for each track.

Track # (RO)	Track date	Vg_{abs} - HFR			Vg_w - HFR			Vg_d - HFR			Vg_{d+w} - HFR			HFR		Zonal wind
		r	RMSE (cm s^{-1})	NRMSE	r	RMSE (cm s^{-1})	NRMSE	r	RMSE (cm s^{-1})	NRMSE	r	RMSE (cm s^{-1})	NRMSE	avg ± std. (cm s^{-1})	Range (cm s^{-1})	avg ± std ($m\ s^{-1}$)
#4266	17-Oct-2013	0.30	15.48	2.39	0.49	16.56	2.56	0.88	14.86	2.30	0.92	15.95	2.47	7.65 ± 1.90	6.47	−0.47 ± 0.16
#2644	30-Jun-2014	0.90	23.34	1.22	0.65	13.85	0.72	0.88	23.18	1.21	0.70	13.70	0.72	15.16 ± 6.14	19.12	3.81 ± 0.47
#1804	06-May-2015	0.54	6.03	0.23	0.65	3.64	0.14	0.55	5.95	0.23	0.60	3.7	0.14	2.05 ± 4.18	25.67	1.65 ± 0.47
#2224	04-Jun-2015	0.59	12.72	0.49	0.81	2.24	0.09	0.49	12.65	0.49	0.80	2.14	0.08	−4.47 ± 1.94	26.00	−4.70 ± 1.96
#4407	23-Oct-2015	0.62	13.17	1.57	0.75	4.93	0.59	0.55	13.00	1.55	0.73	4.82	0.57	−12.22 ± 3.10	8.41	−3.29 ± 0.81
#2644	09-Jul-2017	0.93	5.21	1.29	0.93	4.02	1.00	0.89	5.30	1.32	0.89	3.46	0.86	13.57 ± 6.50	4.03	2.50 ± 0.26
#3035	05-Aug-2017	0.81	12.59	0.76	0.83	6.65	0.40	0.87	12.26	0.74	0.88	6.31	0.38	5.21 ± 5.28	16.46	1.11 ± 1.00
#4266	29-Oct-2017	0.28	13.49	1.84	0.51	3.43	0.47	0.23	13.07	1.79	0.52	2.91	0.40	−6.67 ± 1.57	7.31	−5.03 ± 1.91
#153	21-Jan-2018	0.73	5.08	0.52	0.78	5.42	0.56	0.77	4.92	0.50	0.81	5.25	0.54	3.25 ± 2.08	9.76	−0.34 ± 0.24
#1804	15-May-2018	0.64	5.97	0.28	0.62	4.15	0.20	0.69	5.62	0.27	0.68	3.76	0.18	2.25 ± 5.98	21.09	−0.61 ± 1.33
#2224	13-Jun-2018	0.73	20.04	1.13	0.88	11.25	0.63	0.69	20.00	1.13	0.88	11.24	0.63	12.68 ± 7.68	17.77	3.97 ± 0.79
#2644	12-Jul-2018	0.45	17.99	2.88	0.71	10.86	1.74	0.39	17.83	2.86	0.74	10.72	1.72	13.76 ± 7.64	6.24	4.05 ± 1.13
#4266	01-Nov-2018	0.84	29.76	2.99	0.84	22.70	2.28	0.83	28.19	2.83	0.83	20.99	2.11	23.22 ± 2.86	9.97	2.91 ± 0.46
#153	25-Jan-2019	0.78	7.19	0.29	0.78	6.92	0.28	0.78	5.56	0.22	0.78	5.29	0.21	0.78 ± 1.11	24.99	0.79 ± 0.21
Average value		0.61	12.54	1.19	0.68	7.77	0.78	0.63	12.16	1.16	0.72	7.35	0.73	5.71 ± 3.86	13.55	

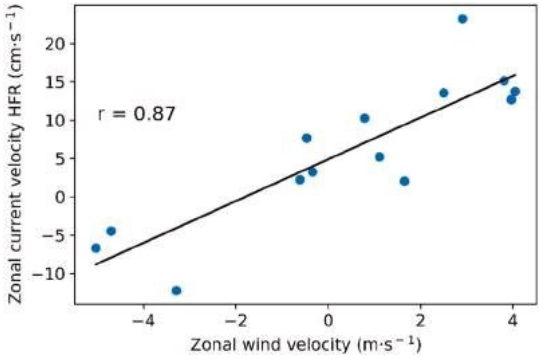

Fig. 5. Scatter plot of the relation among average along-track zonal wind velocity and zonal surface current from HFR for each track. The linear Pearson's correlation coefficient is also shown (confidence level: 95%).

The track-to-track statistical values for Vg_w are given in Table 3. A significant improvement is observed in r/RMSE/NRMSE in most of the tracks (0.68/7.77 cm·s^{-1}/0.78 in average), with respect to Vg_{abs}. In terms of RMSE this implies a reduction of almost 40%; also, the improvement in the NRMSE (from 1.19 to 0.78) shows the importance of the wind, which reduces this difference in intensity. The effectiveness of the wind-related correction is clearly shown in track #2644 (12-Jul-2018), where r improves from 0.45 (Vg_{abs}) to 0.71 (Vg_w), proving the important control of the wind over the surface circulation as depicted in Fig. 5.

The ageostrophic correction due the bottom friction slightly improved the comparison with respect to Vg_{abs} in terms of r, RMSE and NRMSE in most of the tracks. The improvement in the correlation in track #4266 (17-Oct-2013) is particularly evident. The bottom friction component improved r = 0.88 (0.30) and RMSE = 14.86 cm·s^{-1} (15.48 cm·s^{-1}). This correction seems to be less effective than the one based on the wind effect, since it is restricted to shallower areas.

The combined use of both ageostrophic corrections (Vg_{d+w}) improved the comparison (r, RMSE and NRMSE) against HFR_u in most of the tracks. This is clearly observed in the averaged values in Table 3. As mentioned previously, the wind effect component has a major impact on increasing/reducing r/NRMSE considering the ageostrophic components. Tracks with good comparisons considering only the geostrophic component (Vg_{abs}), generally maintain good results when applying the different corrections, so the ageostrophic components seem to be circumstantially beneficial. Despite the variability of the wind field in the GoC, the wind correction might improve the results under different scenarios. Fig. 6 gives the along-track averaged correlation (Fig. 6a, b) and NRMSE (Fig. 6c, d), split in two sectors: coastal (3–25 km) and offshore (> 25 km) considering the distance to the coastline. For the coastal sector, the use of the wind correction produces a strong improvement of the results, increasing/decreasing r/NRMSE. The effect of the bottom-friction correction is less important, but it still improves the results compared with the uncorrected measurements. The application of the ageostrophic component considering the bottom friction and wind (Vg_{d+w}) gives the best comparison against HFR_u. Offshore, r

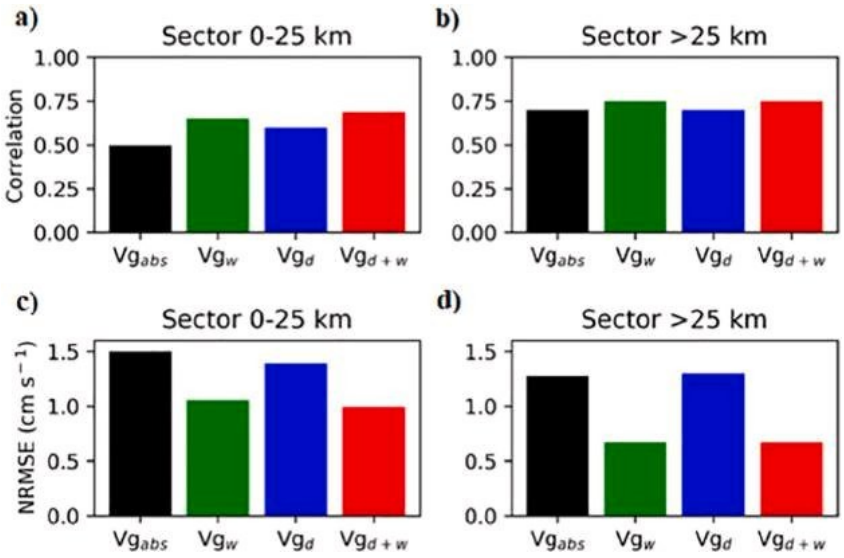

Fig. 6. **(a)** Averaged correlation coefficient from the along-track comparison among Vg_{abs}, Vg_{w}, Vg_{d}, Vg_{d+w} from CS2 and surface zonal velocity from HFR for the 14 analysed tracks in the sector 3–25 km from the coastline; (b) Same as (a) for the offshore sector (>25 km from the coastline). (c) Same as (a) for the NRMSE; (d) Same as (b) for the NRMSE.

shows a good performance even for the uncorrected measurements suggesting that the effect of the ageostrophic components further than 25 km is less significant. Again, the wind correction improves the results with respect to the bottom friction, and the best comparison is given when both corrections are added (more evident in NRMSE).

Fig. 7 gives the along-track averaged values of HFR_u, Vg_{abs}, Vg_d, Vg_w, Vg_{d+w} from the 14 analysed tracks depicted against the distance to the coastline (only the coastal sector is shown). The wind correction increased the altimeter-derived zonal velocity to the level observed in the radar close to the coast ([3–8] km). The effect of the bottom friction correction is clearly noticeable for distances closer than 5 km to the coast. The use of both corrections seems to underestimate Vg_{d+w} with respect to HFR_u in the [9–25] km sector.

4.2. Observability of fine-scale surface circulation

The surface circulation over the coastal area in the GoC is characterised by complex dynamics, regarding its spatio-temporal variability. The capability of CS2 measurements for detecting fine-scale circulation variations over the study area is assessed in this section. Two examples are shown in which Vg_{d+w} and HFR measurements detect small variations in surface circulation related to the high variability of the coastal zone. Fig. 8.a and c show the total surface circulation in the GoC detected by the HFR and the 8-day SST. The along-track zonal CS2-Vg_{d+w} and HFR_u current velocity are compared in Fig. 8.b and d). The details of the CS2 tracks used are presented in Table 2. Fig. 8.a and b refer to CS2 track #1804 (06-May-2015). The surface circulation inferred from the HFR map is highly variable in the coastal area, while further south the circulation is mainly south-eastward. As depicted by SST data, a pool of warmer water close to the coastal area in the eastern sector of the GoC seems to exist, which could be generating an imbalance of the pressure gradient and, therefore, a possible west-bound current (Criado-Aldeanueva et al., 2006). Such a spatial variability is captured by the corrected altimetry data (Vg_{d+w}) in the same way as in HFR, but with a slight overestimation. Surface circulation from #2644 (09-Jul-2017) is presented in Fig. 8.c and d. An eastward current is observed along the whole transect from HFR, with decreasing velocities from coast to off shore. The same pattern is captured by the CS2 Vg_{d+w} measurements with a high level of agreement. This ocean surface variability could be related to a frontal structure generated by the vertical pumping of cold water (Barale et al., 2010) in the western sector of the area, as confirmed by the gradient in the water temperature close to the coast observed in the SST map.

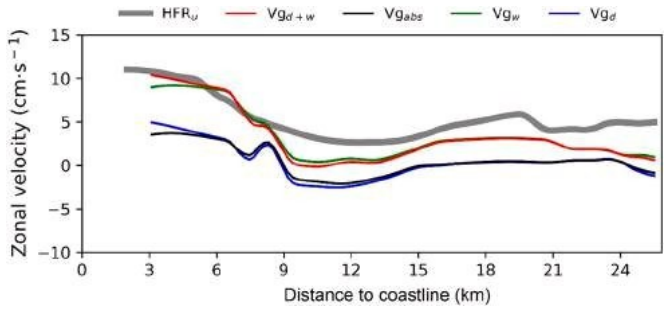

Fig. 7. Along-track surface averaged velocities from Vg_{abs}, Vg_{w}, Vg_{d}, Vg_{d+w} and HFr_u.

5. Conclusions

This study assessed the performance of altimetry data from the CryoSat-2 SIRAL instrument in SAR-mode for estimating the surface circulation in coastal areas, along with the use of wind and bottom friction ageostrophic corrections to analyse the agreement with high-frequency radar measurements. In order to do this, we estimated cross-track surface velocities using along-track low-pass filtered Absolute Dynamic Topography measurements from 14 CS2 tracks over the area covered with valid HFR data in the GoC. The filtering strategy followed in this work is dependent on the HFR measurements for each track. This will be solved in future studies, in order to use HFR data only for validation purposes, avoiding their use in the processing of altimeter data to obtain along-track estimates of absolute dynamic topography. From the obtained results, the following conclusions are highlighted.

The absolute surface geostrophic velocity obtained from 20-Hz altimetry data (Vg_{abs}) agreed well ($r > 0.60$) with HFR data (HFR_u) at along-track distances further than 25 km from land. In general, the geostrophic assumption needs to be considered with care in the GoC for distances between 3 and 25 km to the coast, since it is not realistic at these depths. The use of the wind ageostrophic component (Vg_w) improved the agreement in most of the tracks, despite the variability of the wind field along the time period analysed. Overall, we observed a

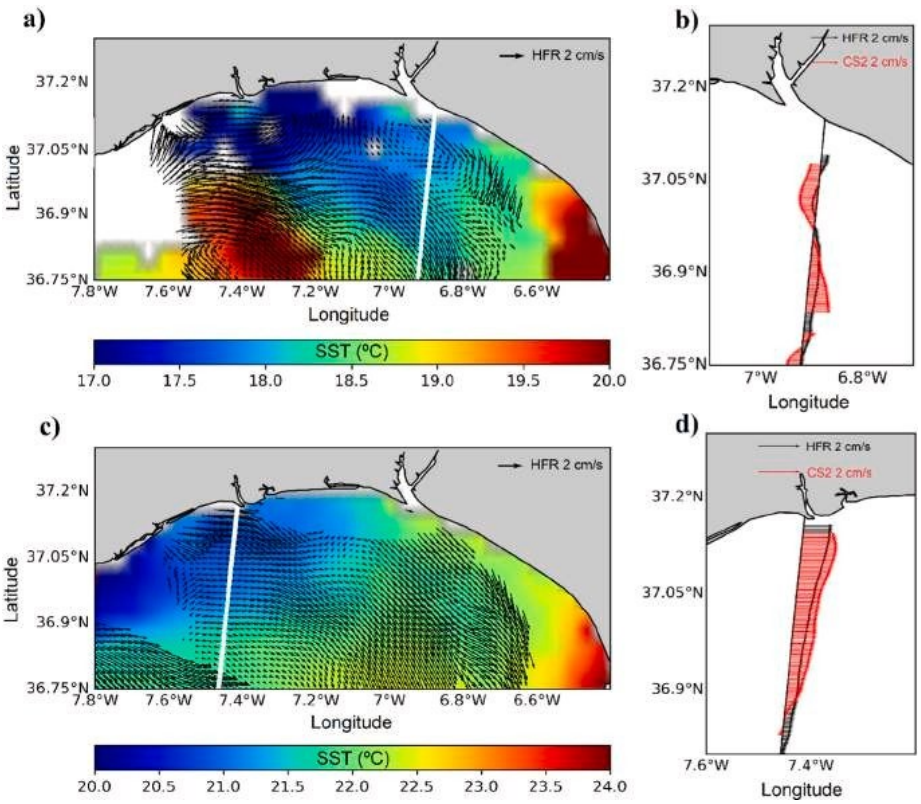

Fig. 8. (a) Surface circulation observed from HFR overlaid with satellite SST for track #1804 (06-May-2015); (b) zonal surface circulation observed from CS2-Vg_{d+w} overlaid with zonal HFR surface velocity for track #1804; (c) same as (a) for track #2644 (09-Jul-2017); (d) same than (b) for track #2644.

reduction in NRMSE of ca. 35% once the wind correction was used in the estimates of the zonal velocity. The bottom friction ageostrophic component (Vg_d) just slightly improved the comparison (mainly for RMSE/NRMSE) in most of the tracks since the applied correction is inherently a linear simplification. The use of both corrections (Vg_{d+w}) gave the best results in terms of r, RMSE, and NRMSE. This improvement was more significant in the 3–25 km sector. We concluded that ageostrophy plays a key role in the coastal fringe of the GoC (3–25 km). This study is a first attempt to consider the effect of the bottom friction on satellite altimetry data. Further studies are needed in order to obtain a better characterisation of the wind effect. A proper characterisation of ageostrophy could be of great benefit for the future of coastal altimetry and the understanding of the near-shore ocean dynamics, especially in coastal areas not covered by HFRs.

The qualitative comparison of the wind and bottom friction corrected altimetry surface measurements (Vg_{d+w}) with the HFR velocities along with SST data, exhibits the high potential of altimetry measurements for the study of dynamics and patterns of coastal areas. Surface velocities derived from CS2 detected surface structures and high-variability surface dynamics, with rapid changes in the current direction even for low velocities.

Satellite altimetry derived surface current velocities gave accurate measurements in coastal areas when the ageostrophic signals were corrected. Differences could be due to unsolved ageostrophic local factors which may also affect surface circulation such as the along-shore pressure variations, since our proposed ageostrophic corrections are just intended to address common issues for all coastal areas, which are the wind and bottom friction effect. The knowledge of ageostrophic and local processes in coastal areas is necessary for a better exploitation of altimetry data in coastal areas since they are highly tied to local meteocean agents and their effects are not entirely understood. Our validation method has shown that the synergy between altimetry and HFR helped to unravel the effects of ageostrophic processes in coastal areas. This will help the validation of present (CryoSat-2, Sentinel-3A/B) and future (Jason-CS/Sentinel-6A/B and SWOT) missions. Thanks to this, it will be possible to: (i) make use of the whole dataset of satellite altimetry data since 1993 in order to obtain estimates of current velocities back in time when no HFR data were available in our (and other) regions of the coastal zones around the world; and (ii) to extend this methodology to other areas where HFR are hardly available (e.g. Africa or South America) or countries which cannot cover all coastlines (e.g. Australia). Furthermore, the good agreement suggests that HFR systems may be a solid tool for the validation of altimetry derived surface currents in coastal areas. The methodology presented here will serve as a proof of concept for the validation of 2-D interferometric SAR altimeter missions (e.g. SWOT).

Declaration of Competing Interest

The authors declare that they have no known competing financial interests or personal relationships that could have appeared to influence the work reported in this paper.

Acknowledgements

Roberto Mulero is financed by the European Social Fund and the Youth Employment Initiative through the "Programa Operativo de Empleo Juvenil". The authors thank all the team members of GPOD for their technical support. This paper was partially funded by the European Union's Interreg V-A Espan˜a – Portugal (POCTEP) 2014-2020 project: OCASO, under grant agreement: GA 0223_OCASO_5_E; and by the Spanish Project: Circulation and transport processes in the estuaries of the GoC: Current situation and projections of future climate change scenarios (TRUCO) (Ref.: RTI2018-100865-B-C22).

References

Aguiar, E., Mourre, B., Juza, M., Reyes, E., Hern´andez-Lasheras, J., Cutolo, E., Mason, E., Tintor´e, J., 2020. Multi-platform model assessment in the Western Mediterranean Sea: impact of downscaling on the surface circulation and mesoscale activity. Ocean Dyn. 70, 273–288. https://doi.org/10.1007/s10236-019-01317-8.

Aldarias, A., Gomez-Enri, J., Laiz, I., Tejedor, B., Vignudelli, S., Cipollini, P., 2020. Validation of sentinel-3A SRAL coastal sea level data at high posting rate: 80 Hz. IEEE Trans. Geosci. Remote Sens. 1–13. https://doi.org/10.1109/tgrs.2019.2957649.

Amante, C., Eakins, B.W., 2009. {ETOPO}1 Global Relief Model Converted to {PanMap} Layer Format. NOAA-National Geophys, Data Cent.

Ambar, I., Howe, M.R., 1979. Observations of the mediterranean outflow-II the deep circulation in the vicinity of the gulf of cadiz. Deep Sea Res. Part A, Oceanogr. Res. Pap. https://doi.org/10.1016/0198-0149(79)90096-7.

Andersen, O.B., Scharroo, R., 2011. Range and geophysical corrections in coastal regions: And implications for mean sea surface determination. In: Coastal Altimetry. https://doi.org/10.1007/978-3-642-12796-0_5.

Andersen, O., Knudsen, P., Stenseng, L., 2018. A New DTU18 MSS Mean Sea Surface – Improvement from SAR Altimetry. In: 25 Years of Progress in Radar Altimetry Symposium, Portugal.

Barale, V., Gower, J.F.R., Alberotanza, L., 2010. Oceanography from Space: Revisited, Oceanography from Space: Revisited. https://doi.org/10.1007/978-90-481-8681-5.

Bouffard, J., Pascual, A., Ruiz, S., Faug`ere, Y., Tintor´e, J., 2010. Coastal and mesoscale dynamics characterization using altimetry and gliders: a case study in the Balearic Sea. J. Geophys. Res. Ocean. 115, 1–17. https://doi.org/10.1029/2009JC006087.

Bouffard, J., Naeije, M., Banks, C.J., Calafat, F.M., Cipollini, P., Snaith, H.M., Webb, E., Hall, A., Mannan, R., F´em´enias, P., Parrinello, T., 2018. CryoSat Ocean product quality status and future evolution. Adv. Sp. Res. https://doi.org/10.1016/j.asr.2017.11.043.

Bowden, K.F., 1984. Physical oceanography of coastal waters. In: Ellis Horwood Ser. Mar. Sci. John Wiley & Sons, Inc, Somerset, N.J, p. 302.

Calafat, F.M., Cipollini, P., Bouffard, J., Snaith, H., F´em´enias, P., 2017. Evaluation of new CryoSat-2 products over the ocean. Remote Sens. Environ. 191, 131–144. https://doi.org/10.1016/j.rse.2017.01.009.

Capodici, F., Cosoli, S., Ciraolo, G., Nasello, C., Maltese, A., Poulain, P.M., Drago, A., Azzopardi, J., Gauci, A., 2019. Validation of HF radar sea surface currents in the Malta-Sicily Channel. Remote Sens. Environ. https://doi.org/10.1016/j.rse.2019.02.026.

Carvalho, D., Rocha, A., Go´mez-Gesteira, M., Silva Santos, C., 2014. Sensitivity of the WRF model wind simulation and wind energy production estimates to planetary boundary layer parameterizations for onshore and offshore areas in the Iberian Peninsula. Appl. Energy. https://doi.org/10.1016/j.apenergy.2014.08.082.

Cipollini, P., Benveniste, J., Bouffard, J., Emery, W., Gommenginger, C., Griffin, D., Hoyer, J., Madsen, K., Mercier, F., Miller, L., Pascual, A., Ravichandran, M., Shillington, F., Snaith, H., Strub, T., Vandemark, D., Vignudelli, S., Wilkin, J., Woodworth, P., Zavala-Garay, J., 2010. The Role of Altimetry in Coastal Observing Systems. https://doi.org/10.5270/oceanobs09.cwp.16.

Cleveland, W.S., Devlin, S.J., 1988. Locally weighted regression: an approach to regression analysis by local fitting. J. Am. Stat. Assoc. https://doi.org/10.1080/01621459.1988.10478639.

Cosoli, S., Bolzon, G., 2015. Accuracy of surface current mapping from high-frequency (HF) ocean radars. Boll. Geofis. Teor. Appl. 56, 55–70. https://doi.org/10.4430/bgta0132.

Cosoli, S., Ga˘ci´c, M., Mazzoldi, A., 2005. Comparison between HF radar current data and moored ADCP currentmeter. Nuovo Cim. della Soc. Ital. di Fis. C. https://doi.org/10.1393/ncc/i2005-10032-6.

Cosoli, S., Mazzoldi, A., Ga˘ci´c, M., 2010. Validation of surface current measurements in the northern Adriatic Sea from high-frequency radars. J. Atmos. Ocean. Technol. https://doi.org/10.1175/2009JTECHO680.1.

Criado-Aldeanueva, F., García-Lafuente, J., Vargas, J.M., Del Río, J., Sa´nchez, A., Delgado, J., S´anchez, J.C., 2006. Wind induced variability of hydrographic features and water masses distribution in the Gulf of Cadiz (SW Iberia) from in situ data. J. Mar. Syst. 63, 130–140. https://doi.org/10.1016/j.jmarsys.2006.06.005.

Dinardo, S., Fenoglio-Marc, L., Buchhaupt, C., Becker, M., Scharroo, R., Joana Fernandes, M., Benveniste, J., 2018. Coastal SAR and PLRM altimetry in German bight and West Baltic Sea. Adv. Sp. Res. 62, 1371–1404. https://doi.org/10.1016/j.asr.2017.12.018.

Drinkwater, M.R., Francis, R., Ratier, G., Wingham, D.J., 2004. The European Space Agency's Earth Explorer Mission. Measuring variability in the cryosphere. Ann. Glaciol, CryoSat. https://doi.org/10.3189/172756404781814663.

Fenoglio-Marc, L., Dinardo, S., Scharroo, R., Roland, A., Dutour Sikiric, M., Lucas, B., Becker, M., Benveniste, J., Weiss, R., 2015. The German bight: a validation of CryoSat-2 altimeter data in SAR mode. Adv. Sp. Res. https://doi.org/10.1016/j.asr.2015.02.014.

Fu, L.-L., Chelton, D., Zlotnicki, V., 1988. Satellite altimetry: observing ocean variability from space. Oceanography. https://doi.org/10.5670/oceanog.1988.01.

Fu, L.L., Chelton, D.B., Le Traon, P.Y., Morrow, R., 2010. Eddy dynamics from satellite altimetry. Oceanography 23, 15–25. https://doi.org/10.5670/oceanog.2010.02.

García-Lafuente, J., Delgado, J., Criado-Aldeanueva, F., Bruno, M., del Río, J., Miguel Vargas, J., 2006. Water mass circulation on the continental shelf of the Gulf of C´adiz. Deep. Res. Part II Top. Stud. Oceanogr. https://doi.org/10.1016/j.dsr2.2006.04.011.

Garel, E., Laiz, I., Drago, T., Relvas, P., 2016. Characterisation of coastal counter-currents on the inner shelf of the Gulf of Cadiz. J. Mar. Syst. 155, 19–34. https://doi.org/10.1016/j.jmarsys.2015.11.001.

Godin, G., Martinez, A., 1994. Friction on the propagation O F tides in a channel. Cont. Shelf Res. 14, 723–748.

Go´mez-Enri, J., Vignudelli, S., Quartly, G.D., Gommenginger, C.P., Cipollini, P., Challenor, P.G., Benveniste, J., 2010. Modeling Envisat RA-2 waveforms in the coastal zone: case study of calm water contamination. IEEE Geosci. Remote Sens. Lett. https://doi.org/10.1109/LGRS.2009.2039193.

Go´mez-Enri, J., Vignudelli, S., Cipollini, P., Coca, J., Gonza´lez, C.J., 2018. Validation of CryoSat-2 SIRAL Sea level data in the eastern continental shelf of the Gulf of Cadiz (Spain). Adv. Sp. Res. https://doi.org/10.1016/j.asr.2017.10.042.

Gommenginger, C., Thibaut, P., Fenoglio-Marc, L., Quartly, G., Deng, X., Go´mez-Enri, J., Challenor, P., Gao, Y., 2011. Retracking altimeter waveforms near the coasts. In: Coastal Altimetry. https://doi.org/10.1007/978-3-642-12796-0_4.

Han, W., Stammer, D., Thompson, P., Ezer, T., Palanisamy, H., Zhang, X., Domingues, C. M., Zhang, L., Yuan, D., 2019. Impacts of basin-scale climate modes on coastal sea level: a review. Surv. Geophys. https://doi.org/10.1007/s10712-019-09562-8.

Handoko, E.Y., Fernandes, M.J., L´azaro, C., 2017. Assessment of altimetric range and geophysical corrections and mean sea surface models-impacts on sea level variability around the Indonesian seas. Remote Sens. https://doi.org/10.3390/rs9020102.

Kantha, L.H., Clayson, C.A., 2013. Numerical models of oceans and oceanic processes. Int. Geophys. Ser. https://doi.org/10.1016/S0074-6142(00)80027-3.

Keulegan, G.H., 1951. Wind tides in small closed channels. J. Res. Natl. Bur. Stand. 1934 https://doi.org/10.6028/jres.046.041.

Kim, S.Y., Cornuelle, B.D., Terrill, E.J., 2010. Decomposing observations of high-frequency radar-derived surface currents by their forcing mechanisms: locally wind-driven surface currents. J. Geophys. Res. Ocean. https://doi.org/10.1029/2010JC006223.

Knudsen, P., Andersen, O.B., Maximenko, N., 2016. The updated geodetic mean dynamic topography model – DTU15MDT. In: In: Presented at the ESA Living Planet Symposium, 2016. Prague, Czech Republic.

Laiz, I., Go´mez-Enri, J., Tejedor, B., Aboitiz, A., Villares, P., 2013. Seasonal Sea level variations in the gulf of Cadiz continental shelf from in-situ measurements and satellite altimetry. Cont. Shelf Res. https://doi.org/10.1016/j.csr.2012.12.008.

Laiz, I., Plecha, S., Teles-Machado, A., Gonz´alez-Ortego´n, E., S´anchez-Quiles, D., Cobelo-García, A., Roque, D., Peliz, A., S´anchez-Leal, R.F., Tovar-Sa´nchez, A., 2019. The role of the Gulf of Cadiz circulation in the redistribution of trace metals between the Atlantic Ocean and the Mediterranean Sea. Sci. Total Environ. https://doi.org/10.1016/j.scitotenv.2019.134964.

Lipa, B., Nyden, B., Ullman, D.S., Terrill, E., 2006. SeaSonde radial velocities: Derivation and internal consistency. IEEE J. Ocean. Eng. https://doi.org/10.1109/JOE.2006.886104.

Liu, Y., Weisberg, R.H., Vignudelli, S., Mitchum, G.T., 2014. Evaluation of altimetry-derived surface current products using Lagrangian drifter trajectories in the eastern Gulf of Mexico. J. Geophys. Res. Ocean. https://doi.org/10.1002/2013JC009710.

Lorente, P., Piedracoba, S., Fanjul, E.A., 2015. Validation of high-frequency radar ocean surface current observations in the NW of the Iberian Peninsula. Cont. Shelf Res. https://doi.org/10.1016/j.csr.2014.11.001.

Madsen, O.L., 1977. A realistic model of the wind-induced Ekman boundary layer. J. Phys. Oceanogr. https://doi.org/10.1175/1520-0485(1977)007<0248:ARMOTW>2.0.CO;2.

Mandal, S., Sil, S., Pramanik, S., Arunraj, K.S., Jena, B.K., 2019. Characteristics and evolution of a coastal mesoscale eddy in the Western Bay of Bengal monitored by high-frequency radars. Dyn. Atmos. Oceans 88, 101107. https://doi.org/10.1016/j.dynatmoce.2019.101107.

Manso-Narvarte, I., Caballero, A., Rubio, A., Dufau, C., Birol, F., 2018. Joint analysis of coastal altimetry and high-frequency (HF) radar data: Observability of seasonal and mesoscale ocean dynamics in the Bay of Biscay. Ocean Sci. 14, 1265–1281. https://doi.org/10.5194/os-14-1265-2018.

Meloni, M., Bouffard, J., Doglioli, A.M., Petrenko, A.A., Valladeau, G., 2019. Toward science-oriented validations of coastal altimetry: application to the Ligurian Sea. Remote Sens. Environ. https://doi.org/10.1016/j.rse.2019.01.028.

Morrow, R., Le Traon, P.Y., 2012. Recent advances in observing mesoscale ocean dynamics with satellite altimetry. Adv. Sp. Res. https://doi.org/10.1016/j.asr.2011.09.033.

Morrow, R., Carret, A., Birol, F., Nino, F., Valladeau, G., Boy, F., Bachelier, C., Zakardjian, B., 2017. Observability of fine-scale ocean dynamics in the northwestern Mediterranean Sea. Ocean Sci. https://doi.org/10.5194/os-13-13-2017.

Neumann, B., Vafeidis, A.T., Zimmermann, J., Nicholls, R.J., 2015. Future coastal population growth and exposure to sea-level rise and coastal flooding - a global assessment. PLoS One. https://doi.org/10.1371/journal.pone.0118571.

Peliz, A., Dubert, J., Marchesiello, P., Teles-Machado, A., 2007. Surface circulation in the Gulf of Cadiz: Model and mean flow structure. J. Geophys. Res. Ocean. https://doi.org/10.1029/2007JC004159.

Peliz, A., Marchesiello, P., Santos, A.M.P., Dubert, J., Teles-Machado, A., Marta-Almeida, M., Le Cann, B., 2009. Surface circulation in the Gulf of Cadiz: 2. Inflow-outflow coupling and the Gulf of Cadiz slope current. J. Geophys. Res. Ocean. https://doi.org/10.1029/2008JC004771.

Pinardi, N., Pistoia, J., Cipollini, P., Doglioni, F., 2017. Coastal Altimetry for the Computation of a Mean Dynamic Topography in the Mediterranean Sea. Alma Mater Studiorum-Universit`adi Bologna.

Powell, B.S., Leben, R.R., 2004. An optimal filter for geostrophic mesoscale currents from along-track satellite altimetry. J. Atmos. Ocean. Technol. 21, 1633–1642. https://doi.org/10.1175/1520-0426(2004)021<1633:AOFFGM>2.0.CO;2.

Roesler, C.J., Emery, W.J., Kim, S.Y., 2013. Evaluating the use of high-frequency radar coastal currents to correct satellite altimetry. J. Geophys. Res. Ocean. 118, 3240–3259. https://doi.org/10.1002/jgrc.20220.

Stanichny, S.V., Kubryakov, A.A., Soloviev, D.M., 2016. Parameterization of surface wind-driven currents in the Black Sea using drifters, wind, and altimetry data. Ocean Dyn. 66, 1–10. https://doi.org/10.1007/s10236-015-0901-3.

Teles-Machado, A., Peliz, A´., Dubert, J., Sa´nchez, R.F., 2007. On the onset of the Gulf of Cadiz coastal countercurrent. Geophys. Res. Lett. https://doi.org/10.1029/2007GL030091.

Troupin, C., Pascual, A., Valladeau, G., Pujol, I., Lana, A., Heslop, E., Ruiz, S., Torner, M., Picot, N., Tintor´e, J., 2015. Illustration of the emerging capabilities of SARAL/AltiKa in the coastal zone using a multi-platform approach. Adv. Sp. Res. 55, 51–59. https://doi.org/10.1016/j.asr.2014.09.011.

Vignudelli, S., Kostianoy, A.G., Cipollini, P., Benveniste, J., 2011. Coastal altimetry. In: Coastal Altimetry. https://doi.org/10.1007/978-3-642-12796-0.

Vignudelli, S., Birol, F., Benveniste, J., Fu, L.L., Picot, N., Raynal, M., Roinard, H., 2019. Satellite altimetry measurements of sea level in the coastal zone. Surv. Geophys. https://doi.org/10.1007/s10712-019-09569-1.

Webb, E., Hall, A., 2016. Geophysical corrections in level 2 CryoSat data products. In: IDEAS-VEG-IPF-MEM-1288 Version, 5.

Weber, J.E., 1983. Steady wind- and wave-induced currents in the Open Ocean. J. Phys. Oceanogr. https://doi.org/10.1175/1520-0485(1983)013<0524:swawic>2.0.co;2.

Wingham, D.J., Francis, C.R., Baker, S., Bouzinac, C., Brockley, D., Cullen, R., de Chateau-Thierry, P., Laxon, S.W., Mallow, U., Mavrocordatos, C., Phalippou, L., Ratier, G., Rey, L., Rostan, F., Viau, P., Wallis, D.W., 2006. CryoSat: a mission to determine the fluctuations in Earth's land and marine ice fields. Adv. Sp. Res. https://doi.org/10.1016/j.asr.2005.07.027.

Wu, J., 1975. Wind-induced drift currents. J. Fluid Mech. https://doi.org/10.1017/S0022112075000687.

Wyatt, L.R., 2014. High frequency radar applications in coastal monitoring, planning and engineering. Aust. J. Civ. Eng. https://doi.org/10.7158/C13-023.2014.12.1.

Universidad de Cádiz
Escuela de Doctorado UCA
Edificio Hospital Real
Plaza Falla nº 8
11003 Cádiz
http://escueladoctoral.uca.es/
escuela.doctoral@uca.es

Modelo de consentimiento de coautores para inclusión de trabajos en la modalidad de tesis por compendio de publicaciones

Los investigadores/as:

Román-Cascón, C., Mañanes, R., Izquierdo, A., Bruno, M., y Gómez-Enri, J., como coautores/as del artículo/libro/capítulo de libro:

The Use of Sentinel-3 Altimetry Data to Assess Wind Speed from the Weather Research and Forecasting (WRF) Model: Application over the Gulf of Cadiz, publicado en *Remote Sensing*, por la presente dan su consentimiento para que esta publicación sea incorporada a la tesis doctoral titulada *Coastal surface circulation of the Gulf of Cadiz from satellite altimetry measurements* cuyo autor/a es Roberto Mulero Martínez, renunciando a presentar estos resultados como parte de otra tesis doctoral en cualquier Universidad.

En Cádiz, a 06 de marzo de 2024

Fdo. Carlos Román Cascón

ROMAN CASCON CARLOS - 48893754D

Firmado digitalmente por ROMAN CASCON CARLOS - 48893754D
Fecha: 2024.03.07 09:56:38 +01'00'

Fdo. Rafael Mañanes Salinas

Firmado por MAÑANES SALINAS RAFAEL - ***0751** el día 07/03/2024 con un certificado emitido por AC FNMT Usuarios

Fdo. Alfredo Izquierdo González

IZQUIERDO GONZALEZ ALFREDO - 34846311T

IZQUIERDO GONZALEZ ALFREDO - 34846311T
2024.03.07 13:14:19 +01'00'

Fdo. Jesús Gómez Enri

GOMEZ ENRI JESUS - 34048944C

Firmado digitalmente por GOMEZ ENRI JESUS - 34048944C
Nombre de reconocimiento (DN): cn=GOMEZ ENRI JESUS - 34048944C, sn=GOMEZ ENRI, givenName=JESUS, c=ES, serialNumber=IDCES-34048944C
Fecha: 2024.03.07 15:07:14 +01'00'

remote sensing

MDPI

Article

The Use of Sentinel-3 Altimetry Data to Assess Wind Speed from the Weather Research and Forecasting (WRF) Model: Application over the Gulf of Cadiz

Roberto Mulero-Martinez *, Carlos Román-Cascón, Rafael Mañanes, Alfredo Izquierdo, Miguel Bruno and Jesús Gómez-Enri

Department of Applied Physics, University of Cádiz, CASEM, 11510 Puerto Real, Spain

* Correspondence: roberto.mulero@uca.es

Abstract: This work presents the quality performance and the capabilities of altimetry derived wind speed (WS) retrievals from the altimeters on-board Copernicus satellites Sentinel-3A/B (S3A/B) for the spatial assessment of WS outputs from the weather research and forecasting (WRF) model over

the complex area of the Gulf of Cádiz (GoC), Spain. In order to assess the applicability of the altimetry data for this purpose, comparisons between three different WS data sources over the area were evaluated: in situ measurements, S3A/B 20 Hz altimetry data, and WRF model outputs. Sentinel- 3A/B WS data were compared against two different moored buoys to guarantee the quality of the data over the GoC, resulting in satisfying scores (average results: RMSE = 1.21 m/s, r = 0.93 for S3A and RMSE = 1.36 m/s, r = 0.89 for S3B). Second, the WRF model was validated with in situ data from four different stations to ensure the correct performance over the area. Finally, the spatial variability of the WS derived from the WRF model was compared with the along-track altimetry-derived WS. The analysis was carried out under different wind synoptic conditions. Qualitative and quantitative results (average RMSE < 1.0 m/s) show agreement between both data sets under low/high wind regimes, proving that the spatial coverage of satellite altimetry enables the spatial assessment of high-resolution numerical weather prediction models in complex water-covered zones.

Keywords: wind speed; satellite altimetry; WRF; model validation; sea surface

Citation: Mulero-Martinez, R.; Román-Cascón, C.; Mañanes, R.; Izquierdo, A.; Bruno, M.; Gómez-Enri, J. The Use of Sentinel-3 Altimetry Data to Assess Wind Speed from the Weather Research and Forecasting (WRF) Model: Application over the Gulf of Cadiz. *Remote Sens.* **2022**, *14*, 4036. https://doi.org/10.3390/rs14164036

Academic Editor: Sergey A. Lebedev

Received: 6 July 2022
Accepted: 15 August 2022
Published: 18 August 2022

1. Introduction

Sea surface wind (SSW) plays an essential role in driving surface ocean currents, since it modulates the amount of energy available for the generation of ageostrophic Ekman currents [1]. Wind speed influences ocean surface circulation as well as climate variability, which is why surface wind speed and direction are included as essential climate variables (ECV) in the Global Climate Observing System inventory [2]. Close to coastal areas, due to the occurrence of atmospheric thermal gradients, along with the existence of orographic constraints [3], SSW is highly variable in the spatio-temporal domain. Accurate SSW maps are crucial in coastal areas for better monitoring and prediction of wind-related hazards, such as storm surges or flooding [4]. Moreover, SSW plays a key role in the estimation of realistic total ocean surface currents from altimetry, especially in coastal areas [5,6]. The effect of the SSW on sea surface dynamics is the focus of coastal altimetry and oceanog- raphy research in recent years. Significant progress was made with products, such as GlobCurrent [7] and the Near-Real-Time Version of the Cross-Calibrated Multiplatform (CCMP) ocean surface wind velocity data set [8]. However, the spatial resolution of SSW products is still linked to scatterometer measurements, which generally contain a 25–50 km wide blind zone along the coast [9], except for specific products, such as ASCAT 6.25 km, with a true spatial resolution of about 17 km. This is essential for studying dynamical mesoscale features, although they still present a significant coastal gap [10], which limits the characterisation of mesoscale and fine scale circulation near the coast. The lack of

information in the coastal fringe is also transferred to global atmospheric analysis and reanalysis products, which combine numerical weather prediction (NWP) with scatterome- ters and in situ measurements, restricting the achievement of a realistic assessment of local conditions in coastal areas [11]. In this context, WS retrievals from synthetic aperture radar (SAR) imagery [12,13], improved by new deep-learning based models [14,15], along with altimeter-based techniques derived by the measurement of the backscattering coefficient (σ0) of the sea surface, are of great value since they can provide high-resolution data under complex conditions.

Wind speed altimetry products provide WS at 10 m over the ocean surface (U_{10}) [16], derived at along-track posting rates ranging from 1 Hz to 80 Hz (7 km/85 m between con- secutive measurements, respectively). Wind speed from altimetry is empirically estimated from the radar power returned from the sea surface. The returned power waveforms are affected by the sea surface roughness in the footprint area, which might be dominated by the wind-induced capillary waves. As wind increases, the sea surface roughness also increases and the backscattering coefficient (σ0) of the sea surface decreases, as measured by the altimeter [17]. Altimeter measurements of σ0 are therefore inversely related to sea surface WS. It was proven by [18] that consistency in the accuracy of WS data de- rived from Sentinel-3A/B (S3A/B) altimeters when validated against data from more than 80 moored buoys at different locations, with root mean square errors (RMSE) of 1.19 m/s and 1.13 m/s for S3A (from 1 March 2016 to 31 October 2019) and S3B (from 10 November 2018 to 31 October 2019), respectively. Wind speed data from the Sentinel-3 mission are routinely evaluated by the Sentinel-3 Mission Performance Centre (S3MPC) tasked by the European Space Agency (ESA) to monitor and guarantee the provision of high-quality data to the users [19]. As officially reported in the S3 Wind and Waves Cyclic Performance Report [20] for the period from December 2020 to January 2021, the standard deviation of the difference (a proxy to the random error) is around 1.70 m/s and 1.80 m/s for S3A and S3B, when compared to in situ (mainly buoys) measurements, using a maximum acceptable collocation distance and time interval between the collocated altimeter and buoy observation of 200 km and 2 h, respectively.

Numerical weather prediction models, such as the weather research and forecasting (WRF) model [21,22], set with appropriate parameterisations, can provide wind speed data with high spatial and temporal resolution for any terrestrial, coastal, or open ocean area of the globe [10]. WRF is a mesoscale numerical weather prediction system designed for both atmospheric research and operational forecasting applications [21]. Commonly, NWP models, such as WRF, are calibrated/validated using in situ observations from meteorological stations and buoys; however, due to the spatial scarcity of these sources, the uncertainty in the WS of the coastal band persists [9]. Therefore, there is a need for high-resolution measurements of the SSW over coastal areas for assessing NWP models, not only to enhance our knowledge in the mesoscale atmospheric circulation in these areas, but also for a realistic characterisation of the surface current variability linked to it.

Although WS derived from altimetry is used for assimilation into forecasting mod- els [23], to our knowledge it is not yet used for the spatial evaluation of NWP models in coastal areas, where scatterometer data are not available. Satellite altimeter WS measure- ments can be used to calibrate and validate wind models at any coastal area covered by the orbital configuration of the satellite, enabling the fine-tuning of NWP models over the complex land–sea transition zones.

The main objective of this study is to analyse the capability of S3A/B altimeters U_{10} retrievals to perform extensive spatial assessments of U_{10} from the WRF model over complex areas, such as the Gulf of Cádiz (Figure 1), focusing on the possibilities of data comparison in the coastal area (up to 5 km from land due to altimeter limitations). Both datasets are also assessed through comparisons with moored buoy and weather station data. In addition, fine scale spatial variability of the wind at different dominant regimes in the study area is analysed using the outputs of the WRF model and the Sentinel-3 mission. The paper is organised as follows: Section 2 describes the study area (Gulf of Cádiz). Section 2

provides details of the datasets and methods used to compare the different data sources. The results are presented and discussed in Section 3. Conclusions and future perspectives are presented in Section 4.

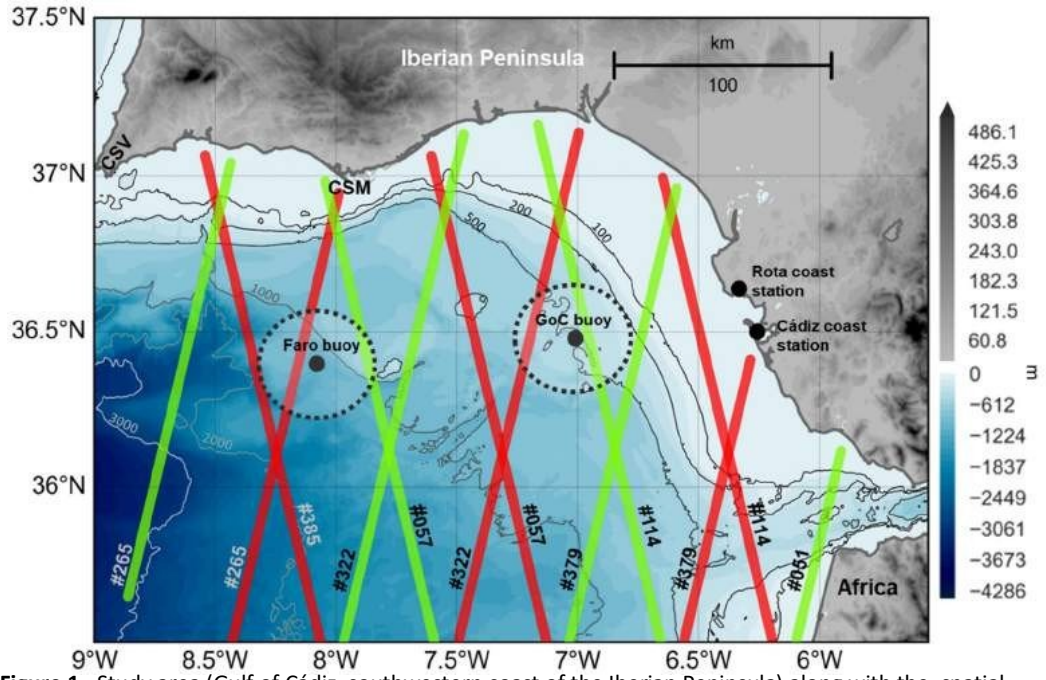

Figure 1. Study area (Gulf of Cádiz, southwestern coast of the Iberian Peninsula) along with the spatial distribution of the data sources used in this work and some geographical features: S3A tracks (red line), S3B tracks (green line), location of the moored (GoC buoy and Faro buoy) along with the 25 km radius area used to select S3A/B data for its validation (dotted contoured area), location of the land-based meteorological stations from the Spanish Meteorological Office (Cádiz coast station and Rota coast station), Cape Santa Maria (CSM), and Cape San Vicente (CSV).

2. Materials and Methods

2.1. Study Area

The study area extends from Cape San Vicente (CSV) to the entrance of the Strait of Gibraltar (SG) (Figure 1), covering the Gulf of Cádiz (GoC), southern Spain. This area is characterised by abrupt changes in the orientation of the coastline, very complex coastal topography, and links between two basins with different characteristics. Such features favour the existence of a heterogeneous wind field, with topography-induced atmospheric flows [24] that strongly control the zonal sea surface circulation [25,26] and therefore, modulate variables of interest, such as sea surface temperature (SST) and chlorophyll concentration [27]. Such sea surface circulation over the continental shelf alternates west- ward/eastward modes, the former characterised by a coastal countercurrent, and the latter for inducing cold water upwellings along the coast [6,28]. Moreover, due to differences in the surface temperatures of the land and the sea, the coastal area of the GoC, is characterised by a land–sea breeze circulation, which is generally perpendicular to the coastline and can be extended up to 200 km inland [29]. Apart from the local geographic characteristics, the wind field in the area is also controlled by the large scale. Different studies demonstrated that the North Atlantic oscillation (NAO) is significantly related to the wind field in the area through the modulation of the Azores anticyclone [30,31]. The zonal component of the SSW is the most important meteorological agent affecting the ocean circulation in the area. Its variability is directly related to the sea surface circulation over the GoC [6], but also to the across shore sea level variability of the strait, contributing to the modulation of the water exchange through it, as observed from modelling studies [32], in situ [33], and altimeter data [34].

2.2. Altimetry Data

The along-track WS data from altimetry are retrieved from the retracking of the altimeter waveforms. The satellites have a repeat cycle of 27 days. The radar instrument, synthetic aperture radar altimeter (SRAL), has two measurement modes: low resolution (LRM) and SAR, the latter being the high-resolution along-track mode commonly used over the global ocean. Furthermore, the S3A/B SRAL generates level-2 data at 1 Hz and 20 Hz of the Ku and C bands (for more details see Sentinel-3 Altimetry Document Library at https://sentinel.esa.int/web/sentinel, accessed on 1 January 2022). The S3A/B level 2 data used were provided by the ESA Earth Console Parallel Processing Service (P-PRO) SAR versatile altimetric toolkit for ocean research and exploitation (SARvatore) service (https:// ui-ppro.earthconsole.eu/, accessed on 1 January 2022), applying the pre-defined processing setup for coastal zones. The SAR Altimetry MOde Studies and Applications (SAMOSA++) model (Dinardo et al., 2020) is used in the retracking process and the final product is posted at 20 Hz, which results in ~330 m along-track spatial resolution measurements. Along-track WS data come from 12 S3A/B tracks over the GoC, detailed in Table 1. For the validation of the altimetry WS data with in situ measurements from the GoC buoy, only S3A/B data in a radius of 25 km around the position of the buoy were used, so the altimetry data can be considered co-located with the in situ data [18]. Only data from relative orbits #265, #322, #385 from S3A, and #057 and #114 from S3B satisfy the 25 km radius criteria (see Figure 1). Raw 20-Hz along-track WS data were edited eliminating the first 5 km of data closer to the coast, since demonstrated by [35], S3-SRAL altimeters start to give accurate data 5 km from the coast, due to coastal and land reflections that might contaminate the radar waveforms, making the retrieval of estimates of the derived geophysical parameters less accurate [36]. Furthermore, the methods presented in [37] were applied, in order to remove outliers and filter out noise signals. The aforementioned editing methodology consists of removing values larger than three times the standard deviation and replacing them with linearly interpolated values; this processing was applied in a 10-times loop [37,38].

Table 1. Sentinel-3 A/B data availability (number of cycles, relative orbits and orientation) for the different comparisons among the datasets (the orientation of the different tracks is presented as ascending (A) or descending (D)).

Sentinel 3A				Sentinel 3B			
Relative Orbit	**N° Cycles S3A vs. WRF**	**N° Cycles S3A vs. Buoy**	**Orientation**	**Relative Orbit**	**N° Cycles S3B vs. WRF**	**N° Cycles S3B vs. Buoy**	**Orientation**
#057	13	-	A	#051	14	-	D
#114	13	-	A	#057	14	26	A
#265	14	33	D	#114	14	29	A
#322	14	53	D	#265	13	-	D
#379	14	-	D	#322	13	-	D
#385	14	34	A	#379	13	-	D
Analysed period	From January 2020 to December 2020	From January 2017 to December 2020			From January 2020 to December 2020	From November 2018 to December 2020	

2.3. In Situ Data

The in situ coastal wind data were extracted from four sources; (i) hourly time series of 10 m height WS and direction (WD), recorded by the weather station deployed by the Spanish Meteorology Agency (AEMET) in the city of Cádiz, (Cádiz coast station, Figure 1); (ii) same as (i), but located in Rota, (Rota coast station, Figure 1); (iii) in situ offshore wind data collected by two moored multi-instrument buoys. These buoys (GoC buoy and Faro buoy, Figure 1) provide an hourly time series of 3 m height WS and WD and are operated and maintained by the Spanish Port Authorities and the Hydrographic Institute of Portugal, respectively. The hourly data, distributed for public use, are built from averaging 10 min of raw data each hour. It is worth noting that these averages, related to spatially smoother wind fields (removing, for instance, small-scale variability due to eddies), should match

better with the S3A/B data, which are averaged over the track segment inside the circular area with a radius of 25 km. Considering that the buoy registers wind parameters at 3 m over the surface, it is necessary to extrapolate the buoy data to a 10 m height wind speed, so it can be compared with altimetry derived WS data. For this purpose, the typically accepted logarithmic wind profile method [39–41] was applied to extrapolate the measured winds by the buoy from 3 to 10 m over the sea. Although there are several methods and variations used for this purpose, e.g., stress equivalent winds [42] that consider the air mass density and stability, for practical reasons, here we used the logarithmic wind profile method, which is suitable for our aim, requiring only WS and WD measurements and proven to be consistent over the first 30 m of sea surface [43,44].

2.4. Weather Research and Forecasting Model Data

Model data were obtained using the mesoscale, non-hydrostatic WRF model version 4.2 [22]. The model was used to produce dynamically downscaled hourly 10 m WS and WD over the complete study area during 2020, with a temporal resolution of 1 h and 3 km grid (d02). The d02 domain was one-way nested within a parent domain of 9 km grid (d01), as depicted in Figure 2, in order to allow communication from the parent (lower resolution) to the child domain (higher resolution), but not vice versa.

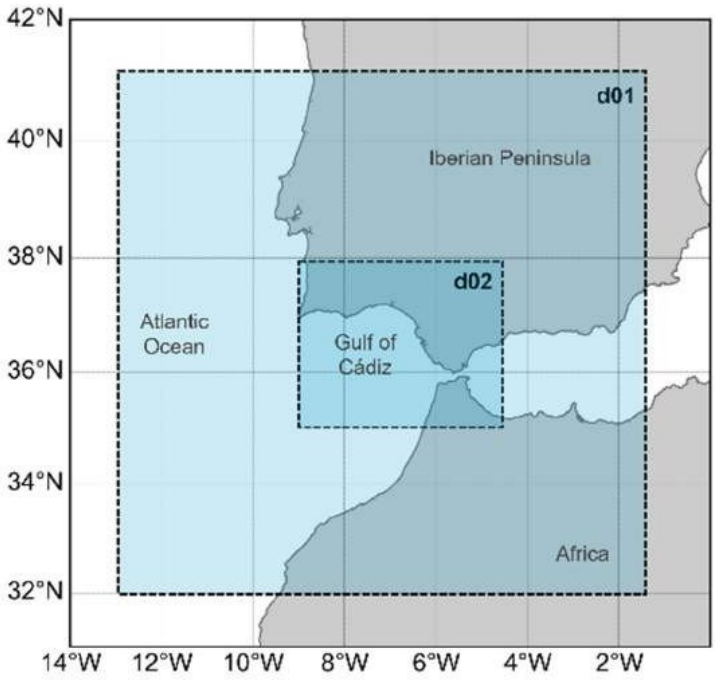

Figure 2. WRF model domains d01 (9 km grid) and d02 (3 km grid).

The initial and boundary conditions were supplied by the NCEP/NCAR operational Global Forecast System (GFS) with 0.25° of spatial resolution and 6 h of temporal sampling (National Centers for Environmental Prediction/National Weather Service/NOAA/US Department of Commerce, 2015). Boundary conditions were applied to the parent domain (d01). The dynamical setup of the simulation was based on the optimised design presented by [45] after performing 4150 daily simulations over southern Spain (Table 2). Unlike previous studies in the area [40,44,45], which consider constant sea surface temperature (SST), in our study, the SST was updated every 6 h. Although the overall impact is expected to be small, it is a more realistic approach and might have an impact under specific conditions or in specific areas [46].

Table 2. Configuration options selected for the WRF simulations, based on [45].

Scheme or Parameterization	Selected Option
Initialization	NCEP/NARC GFS 0.25°
Microphysics	SBU-Lin
Longwave radiaion	RRTMG
Shortwave radiation	Dudhia
Cumulus	Kain-Fritsch
Surface layer	MM5 similarity
Planetary boundary layer	YSU
Vertical levels number	36
Diffusion 6th order option	Knievel
Damping	Rayleigh
Topography model	GTOPO30
Land uses	GLC
Nudging	Grid nudging (d01)/Observational nudging (d02) Sea
surface temperature	Updated every 6 h

2.5. Assessment of Altimeter and Model Data

Prior to the comparisons, the WRF wind data were linearly interpolated to the position of in situ instruments, as well as to the S3A/B along-track measurement positions. Several statistical parameters were used to compare the wind speed and direction from the altimeter and model, according to previous studies [44,47,48]. Root mean square error (RMSE) (1), normalised root mean square error (NRMSE) (2), bias (3), and Pearson's correlation coefficient (r) (4) were used to evaluate wind speed, while bias and standard deviation error (STDE) (5) were applied to the wind direction comparisons results.

$$RMSE = \sqrt{\frac{\sum_{i=1}^{n} (P_i - O_i)^2}{n}} \quad (1)$$

$$NRMSE = \frac{RMSE}{max_i O - min_i O} \quad (2)$$

$$bias = \frac{\sum_{i=1}^{n} (P_i - O_i)}{n} \quad (3)$$

$$r = \frac{\sum_{i=1}^{n} (O_i - \bar{O})(P_i - \bar{P})}{\left[\sum_{i=1}^{n} (O_i - \bar{O})^2 \sum_{i=1}^{n} (P_i - \bar{P})^2\right]^{\frac{1}{2}}} \quad (4)$$

$$STDE = \left[(RMSE)^2 - (bias)^2\right]^{\frac{1}{2}} \quad (5)$$

where P represents the co-located WS or WD from the data source that is being evaluated (model: WS, WD, and altimetry: WS); O denotes the co-located WS or WD from the reference data source (in situ stations). Note that WD is an angular variable, therefore, to avoid errors related to 0° and 360° overlapping, WD bias and WD STDE were calculated for a new circular variable (d) (6), bounded between [−180, 180], and obtained from the observed (O) and predicted (P) wind directions as follows:

$$d_i = \begin{cases} d_i^p - d_i^o \; if \; d_i^p - d_i^o < 180 \\ d_i^p - d_i^o - 360 \; if \; d_i^p - d_i^o > 180 \\ d_i^p - d_i^o + 360 \; if \; d_i^p - d_i^o < -180 \end{cases} \quad (6)$$

3. Results and Discussion

3.1. Preliminary Validation of the Data Sources

3.1.1. Altimetry Wind Speed Validation Using In Situ Data

All available WS data derived from altimetry and corresponding to relative orbits #265, #322, and #385 from S3A, as well as #057 and #114 from S3B that matched the 25 km radius criteria (presented in Section 2.2) from 6 January 2017 to 31 December 2020, were compared against the moored GoC buoy and the Faro buoy, using some of the statistical parameters presented in Section 2.4, to ensure the correct performance of the altimetry sensors over the area of interest. The results from the comparison are shown in Figure 3. The scatterplots present the GoC buoy (Figure 3a) and Faro buoy (Figure 3b) WS measurements against the average of all the S3A and S3B measurements within the 25-km radius around the buoys; the corresponding standard deviation threshold of each track segment is also shown. Due to the different starting points of S3A (since 2016) and S3B (since 2018), the number of available data for the latter is lower than that of S3A.

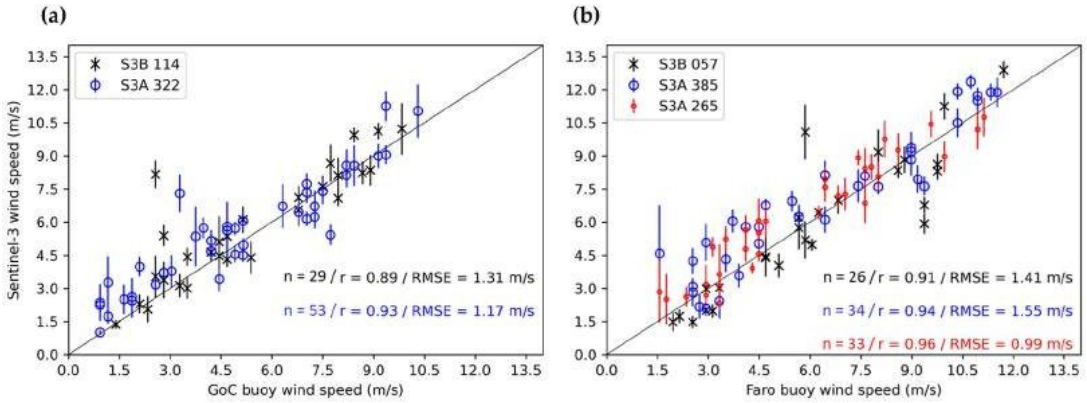

Figure 3. Scatterplot of the WS comparison among S3A (**a**)/S3B (**b**) and in situ measurements from the GoC buoy. Vertical lines represent the standard deviation for each point based on the Sentinel-3 data inside the 25 km radius area (see Figure 1).

These results are in line with the reported accuracy in the S3 Wind and Waves Cyclic Performance Report for the period from December 2020 to January 2021 [20]. They are also in agreement with those reported by [18], who compared WS from S3A/B with more than 80 moored buoys. There is a strong linear relationship between the altimeters and the GoC buoy dataset according to the average r coefficients (0.94 for S3A and 0.90 for S3B, 99% of confidence level). As it was expected, the best results correspond with the relative orbits closer to the location of the buoys S3A #265.

The differences observed between the two data sources might be related with the representativeness of the spatio-temporal domains. Firstly, in the spatial domain, the in situ data represent a local estimate and therefore include the wind variability over all scales [49]. However, the radar altimeter considers the entire footprint [50]. Secondly, the time difference between the satellite passing over the buoy and the operating period of the in situ instrument; this difference was calculated to be 30 min maximum. This temporal difference could also explain the presence of outliers, since unlike the in situ data, the altimeter WS is estimated from instantaneous measurements of the sea surface state. An example is the outlier observed in the S3B #114 vs. GoC buoy scatterplot (Figure 3a), which affects the statistical scores and could compromise the comparisons. This mismatch represents a S3B WS value of 8.00 m/s against an in situ measurement of 2.50 m/s, approximately, and corresponds to 21:00 UTC in situ data and 21:26 UTC altimetry data of 25 November 2020. As depicted in Figure 4e, where hourly WS from the GoC buoy for that day is presented, WS was highly variable during the entire day, especially between 14:00 UTC and 23:00 UTC, with WS ranging from 2.00 m/s to 11.50 m/s. Sentinel-3B passed over the GoC buoy position at 21:26 UTC and detected high variability

in the spatial domain, as shown in Figure 4a. The radargram of the power waveforms for S3B relative orbit #144 in the vicinity of the buoy is shown in Figure 4c, together with the along-track WS (Figure 4a) and the along-track backscattering coefficient (σ0) (Figure 4b). Note that only the power from gates 320 to 365 are shown in the radargram; moreover, since the product used to generate this radargram is not yet corrected by the retracking process, a leading edge deviation over latitude 36.30°N is observed. Regarding the power represented in the radargram (Figure 4c), a fall is clearly observed in the segment between latitudes 35.80°N and 36.25°N. The strong decrease in power affects the retracking of the waveforms and, therefore, the retrieval of the geophysical parameters, as shown in [35]. The retracking of these waveforms results in a strong decrease in the retrieved σ0 and therefore, a rise in the derived along-track WS. This may be related to the existence of a strong and sporadic wind gust, which would agree with the high spatio-temporal variability observed during the day by the in situ sensor. Wind gusts can exceed 20 m/s over the area [51], also dramatically increasing the roughness of the sea surface. If the satellite crosses the area affected by the wind gust, a decrease in the returning signal received by the altimeter should be observed. However, this cannot be confirmed by the buoy data due to its sampling time (measurement recorded 26 min before the satellite pass).

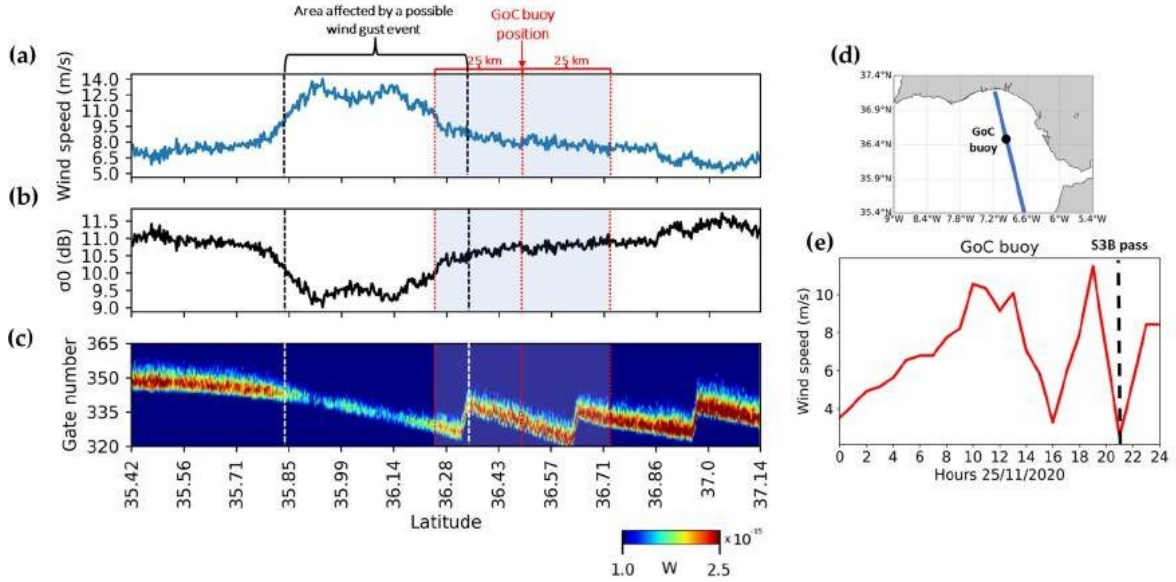

Figure 4. Along-track WS (**a**), σ0 parameter (**b**) and radargram of the waveforms (**c**) from the S3B relative orbit #144 (25 November 2020 at 21:26 UTC). Red dashed lines indicate the GoC buoy position and 25 km radius area; black dashed lines indicate the area affected by a possible wind gust.
(**d**) Satellite track (blue line) and GoC buoy position (black dot). (**e**) Hourly WS from the GoC buoy for the 25 November 2020.

3.1.2. WRF Model Wind Velocity Validation against In Situ Data

In this section, hourly WS and WD data for 2020, obtained from the WRF model stations and the GoC and Faro buoys to ensure that the model performance over the study simulations, are compared to in situ data from the Cádiz and Rota coast meteorological area is adequate. The wind rose diagrams representing the WD and WD data used to estimate the statistical parameters represented in Table 3 are shown in Figure 5, where the predominant zonal component of the wind over the area can be observed. The four figures depict the high variability of the wind over the study area. The resulting scores, shown in Table 3, demonstrate the overall good performance of the dynamical setup applied to the model, which are in line with similar studies [40,44] usually performed only for open ocean

GoC buoy and Rota coast station/Cádiz coast station positions, respectively, as indicated comparisons. However, the model overestimates/underestimates the WS at the Faro and for the bias scores in Table 3. Although there are differences among WS RMSE from the

three stations, once the parameter is normalised (NRMSE) using the range of variation in the WS, these differences are reduced. The best results are obtained for the Faro buoy site, which is the farthest location from the coast.

Table 3. Statistical scores from the comparison among in situ data from the different stations and buoys against simulations from the WRF model.

	Wind Speed				Wind Direction	
In Situ Station	**Bias (m/s)**	**RMSE (m/s)**	**NRMSE (m/s)**	**r**	**Bias (°)**	**STDE (°)**
GoC buoy	0.74	1.93	0.12	0.80	6.74	47.10
Cádiz coast station	−0.13	1.74	0.12	0.74	5.78	54.49
Rota coast station	0.44	1.65	0.16	0.74	8.35	48.68
Faro buoy	0.33	1.59	0.10	0.85	5.54	33.84

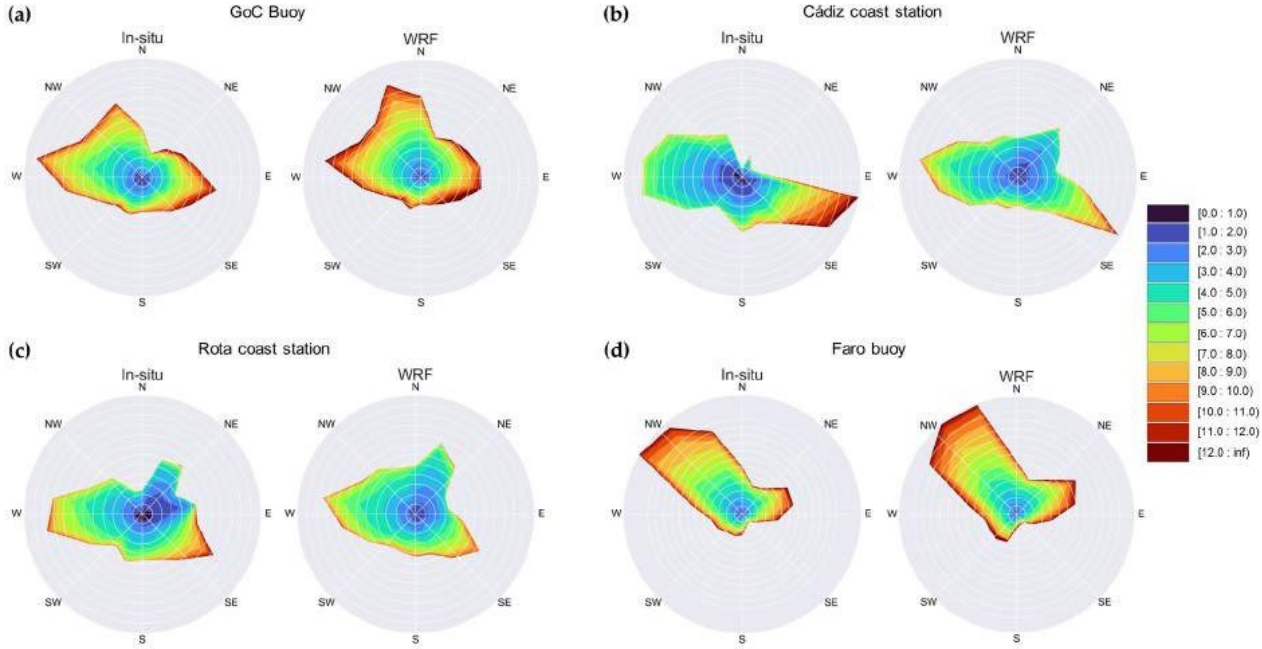

Figure 5. Wind rose diagrams (m/s) calculated at (**a**) GoC buoy, (**b**) Cádiz coast station, (**c**) Rota coast station and (**d**) Faro buoy, over the period January 2020 to December 2020 from both in situ measurements and WRF simulations.

3.2. WRF Model Spatial Assessment Using Altimetry Data

In this section, the innovative use of altimetry WS for the spatial evaluation of WS from the WRF model over the study area is carried out through quantitative comparisons using WS retrievals from S3A and S3B altimeters. Special focus is on the coastal fringe, where other sensors, such as the scatterometers, cannot provide useful data for validating the model. The statistical results from the evaluation of WS data from the WRF model simulations with WS from the S3A/B tracks over the study area are presented here. In order to assess the accuracy of the WRF WS spatial variability, model outputs were linearly interpolated over the positions of the satellite track measurements for 2020. As depicted in Figure 6a,b, the averaged WS spatial variability obtained from both altimetry (Figure 6a) and the WRF model (Figure 6b) matches for almost the whole study area. This agreement between the WRF model and the S3A/B WS data for the set of tracks used is confirmed by the r Pearson's values, which are mostly over 0.80, being the average correlation value for all the tracks 0.85 (confidence level: 99%, Figure 6c). The RMSE (Figure 6d) is small for all tracks, frequently below 1.0 m/s (average RMSE: 0.65 m/s). Lower correlations and larger RMSEs are generally found near the coastal fringe. In the sector [5–20 km] from land, the averages of the statistical parameters are r = 0.79 and RMSE 0.88 m/s, which is also evident

in the WS average maps, since altimetry WS is slightly lower over the coastal area than the WS from WRF. Considering that the altimetry data over the 5 km closest to land were removed, the decrease in the statistical scores from the comparison adjacent to the coast is not due to the land contamination of the altimetry signal, but rather to the WRF simulations. The model WS overestimation in coastal areas is an issue previously described by different authors [39,52,53] and is most likely caused by the high spatial variability of the wind field over these areas due to the thermal atmospheric gradients [3], which may not be properly reproduced by the WRF model at fine scales. Such misrepresentation could be related to the lack of information and crude representation of the land surface that can considerably affect the simulation of the fluxes driving the associated boundary layer processes [54]. Although satellite tracks do not cover the entire WRF domain area, the results prove that using along-track WS from altimetry enables the estimation of the correlation coefficient and RMSE spatial maps for the area, which facilitate the assessment of the WRF model performance over the study area. Moreover, the presence of altimetry data up to 5 km from land allows the detection of weaknesses in the model performance over the complex land–sea transition fringe.

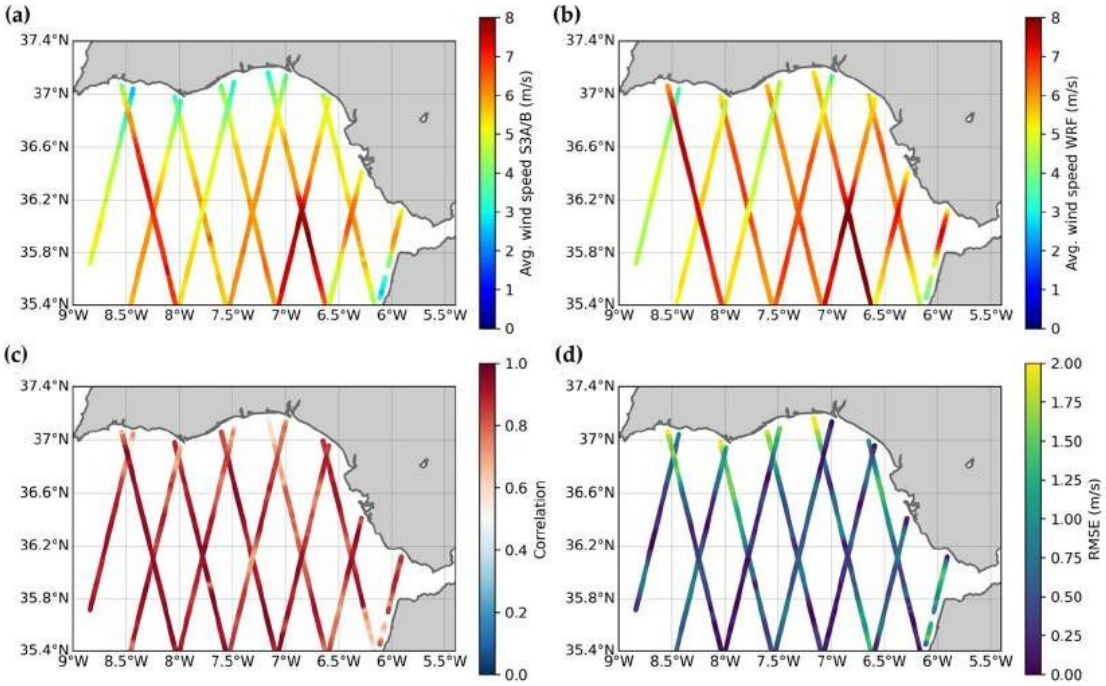

Figure 6. Average WS from S3A/B (**a**) and WRF (**b**); spatial distribution of the r Pearson's parameter (**c**) and RMSE (**d**) from the comparison among WS data from the WRF model and S3A/B tracks over the study area.

3.3. Observability of Spatial Variability

The wind field over the GoC is characterised by its high spatial variability and high- intensity events. In this section, a qualitative comparison of the spatial variability of the WS reproduced by the WRF model with the S3A/B data is presented to investigate the capabilities of using altimetry data for assessing the WRF model under complex conditions. For this purpose, WS from three S3A/B tracks under different atmospheric situations are compared with the wind field obtained from the corresponding WRF model simulations. The comparisons are shown in Figure 7. Figure 7a depicts the simulated wind field on 31 December 2020 at 11:00 UTC. The satellite crossed the area at 10:35 UTC. A weak northerly wind dominated over the whole GoC. The along-track spatial variability observed from the altimeter measurements agrees with the outputs of the WRF model, especially for the northernmost part of the track, stating the good performance of the WRF model even at the positions closer to the coast.

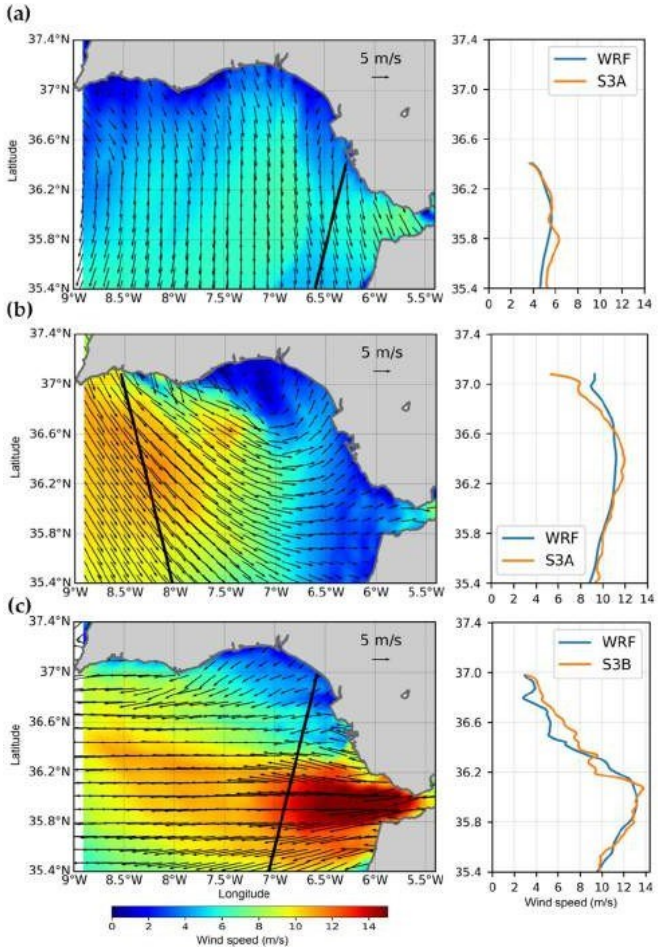

Figure 7. Wind field simulated by the WRF model overlaid with S3A/B track (left) and wind speed observed by S3A/B overlaid with interpolated WRF model data at the same positions for the closest available time. (**a**) 31 December 2020, WRF outputs for 11:00 UTC overlaid with S3A track at 10:35 UTC; (**b**) 25 June 2020, WRF outputs for 22:00 UTC overlaid with S3A track at 21:32 UTC; (**c**) 21 February 2020, WRF outputs for 11:00 UTC overlaid with S3B track at 10:37 UTC.

During the satellite pass on 25 June 2020 at 21:32 UTC the wind field reproduced by the model at 22:00 UTC (Figure 7b) over the GoC can be divided into two sectors: the westernmost area is dominated by mid intensity northwesterlies, while in the sector to the east, the wind is weaker and from west. Furthermore, as also shown by the along-track S3A WS, the intensity increases further from the coast from 6 to 10–12 m/s. Such spatial variability of the WS is well represented by both data sets; however, close to the coast, the differences among the altimeter derived WS and the WRF model output increase. Such disagreement may be caused by two factors as previously mentioned in Section 3.1: the time difference between the satellite pass and the model simulation; and the precision of the WRF model at fine scales close to the complex land–sea boundary. Such discrepancies in the WRF model can be detected thanks to the presence of altimetry data in the coastal fringe.

Finally, Figure 7c shows an example of dominant easterlies over the GoC, as simulated by the WRF for 21 February 2020 at 11:00 UTC. S3B crossed the area at 10:37 UTC. WRF output displays a heterogeneous wind field over the area, with a remarkable easterly jet coming from the Strait of Gibraltar and a generalised decrease towards the northern coast. However, over 36.8° latitude, a slight underestimation from the WRF model is observed, which coincides with the area covered by the Guadalquivir River mouth, an area characterised by high contrasts and variability.

4. Conclusions

This study presents the quality and capabilities of WS from satellite altimetry for the spatial assessment of WS outputs from the WRF model over the complex area of the GoC. In order to achieve this, three WS data sources were compared: in situ measurements, S3A/B satellite altimetry derived measurements at 20 Hz, and the WRF model simulations from a nested domain of 3 km grid and 1 h temporal resolution. From the results of the different comparisons, we conclude that the quality of the high-resolution (20 Hz) S3A/B WS data satisfies the general mission requirements over the study area, and even though the GoC buoy is located in a complex area affected by coastal-related processes, the results are in line with previous studies focused on the open ocean. Regarding the validation of the WRF model against in situ data, the simulations of the surface WS over the area are of good quality; this confirms the goodness of the dynamical parameterisations proposed by [45]. Note that we introduced a modification in the configuration by updating the SST every 6 h instead of maintaining a constant value, which makes the setup more realistic. The spatial variability of the WS derived from the model was compared to along-track altimetry-derived WS data. This comparison, and considering the complex characteristics of the analysed region, exhibits the potential of the altimetry data for the spatial evaluation of numerical models. In this case, the altimetry data enable the detection of a certain level of degradation of the WRF outcomes near the coastal fringe, which is in line with previously detected WS overestimation of the WRF model in coastal areas, which supports the need to conduct further analyses into the dynamical phenomena and the effect of using a more accurate surface representation. It is important to note that these model deficiencies in the coastal band are detected thanks to the presence of altimetry data up to 5 km from the land, enabling the fine tuning and evaluation of NWP models over the complex coastal fringe. Qualitatively, we proved the agreement between altimetry and WRF model data sets under low/high wind speed conditions. However, it is important to note the limitations related to altimetry, as it is not possible to obtain the wind direction. Furthermore, altimetry data are instantaneous and events of time scales shorter than the time resolution of the model may lead to mismatches. Moreover, perpendicular to the track, the altimeters do not measure the variability in scales smaller than the across track footprint length. In this sense, it is important to highlight the need for the continuous improvement of satellite altimetry and model outputs in the coastal fringe in order to obtain realistic geophysical parameters in these areas. Present and future satellite altimetry missions will allow the exploitation of fully focused SAR data for a better characterisation of ocean processes in the 0–5 km coastal band. This study proves the high quality of Sentinel-3A/B WS retrievals over complex areas, and aims to foster the use of this data for the improvement of knowledge of WS and sea surface circulation over areas where the availability of in situ measurements is limited or inexistent. We showed how the spatial coverage of satellite altimetry enables the spatial assessment of high-resolution NWP models in water-covered surfaces, including coastal areas up to 5 km from land, a feature that sets altimetry as a complementary data source to improve the study and prediction of the wind in coastal areas together with some of the current systems, such as scatterometers, high frequency radars, and SAR wind fields.

Author Contributions: Conceptualization, R.M.-M., C.R.-C., R.M., A.I., M.B. and J.G.-E.; Formal analysis, R.M.-M. and C.R.-C.; Funding acquisition, R.M. and M.B.; Investigation, R.M.-M., C.R.-C., A.I., M.B. and J.G.-E.; Methodology, R.M.-M. and J.G.-E.; Supervision, R.M. and J.G.-E.; Valida- tion, R.M.-M.; Visualization, R.M.-M.; Writing—original draft, R.M.-M.; Writing—review & editing, C.R.-C., R.M., A.I., M.B. and J.G.-E. All authors have read and agreed to the published version of the manuscript.

Funding: This article is part of a PhD thesis supported by the program "Earth and Marine Science", funded by the Spanish Project: circulation and transport processes in the estuaries of the GoC: current situation and projections of future climate change scenarios (TRUCO) (Ref.: RTI2018-100865-B-C22).

of the University of Cádiz (Spain) and the University of Ferrara (Italy). This paper was partially

Data Availability Statement: The altimetry data used in this article were obtained from the ESA- GPOD web page, and the in situ data were provided by the Spanish Ports Authorities, the AEMET and the Hydrographic Institute of Portugal.

Conflicts of Interest: The authors declare no conflict of interest.

References

1. Kelly, K.A.; Dickinson, S.; Yu, Z. NSCAT Tropical Wind Stress Maps: Implications for Improving Ocean Modeling. *J. Geophys. Res. Ocean.* **1999**, *104*, 11291–11310. [CrossRef]
2. GCOS. The Global Observing System for Climate Implementation Needs. *World Meteorol. Organ.* **2016**, *200*, 316.
3. Cerralbo, P.; Grifoll, M.; Moré, J.; Bravo, M.; Sairouní Afif, A.; Espino, M. Wind Variability in a Coastal Area (Alfacs Bay, Ebro River Delta). *Adv. Sci. Res.* **2015**, *12*, 11–21. [CrossRef]
4. Lu, Y.; Zhang, B.; Perrie, W.; Mouche, A.; Li, X.; Wang, H. A C-Band Geophysical Model Function for Determining Coastal Wind Speed Using Synthetic Aperture Radar. *Prog. Electromagn. Res. Symp.* **2018**, *11*, 2417–2428. [CrossRef]
5. Bôas, A.B.V.; Ardhuin, F.; Ayet, A.; Bourassa, M.A.; Brandt, P.; Chapron, B.; Cornuelle, B.D.; Farrar, J.T.; Fewings, M.R.; Fox-Kemper, B.; et al. Integrated Observations of Global Surface Winds, Currents, and Waves: Requirements and Challenges for the next Decade. *Front. Mar. Sci.* **2019**, *6*, 1–34. [CrossRef]
6. Mulero-Martínez, R.; Gómez-Enri, J.; Mañanes, R.; Bruno, M. Assessment of Near-Shore Currents from CryoSat-2 Satellite in the Gulf of Cádiz Using HF Radar-Derived Current Observations. *Remote Sens. Environ.* **2021**, *256*, 112310. [CrossRef]
7. Rio, M.H.; Mulet, S.; Picot, N. Beyond GOCE for the Ocean Circulation Estimate: Synergetic Use of Altimetry, Gravimetry, and in Situ Data Provides New Insight into Geostrophic and Ekman Currents. *Geophys. Res. Lett.* **2014**, *41*, 8918–8925. [CrossRef]
8. Mears, C.A.; Scott, J.; Wentz, F.J.; Ricciardulli, L.; Leidner, S.M.; Hoffman, R.; Atlas, R. A Near-Real-Time Version of the Cross-Calibrated Multiplatform (CCMP) Ocean Surface Wind Velocity Data Set. *J. Geophys. Res. Ocean.* **2019**, *124*, 6997–7010. [CrossRef]
9. Astudillo, O.; Dewitte, B.; Mallet, M.; Frappart, F.; Rutllant, J.A.; Ramos, M.; Bravo, L.; Goubanova, K.; Illig, S. Surface Winds off Peru-Chile: Observing Closer to the Coast from Radar Altimetry. *Remote Sens. Environ.* **2017**, *191*, 179–196. [CrossRef]
10. Vogelzang, J.; Stoffelen, A.; Lindsley, R.D.; Verhoef, A.; Verspeek, J. The ASCAT 6.25-Km Wind Product. *IEEE J. Sel. Top. Appl. Earth Obs. Remote Sens.* **2017**, *10*, 2321–2331. [CrossRef]
11. Carvalho, D.; Rocha, A.; Gómez-Gesteira, M.; Silva Santos, C. Offshore Winds and Wind Energy Production Estimates Derived from ASCAT, OSCAT, Numerical Weather Prediction Models and Buoys—A Comparative Study for the Iberian Peninsula Atlantic Coast. *Renew. Energy* **2017**, *102*, 433–444. [CrossRef]
12. Korsbakken, E.; Johannessen, J.A.; Johannessen, O.M. Coastal Wind Field Retrievals from ERS SAR Images. In Proceedings of the IGARSS'97. 1997 IEEE International Geoscience and Remote Sensing Symposium Proceedings. Remote Sensing-A Scientific Vision for Sustainable Development, Singapore, 3–8 August 1997; Volume 103, pp. 1211–1216. [CrossRef]
13. Zhou, L.; Zheng, G.; Li, X.; Yang, J.; Ren, L.; Chen, P.; Zhang, H.; Lou, X. An Improved Local Gradient Method for Sea Surface Wind Direction Retrieval from SAR Imagery. *Remote Sens.* **2017**, *9*, 671. [CrossRef]
14. Mu, S.; Li, X.; Wang, H. The Fusion of Physical, Textural, and Morphological Information in SAR Imagery for Hurricane Wind Speed Retrieval Based on Deep Learning. *IEEE Trans. Geosci. Remote Sens.* **2022**, *60*, 1–13. [CrossRef]
15. Sar, S.C.; Yu, P.; Xu, W.; Zhong, X.; Johannessen, J.A.; Yan, X.; Geng, X.; He, Y.; Lu, W. A Neural Network Method for Retrieving Sea Surface Wind Speed for C-Band SAR. *Remote Sens.* **2022**, *14*, 2269.
16. Abdalla, S. Ku-Band Radar Altimeter Surface Wind Speed Algorithm. *Mar. Geod.* **2012**, *35*, 276–298. [CrossRef]
17. Witter, D.L.; Chelton, D.B. A Geosat Altimeter Wind Speed Algorithm and a Method for Altimeter Wind Speed Algorithm Development. *J. Geophys. Res.* **1991**, *96*, 8853–8860. [CrossRef]
18. Yang, J.; Zhang, J.; Jia, Y.; Fan, C.; Cui, W. Validation of Sentinel-3A/3B and Jason-3 Altimeter Wind Speeds and Significant Wave Heights Using Buoy and ASCAT Data. *Remote Sens.* **2020**, *12*, 2079. [CrossRef]
19. Quartly, G.D.; Nencioli, F.; Raynal, M.; Bonnefond, P.; Garcia, P.N.; Garcia-Mondéjar, A.; de la Cruz, A.F.; Cretaux, J.F.; Taburet, N.; Frery, M.L.; et al. The Roles of the S3MPC: Monitoring, Validation and Evolution of Sentinel-3 Altimetry Observations. *Remote Sens.* **2020**, *12*, 1763. [CrossRef]
20. Abdalla, S.; Centre (MPC) for the Copernicus. *Sentinel-3 Mission S3 Wind and Waves Cyclic Performance Report*; Cycle No. 066-A End Date: 31 December 2020 Cycle No. 047-B; European Space Agency: Paris, France, 2021.
21. Powers, J.G.; Klemp, J.B.; Skamarock, W.C.; Davis, C.A.; Dudhia, J.; Gill, D.O.; Coen, J.L.; Gochis, D.J.; Ahmadov, R.; Peckham, S.E.; et al. The Weather Research and Forecasting Model: Overview, System Efforts, and Future Directions. *Bull. Am. Meteorol. Soc.* **2017**, *98*, 1717–1737. [CrossRef]
22. Skamarock, W.C.; Klemp, J.B.; Dudhia, J.; Gill, D.O.; Zhiquan, L.; Berner, J.; Wang, W.; Powers, J.G.; Duda, M.G.; Barker, D.M.; et al. *A Description of the Advanced Research WRF Model Version 4*; National Center for Atmospheric Research: Boulder, CO, USA, 2019; Volume 145, p. 145.
23. Bhowmick, S.A.; Modi, R.; Sandhya, K.G.; Seemanth, M.; Balakrishnan Nair, T.M.; Kumar, R.; Sharma, R. Analysis of SARAL/AltiKa Wind and Wave over Indian Ocean and Its Real-Time Application in Wave Forecasting System at ISRO. *Mar. Geod.* **2015**, *38*, 396–408. [CrossRef]

24. Carvalho, D.; Rocha, A.; Gómez-Gesteira, M.; Silva Santos, C. Sensitivity of the WRF Model Wind Simulation and Wind Energy Production Estimates to Planetary Boundary Layer Parameterizations for Onshore and Offshore Areas in the Iberian Peninsula. *Appl. Energy* **2014**, *135*, 234–246. [CrossRef]
25. Peliz, A.; Dubert, J.; Marchesiello, P.; Teles-Machado, A. Surface Circulation in the Gulf of Cadiz: Model and Mean Flow Structure. *J. Geophys. Res. Ocean.* **2007**, *112*, C11015. [CrossRef]
26. Navarro, G.; Escudier, R.; Pascual, A.; Caballero, I.; Vázquez, A. Singular Value Decomposition of Ocean Surface Chlorophyll and Sea Level Anomalies in the Gulf of Cadiz (South-Western Iberian Peninsula). In Proceedings of the 20 Years of Progress in Radar Altimetry Conference, Venice, Italy, 24–29 September 2012.
27. Garel, E.; Laiz, I.; Drago, T.; Relvas, P. Characterisation of Coastal Counter-Currents on the Inner Shelf of the Gulf of Cadiz. *J. Mar. Syst.* **2016**, *155*, 19–34. [CrossRef]
28. Hernández-Ceballos, M.A.; Adame, J.A.; Bolívar, J.P.; De la Morena, B.A. A Mesoscale Simulation of Coastal Circulation in the Guadalquivir Valley (Southwestern Iberian Peninsula) Using the WRF-ARW Model. *Atmos. Res.* **2013**, *124*, 1–20. [CrossRef]
29. Folkard, A.M.; Davies, P.A.; Fiuza, A.F.G.; Ambar, I. Remotely Sensed Sea Surface Thermal Patterns in the Gulf Of Cadiz and the Strait of Gibraltar: Variability, Correlations, and Relationships with the Surface Wind Field. *J. Geophys. Res. Ocean.* **1997**, *102*, 5669–5683. [CrossRef]
30. Hidalgo, P.; Gallego, D. A Historical Climatology of the Easterly Winds in the Strait of Gibraltar. *Atmosfera* **2019**, *32*, 181–195. [CrossRef]
31. Brandt, P.; Rubino, A.; Sein, D.V.; Baschek, B.; Izquierdo, A.; Backhaus, J.O. Sea Level Variations in the Western Mediterranean Studied by a Numerical Tidal Model of the Strait of Gibraltar. *J. Phys. Oceanogr.* **2004**, *34*, 433–443. [CrossRef]
32. Ross, T.; Garrett, C.; Traon, P.Y. Le Western Mediterranean Sea-Level Rise: Changing Exchange Flow through the Strait of Gibraltar. *Geophys. Res. Lett.* **2000**, *27*, 2949–2952. [CrossRef]
33. Gómez-Enri, J.; González, C.J.; Passaro, M.; Vignudelli, S.; Álvarez, O.; Cipollini, P.; Mañanes, R.; Bruno, M.; López-Carmona, M.P.; Izquierdo, A. Wind-Induced Cross-Strait Sea Level Variability in the Strait of Gibraltar from Coastal Altimetry and in-Situ Measurements. *Remote Sens. Environ.* **2019**, *221*, 596–608. [CrossRef]
34. Aldarias, A.; Gomez-Enri, J.; Laiz, I.; Tejedor, B.; Vignudelli, S.; Cipollini, P. Validation of Sentinel-3A SRAL Coastal Sea Level Data at High Posting Rate: 80 Hz. *IEEE Trans. Geosci. Remote Sens.* **2020**, *58*, 3809–3821. [CrossRef]
35. Gómez-Enri, J.; Vignudelli, S.; Cipollini, P.; Coca, J.; González, C.J. Validation of CryoSat-2 SIRAL Sea Level Data in the Eastern Continental Shelf of the Gulf of Cadiz (Spain). *Adv. Space Res.* **2018**, *62*, 1405–1420. [CrossRef]
36. Bouffard, J.; Pascual, A.; Ruiz, S.; Faugère, Y.; Tintoré, J. Coastal and Mesoscale Dynamics Characterization Using Altimetry and Gliders: A Case Study in the Balearic Sea. *J. Geophys. Res. Ocean.* **2010**, *115*, 1–17. [CrossRef]
37. Meloni, M.; Bouffard, J.; Doglioli, A.M.; Petrenko, A.A.; Valladeau, G. Toward Science-Oriented Validations of Coastal Altimetry: Application to the Ligurian Sea. *Remote Sens. Environ.* **2019**, *224*, 275–288. [CrossRef]
38. Paulson, C.A. The Mathematical Representation of Wind Speed and Temperature Profiles in the Unstable Atmospheric Surface Layer. *J. Appl. Meteorol.* **1970**, *9*, 857–861. [CrossRef]
39. Powell, M.D.; Vickery, P.J.; Reinhold, T.A. Reduced Drag Coefficient for High Wind Speeds in Tropical Cyclones. *Nature* **2003**, *422*, 279–283. [CrossRef]
40. Carvalho, D.; Rocha, A.; Gómez-Gesteira, M.; Santos, C. A Sensitivity Study of the WRF Model in Wind Simulation for an Area of High Wind Energy. *Environ. Model. Softw.* **2012**, *33*, 23–34. [CrossRef]
41. De Kloe, J.; Stoffelen, A.; Verhoef, A. Improved Use of Scatterometer Measurements by Using Stress-Equivalent Reference Winds. *IEEE J. Sel. Top. Appl. Earth Obs. Remote Sens.* **2017**, *10*, 2340–2347. [CrossRef]
42. Emeis, S.; Turk, M. Comparison of Logarithmic Wind Profiles and Power Law Wind Profiles and Their Applicability for Offshore Wind Profiles. In *Wind Energy*; Springer: Berlin/Heidelberg, Germany, 2007; pp. 61–64. [CrossRef]
43. Peña, A.; Gryning, S.E.; Hasager, C.B. Measurements and Modelling of the Wind Speed Profile in the Marine Atmospheric Boundary Layer. *Bound.-Layer Meteorol.* **2008**, *129*, 479–495. [CrossRef]
44. Arasa, R.; Porras, I.; Domingo-Dalmau, A.; Picanyol, M.; Codina, B.; González, M.Á.; Piñón, J. Defining a Standard Methodology to Obtain Optimum WRF Configuration for Operational Forecast: Application over the Port of Huelva (Southern Spain). *Atmos. Chem. Sci.* **2016**, *6*, 329–350. [CrossRef]
45. Salvação, N.; Guedes Soares, C. Wind Resource Assessment Offshore the Atlantic Iberian Coast with the WRF Model. *Energy* **2018**, *145*, 276–287. [CrossRef]
46. Li, H.; Claremar, B.; Wu, L.; Halgren, C.; Körnich, H.; Ivanell, S.; Sahlée, E. A Sensitivity Study of the WRF Model in Offshore Wind Modeling over the Baltic Sea. *Geosci. Front.* **2021**, *12*, 101229. [CrossRef]
47. Marta-Almeida, M.; Teixeira, J.C.; Carvalho, M.J.; Melo-Gonçalves, P.; Rocha, A.M. High Resolution WRF Climatic Simulations for the Iberian Peninsula: Model Validation. *Phys. Chem. Earth Parts A/B/C* **2016**, *94*, 94–105. [CrossRef]
48. Carvalho, D.; Rocha, A.; Gómez-Gesteira, M. Ocean Surface Wind Simulation Forced by Different Reanalyses: Comparison with Observed Data along the Iberian Peninsula Coast. *Ocean Model.* **2012**, *56*, 31–42. [CrossRef]
49. Stoffelen, A. Toward the True Near-Surface Wind Speed: Error Modeling and Calibration Using Triple Collocation. *J. Geophys. Res. Ocean.* **1998**, *103*, 7755–7766. [CrossRef]
50. Passaro, M.; Cipollini, P.; Vignudelli, S.; Quartly, G.D.; Snaith, H.M. ALES: A Multi-Mission Adaptive Subwaveform Retracker for Coastal and Open Ocean Altimetry. *Remote Sens. Environ.* **2014**, *145*, 173–189. [CrossRef]

51. Adame, J.A.; Lope, L.; Hidalgo, P.J.; Sorribas, M.; Gutiérrez-Álvarez, I.; del Águila, A.; Saiz-Lopez, A.; Yela, M. Study of the Exceptional Meteorological Conditions, Trace Gases and Particulate Matter Measured during the 2017 Forest Fire in Doñana Natural Park, Spain. *Sci. Total Environ.* **2018**, *645*, 710–720. [CrossRef]
52. Ngan, F.; Kim, H.; Lee, P.; Al-Wali, K.; Dornblaser, B. A Study of Nocturnal Surface Wind Speed Overprediction by the WRF-ARW Model in Southeastern Texas. *J. Appl. Meteorol. Climatol.* **2013**, *52*, 2638–2653. [CrossRef]
53. Misaki, T.; Ohsawa, T.; Konagaya, M.; Shimada, S.; Takeyama, Y.; Nakamura, S. Accuracy Comparison of Coastal Wind Speeds between WRF Simulations Using Different Input Datasets in Japan. *Energies* **2019**, *12*, 2754. [CrossRef]
54. Román-Cascón, C.; Lothon, M.; Lohou, F.; Hartogensis, O.; Vila-Guerau De Arellano, J.; Pino, D.; Yagüe, C.; Pardyjak, E.R. Surface Representation Impacts on Turbulent Heat Fluxes in the Weather Research and Forecasting (WRF) Model (v.4.1.3). *Geosci. Model Dev.* **2021**, *14*, 3939–3967. [CrossRef]

UCA Universidad de Cádiz

educa
Escuela de Doctorado UCA

Edificio Hospital Real
Plaza Falla nº 8
11003 Cádiz
http://escueladoctoral.uca.es/
escuela.doctoral@uca.es

Modelo de consentimiento de coautores para inclusión de trabajos en la modalidad de tesis por compendio de publicaciones

Los investigadores/as:

Gómez-Enri, J.; De Oliveira Júnior, L.; Garel, E.; Relvas, P.; Mañanes, R., como coautores/as del artículo/libro/capítulo de libro:

Spatiotemporal variability of the coastal circulation in the northern Gulf of Cadiz from Copernicus Sentinel-3A satellite radar altimetry measurements, publicado en *Advances in Space Research*, por la presente dan su consentimiento para que esta publicación sea incorporada a la tesis doctoral titulada *Coastal surface circulation of the Gulf of Cadiz from satellite altimetry measurements* cuyo autor/a es Roberto Mulero Martínez, renunciando a presentar estos resultados como parte de otra tesis doctoral en cualquier Universidad.

En Cádiz, a 06 de marzo de 2024

GOMEZ ENRI JESUS - 34048944C

Firmado digitalmente por GOMEZ ENRI JESUS - 34048944C
Nombre de reconocimiento (DN): cn=GOMEZ ENRI JESUS - 34048944C, sn=GOMEZ ENRI, givenName=JESUS, c=ES, serialNumber=IDCES-34048944C
Fecha: 2024.03.07 15:07:43 +01'00'

Fdo. Jesús Gómez Enri

Fdo. Luciano De Oliveira Junior

Fdo. Erwan Garel

Digitally signed by Erwan Garel
DN: cn=Erwan Garel, o=Universidade do Algarve, ou=CIMA, email=egarel@ualg.pt, c=PT
Date: 2024.03.06 16:27:50 Z

Fdo. Paulo Relvas

Firmado por MAÑANES SALINAS RAFAEL - ***0751** el día 07/03/2024 con un certificado emitido por AC FNMT Usuarios

Fdo. Rafael Mañanes Salinas

Journal Pre-proofs

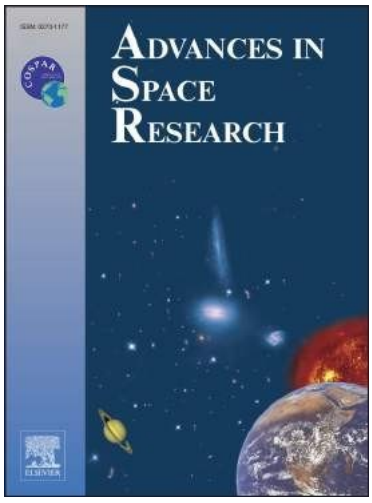

Spatiotemporal variability of the coastal circulation in the northern Gulf of Cadiz from Copernicus Sentinel-3A satellite radar altimetry measurements

R. Mulero-Martinez, J. Gómez-Enri, L. De Oliveira Júnior, E. Garel, P. Relvas, R. Mañanes

PII: S0273-1177(24)00197-2
DOI: https://doi.org/10.1016/j.asr.2024.02.054
Reference: JASR 17301

To appear in: *Advances in Space Research*

Received Date: 29 November 2023
Revised Date: 24 February 2024
Accepted Date: 27 February 2024

Please cite this article as: Mulero-Martinez, R., Gómez-Enri, J., De Oliveira Júnior, L., Garel, E., Relvas, P., Mañanes, R., Spatiotemporal variability of the coastal circulation in the northern Gulf of Cadiz from Copernicus Sentinel-3A satellite radar altimetry measurements, *Advances in Space Research* (2024), doi: https://doi.org/ 10.1016/j.asr.2024.02.054

Spatiotemporal variability of the coastal circulation in the northern Gulf of Cadiz from Copernicus Sentinel-3A satellite radar altimetry measurements

Mulero-Martinez, R. (roberto.mulero@uca.es); Gómez-Enri, J. (jesus.gomez@uca.es); De Oliveira Júnior, L. (lojunior@ualg.pt); Garel, E. (egarel@ualg.pt); Relvas, P. (prelvas@ualg.pt); Mañanes, R. (rafael.salinas@uca.es)

Full title: Spatiotemporal variability of the coastal circulation in the northern Gulf of Cadiz from Copernicus Sentinel-3A satellite radar altimetry measurements

Authors:

Mulero-Martinez, Roberto [1]; orcid: 0000-0002-1736-907X

Gómez-Enri, Jesús [1]; orcid: 0000-0001-6053-5160

De Oliveira Júnior, Luciano [2]; orcid: 0000-0001-5899-2979

Garel, Erwan [2]; orcid: 0000-0002-4584-9759

Relvas, Paulo [3]; orcid: 0000-0002-6404-5895

Mañanes, Rafael [1]; orcid: 0000-0003-1987-478X

Affiliations:

[1]Department of Applied Physics, Faculty of Marine and Environmental Sciences, University of Cadiz, Puerto Real, 11510, Spain

[2]Centre for Marine and Environmental Research (CIMA), University of Algarve, Faro, 8005-139, Portugal

[3]Centre of Marine Sciences (CCMAR), University of Algarve, Faro, 8005-139, Portugal

Contact information for the corresponding author:

roberto.mulero@uca.es (R. Mulero-Martínez)

Abstract

This study presents a generalised characterisation of the surface circulation over the northern shelf of the Gulf of Cadiz, based on 4 years of high-resolution satellite altimetry data from Sentinel-3A and wind model data. The altimetry-based surface zonal currents, adjusted for bottom-drag and wind effects, are compared with a generic CMEMS product and validated against in-situ ADCP measurements. The proposed altimetry product demonstrates superior performance than the CMEMS product, accurately reflecting surface circulation direction compared to in-situ measurements ($r = 0.77$, RMSE = 0.10 m/s, bias = 0.01 m/s). The use of the bottom-drag and wind-corrected/uncorrected altimetry product for spatiotemporal analysis of the shelf circulation revealed the distinct contributions of wind-driven and geostrophic components in different basin sectors. The results show that over the western basin, positive (eastward) surface currents were predominantly driven by westerly winds, while only occasionally, westward flows coincided with easterly winds, suggesting a higher control of the geostrophic component over the westward flows. In contrast, over the eastern basin, both eastward and westward flows were found to be primarily driven by favourable winds. Additionally, the analysis of Absolute Dynamic Topography (ADT) values along the whole basin showed the presence of ADT gradients both along-shore and cross-shore over the shelf, contributing to geostrophic flows. Finally, the seasonal analysis showed that eastward circulation tends to dominate during the spring and summer months, related to the upwelling season in the Gulf of Cadiz and associated westerly winds. Westward flows prevail during the winter months, related to easterly winds and the rebalancing of the along-shore sea level gradient during relaxed upwelling conditions. The findings demonstrate a significant improvement in the use of satellite altimetry data to study complex oceanographic dynamics in coastal areas, where both spatial and temporal variability are high. Moreover, the similarity of our results to those obtained from in-situ systems supports the use of altimetry data and publicly available wind models to support oceanographic studies in remote or resource-limited areas.

1 Introduction

The use of satellite altimetry had a transformative impact on the discipline of physical oceanography by providing a comprehensive global perspective on ocean topography from space (Fu et al. 2010). This advancement has made significant contributions to our understanding of large-scale circulation patterns and processes in the open ocean through the application of geostrophic approximation methods. Studying ocean dynamics becomes notably complex in coastal areas and smaller sub-basins where the geostrophic approximation by itself might not be enough to explain the circulation due to local phenomena and non-geostrophic factors like complex variations in wind fields, shallow bottom topographies, river discharges, and interactions between different water masses (Criado-Aldeanueva et al. 2006; Mulero-Martínez et al. 2021). Nonetheless, more in-depth knowledge of the ocean dynamics over coastal areas (including the potential effects of sea level rise) has significant socio-economic and environmental implications, potentially improving the management of activities such as fisheries, offshore energy or navigation-related risks.

Recent advancements in radar altimetry have greatly enhanced the accuracy and resolution of sea surface height (SSH) measurements along the satellite's tracks, allowing the study of coastal ocean circulation by providing observations at short spatial scales critical for coastal regions (Morrow et al. 2017; Raney 2012). In particular, Synthetic Aperture Radar (SAR) Delay-Doppler altimetry achieves a resolution which is an order of magnitude finer compared to conventional radar altimetry. The Sentinel-3A (S3A) satellite altimeter currently provides SAR-mode data in the whole ocean enabling the application of this innovative data processing approach to coastal ocean studies (Feng et al. 2023). Besides, satellite altimetry continues evolving and represents a fast-developing technology, exemplified by the recent launch of the Surface Water and Ocean Topography (SWOT) mission that will collect data across a 120 km wide swath (Srinivasan and Tsontos 2023).

This study aims to present the capacities of S3A SAR mode datasets for assessing coastal sea surface circulation over the Gulf of Cadiz. In addition, the study shows how the value of such a dataset, characterised by its enhanced and consistent time and spatial coverage, can be improved when accounting for the effect of ageostrophic factors such as the bottom-drag effects and the wind-driven surface circulation. On a final basis, this work aims to contribute to achieving a level of understanding of ocean circulation in coastal zones from altimetry similar to that of the open ocean (Troupin et al. 2015), even in areas with a lack of either in-situ measurements or local hydrodynamical models. The overarching goal of this study is to complement regional coastal oceanographic studies by providing the highest quality altimeter measurements of Absolute Dynamic Topography (ADT) and ADT-derived geostrophic current (V_t), over the northern GoC coastal zone. This objective entails an investigation into the quality of different altimetry-based products but also about the different mechanisms affecting the sea surface circulation over the continental shelf of the GoC along its sub-basins. The approach relies upon previous coastal oceanographic studies (Manso-Narvarte et al. 2018a; Mulero-Martínez et al. 2021) based on altimetry and local oceanographic studies (Garel et al. 2016; De Oliveira Júnior, Garel, and Relvas 2021; De Oliveira Júnior, Relvas, and Garel 2022) based on various measurement devices such as high-frequency radar (HFR) and Acoustic Doppler current profiler (ADCP).

The paper is organized as follows. Section 2 provides a concise overview of the study region and presents recent research findings about the ocean circulation in the area. Section 3 describes the datasets and methods applied, including the detailed filtering strategy applied to the raw altimetry data and the approach to obtain estimates of the geostrophic velocity. Results and discussions are presented in Section 4, starting with the comparison of altimetry-derived surface current velocity from different products with in-situ ADCP measurements. Next, the GoC shelf circulation is characterised based on current velocity estimated with the most accurate product from the previous comparison with ADCP, including the assessment of the alongshore ADT gradients, the different contributions of both the bottom-drag corrected geostrophic and the wind-driven circulation to the total circulation and the spatiotemporal variability of the circulation over the shelf. Finally, the summary and conclusions are presented in Section 5.

2 Study area

The GoC is located between the northwestern coast of Africa and the southwestern tip of the Iberian Peninsula. The northern shelf spans from the eastern Strait of Gibraltar to Cape San Vicente (CSV) in the west. It is divided by Cape Santa Maria (CSM) into a narrower western shelf and a broader eastern shelf (Figure 1). The complex dynamics of the surface circulation in this region are influenced by factors such as bathymetry, wind patterns, river discharges and water mass exchanges through the Strait of Gibraltar (Criado-Aldeanueva et al. 2006; García-Lafuente et al. 2006).

The wind field along the GoC is influenced by various factors, including topography, atmospheric flows, and temperature variations between land and sea (Carvalho et al. 2014; Mulero-martinez et al. 2022). The wind patterns in the GoC exhibit alternating flows known as Ponientes (westerly) and Levantes (easterly). These winds can occur consistently throughout the year with a periodicity of approximately 2-3 days (De Oliveira Júnior et al. 2021) but generally respond to a seasonal cycle forced by the seasonal displacement of the Azores high (Criado-Aldeanueva et al. 2009; Ortega et al. 2023). During the winter and autumn months (December to February and September to November, respectively), there is a high degree of variability in wind direction accompanied by frequent intense weather events, including strong Levantes. In spring, northwest winds become less dominant, occasionally giving way to stronger eastward winds. Summer experiences predominantly calm winds with a prevailing northwest component (De Oliveira Júnior et al. 2021). Northerly winds along western Portugal rotate anti-clockwise from CSV, providing the conditions for local upwelling along the southern coast. East of Cape Santa Maria, the intensity of the wind-related upwelling events decreases due to the widening continental shelf being non-significant by the middle of the eastern basin (De Oliveira Júnior et al. 2022).

The large-scale (> 100 km) sea surface circulation in the GoC generally displays a south-eastward background circulation superimposed on the anticyclonic pattern delineated by the presence of the Gulf of Cadiz Current (GCC) that is strongest in summer (Criado-Aldeanueva et al. 2006; García-Lafuente et al. 2006; Garel et al. 2016; Sánchez and Relvas 2003). Shifts to north-westward flow can be observed throughout the year, but predominantly in late autumn and early winter, particularly in December and January (Folkard et al. 1997; Sánchez and Relvas 2003). Over the continental shelf, the flow is alongshore, alternating between eastward and westward at a time scale of 2-3 days, following a similar pattern to the wind field. The alongshore velocities, mostly zonal due to the coastline orientation, can reach up to approximately 0.4 m/s, while cross-shore

(meridional) velocities, mainly dominated by tidal forces, are one order of magnitude weaker (Garel et al. 2016; De Oliveira Júnior et al. 2021). The shelf circulation along the GoC is highly linked to the southward flows along Portugal's western coast and its upwelling system. Eastward cold-water flows along the GoC shelf originated either under northerly winds, due to the rotation of the poleward Portugal's current around CSV or locally under westerly wind conditions (Folkard et al. 1997; De Oliveira Júnior et al. 2022). In contrast, westward coastal flows, commonly expressed as Coastal Counter Currents (CCC) (Garel et al. 2016; Laiz et al. 2019; De Oliveira Júnior et al. 2021, 2022; Teles-Machado et al. 2007) due to their opposite direction to the characteristic south-eastward slope of the GCC, develop along a relatively narrow strip spanning up to 15-20 km off the coast (De Oliveira Júnior et al. 2021). Recent studies of surface currents derived from High-Frequency Radar (HFR) and numerical model simulations found the coastal margin of the westernmost side of the Strait of Gibraltar as the initiation point of the CCCs events (Sirviente et al. 2023). Opposite to the eastward flows, CCCs tend to increase coastal temperatures during summer through the transport of warm water from areas surrounding the mouth of the Guadalquivir River and Cadiz Bay marshes (Relvas and Barton 2002). Such transport does not only affect water temperature but also nutrient availability and the transport of pollutants throughout the basin, playing a key role in the biogeochemistry of the area (Laiz et al. 2019). The occurrence of CCCs has been associated with an unbalanced along-shore pressure gradient during periods of weakened upwelling-favourable winds (Garel et al. 2016; De Oliveira Júnior et al. 2021, 2022). In addition to local wind stress, it is crucial to take into account the impact of remote factors such as wind forcing over the Alboran Sea and the eastern side of the Strait of Gibraltar. A recent study also suggested a potential relation with the sea level atmospheric pressure forcing over the Ligurian Sea (Sirviente et al. 2023). However, understanding the primary driving mechanisms for CCCs in this region is challenging since those events result from various intricated factors that vary spatially and temporally.

Considering the different features that characterise the GoC circulation, a generic glimpse of the ocean surface circulation can be defined as a predominant anticyclonic system, regarding the open ocean circulation, with episodic inversions to north-westward circulation under strong and persistent easterly winds. The shelf circulation is characterised by the presence of two transient cyclonic cells over the eastern and western basins, driven by CCC events in the north and delimited by the GCC in the south (Criado-Aldeanueva et al. 2009).

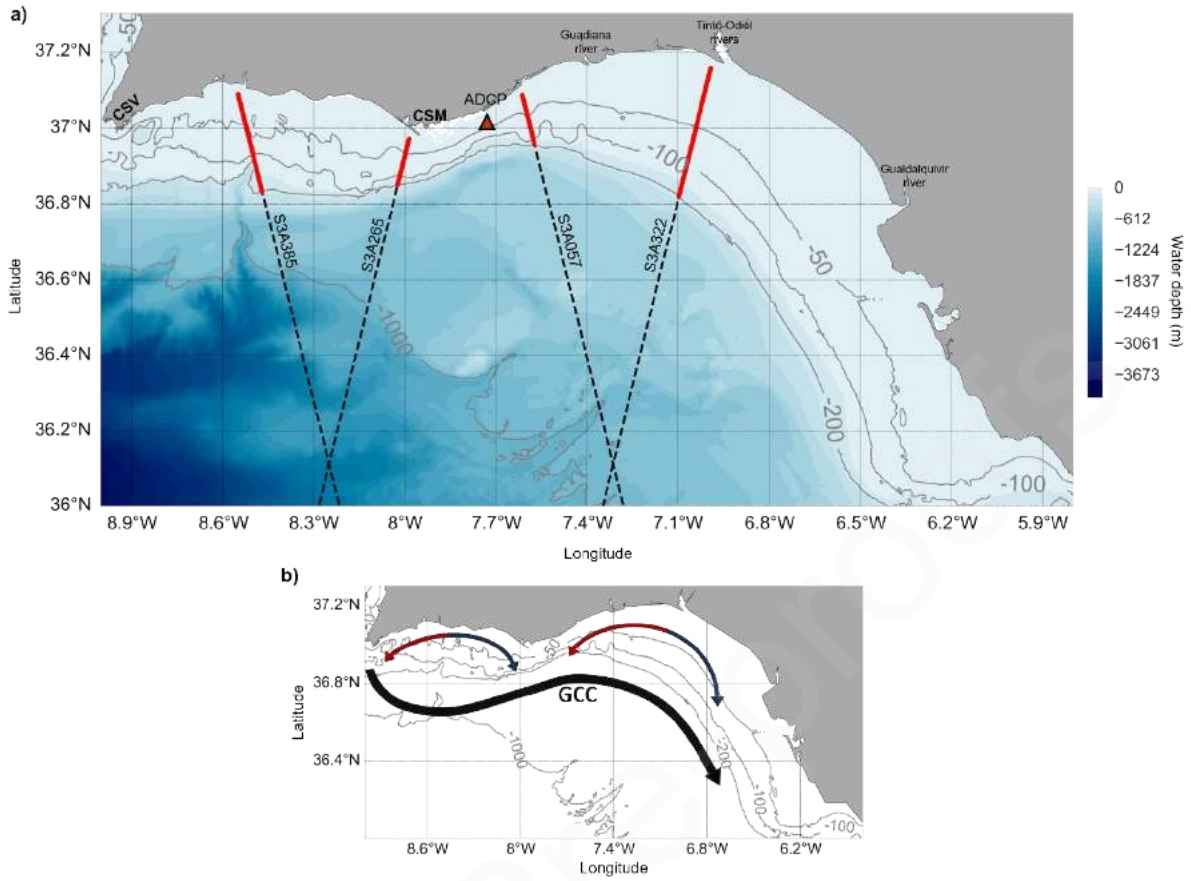

Figure 1. (a) Study area along with the Sentinel-3A tracks (red lines indicate the sectors considered over the continental shelf, with depth ≤ 200 m) selected for the study and the location of the Armona ADCP. The main geographical characters are also presented: Cape San Vicente (CSV); Cape Santa Maria (CSM). (b) Representative scheme of the surface circulation in the northern margin of the GoC based on (De Oliveira Júnior et al. 2022)*, where the GCC remains stable almost all year round, while over the shelf, the blue lines represent the circulation under favourable upwelling conditions and the red lines represent the circulation under weakened upwelling conditions and/or strong Levantes.*

3 Data and methods

3.1 Satellite altimetry data from Sentinel-3A

This study is based on high-resolution along-track ADT obtained from Sea Level Anomaly (SLA) measurements from 4 different Sentinel-3A tracks crossing the continental shelf of the GoC (Figure 1), during the period: 2017-2021. Each track has a repeat cycle of 27 days and is identified by its specific relative orbit number: S3A-385, S3A-265, S3A-057 and S3A-322.

The synthetic aperture radar altimeter (SRAL) instrument onboard Sentinel-3A can measure in two different modes, namely, low resolution (LRM) and synthetic aperture radar (SAR). The latter mode, SAR, is renowned for its high-resolution along-track capabilities and is widely utilised across the global ocean. Additionally, the data from the SRAL instrument on Sentinel-3A can be post-processed to generate level-2 data at frequencies of 1 Hz, 20 Hz and 80 Hz for the Ku and C bands. Detailed information regarding these data can be found in the Sentinel-3 Altimetry Document Library,

accessible at https://sentinel.esa.int/web/sentinel. Sentinel-3A level 2 data for this study were accessed through the ESA Earth Console Parallel Processing Service (P-PRO) SAR versatile altimetric toolkit for ocean research and exploitation, known as P-PRO SARvatore (https://ui-ppro.earthconsole.eu). These data were processed using the predefined setup designed for coastal zones. In addition, the retracking process was based on the SAR Altimetry MOde Studies and Applications (SAMOSA++) model (Dinardo et al. 2021). The product extracted consists of SLA measurements at a frequency of 20 Hz, yielding an along-track spatial resolution of approximately 330 meters. Finally, a set of range and geophysical corrections, presented in Table 1, are applied following the recommendations in (Feng et al. 2023; Fenoglio-Marc et al. 2015; Gómez-Enri et al. 2018; Mulero-Martínez et al. 2021), including a sea state bias (SSB) correction based on 5% of the significant wave height (SWH), as suggested by (Fenoglio-Marc et al. 2015; Gómez-Enri et al. 2018).

Table 1. Range and geophysical corrections applied to the original Sea Level Anomaly (SLA) measurements.

Range corrections	**Geophysical corrections**	
Atmospheric	**Tidal**	**Ocean surface**
Dry Tropospheric	Ocean Tide (TPXO8-atlas model)	Dynamic Atmospheric Correction
Wet Tropospheric	Long-Period Equilibrium Tide	Sea State Bias (5% Significant Wave Height)
Ionospheric	Ocean Loading Tide	
	Solid Earth Tide	
	Geocentric Polar Tide	

3.1.1 Sea level anomaly (SLA) filtering strategy

To obtain valid SLA data up to 3 km from the coast over the GoC, 20-Hz along-track SLA data from 4 different Sentinel-3A relative orbits over the area for the period 2017-2021 were edited as follows: Firstly, raw SLA values closer than 3 km to the coastline were rejected to maintain a distance of good quality. This criterion is based on Aldarias et al. (2020), which suggested that good quality data can be obtained within S3-A tracks up to 3 km from the coast in our study area. Secondly, values larger than three times the standard deviation of the SLA were removed and replaced by linearly interpolated values; this process was applied 10 times to remove most outliers in SLA estimates (Bouffard et al. 2010; Meloni et al. 2019; Mulero-Martínez et al. 2021). Finally, a LOESS (locally weighted smoothing) filter (Cleveland and Devlin 1988) was applied along each track segment individually to filter out high-frequency noise (Manso-Narvarte et al. 2018b); this is a common and proven valid processing procedure for the study of oceanic mesoscale phenomena (Morrow et al. 2017; Mulero-Martínez et al. 2021). After applying this procedure, the resulting SLA is suitable for being used for oceanographic purposes. Figure 2 shows an example of track S3A-057 before (Fig. 2.a) and after (Fig. 2.b) the filtering process.

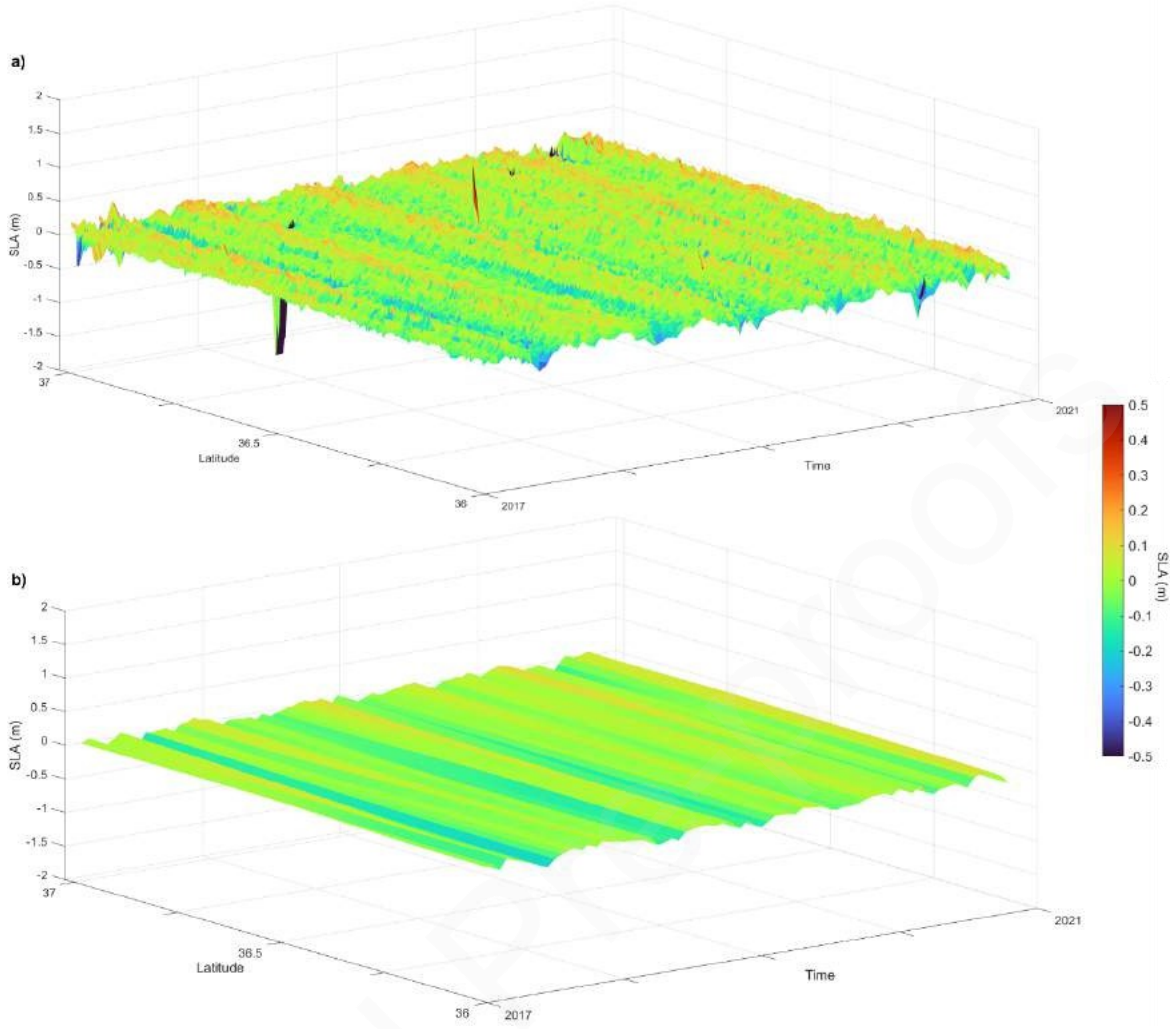

Figure 2. Latitude-time variability of the SLA from S3A-057 before (a) and after (b) applying the filtering strategy.

3.1.2 Absolute Dynamic Topography (ADT) and surface circulation.

Absolute dynamic topography (ADT) profiles were estimated by adding the mean dynamic topography (MDT) to the SLA. Though the ADT can also be computed by extracting a geoid model from the sea surface height (SSH), the MDT-based approach has been found to provide the best estimates when used to calculate derived geostrophic velocities, as it is exposed in Section 4.1.1. The DTU15MDT model (Knudsen, Andersen, and Maximenko 2016) was used to calculate the final ADT. This MDT model has been previously used by (Mulero-Martínez et al. 2021) over the eastern basin of the GoC for estimating geostrophic currents from CryoSat-2 satellite altimetry data with good results. While the MDT data were interpolated from the original model grid to the satellite' tracks positions, the EGM2008 (Pavlis et al. 2008) and EIGEN6C4 (Förste et al. 2014) geoid models data tested in Section 4.1.1 were extracted along with the raw altimetry data from the P-PRO SARvatore service, at the same 20 Hz posting rate.

Given that the ADT characterises the dynamic signal denoting displacement relative to the equipotential surface (geoid) influenced by interactions involving the atmosphere and

the topographical features of the ocean floor and its boundaries, it is feasible to derive an estimate of the absolute surface geostrophic circulation using altimeter measurements. This estimation relies on analysing the spatial fluctuations in ADT while accounting for the impact of the Earth's rotational motion, represented by the Coriolis force. Briefly, it is possible to obtain estimates of the absolute geostrophic component of the surface circulation (V_{gAbs}) normal to the satellite tracks using the following Eq. (1):

$$V_{gAbs} = \frac{-g}{f} \cdot \frac{\partial ADT}{\partial y}$$

where g (m·s^{-2}) is the gravitational acceleration; y (m) is the along-track distance; f (s^{-1}) is the Coriolis parameter ($f = 2\Omega sin\varphi$, where Ω is the angular rotation velocity of the Earth and φ the latitude). The along-track ADT (m) gradient (slope) is estimated by using the optimal filter developed by (Powell and Leben 2004). In addition, (Mulero-Martínez et al. 2021) suggested that, in coastal areas, the effect of both the wind-induced velocity component and the bottom friction must be considered to improve estimates of the surface circulation. Following (Mulero-Martínez et al. 2021), Eq. (2) and Eq. (3) provide an estimation of the bottom-drag corrected surface geostrophic velocity (V_{gd}, m·s^{-1}) and the zonal surface wind-driven velocities (V_w, m·s^{-1}), respectively:

$$V_{gd} = \frac{-g}{f + \left(\frac{r^2}{f}\right)} \cdot \frac{\partial ADT}{\partial y}$$

$$V_w = 0.03 \cdot U_{10} \cdot \cos(10°),$$

where $r = (0.35C_d)/d$ (m^{-1}) is a depth-dependent parameter, using a typically accepted value of $C_d = 2.0\ 10^{-3}$ (Bowden 1983), and U_{10} (m·s^{-1}) is the zonal component of the wind speed at 10 m above the mean sea level.

Finally, Eq. (4) allows the estimation of a more complete along-track total surface velocity (V_t), accounting for the main geostrophic component derived from altimetry and corrected for the bottom friction and wind drag effects on the surface circulation, as proposed by (Mulero-Martínez et al. 2021).

$$V_t = \frac{-g}{f + \left(\frac{r^2}{f}\right)} \cdot \frac{\partial ADT}{\partial y} + 0.03 \cdot U_{10} \cdot \cos(10°) \quad (4)$$

where r is a depth-dependent parameter and U_{10} is the zonal component of the wind speed. An in-depth development of Eq. (2) can be found in (Mulero-Martínez et al. 2021). In addition, the resulting cross-track velocities are rotated to obtain the zonal component of the current.

Figure 3 summarizes the complete methodology from the original raw SLA measurements to the final V_t product.

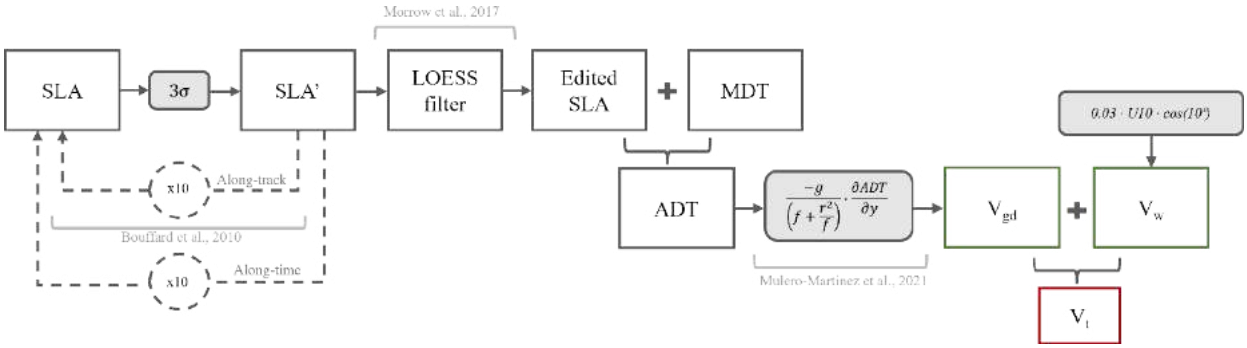

Figure 3. Schematic representation of the complete methodology for editing satellite sea level anomaly and calculating the along-track total surface velocity.

3.2 Model wind data

Wind data used to compute the wind component of the circulation for the period 2017-2021 was extracted from the National Center for Environmental Prediction (NCEP) operational Global Forecast System (GFS) with 0.25˚ (approximately 25 km) of grid resolution and 6 h of temporal sampling (https://rda.ucar.edu/datasets/ds084.1/). A previous study on the GoC found the NCEP-GFS model as a reliable source of wind data, obtaining the best results in terms of error and correlation, for both wind speed and direction, when assessed against in-situ measurements and compared with other equivalent publicly available models (Carvalho et al. 2014). NCEP GFS wind data was used for the estimation of the wind-driven surface current in Section 4.2. However, for the detailed evaluation of surface current velocities from different altimetry-based products against ADCP measurements during the period 2020-2021, presented in Section 4.1, an alternative source with higher spatial and temporal resolutions, and locally calibrated, was used to accurately reproduce the wind conditions, though with a higher computation cost. Specifically, the wind data for the study was obtained using the Weather Research and Forecasting (WRF) model v.4.2 (Skamarock et al. 2019), which is a mesoscale non-hydrostatic model. The WRF model was used to produce dynamically downscaled hourly 10 m wind speed and direction over the complete GoC area. The 3 km resolution domain was one-way nested within a larger parent domain with a resolution of 9 km. The initial and boundary conditions were provided by the NCEP-GFS model described earlier and applied to the parent domain. The dynamical set-up of the simulations follows the scheme presented in (Mulero-Martinez et al. 2022), as it was proved to successfully reproduce the wind conditions in the area.

3.3 In-situ ADCP measurements

Acoustic Doppler current profiler (ADCP) measurements were obtained from Armona coastal station (37.0108ºN, 7.7413ºW) (Figure 1), where the water depth is 22 m. For the data collection a Sentinel V 500 kHz ADCP, manufactured by TRDI, was bottom-mounted 4 times for periods ranging from January 2020 to December 2021. The instrument recorded hourly velocities in cells of 0.5 m thick along the water column. The resulting data was de-tided by applying a low-pass filter of a 40-h cut-off period. This study was based only on the spatial average of the two uppermost valid cells (Garel et al. 2016), typically within the initial 2 to 3 meters from the water surface. For the comparisons against satellite altimetry data, presented in Section 4.1, 72 h averages of ADCP measurements previous to the satellite pass were used. Using 72 h averages is suggested in (Mulero-Martínez et al. 2021; Roesler, Emery, and Kim 2013) for

comparisons with altimetry data since it is representative of a synoptic circulation, similar to the estimates using altimetry data, mainly based on geostrophic processes.

3.4 CMEMS gridded product

Gridded absolute geostrophic current velocities were gathered from the Copernicus Marine Environment Monitoring Service (CMEMS). The gridded product is based on multi-mission satellite altimetry (including Sentinel-3A) SLA measurements. The final gridded data is estimated by optimal interpolation, merging the level-3 along-track measurement from the different altimeter missions available and providing daily estimates with a 1/8°x1/8° spatial resolution. A more detailed description of the development and quality of the products can be found in https://doi.org/10.48670/moi-00142.

4 Results and discussion

4.1 Comparison and validation with in-situ current measurements

The S3A-057 satellite track passes over the GoC southbound (descending track), covering a narrow part of the continental shelf east of the CSM (Figure 1). The Armona ADCP was moored 15 km from this track. Different surface current estimates from S3A-057 altimetry measurements and gridded CMEMS products were compared with in situ measurements from the ADCP moored at Armona station.

4.1.1 Evaluation of ADT constructions

Results of the comparison between ADCP surface zonal velocities and the three different S3-V_t products, computed with ADTs from the different approaches (S3-V_tMDT, S3-V_tEGM and S3-V_tEIGEN), are presented in Figure 4. The comparison of different methods yielded the best result in terms of Pearson's correlation and root mean square error when using S3-V_tMDT (correlation coefficient=0.77; RMSE=0.10 m/s). The S3-V_tEGM and S3-V_tEIGEN estimates also performed well but had slightly lower correlation coefficients and larger RMSE compared to S3-V_tMDT. This finding aligns with a previous study (Feng et al. 2023) conducted in the Northwest Atlantic Shelf, particularly in the Gulf of Maine, which also concluded that constructing ADT based on MDT provides more accurate results when used for geostrophic current estimations, mainly due to increasing geoid errors near the coast.

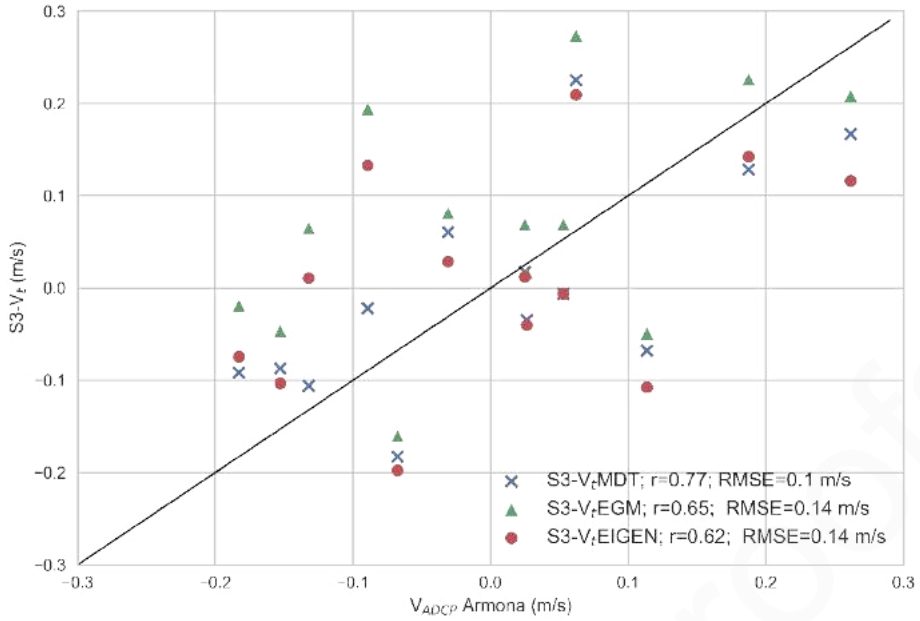

Figure 4. *Scatter plot of the different satellite altimetry-derived surface geostrophic velocity approaches against in-situ ADCP measurements. S3-V_tMDT refers to geostrophic velocities estimated using the ADT based on MDT, while S3-V_tEGM and S3-V_tEIGEN refer to the geostrophic velocities estimated using geoid models EGM2008 and EIGEN6C4, respectively.*

4.1.2 Inter-products comparison

The comparison presented in Figure 5 shows the current velocity estimated from several altimetry-based products against in-situ ADCP surface current measurements. Specifically, the altimetry-based products are the bottom-friction corrected geostrophic current (V_{gd}), the total current velocity accounting for the bottom-friction corrected geostrophic and wind components (V_t), generated from both high-resolution altimetry data along S3A-057 (S3-V_{gd} and S3-V_t) and the CMEMS product (C-V_{gd} and C-V_t). The wind information used for the estimation of the V_t was extracted from the high-resolution locally downscaled WRF model. The statistical parameters resulting from the comparison (r-correlation, RMSE, and bias) used to quantify the performance of the different products are presented in Table 2.

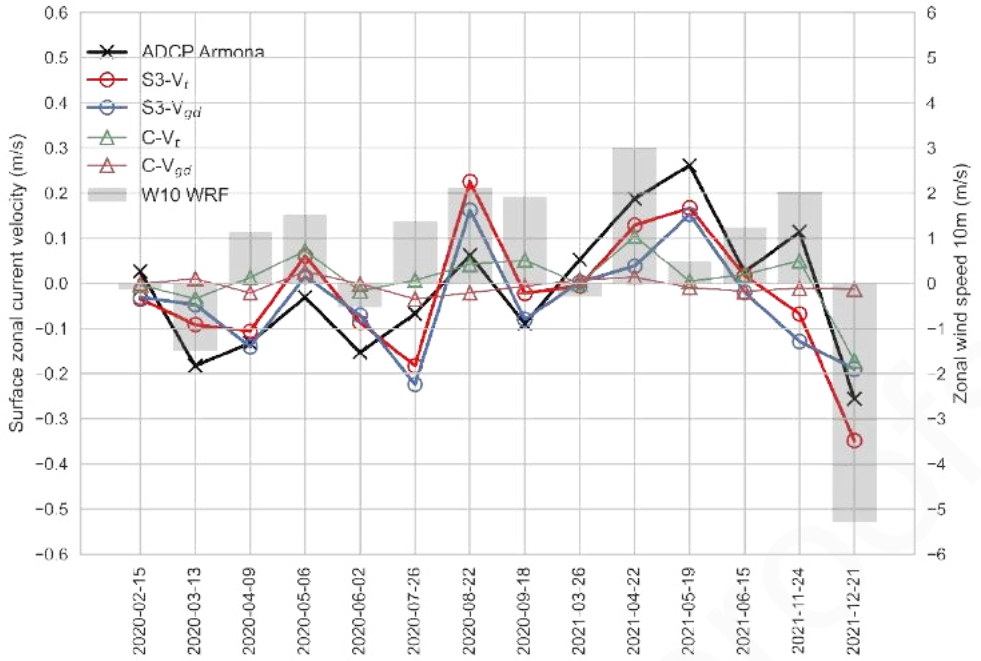

Figure 5. Match-up time series of altimetry-based current velocities (S3-V_{gd}, S3-V_t, C-V_{gd}, C-V_t) and in-situ ADCP Armona surface current velocities, along with the simultaneous zonal wind speed from WRF. Note that the time interval is not constant.

The comparison with in-situ measurements shows that the C-V_{gd} product produced the worst results (r = 0.10, RMSE = 0.14 m/s, Bias = -0.01 m/s), which is expected considering that it mainly represents the geostrophic current, corrected only for the bottom friction, in addition to the low resolution and high smoothing of both the final product and altimetric data (1 Hz) used for its development. The CMEMS product improved when applying an estimate of surface wind current (C-V_t), (r = 0.62, RMSE = 0.12 m/s, Bias = 0.01 m/s), especially in terms of correlation. This improvement is due to the greater similarity between the compared variables, resulting from the important role of the wind on the surface circulation of the GoC (Mulero-Martínez et al. 2021; De Oliveira Júnior et al. 2022).

The best results of the comparison derive from the use of the products generated with high-resolution altimetric measurements (20 Hz), S3-V_{gd} and S3-V_t. S3-V_{gd} showed a higher correlation than C-V_t, even without the application of wind current estimation (r = 0.67, RMSE = 0.11 m/s, Bias = 0.03 m/s). The higher spatial resolution of the altimetric data used to generate this product allows for a better representation of nearshore circulation along the continental shelf. However, the lack of a wind component penalizes the results of this comparison in terms of bias. Finally, the S3-V_t product provided the best representation of the surface circulation, with the best results for all calculated statistics (r = 0.77, RMSE = 0.10 m/s, Bias = 0.01 m/s). The S3-V_t product not only has the advantage of being generated with high spatial resolution altimetric data but also includes the variability provided by the estimation of the wind-induced current component. The high variability of the zonal circulation in the continental shelf sector during the analysis period can be observed. This variability, which is highly dependent on the wind field in the area, is well represented by the S3-V_t product, which correctly reproduced the ADCP current direction more than 70% of the time, even considering weak flows that might be produced by surface gradients of low magnitude, difficult to be resolved by altimetry (Marechal et al. 2020).

Despite the good results, it should be noted that the comparison shows current values obtained independently and in various ways. The ADCP measures at a single point and directly measures the total circulation that is taking place at each moment, while the altimetric products estimate the geostrophic component of the circulation based on the elevation gradient of the ocean surface along the satellite track (Feng et al. 2023). In addition, the distance between the satellite track and the ADCP could also affect the comparison. Such differences stand a limitation when performing this kind of comparison and should be considered when interpreting the statistical results. These results demonstrate the benefits of including the wind effect in the estimation of the surface circulation from altimetry.

Table 2. Statistical results (correlation coefficient, r; root mean square error, RMSE; and bias, Bias) from the comparison between altimetry-based current velocities (S3-V_{gd}, S3-V_t, C-V_{gd}, C-V_t) and in-situ ADCP Armona surface current velocities.

Product	r	p-value	RMSE (m/s)	Bias (m/s)
C-V_{gd}	0.10	0.742	0.14	-0.01
C-V_t	0.62	0.018	0.12	0.01
S3-V_{gd}	0.67	0.009	0.11	0.03
S3-V_t	0.77	0.001	0.10	0.01

4.2 Characterisation of the GoC shelf circulation

Since S3-V_t showed the best validation results, the same methodology has been extended to tracks S3A-385, 265, and 322, in addition to the already mentioned 057, for a longer period: 2017-2021. The use of different satellite tracks along the area allows for analysing the spatiotemporal variability of the surface circulation along the continental shelf in the GoC. It is worth mentioning that unlike in the previous section, the S3-V_t products analysed in this section, have been generated with an estimation of the wind-induced surface current (V_w) based on lower resolution data from NCEP-GFS instead of the locally calibrated WRF downscaling, due to computation limitations. Since the NCEP-GFS was used as boundary conditions for the WRF model, they were found to equivalently represent the synoptic conditions.

4.2.1 Contribution of the geostrophic and wind components

The different timeseries presented in Figure 6 show the along-track average zonal circulation along the continental shelf of the GoC, from tracks S3A-385 (a), 265 (b), 057 (c) and 322 (d), respectively. Specifically, estimates of the total current (V_t), the bottom-friction corrected geostrophic components (V_{gd}) and the wind component (V_w) of the surface circulation are presented to provide a comprehensive understanding of how the different components contribute to the alongshore circulation in the GoC northern shelf.

Tracks S3A-285, 265 and 057 (Figure 6a-c) present similar characteristics regarding the contribution of V_{gd} and V_w to V_t. Positive flows are mainly driven by westerly winds, as indicated by the correspondence of positive V_t and V_w, agreeing with the wind field over the area, since west of CSM westerly and north-westerly winds dominate (Folkard et al. 1997; De Oliveira Júnior et al. 2022), while easterlies are less recurrent and weaker than

over the southern part of the eastern basin (Mulero-martinez et al. 2022). In contrast, westward V_t flows are likely to occur along with both westward V_{gd} and V_w, but also just linked to V_{gd}, suggesting that westward flows, such as CCCs, are not necessarily linked to strong easterly winds, but also to geostrophic adjustments. Marked events (E1, 2, 3, 4 and 5) in Figure 6a represent the different scenarios detected with track S3A-385 along the western basin regarding the contribution of both V_{gd} and V_w to the westward flows. Events E1 (21-Apr-2017), E4 (25-Feb-2019) and E5 (23-Feb-2021) show V_t negative flow events driven by both westward V_{gd} and V_w, while during events E2 (30-Sep-2017) and E3 (6-Dec-2018) the V_t flows directed to the west are purely controlled by a negative V_{gd} flow. Several authors have suggested the existence of an alongshore pressure (sea level) gradient over the shelf that is likely to promote westward flows without favourable winds and would explain most of the flow variability during CCCs events in the western basin (Garel et al. 2016; De Oliveira Júnior et al. 2021, 2022). The new findings show that the cross-shore gradients may contribute as well to these events. The actual presence of both sea level gradients (i.e., cross-shore and alongshore) over the shelf is further analysed in Section 4.2.2. Regarding track S3A-322 (Figure 6d), crossing the eastern basin of the GoC, both V_{gd} and V_w components agree on most of the occasions on the direction of the circulation, aligning with V_t. This observation suggests that in contrast to the western basin, both eastward and westward flows along the shelf in this region are predominantly driven by favourable winds as suggested by previous studies using ADCP measurements (Criado-Aldeanueva et al. 2009). These winds also contribute to the development of cross-shelf sea level gradients through the piling up or down of water at the coast by Ekman transport, as previously reported in nearby areas (Gómez-Enri et al. 2019), which enhances the total flow through the additional contribution of a geostrophic component. The different V_{gd}-V_w interplays along the different basins are reassured when comparing with ADCP measurements with the correlation coefficients for V_{gd}-V_w, being 0.12 for S3A-385 (western basin) and 0.46 for S3A-322 (eastern basin). It can be also observed that, on average, the wind-driven flow is eastward for all the tracks, due to the dominance of westerly winds over the area, while the geostrophic flow tends to be westward along the whole basin.

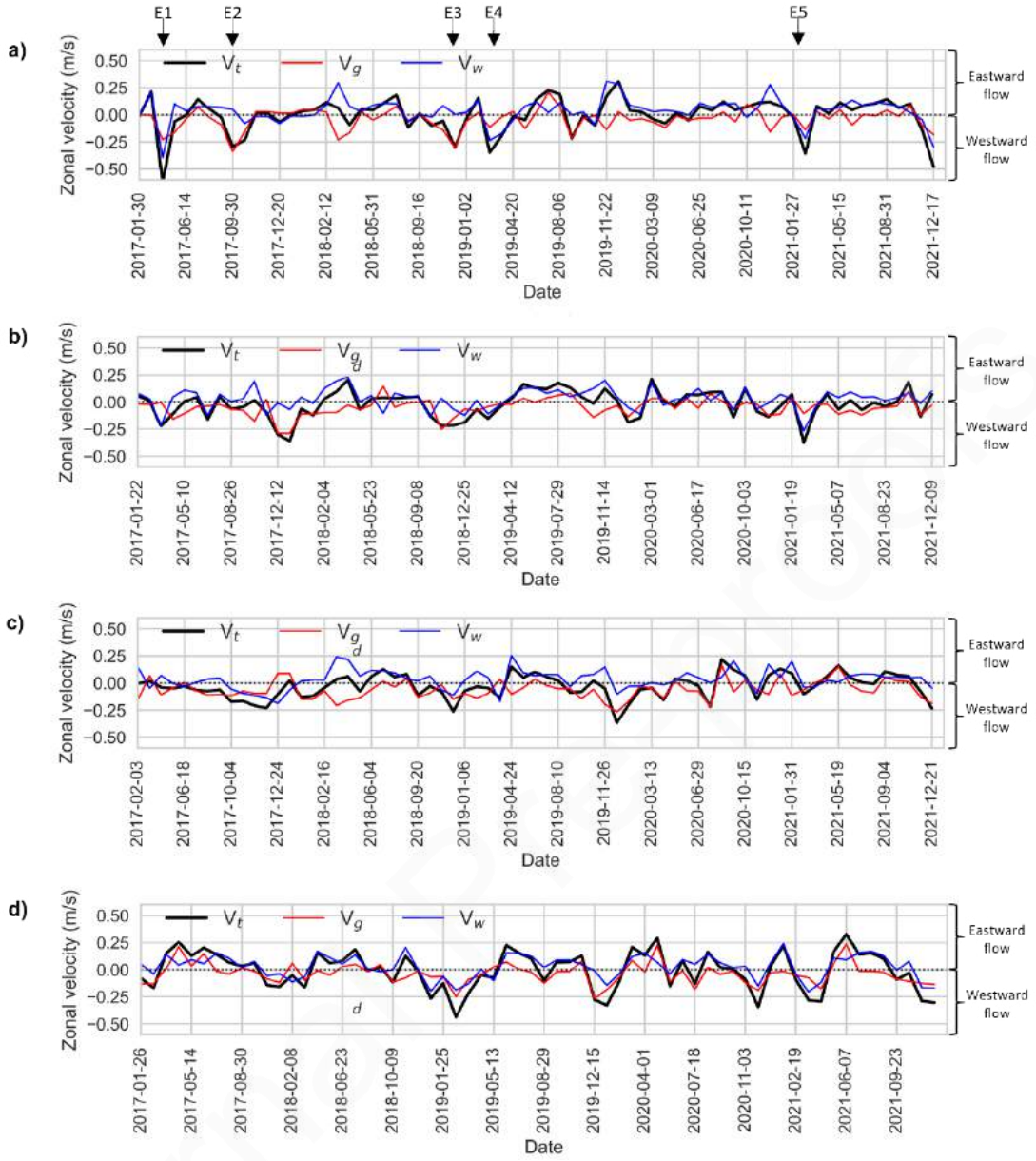

Figure 6. Time series of shelf average V_{gd} (red lines), V_w (blue lines) and V_t (black lines) from tracks S3A-385 (a), S3A-265 (b), S3A-057 (c) and 322 (d).

4.2.2 Alongshore and cross-shore sea level gradients

The 5 years average (2017-2021) of ADT for the continental shelf sector traversed by the different tracks is presented in Figure 7. The results show the existence of ADT gradients both alongshore and cross-shore, the former of much larger amplitude. Alongshore ADT average differences reach up to 4 cm between the easternmost and the westernmost tracks. This result is in line with previous studies, such as (Relvas and Barton 2002; Sánchez et al. 2006), that estimated an average slope of 5 cm/100 km for the same area based on tide gauges. This difference in ADT along the basin implies the existence of an unbalance in the along-shore pressure gradient. To be rebalanced, such alongshore gradient would lead to a westward flow (García-Lafuente et al. 2006; De Oliveira Júnior et al. 2021) during

periods of weakened westerly winds and would be enhanced under easterly wind conditions. Additionally, the cross-shore sea level gradients would also support the westward circulation over the shelf, as for the physical basis of this research, a north-south ADT gradient (higher ADT values close to the coast and lower off the coast) would develop a westward geostrophic flow. Such interpretation of the potential effects of the alongshore and cross-shore sea level gradients (ADT gradients) matches with the previously analysed contribution of the different components to the total shelf circulation at the different locations. The results also agree with several studies that suggested the existence of an alongshore pressure gradient as the main factor driving the commonly known coastal countercurrent (CCC) over the GoC shelf during weak wind conditions (Garel et al. 2016; De Oliveira Júnior et al. 2021, 2022) and with the observations from (Sirviente et al. 2023) of sea surface height across-shore gradients directed seawards for days when the CCC in the GoC is present. The average net geostrophic flow resulting from the existence of the ADT gradients presented in Figure 7 can be summed up as a westward flow in the absence of any other components. Such a flow would support the circulation represented by red lines in Figure 1.

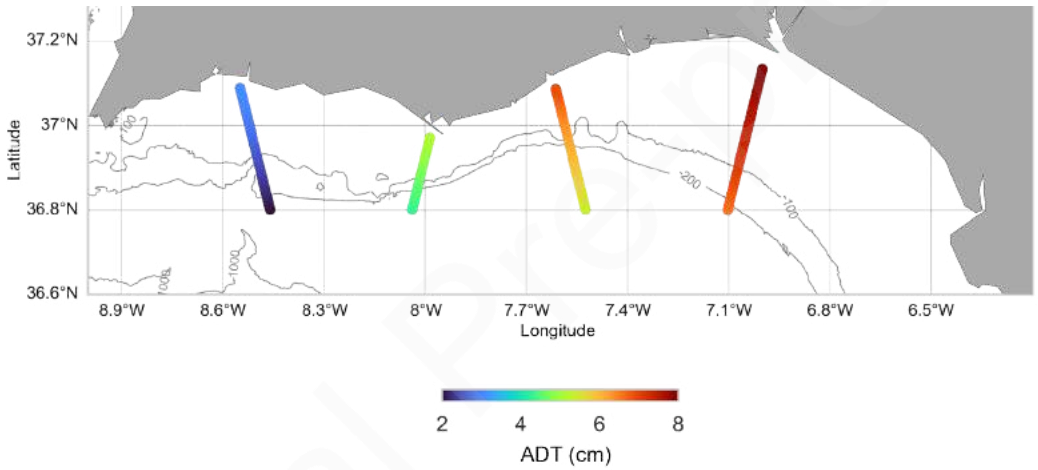

Figure 7. Along-track ADT average for the period 2017-2021 over the continental shelf of the GoC.

4.2.3 Spatio-temporal variability

The spatial and temporal variability of the zonal component of surface circulation along the GoC is evaluated by a Hovmöller (HM) diagram (Figure 8). The figure shows an HM diagram of the satellite total zonal velocity (V_t) variability against latitude and time for the tracks S3A-385 (a) and S3A-322 (b), representing the western and eastern basins, respectively. Tracks S3A-265 and S3A-057 are not presented due to the narrowness of the shelf at these locations. The use of time-latitude HM diagrams enables qualitatively identifying the alternance among periods dominated by either eastward or westward circulation, in addition, to providing the latitudinal variability of the main flows. Even though the different tracks are not contemporary, it is possible to appreciate a generic and common winter-summer seasonality.

For track S3A-385 (Figure 8a), the HM diagram shows some intense westward events extending along the entire transect (E1, E4 and E5). Those events can also be identified in Figure 6 and seem to be the result of the joint action of both V_w and V_{gd} west-bounded components. These events are not limited to the shelf section but extend further offshore,

potentially due to the action of Levantes along the whole basin. Additional westward events can be found more limited to the northern section and the shelf (i.e., E2 and E3), agreeing with the expected configuration of intense CCC events. As can be observed in Figure 6, E2 and E3 are mainly explained by the V_{gd} flow, suggesting that westward flows due to geostrophic forces might result in narrower coastal flows than those where also the V_w contribute. Considering that the wind-driven flows would be due to a homogeneous wind field blowing toward the west all over the GoC, they can be expected to cover an extension as wide as the mentioned wind field. On the other hand, the extension of westward flows caused only or mainly by geostrophic forces could result in narrower extensions due to constraints such as bathymetry. The southern half of the HM diagram in Figure 8a presents the highest positive flow velocities mostly limited up to 36.6ºN, agreeing with the spatial characteristics of the GoC Current (GCC). Results from track S3A-322 (Figure 8b) show remarkably high-intensity negative flows over the southern section of the analysed transect, which most of the time extend up to the northern limits. As previously mentioned, (De Oliveira Júnior et al. 2022) performed a similar analysis based on HFR data over the GoC, and, for the eastern basin found that negative flows tend to occur mostly over the outer shelf, in line with these results that show how the most intense negative flows tend to occur more detached from the coast. Such setup of the circulation might be explained by the proximity to the Strait of Gibraltar where easterly winds are canalised into the GoC and would drive the surface circulation since, as previously stated, is mainly controlled by the wind component over the eastern basin.

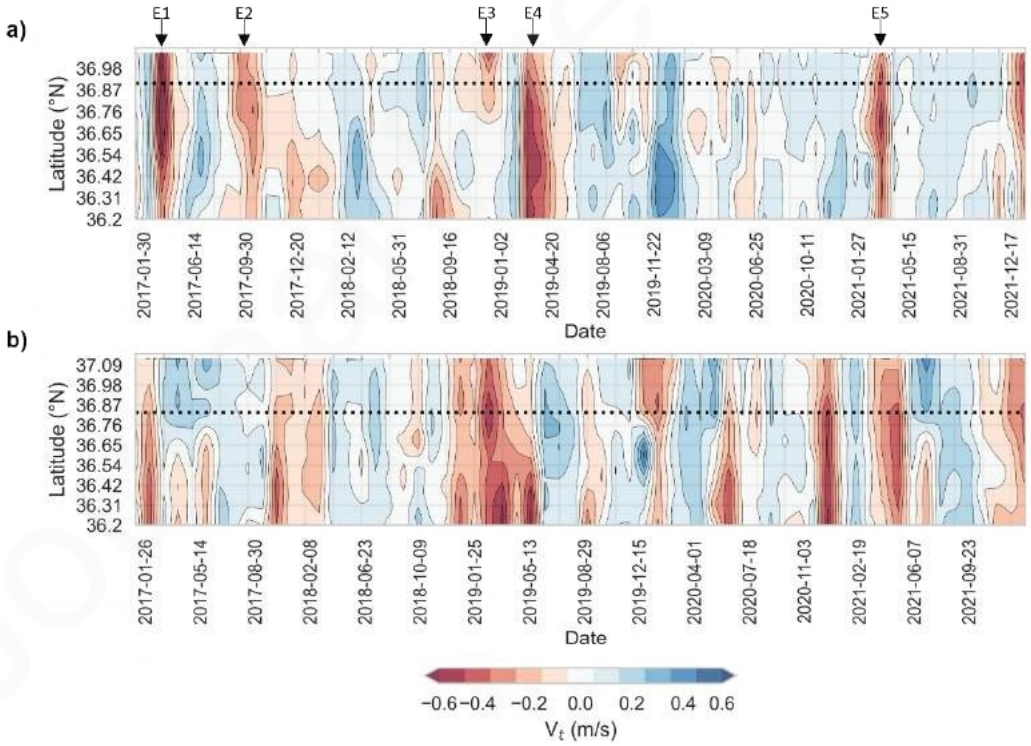

Figure 8. Latitude-time Hovmöller diagrams of the total surface zonal velocity for the period 2017-2021 from tracks S3A-385 (a) and S3A-322 (b) Horizontal dotted lines indicate the latitude corresponding to the 200 m depth isobath.

The percentage of occurrence of positive and negative flows over the different months, as estimated from the different tracks for the shelf section are presented in **Table 3**. This table provides a global perspective of the temporal and seasonal variability of the dominant flow direction along the year. For all four tracks, eastward circulation prevails

during May, June, July and August. The prevalence of eastward flows during the spring-summer months agrees with the upwelling season, though such seasonality over the GoC is not clearly defined, during these months westerly winds are most likely to drive the surface circulation over the area (Garel et al. 2016; De Oliveira Júnior et al. 2022; Sánchez and Relvas 2003). The opposite situation is observed for winter months, from December to February, when the circulation is predominantly westward. More prevailing westward flows during winter months are associated with strong easterly winds and the effect of the along-shore sea level gradient during relaxed upwelling conditions. The resulting all-year percentages for all tracks are mainly balanced, agreeing with the results presented in (Teles-Machado et al. 2007), and with the latest study over the area (Sirviente et al. 2023) which, based on HFR measurements and numerical model simulations, found that for summer months westward flows are of smaller amplitude, and greater amplitudes are observed in eastward flows. It is worth noting that the values presented in **Table 3** are based on satellite passes with 27-day cycles, resulting in approximately 5 passes per track and month for the whole period analysed.

Table 3. Monthly percentage of occurrence of westward and eastward circulation and zonal wind over the continental shelf of the GoC from Sentinel-3A tracks #385, #365, #057, #322 and NCEP-GFS wind model. Periods coloured in blue represent the dominance of eastward circulation, while those coloured in red stand for the dominance of westward circulation.

S3A Tracks	V_t Direction	Jan	Feb	Mar	Apr	May	Jun	Jul	Aug	Sep	Oct	Nov	Dec
#385	Westward	42.86	50.00	40.00	80.00	42.86	20.00	0.00	16.67	57.14	60.00	33.33	42.86
	Eastward	57.14	50.00	60.00	20.00	57.14	80.00	100.00	83.33	42.86	40.00	66.67	57.14
#365	Westward	66.67	60.00	42.86	60.00	20.00	16.67	28.57	40.00	40.00	50.00	83.33	66.67
	Eastward	33.33	40.00	57.14	40.00	80.00	83.33	71.43	60.00	60.00	50.00	16.67	33.33
#057	Westward	66.67	100.00	66.67	40.00	40.00	33.33	33.33	40.00	60.00	50.00	100.00	66.67
	Eastward	33.33	0.00	33.33	60.00	60.00	66.67	66.67	60.00	40.00	50.00	0.00	33.33
#322	Westward	75.00	100.00	60.00	33.33	40.00	0.00	16.67	28.57	20.00	60.00	60.00	83.33
	Eastward	25.00	0.00	40.00	66.67	60.00	100.00	83.33	71.43	80.00	40.00	40.00	16.67
Zonal Wind	**Direction**	**Jan**	**Feb**	**Mar**	**Apr**	**May**	**Jun**	**Jul**	**Aug**	**Sep**	**Oct**	**Nov**	**Dec**
	Westward	47.52	52.66	45.97	40.67	37.16	18.33	15.16	24.68	41.00	50.81	43.67	50.97
	Eastward	52.48	47.34	54.03	59.33	62.84	81.67	84.84	75.32	59.00	49.19	56.33	49.03

5 Summary and conclusions

This study presents a generic methodology for assessing the surface circulation over the northern shelf of the Gulf of Cádiz, based on satellite altimetry measurements and considering the effects of ageostrophic factors such as the bottom-drag and wind-driven circulation. The results from the applied methodology were validated against in-situ measurements over the GoC's shelf. After ensuring the good performance of the methods, the outputs were applied for a characterisation of the surface circulation over the GoC northern shelf, specifically, based on 4 years of high-resolution satellite altimetry data from Sentinel-3A and wind model data. The resulting spatiotemporal characteristics agree with the general description of the literature, furthermore, the results bring additional details about the sea level variability along the GoC.

The use of the ADT construction employing MDT, for computing surface geostrophic velocities, yielded the best correlation (0.77) and the lowest root mean square error (0.10 m/s) when compared to ADCP measurements from near-shore moorings. While geoid-based methods also provided reasonable results, they exhibited slightly lower correlation coefficients and larger RMSE values. This analysis is consistent with results from prior studies in other coastal regions, such as coastal areas over the Northwest Atlantic Shelf (Feng et al. 2023), emphasizing the importance of constructing ADT based on MDT for

improved accuracy, particularly in areas near the coast. Thus, the present work provides valuable insights into the choice of ADT construction methods for enhancing the reliability of satellite-derived ocean current velocity data in coastal regions.

The comparison of surface bottom-drag corrected geostrophic (V_{gd}) and total (V_t) zonal current velocity estimates derived from different altimetry-based sources, including high-resolution along-track Sentinel-3A data (S3-V_{gd} and S3-V_t) and Copernicus Marine Environment Monitoring Service (CMEMS) products (C-V_{gd} and C-V_t), with in-situ ADCP measurements, revealed that the CMEMS's geostrophic current product (C-V_{gd}) had the poorest performance due to its limited resolution. However, when incorporating wind-driven current estimates (C-V_t), the product improved significantly, emphasizing the importance of wind on the surface circulation (Mulero-Martínez et al. 2021). The best results were achieved with high-resolution altimetry data (S3A-V_{gd} and S3A-V_t). S3A-V_{gd} showed a high correlation even without wind data, with a slight bias. S3-V_t, which included wind-driven current variability, outperformed all other products in terms of statistical metrics, accurately capturing surface circulation direction most of the time. These findings encourage the use of high-resolution altimetry data as inputs for global products/models, even over coastal areas. In addition, they highlight the necessity of properly characterising local effects as wind-driven currents to reach a good understanding of the circulation over complex coastal areas.

The analysis of the surface circulation along the continental shelf aimed to assess the contributions of the bottom-friction corrected geostrophic (V_{gd}) and wind-driven (V_w) flow components to the total surface current (V_t). The results showed distinct characteristics over the different parts of the GoC. Tracks S3A-385 and 265, located in the western basin, suggested that positive (eastward) surface currents were predominantly driven by westerly winds, while only occasionally, westward flows coincided with easterly winds. These patterns suggest a higher control of the geostrophic component over westward flows, which are mainly driven by cross-shore and alongshore sea level gradients. In contrast, track S3A-322, located in the eastern basin, displayed a stronger correspondence between both V_{gd} and V_w with V_t. This fact suggests that both eastward and westward flows along the shelf in this region were primarily driven by favourable winds. These winds also induced cross-shelf sea level gradients through Ekman transport, enhancing the westward geostrophic component of the flow. Related to that, the analysis of ADT values along the whole basin showed the presence of ADT gradients, both along-shore and cross-shore, along the GoC's shelf, with a greater amplitude attributed to alongshore gradients. Notably, average alongshore ADT differences reached up to 4 cm between the easternmost and westernmost tracks. This discrepancy in ADT along the basin supports the fact that an imbalance in the along-shore pressure gradient would induce a westward flow during periods of weakened westerly winds and intensify under easterly wind conditions. These findings are consistent with the observed contributions of different components to the total shelf circulation over the different basins. They also corroborate previous studies suggesting that an alongshore pressure gradient is a primary driver of the coastal CCC under weak wind conditions (De Oliveira Júnior et al. 2021, 2022) and with the observations from (Sirviente et al. 2023) of sea surface height across-shore gradients directed seawards for days when the CCC in the GoC is present.

Regarding the spatiotemporal characterisation of the surface circulation, the results for the continental shelf of the western basin showed the occurrence of westward flows primarily in the northern half of the transect, aligning with the expected configuration of CCC events in this area. The southern half of the transect exhibited a higher occurrence

of positive (eastward) flows, typically limited to latitudes up to 36.6ºN, consistent with the Gulf of Cadiz Current (GCC). These findings supported previous research that found negative flows extending toward the shelf break 60-70% of the time, with positive flows dominating further offshore. In contrast, results for the eastern basin displayed notably high-intensity negative flows, primarily in the southern section of the transect. These observations were in line with previous studies indicating that negative flows tend to occur mostly over the outer shelf and detached from the coast at the eastern basin (De Oliveira Júnior et al. 2022), as easterly winds channelled into the Gulf of Cadiz played a significant role in driving surface circulation. Across all four tracks, the eastward circulation dominated during the spring and summer months (May, June, July, and August). This eastward flow pattern correlated with the upwelling season in the Gulf of Cadiz, driven by westerly winds. In contrast, westward flows prevailed during the winter months (December to February). This westward flow predominance in winter might be associated with a higher occurrence of easterly winds and the rebalancing of the along-shore sea level gradient during relaxed upwelling conditions.

These results represent an advance in the use of satellite altimetry data for oceanographic applications in coastal areas where both the spatial and temporal variability of the circulation are highly complex. Furthermore, considering the similarity of the results with previous studies based on in-situ systems that entail more costs for the user, such as HFR and ADCP, the use of altimetry data and publicly accessible wind models is an advantage for the evaluation of oceanographic characteristics in areas with difficult access or few resources, which can contribute to a better understanding and management of coastal areas.

References

Aldarias, Ana, Jesus Gomez-Enri, Irene Laiz, Begona Tejedor, Stefano Vignudelli, and Paolo Cipollini. 2020. “Validation of Sentinel-3A SRAL Coastal Sea Level Data at High Posting Rate: 80 Hz.” *IEEE Transactions on Geoscience and Remote Sensing* 58(6):3809–21. doi: 10.1109/TGRS.2019.2957649.

Bouffard, Jérôme, Ananda Pascual, Simón Ruiz, Yannice Faugère, and Joaquín Tintoré. 2010. “Coastal and Mesoscale Dynamics Characterization Using Altimetry and Gliders: A Case Study in the Balearic Sea.” *Journal of Geophysical Research: Oceans* 115(10). doi: 10.1029/2009JC006087.

Bowden, K. F. 1983. *Physical Oceanography of Coastal Waters*. Camelot Press Ltd.

Carvalho, D., A. Rocha, M. Gómez-Gesteira, and C. Silva Santos. 2014. “Offshore Wind Energy Resource Simulation Forced by Different Reanalyses: Comparison with Observed Data in the Iberian Peninsula.” *Applied Energy* 134:57–64. doi: 10.1016/j.apenergy.2014.08.018.

Cleveland, William S., and Susan J. Devlin. 1988. “Locally Weighted Regression: An Approach to Regression Analysis by Local Fitting.” *Journal of the American Statistical Association* 83(403):596–610. doi: 10.1080/01621459.1988.10478639.

Criado-Aldeanueva, F., J. Garcia-Lafuente, G. Navarro, and J. Ruiz. 2009. "Seasonal and Interannual Variability of the Surface Circulation in the Eastern Gulf of Cadiz (SW Iberia)." *Journal of Geophysical Research: Oceans* 114(1):0–11. doi: 10.1029/2008JC005069.

Criado-Aldeanueva, Francisco, Jesús García-Lafuente, Juan Miguel Vargas, Jorge Del Río, A. Vázquez, A. Reul, and A. Sánchez. 2006. "Distribution and Circulation of Water Masses in the Gulf of Cadiz from in Situ Observations." *Deep-Sea Research Part II: Topical Studies in Oceanography* 53(11–13):1144–60. doi: 10.1016/j.dsr2.2006.04.012.

Dinardo, Salvatore, Luciana Fenoglio-Marc, Matthias Becker, Remko Scharroo, M. Joana Fernandes, Joanna Staneva, Sebastian Grayek, and Jérôme Benveniste. 2021. "A RIP-Based SAR Retracker and Its Application in North East Atlantic with Sentinel-3." *Advances in Space Research* 68(2):892–929. doi: 10.1016/j.asr.2020.06.004.

Feng, Hui, Alejandro Egido, Doug Vandemark, and John Wilkin. 2023. "Exploring the Potential of Sentinel-3 Delay Doppler Altimetry for Enhanced Detection of Coastal Currents along the Northwest Atlantic Shelf." *Advances in Space Research* 71(1):997–1016. doi: 10.1016/j.asr.2022.09.011.

Fenoglio-Marc, L., S. Dinardo, R. Scharroo, A. Roland, M. Dutour Sikiric, B. Lucas, M. Becker, J. Benveniste, and R. Weiss. 2015. "The German Bight: A Validation of CryoSat-2 Altimeter Data in SAR Mode." *Advances in Space Research* 55(11):2641–56. doi: 10.1016/J.ASR.2015.02.014.

Folkard, Andrew M., Peter A. Davies, Armando F. G. Fiúza, and Isabel Ambar. 1997. "Remotely Sensed Sea Surface Thermal Patterns in the Gulf Of-Cadiz and the Strait of Gibraltar: Variability, Correlations, and Relationships with the Surface Wind Field." *Journal of Geophysical Research C: Oceans* 102(C3):5669–83.

Förste, Ch, S. L. Bruinsma, O. Abrikosov, J. M. Lemoine, T. Schaller, H. J. Götze, J. Ebbing, J. C. Marty, F. Flechtner, G. Balmino, and R. Biancale. 2014. "The Latest Combined Global Gravity Field Model Including GOCE Data up to Degree and Order 2190 of GFZ Potsdam and GRGS Toulouse." 11:25–28.

Fu, Lee Lueng, Dudley B. Chelton, Pierre Yves Le Traon, and Rosemary Morrow. 2010. "Eddy Dynamics from Satellite Altimetry." *Oceanography* 23(4):15–25. doi: 10.5670/OCEANOG.2010.02.

García-Lafuente, Jesús, Javier Delgado, Francisco Criado-Aldeanueva, Miguel Bruno, Jorge del Río, and Juan Miguel Vargas. 2006. "Water Mass Circulation on the Continental Shelf of the Gulf of Cádiz." *Deep-Sea Research Part II: Topical Studies in Oceanography* 53(11–13):1182–97. doi: 10.1016/j.dsr2.2006.04.011.

Garel, E., I. Laiz, T. Drago, and P. Relvas. 2016. "Characterisation of Coastal Counter-Currents on the Inner Shelf of the Gulf of Cadiz." *Journal of Marine Systems* 155:19–34. doi: 10.1016/j.jmarsys.2015.11.001.

Gómez-Enri, J., C. J. González, M. Passaro, S. Vignudelli, O. Álvarez, P. Cipollini, R. Mañanes, M. Bruno, M. P. López-Carmona, and A. Izquierdo. 2019. "Wind-Induced

Cross-Strait Sea Level Variability in the Strait of Gibraltar from Coastal Altimetry and in-Situ Measurements." *Remote Sensing of Environment* 221(October 2018):596–608. doi: 10.1016/j.rse.2018.11.042.

Gómez-Enri, J., S. Vignudelli, P. Cipollini, J. Coca, and C. J. González. 2018. "Validation of CryoSat-2 SIRAL Sea Level Data in the Eastern Continental Shelf of the Gulf of Cadiz (Spain)." *Advances in Space Research* 62(6):1405–20. doi: 10.1016/j.asr.2017.10.042.

Knudsen, Per, Ole Andersen, and Nikolai Maximenko. 2016. "The Updated Geodetic Mean Dynamic Topography Model - DTU15MDT." *EGUGA* 18:EPSC2016-5052.

Laiz, I., S. Plecha, A. Teles-Machado, E. González-Ortegón, D. Sánchez-Quiles, A. Cobelo-García, D. Roque, A. Peliz, R. F. Sánchez-Leal, and A. Tovar-Sánchez. 2019. "The Role of the Gulf of Cadiz Circulation in the Redistribution of Trace Metals between the Atlantic Ocean and the Mediterranean Sea." *Science of the Total Environment*. doi: 10.1016/j.scitotenv.2019.134964.

Manso-Narvarte, Ivan, Ainhoa Caballero, Anna Rubio, Claire Dufau, and Florence Birol. 2018a. "Joint Analysis of Coastal Altimetry and High-Frequency (HF) Radar Data: Observability of Seasonal and Mesoscale Ocean Dynamics in the Bay of Biscay." *Ocean Science* 14(5):1265–81. doi: 10.5194/os-14-1265-2018.

Manso-Narvarte, Ivan, Ainhoa Caballero, Anna Rubio, Claire Dufau, and Florence Birol. 2018b. "Joint Analysis of Coastal Altimetry and High-Frequency (HF) Radar Data: Observability of Seasonal and Mesoscale Ocean Dynamics in the Bay of Biscay." *Ocean Science* 14(5):1265–81. doi: 10.5194/os-14-1265-2018.

Marechal, Gwendal, Fabrice Ardhuin, Gwendal Marechal, and Fabrice Ardhuin. 2020. "Surface Currents and Significant Wave Height Gradients: Matching Numerical Models and High-Resolution Altimeter Wave Heights in the Agulhas Current Region." *Esoar* 105:essoar.10505343. doi: 10.1002/ESSOAR.10505343.1.

Meloni, M., J. Bouffard, A. M. Doglioli, A. A. Petrenko, and G. Valladeau. 2019. "Toward Science-Oriented Validations of Coastal Altimetry: Application to the Ligurian Sea." *Remote Sensing of Environment* 224(February):275–88. doi: 10.1016/j.rse.2019.01.028.

Morrow, Rosemary, Alice Carret, Florence Birol, Fernando Nino, Guillaume Valladeau, Francois Boy, Celine Bachelier, and Bruno Zakardjian. 2017. "Observability of Fine-Scale Ocean Dynamics in the Northwestern Mediterranean Sea." *Ocean Science* 13(1):13–29. doi: 10.5194/OS-13-13-2017.

Mulero-Martínez, R., J. Gómez-Enri, R. Mañanes, and M. Bruno. 2021. "Assessment of Near-Shore Currents from CryoSat-2 Satellite in the Gulf of Cádiz Using HF Radar-Derived Current Observations." *Remote Sensing of Environment* 256:112310. doi: 10.1016/J.RSE.2021.112310.

Mulero-martinez, Roberto, Carlos Román-cascón, Rafael Mañanes, Alfredo Izquierdo, and Miguel Bruno. 2022. "The Use of Sentinel-3 Altimetry Data to Assess Wind Speed from the Weather Research and Forecasting (WRF) Model : Applica- Tion over the Gulf of Cadiz." 1–15.

Mulero-Martinez, Roberto, Carlos Román-Cascón, Rafael Mañanes, Alfredo Izquierdo, Miguel Bruno, and Jesús Gómez-Enri. 2022. "The Use of Sentinel-3 Altimetry Data to Assess Wind Speed from the Weather Research and Forecasting (WRF) Model: Application over the Gulf of Cadiz." *Remote Sensing 2022, Vol. 14, Page 4036* 14(16):4036. doi: 10.3390/RS14164036.

De Oliveira Júnior, L., E. Garel, and P. Relvas. 2021. "The Structure of Incipient Coastal Counter Currents in South Portugal as Indicator of Their Forcing Agents." *Journal of Marine Systems* 214(October 2020):103486. doi: 10.1016/j.jmarsys.2020.103486.

De Oliveira Júnior, Luciano, Paulo Relvas, and Erwan Garel. 2022. "Kinematics of Surface Currents at the Northern Margin of the Gulf of Cádiz." *Ocean Science* 18(4):1183–1202. doi: 10.5194/os-18-1183-2022.

Ortega, María, Enrique Sánchez, Claudia Gutiérrez, María Ofelia Molina, and Noelia López-Franca. 2023. "Regional Winds over the Iberian Peninsula (Cierzo, Levante and Poniente) from High-Resolution COSMO-REA6 Reanalysis." *International Journal of Climatology* 43(2):1016–33. doi: 10.1002/joc.7860.

Pavlis, N. K., S. A. Holmes, S. C. Kenyon, and J. K. Factor. 2008. "An Earth Gravitational Model to Degree 2160: EGM2008." *Geophysical Research Abstracts* 10:2008–01891.

Powell, Brian S., and Robert R. Leben. 2004. "An Optimal Filter for Geostrophic Mesoscale Currents from Along-Track Satellite Altimetry." *Journal of Atmospheric and Oceanic Technology* 21(10):1633–42. doi: 10.1175/1520-0426(2004)021<1633:AOFFGM>2.0.CO;2.

Raney, R. Keith. 2012. "CryoSat SAR-Mode Looks Revisited." *IEEE Geoscience and Remote Sensing Letters* 9(3):393–97. doi: 10.1109/LGRS.2011.2170052.

Relvas, Paulo, and Eric D. Barton. 2002. "Mesoscale Patterns in the Cape São Vicente (Iberian Peninsula) Upwelling Region." *Journal of Geophysical Research: Oceans* 107(C10):28–1. doi: 10.1029/2000JC000456.

Roesler, C. J., W. J. Emery, and S. Y. Kim. 2013. "Evaluating the Use of High-Frequency Radar Coastal Currents to Correct Satellite Altimetry." *Journal of Geophysical Research: Oceans* 118(7):3240–59. doi: 10.1002/JGRC.20220.

Sánchez, R. F., E. Mason, P. Relvas, A. J. da Silva, and Á. Peliz. 2006. "On the Inner-Shelf Circulation in the Northern Gulf of Cádiz, Southern Portuguese Shelf." *Deep Sea Research Part II: Topical Studies in Oceanography* 53(11–13):1198–1218. doi: 10.1016/J.DSR2.2006.04.002.

Sánchez, Ricardo F., and Paulo Relvas. 2003. "Spring-Summer Climatological Circulation in the Upper Layer in the Region of Cape St. Vincent, Southwest Portugal." *ICES Journal of Marine Science*. doi: 10.1016/S1054-3139(03)00137-1.

Sirviente, S., M. Bolado-Penagos, J. J. Gomiz-Pascual, J. Romero-Cózar, A. Vázquez, and M. Bruno. 2023. "Dynamics of Atmospheric-Driven Surface Currents on The Gulf of Cadiz Continental Shelf and Its Link with The Strait of Gibraltar and The

Western Alboran Sea." *Progress in Oceanography* 219. doi: 10.1016/j.pocean.2023.103175.

Skamarock, W. C., J. B. Klemp, Jimy Dudhia, D. O. Gill, Liu Zhiquan, Judith Berner, Wei Wang, J. G. Powers, Michael G. Duda, Dale M. Barker, and Xiang-Yu Huang. 2019. "A Description of the Advanced Research WRF Model Version 4." *NCAR Technical Note NCAR/TN-475+STR* 145.

Srinivasan, Margaret, and Vardis Tsontos. 2023. "Satellite Altimetry for Ocean and Coastal Applications: A Review." *Remote Sensing 2023, Vol. 15, Page 3939* 15(16):3939. doi: 10.3390/RS15163939.

Teles-Machado, Ana, Álvaro Peliz, Jesus Dubert, and Ricardo F. Sánchez. 2007. "On the Onset of the Gulf of Cadiz Coastal Countercurrent." *Geophysical Research Letters* 34(12):1–5. doi: 10.1029/2007GL030091.

Troupin, Charles, Ananda Pascual, Guillaume Valladeau, Isabelle Pujol, Arancha Lana, Emma Heslop, Simón Ruiz, Marc Torner, Nicolas Picot, and Joaquín Tintoré. 2015. "Illustration of the Emerging Capabilities of SARAL/AltiKa in the Coastal Zone Using a Multi-Platform Approach." *Advances in Space Research* 55(1):51–59. doi: 10.1016/J.ASR.2014.09.011.

Conflicts of Interest: The authors declare no conflict of interest.

Summary of Activities

Disciplinary Activities

VI Doctoral days meeting (field trip). University of Cadiz Doctorate School (EDUCA).

Doctoral days meeting (Oral presentation). University of Cadiz Doctorate. School (EDUCA) and International Doctoral School in Marine Studies (EIDEMAR).

Course on GIS and Remote Sensing applied to project management in the marine environment, land and marine environment protection. University of Cadiz Doctorate School (EDUCA).

Artificial intelligence (AI) for Earth monitoring / EUMETSAT, EUROPEAN CENTRE FOR MEDIUM-RANGE WEATHER FORECASTS (ECMWF), MERCATOR OCEAN INTERNATIONAL (MOI) AND EUROPEAN ENVIRONMENT AGENCY (EEA).

Coastal Altimetry Training Programme, February 6 (2023), Cádiz (Spain). European Space Agency (ESA).

OFFSHORE WIND FARM TECHNOLOGY: DESIGN, INSTALLATION AND OPERATION / TUDelft.

Complementary Skills

Training event Career development for doctoral students. European University of the Seas Doctorate School (SEA-EU DOC).

Corso di Lingua Italiana per Stranieri. Centro Linguistico d'Ateneo dell'Università di Ferrara (CLA).

German language course / Centro superior de lenguas modernas (CSLM), Universidad de Cádiz.

Scientific Activities

Publication: Mulero-Martínez, R., Gómez-Enri, J., Mañanes, R., & Bruno, M. (2021). Assessment of nearshore currents from CryoSat-2 satellite in the Gulf of Cádiz using HF radar-derived current observations. Remote Sensing of Environment, 256, 112310. https://doi.org/10.1016/j.rse.2021.112310.

vPICO presentation: How are the coastal breezes affected by changes in the land surface? Analysis from a case study using WRF, EGU General Assembly 2021, 19–30 Apr 2021. https://doi.org/10.5194/egusphere-egu21-4377.

Oral presentation: Assessment of CryoSat-2 altimetry data using high-frequency radar for the study of surface coastal circulation, CryoSat 10th Anniversary 14-17 June 2021. https://earth.esa.int/eogateway/events/cryosat-10th-anniversary-science-conference.

Poster presentation international workshop: Living Planet Symposium 2022, European Space Agency (ESA). 23 May 2022 to 27 May 2022, Bonn (Germany).

Oral presentation national workshop: XIX Congreso de la Asocición Española de Teledetección. 29 Jun 2022 to 01 Jul 2022, Pamplona (Spain).

Publication: Mulero-Martinez, R., Román-Cascón, C., Mañanes, R., Izquierdo, A., Bruno, M., Gómez-Enri, J. (2022). The Use of Sentinel-3 Altimetry Data to Assess Wind Speed from the Weather Research and Forecasting (WRF) Model: Application over the Gulf of Cadiz. Remote Sens. 2022, Volume 14, Issue 16, 4036.

Oral presentation international workshop: 2022 Ocean Surface Topography Science Team (OSTST) meeting, October 31 - November 4 (2022), Venice (Italy). CNES, EUMETSAT.

Oral presentation international workshop: 13th Coastal Altimetry Workshop, February 6-10 (2023), Cádiz (Spain). ESA.

Study abroad period: September 19 – December 19 (2022), Centro de Investigação Marinha e Ambiental (CIMA), Universidade do Algarve (Portugal).

Other Activities

Teaching assistance in the subject Methods in Oceanography, University Degree in Marine Sciences (University of Cádiz).

Teaching assistance in the subject GIS and Remote Sensing, University Degree in Marine Sciences (University of Cádiz).